

**Polar Tris(pyrazolyl)borates for the Modeling of
Zinc Metalloenzymes in Aqueous Solution**

Inaugural-Dissertation
Fakultät für Chemie, Pharmazie und Geowissenschaften der
Albert-Ludwigs-Universität
Freiburg im Breisgau
Deutschland

vorgelegt von
Cristina Pérez Olmo
aus
Jaén (Spanien)
April 2005

Promotionsausschußvorsitzender:	Prof. Dr. G. E. Schulz
Dekan:	Prof. Dr. P. Gräber
Leiter der Arbeit:	Prof. Dr. H. Vahrenkamp
Referent:	Prof. Dr. H. Vahrenkamp
Koreferent:	Prof. Dr. C. Janiak

Tag der Bekanntgabe des Prüfungsergebnisses: 29. April 2005

Danksagung

Die vorliegende Arbeit wurde in der Zeit von Dezember 2000 bis April 2005 im Institut für Anorganische und Analytische Chemie der Albert-Ludwigs-Universität in Freiburg im Breisgau unter der Leitung von Herrn

Prof. Dr. Heinrich Vahrenkamp

angefertigt. Ihm danke ich herzlich dafür, daß ich bei ihm promovieren konnte. Besonders gilt ihm mein Dank für die interessante Themenstellung, den gewährten Freiraum bei der Bearbeitung des Themas und für die Betreuung bei der Abfassung des Manuskripts.

Allen Kolleginnen und Kollegen möchte ich für die gute Arbeitsatmosphäre und die hervorragende Zusammenarbeit danken. Mein besonderer Dank gilt Frau Petra Klose, die mit großem Einsatz zum Gelingen vieler Experimente beigetragen hat. Für die freundliche Unterstützung und Hilfestellungen bei der Röntgendiffraktometer-Messungen danke ich Frau Prof. Dr. Caroline Röhr, Dr. Werner Deck und Dr. Horst Brombacher. Für ihre ungewöhnlichen Ratschläge bei präparativen Probleme danke ich Dr. Mouhai Shu, Dr. Jan Seebacher und Dr. Florian Groß. Bei Frau Gerda Probst und Frau Vera Brucksch bedanke ich mich für ihre Hilfe bei bürokratischen Probleme.

Ich möchte Herrn Prof. Dr. Christoph Janiak für die Übernahme des Koreferats danken, ebenso wie Herrn Prof. Dr. Peter Gräber für seine Bereitschaft, als Dritprüfer an meiner Doktorprüfung mitzuwirken.

A mis padres quisiera agradecerles el apoyo y cariño que han sabido transmitirme a diario durante estos últimos cuatro años a pesar de la distancia. Especialmente me gustaría agradecerle al Dr. D. José A. Maldonado Calvo su ayuda en la resolución de estructuras cristalinas y en las mediciones de RMN y de UV-vis, así como sus numerosas contribuciones a la elaboración de este escrito.

Cristina Pérez Olmo

A Lucía

Table of contents

1. Introduction	1
2. Results and discussion	8
2.1. Carboxyester substituted ligands $\text{Tp}^{\text{C(O)OR,Me}}$	9
2.1.1. Potassium hydrotris(3-carboxyethyl-5-methyl)pyrazolylborate $\text{KTp}^{\text{C(O)OEt,Me}}$	10
2.1.2. Dihydrobis(3-carboxyalkyl-5-methyl)pyrazolylborates $\text{Bp}^{\text{C(O)OR,Me}}$	11
2.1.3. Bisdihydrobis(3-carboxyalkyl-5-methyl)pyrazolylborate zinc complexes $(\text{Bp}^{\text{C(O)OR,Me}})_2\text{Zn}$	13
2.1.4. Modifications: hydrolysis and heteroscorpionates	15
2.2. Pyridyl substituted ligands $\text{Tp}^{4'\text{Py,Me}}$ and $\text{Tp}^{4'(6'\text{Me})\text{Py,Me}}$	18
2.2.1. Potassium hydrotris(3-(4'-pyridyl)-5-methyl)pyrazolylborate and potassium hydrotris(3-(4'-(6'-methyl)-pyridyl)-5-methyl)pyrazolylborate, $\text{KTp}^{4'\text{Py,Me}}$ and $\text{KTp}^{4'(6'\text{Me})\text{Py,Me}}$	19
2.2.2. Hydrotris(3-(4'-pyridyl)-5-methyl)pyrazolylborate zinc halides $\text{Tp}^{4'\text{Py,Me}}\text{Zn-Hal}$	21
2.2.3. Hydrotris(3-(4'-pyridyl)-5-methyl)pyrazolylborate zinc acetate $\text{Tp}^{4'\text{Py,Me}}\text{Zn-OC(O)CH}_3$ and nitrate $\text{Tp}^{4'\text{Py,Me}}\text{Zn-ONO}_2$	22
2.2.4. Hydrotris(3-(4'-pyridyl)-5-methyl)pyrazolylborate zinc aqua and methanol complexes, $[\text{Tp}^{4'\text{Py,Me}}\text{Zn}\cdot\text{OH}_2]\text{ClO}_4$ and $[\text{Tp}^{4'\text{Py,Me}}\text{Zn}\cdot\text{HOMe}]\text{ClO}_4$	24
2.2.5. Hydrotris(3-(4'-pyridyl)-5-methyl)pyrazolylborate zinc hydroxide $\text{Tp}^{4'\text{Py,Me}}\text{Zn-OH}$	27
2.2.6. Heterocumulene insertions	30
2.2.7. Brønsted base properties of $\text{Tp}^{4'\text{Py,Me}}\text{Zn-OH}$ 20	33
2.2.8. Hydrolytic properties of $\text{Tp}^{4'\text{Py,Me}}\text{Zn-OH}$ 20	35
2.2.9. Hydrolytic properties of $[\text{Tp}^{4'\text{Py,Me}}\text{Zn}\cdot\text{OH}_2]\text{ClO}_4$ 18	38
2.3. Carboxamide substituted ligands $\text{Tp}^{\text{C(O)NHR,Me}}$	49
2.3.1. Potassium hydrotris(3-phenylcarboxamide-5-methyl)pyrazolylborate $\text{KTp}^{\text{C(O)NHPH,Me}}$	52
2.3.2. Hydrotris(3-phenylcarboxamide-5-methyl)pyrazolylborate zinc complexes $\text{Tp}^{\text{C(O)NHPH,Me}}\text{Zn-X}$ (X = Cl, ONO_2 and OC(O)CH_3)	53
2.3.3. Bis(hydrotris(3-phenylcarboxamide-5-methyl)pyrazolylborate zinc hydroxide perchlorate $[(\text{Tp}^{\text{C(O)NHPH,Me}}\text{Zn})_2(\mu_2\text{-OH})]\text{ClO}_4$	54
3. Structure determinations.....	56
4. Experimental section.....	97
4.1. General.....	97
4.2. Syntheses	100
4.3. X-ray single crystal determinations	128
5. Summary	167
6. References	171
7. List of compounds	Brochure

List of Abbreviations

acac	acetylacetonate	NMR	nuclear magnetic
b	broad (IR), (NMR)		resonance
benzoylac	benzoylacetone	ONit	p-nitrophenolate
cal	Calculated	Ph	phenyl
dec	decompose	Py	pyridyl
DMSO	dimethyl sulphoxide		pyridine
d	duplet (NMR)	Pz	pyrazolyl
dd	double duplet	q	quartet (NMR)
δ	chemical shift	R	organic rest
Et	ethyl	s	singlet (NMR)
Fig	figure		strong (IR)
Hz	Hertz	t	triplet (NMR)
int	intensity	<i>t</i> -Bu	terc-butyl
IR	infrared	THF	tetrahydrofurane
J	coupling constant	TNP	Tris(p-nitrophenyl)
L	ligand		phosphate
m	multiplet (NMR)	Tp	Tris(pyrazolyl)borate
	middle (IR)	vs	very strong (IR)
Me	methyl	ν	wave number
m. p.	melting point	w	weak (IR)

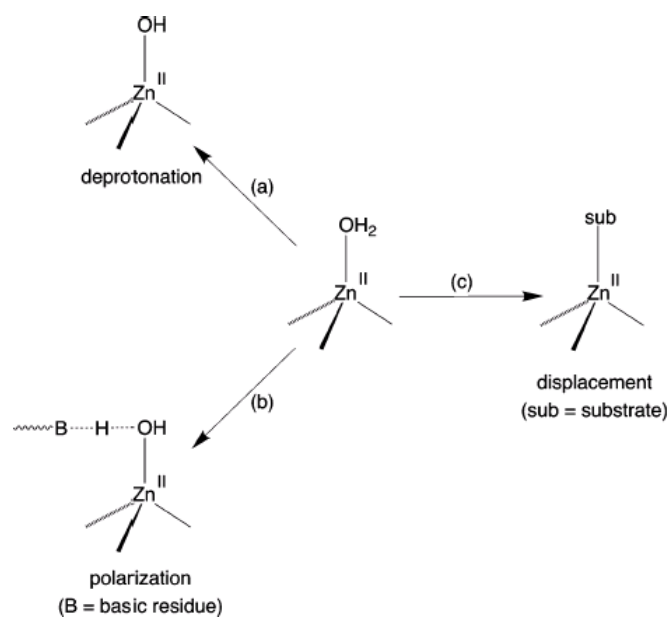
1. Introduction

Water is the most abundant biological molecule, constituting 65 % by weight of the human body, and plays essential roles in biological processes.¹

Water not only hydrates the surface of biological macromolecules, but is an essential component of their three-dimensional topology, which is responsible for a particular biological function. It prevents the oppositely charged moieties of biological macromolecules from aggregating and also plays a role in the entropic formation of the hydrophobic interactions which are of importance in the globular folding of proteins.² In globular proteins, the folding of the polypeptide chain is such that the amino acids with nonpolar side chains are assembled in the interior to form a hydrophobic core, whereas the amino acids with polar and charged side chains tend to be at the surface to interact with the aqueous media. This oil-drop-like distribution of hydrophilic and hydrophobic amino acids determines the ternary structure of a globular protein.

The secondary structure of a protein, α -helix and β -pleated sheet, is stabilized through hydrogen bonds between separated amino acids belonging to the same polypeptide chain. Often water molecules take part in this hydrogen bonding networks. In enzymes, this secondary structure decides which amino acid residues of the polypeptide chain will provide the cavity in which a biochemical reaction must occur.³

Also in the interior of the cavity, known as the “active site” of an enzyme, water molecules can be found to occupy specific locations. Thus, for most zinc-metalloenzymes known, the resting state of the active site can be generally represented by a tetrahedral Zn(II) ion attached to the protein backbone by three amino acid residues, with the fourth site being occupied by a catalytically important water ligand.⁴ This water is often hydrogen bonded to other residues in the cavity and/or to other water molecules. The mechanism of action of most zinc enzymes centers around the Zn-OH₂ function,^{4,5} which participates in the catalytic cycle by a variety of means, as illustrated in Scheme 1.1.^{4,6,7,8}



Scheme 1.1. Basic mechanisms of action of the Zn-OH₂ function in zinc enzymes.

Most commonly, the Lewis acidic Zn(II) center activates the coordinated water towards deprotonation, thereby generating zinc-bound hydroxide close to neutral pH, as shown in mechanism (a). This is the case of carbonic anhydrase (CA).

Mechanism (b) is displayed by carboxypeptidase A which incorporates an anionic glutamate residue at the active site avoiding the full deprotonation of the zinc-bound water molecule at neutral pH. For such situations, further activation is necessary for generating a zinc-bound hydroxide, and this is achieved by interaction with an adjacent protein glutamate basic residue.

Mechanism (c) involves complete displacement of the coordinated water to allow access of the substrate to the zinc center. This type of mechanism is exemplified by liver alcohol dehydrogenase, in which the coordinated water is displaced by an alcohol. Liver alcohol dehydrogenase (LADH) favors a displacement mechanism because the presence of two negative cysteinyl ligands inhibits deprotonation.

Our deduction from these studies should be that water is not just another component of the complex enzymatic structures. More important, water displays a determinant function in the biochemical processes catalyzed by such enzymes, and the regeneration of the zinc-bound water species in the aqueous living media should be investigated as a fundamental step of the catalytic cycle of zinc metalloenzymes.

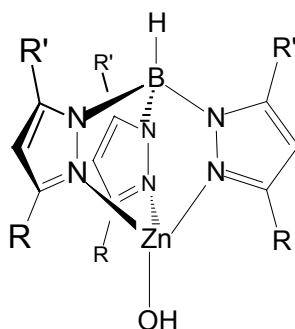
Thanks to the growing application of new spectroscopic and magnetic methods in enzymology, and to the dazzling progress in protein crystallography, structural details of the enzyme binding sites inconceivable a decade ago are nowadays well established. Thus, X-ray diffraction studies on a variety of forms of the human carbonic anhydrase II (HCAII) have demonstrated that the Zn(II) ion is coordinated to a water molecule, which is involved in a hydrogen-bonding network with Thr199, Glu106 and a second water molecule present in the active site.⁹ The function of the protein residues in the mechanism of biocatalyzed processes can also be clarified via site-specific mutagenesis. Parallel *in vitro* metal-substitution in zinc metalloenzymes helps to determine the constraints imposed by the zinc centre.¹⁰

In addition to the above mentioned advances in enzymology, bioinorganic chemistry has succeeded in determining reaction pathways using “synthetic analogues”. They are low molecular weight coordination compounds that mimic the structural and functional sites of the metalloenzymes, and are more amenable to structural, spectroscopic, and mechanistic studies than those.^{11,12} For example, in carbonic anhydrase (CA), the first enzyme recognized to contain zinc,^{13,14} and in the recently discovered matrix metalloproteinases^{15,16,17,18} (MMPs), catalytic zinc is placed in a nitrogen rich environment supported by three histidine imidazole residues, and one water molecule. Therefore, appropriate synthetic analogues need to be constructed using tridentate nitrogen donor ligands (N₃) that approach the tetrahedral geometry enforced by histidine residues around zinc in the enzyme.¹⁹

With this aim, various neutral tripodal ligands containing three imidazole donors have been synthesized^{20,21,22,23,24,25,26,27} but only one tetrahedral zinc hydroxide complex based on a sterically demanding tris(imidazolyl)phosphine could be structurally characterized.²⁸ More accurate structural models have been prepared with cavitant ligands which provide a hydrophobic core fitted with three zinc binding imidazolyl arms. For example, in 2001 Reinaud published an aqua model complex based on a tris(imidazolyl) calixarene ligand,^{29,30} and more recently, Riordan has characterized an aqua complex based on a tris(imidazolyl)benzene ligand.³¹ Other tripodal N₃-ligands, i.e. tris(pyrazolyl)methane and tris(pyridyl)methanol, were found not to support mononuclear tetrahedral zinc hydroxide or aqua complexes.^{32,33} In the case of macrocyclic triamines the absence of steric protection prevents the formation of

mononuclear zinc hydroxide complexes.^{34,35} However, various derivatives of macrocyclic triamines and tetraamines have been successfully used by Kimura to understand the intrinsic properties of substrate or inhibitor recognition by zinc at the active centers of carbonic anhydrase and carboxypeptidase.³⁶ Other systems that have been shown to exhibit a functional equivalence to carbonic anhydrase are exemplified by five-coordinate tris(benzimidazolyl)zinc aqua complexes.^{37,38,39}

But without doubt the best ligands for a biomimetic chemistry of zinc have been the famous tris(pyrazolyl)borates (Tp) introduced by S. Trofimenko.^{40,41,42} The development of a “second generation” of Tp ligands bearing bulky substituents (R) such as *t*Bu, Ph or Cum, on the 3-position of the pyrazoles afforded the first isolation of monomeric tetrahedral zinc hydroxide complexes of the type $\text{Tp}^{\text{R,R'}}\text{ZnOH}$,^{43,44,45,46,47,48} where R' can be H, Me or *t*Bu substituents in the 5-position of the pyrazoles.



$\text{Tp}^{\text{R,R'}}\text{ZnOH}$

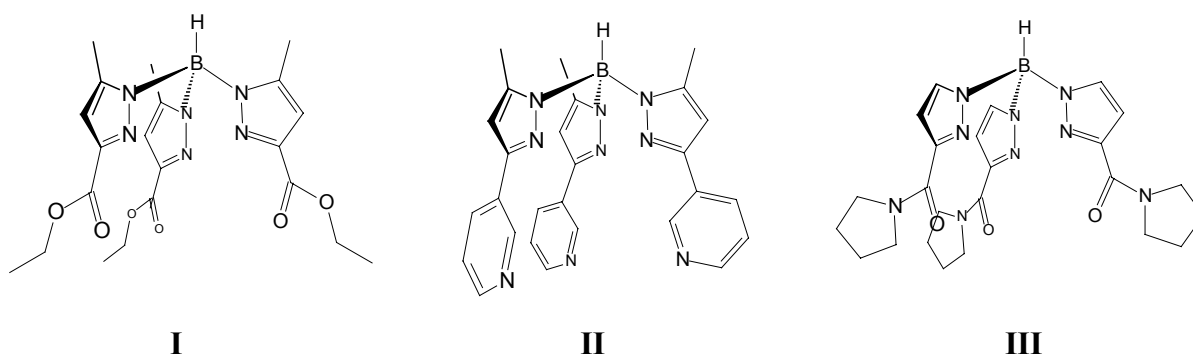
Our own group has contributed the “*Freiburg Enzyme Model*”⁴⁹ for a wide range of investigations on the modeling chemistry of zinc enzymes. Thus, the latest results about the solvolytic chemistry and basic properties of $\text{Tp}^{\text{R,R'}}\text{Zn}$ -alkoxides^{50,51,52} attempt to provide a better understanding of the alcohol dehydrogenation catalyzed by liver alcohol dehydrogenase (LADH) in living organisms and of the modeling of carbonic anhydrase (CA) studied with $\text{Tp}^{\text{R,R'}}\text{Zn}$ -hydroxides previously.^{44,47,53}

The Tp platform has succeeded in clarifying mechanistic details of many biotransformations catalyzed by zinc, but it has required extremely hydrophobic and water-free conditions. However, the catalytic activity of “biological zinc” can not only be understood as a result of hydrophobic effects but also of hydrophilic interactions of

the substrates with polar protein side chains and water molecules in the active site of the enzyme. Therefore, we and others are interested in the further development of the Tp ligands to provide a hydrophobic cavity within a hydrophilic system bearing H-bonding groups on the pyrazole rings and being soluble in aqueous solution.

First attempts to synthesize water soluble tripodal N₃-ligands were made by Kläui.⁵⁴ The insertion of an anionic sulfonate group on neutral tris(pyrazolyl)methane ligands allowed the isolation of zinc complexes very stable towards hydrolysis and soluble in polar solvents like wet methanol. Since these ligands do not always afford the desired N₃-coordination array around zinc,⁵⁵ Kläui has recently prepared the water soluble tris(2-isopropylimidazol-4(5)-yl)phosphane for a more appropriate biomimetic chemistry of zinc in aqueous solution.⁵⁶

In the case of Tp, the conditions required for the ligand synthesis, which will be described in detail in the following chapter, make the use of pyrazoles with functional substituents particularly difficult. Therefore, only few examples can be found in the literature where polar groups are attached to Tp systems to allow their solubility in protic solvents or water. These comprise the three types depicted below.



Ligand **I** was published by Carrano.⁵⁷ The H-bond accepting -C(O)OEt groups favour the stabilization of zinc-bound water molecules and the isolation of a binuclear hydroxo complex which was shown to catalyse self-transesterification in methanolic solution.⁵⁸ The zinc complexes of **I** are soluble in polar organic solvents but not in water.

Our group developed ligands of type **II** incorporating pyridyl substituents which could also act as H-bond accepting groups.⁵⁹ Yet, in zinc complexes of **II** one pyridyl nitrogen coordinates generally to a second zinc centre and dimeric species, partially stabilized through stacking interactions, are formed.⁶⁰ Thus, the pyridyl nitrogens act as lone pair electron donors for binding additional zinc ions, but not as H-bonding acceptors for increasing the solubility in protic solvents or water.

Ligand type **III** constitutes a third example of Tp ligand with H-bond acceptor properties. It was developed by Trofimenko and found to show a variety of coordination modes with lanthanide ions⁶¹. The H-bonding acceptor character of its ternary amides can be compared to that of the urea residues in Borovik's tris(2-aminoethyl)amine ligands.⁶² Additionally, the urea groups contain H-bonding donors which contribute to the stabilization of monomeric zinc complexes with terminal hydroxo ligands.⁶³

The work described in this thesis was intended to deal with several modifications of the above described Tp systems in order to increase their solubility in water.

First, appropriate conditions for the synthesis of $\text{Tp}^{\text{C(O)OR,Me}}$ ligands of type **I** should be determined. Zinc complexes of the resulting carboxyester substituted ligands should be isolated and used as starting materials for the synthesis of water soluble zinc species. Self-transesterification already reported to be catalysed in methanol by zinc complexes of **I** was hoped to be also observed in the presence of bulky alcohols. This would represent a novel procedure for the synthesis of sterically hindered $\text{Tp}^{\text{C(O)OR,Me}}\text{Zn}$ complexes.

Second, ligands of type **II** should be modified in order to place the pyridyl nitrogens in a more accessible position for H-bonding interactions with the solvent molecules. This was hoped to enhance their solubility in protic solvents and water. The coordination behaviour of the new pyridyl substituted ligands towards zinc was to be studied. A zinc hydroxo complex was hoped to be isolated and structurally characterized. Its reactivity as a Brønsted base and as a nucleophilic species for the cleavage of several substrates was to be investigated. A novel aqua complex was hoped to be structurally characterized and to perform catalytic hydrolyses in aqueous solution.

Third, the introduction of functional groups possessing both H-bond acceptor and donor properties would constitute an important advance in the evolution of Tp ligands.

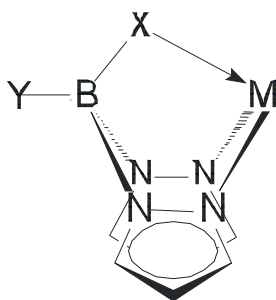
Therefore our target was the synthesis of Tp ligands incorporating secondary carboxyamides $-C(O)NHR$ able to build the desirable cavity around zinc. Zinc complexes of the novel carboxyamide substituted ligands were hoped to possess the desired hydrolytic activity.

The analytical methods employed for the investigations in this work were to be NMR, IR and UV-Vis spectroscopy as well as crystal X-Ray diffraction analysis. NMR and UV-Vis spectroscopy were to be used to follow the hydrolytic reactions. X-Ray diffraction analysis was to provide structural information about the coordination modes of the isolated ligands.

The ultimate aim of this work was to understand the importance of secondary interactions of hydrophilic nature in the catalytic activity of zinc metalloenzymes. Structural and functional models based on novel hydrophilic Tp systems were expected to contribute to this by making possible reactivity studies in aqueous solution.

2. Results and discussion

Poly(pyrazolyl)borates were first described by S. Trofimenko as boron-based chelating ligands of general formula $[XYB(pz)_2]^-$ which contain at least two pyrazolyl nitrogen donors (pz) for coordinating to a metal ion.⁶⁴ As shown below, a third substituent (X) on the tetrasubstituted boron ion (B) can be directed towards the metal (M) interacting with it in a wide variety of forms. This feature, which reminds the hunting habits of a scorpion, gave poly(pyrazolyl)borates the name of “scorpionates”.⁶⁵ In the case that X is identical to the bridging pyrazolyl groups, the ligand $[YB(pz)_3]^-$ acts as a N_3 -chelate of C_{3v} symmetry and receives the name of “homoscorpionate”. In the case that X and Y are both non-identical to the bridging pyrazolyl groups, the ligand receives the name of “heteroscorpionate”.



Scorpionates

The most relevant homoscorpionates in bioinorganic chemistry have been the hydrotris(pyrazol-1-yl)borates, $[HB(pz)_3]^-$, more commonly denoted as “Tp”.⁶⁶ They keep the metal ion in a N_3 -coordination core similar to that supported by three histidine imidazole residues in numerous metalloenzymes. The introduction in the late 1980s of the “second generation” ligands Tp^R bearing bulky substituents (R) on the 3-position of the pyrazole rings,⁶⁷ allowed the steric control of the structure and reactivity of the resulting $Tp^R M$ complexes. Moreover, the structure and function of a wide variety of zinc enzymes could be modeled with sterically hindered $Tp^{R,Me} Zn$ complexes (R = *t*Bu,

Ph, Cum, Tol).¹⁹ On one hand, the methyl groups in the 5-position of the pyrazoles contribute to the stabilization of the hydrolytically unstable B-N bond.⁶⁵ On the other hand, the bulky groups (R) in the 3-position form a pocket around zinc that prevents the formation of saturated $(\text{Tp}^{\text{R,Me}})_2\text{Zn}$ complexes and favors coordination to relevant biological substrates.^{68,69,70,71} In addition, aromatic substituents, i.e. Ph, Cum, Tol, provide a hydrophobicity to the pocket which is responsible for the zinc-bound water to be deprotonated near neutral pH and for the resulting zinc-bound hydroxide to be more nucleophilic.⁴⁹ The Tp platform has been therefore successfully applied to the biomimetic chemistry of zinc enzymes, nevertheless under extremely hydrophobic conditions in contrast to that required by the enzymes.

Attempting to develop $\text{Tp}^{\text{R,Me}}\text{Zn}$ complexes as functional models in aqueous solution, this work was aimed at the synthesis of Tp ligands incorporating novel polar substituents. The general synthesis of Tp ligands involves thermolysis of a mixture of a pyrazole and a borohydride salt, MBH_4 (M = K, Na or Li), either as a melt or in a high-boiling solvent.⁴² Since pyrazoles containing polar substituents such as nitro groups and carboxylic or sulfonic acid groups have been already reported to be incompatible with the borohydride ion,⁴² the selection of a suitably substituted pyrazole for the synthesis of polar Tp ligands seems to be nontrivial. Hence, our efforts were first focused on the use of Tp ligands with polar substituents already reported to be suitable for the synthesis described above, as precursors of water soluble species. Finally, the construction of a protecting pocket around zinc incorporating for the first time NH hydrogen donor groups was particularly successful.

The present chapter covers the synthesis and zinc coordination chemistry of three classes of polar Tp ligands in the following sections: **2.1**) Carboxyester substituted ligands $\text{Tp}^{\text{C(O)OR,Me}}$; **2.2**) Pyridyl substituted ligands $\text{Tp}^{4'\text{Py,Me}}$ and $\text{Tp}^{4'(6'\text{Me})\text{Py,Me}}$; and **2.3**) Carboxamide substituted ligands $\text{Tp}^{\text{C(O)NHR,Me}}$.

2.1. Carboxyester substituted ligands $\text{Tp}^{\text{C(O)OR,Me}}$

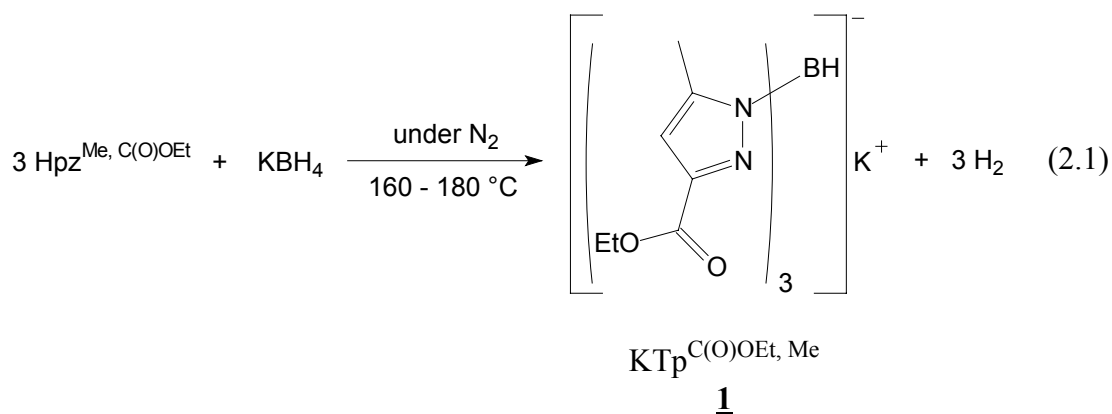
The vicinal oxygen chelate or VOC superfamily⁷² includes a big number of structurally related metalloenzymes which catalyze a very diverse set of reactions with unrelated transition states but a common mechanistic imperative. They all provide a

metal coordination environment with two or three open or readily accessible coordination sites to promote direct electrophilic participation of the metal ion in catalysis. The “open coordination sites” are occupied by labile water molecules that are stabilized by means of hydrogen bonding interactions with the protein residues in the active site. Good structural models for the labile water ligands ubiquitous to the VOC superfamily could be isolated by Carrano using the ester substituted ligand $\text{Tp}^{\text{C(O)OEt, Me}}$ (**I**).⁵⁷ Similarly to the protein backbone, **I** contains hydrogen bonding carbonyl groups which can be directed to the center of the metal binding cavity for helping in the stabilization of the water and hydroxide co-ligands.^{58,73}

This section presents the new ligands obtained from the already published synthesis of the homoscorpionate **I** with different carboxyester substituted pyrazoles of type $\text{Hpz}^{\text{Me, C(O)OR}}$. Some efforts for obtaining carboxyester substituted heteroscorpionates and water soluble systems are included.

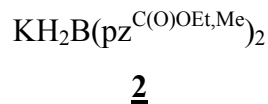
2.1.1. Potassium hydrotris(3-carboxyethyl-5-methyl)pyrazolylborate $\text{KTp}^{\text{C(O)OEt, Me}}$

Following the melting reaction already described by Carrano,⁵⁷ the potassium salt $\text{KTp}^{\text{C(O)OEt, Me}}$ **1** could be prepared as shown in equation 2.1.



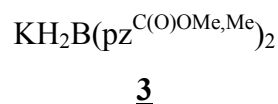
In agreement with that reported by Carrano,⁵⁷ **1** shows a characteristic IR B-H stretching vibration at 2523 cm^{-1} and the ^1H NMR resonances of the CH_3 and CH pyrazolyl protons at 2.41 and 6.28 ppm respectively. However, under the above described reaction conditions the published yield of 70 % could not be reproduced and **1** could be only isolated in 10 % yield by recrystallization from toluene at $-20 \text{ }^\circ\text{C}$. The rest was generally unreacted $\text{Hpz}^{\text{Me, C(O)OEt}}$ and, even more, a second product different to

1 was often found to be the major one in the melting reaction. It was isolated and identified by its ^1H NMR and IR spectra, detailed in section 2.1.2, as the bis(pyrazol-1-yl)borate **2**.



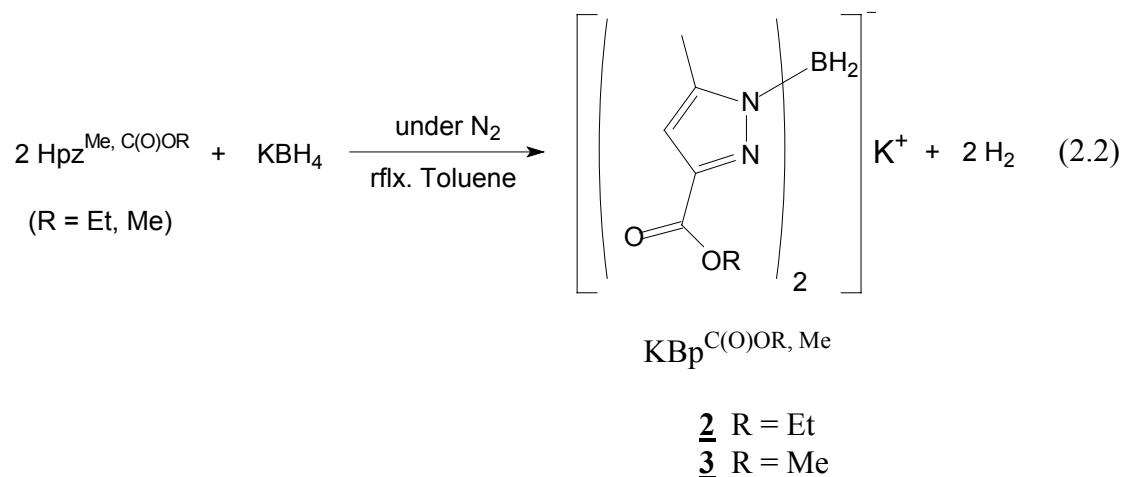
Numerous reactions under different conditions of temperature and stoichiometry were carried out in order to increase the yield of **1**. Unfortunately, the favoured product of the melting reaction was always found to be **2**. The same results were obtained from the reactions in high-boiling solvents such as toluene, 1,4-dioxane and anisole.

Further attempts to synthesize a carboxyester substituted Tp ligand in high yields were made with the methyl ester substituted $\text{Hpz}^{\text{Me,C(O)OMe}}$. The desired $\text{KTp}^{\text{C(O)OMe,Me}}$ could not be isolated, since the formation of the di-substitution product **3** was favoured again.



2.1.2. Dihydrobis(3-carboxyalkyl-5-methyl)pyrazolylborates $\text{Bp}^{\text{C(O)OR,Me}}$

In order to provide a complete characterization of the new ester substituted dihydrobis(pyrazol-1-yl)borates **2** and **3**, they were prepared in an appropriate manner.⁴² Thus, according to equation 2.2, $\text{Hpz}^{\text{Me,C(O)OR}}$ and KBH_4 were refluxed in anhydrous toluene to give $\text{KH}_2\text{B}(\text{pz}^{\text{C(O)OR,Me}})_2$, conventionally denoted as $\text{KBp}^{\text{C(O)OR,Me}}$.



While **2** could be separated from the solution by filtration in 85 % yield, **3** needed further purification by reaction with TlNO_3 in aqueous DMF. The thallium salt **4** precipitated immediately in the solution.



4

The most characteristic spectroscopic features of **2**, **3** and **4** are given in table 2.1. It is noteworthy that the two B-H vibration bands typical of Bp ligands and two different types of C=O groups can be detected in the IR spectra of the potassium salts **2** and **3**, but not in that of the thallium salt **4**.

Table 2.1. Selected IR vibrations (cm^{-1} , in KBr) and ^1H NMR proton resonances (ppm, in CDCl_3) of **2**, **3** and **4**.

	ν (B-H) (cm^{-1})	ν (C=O) (cm^{-1})	δ [$\text{CH}(\text{pz})$] (ppm)	δ [$\text{CH}_3(\text{pz})$] (ppm)
2	2451, 2424	1719, 1703	6.31	2.33
3	2446, 2402	1717, 1705	6.27	2.27
4	2444	1734	6.37	2.37

3 could be obtained as colourless crystals. As shown in figure 2.1, an X-ray structure determination revealed a polymeric structure and verified the existence of two types of carbonyl groups already observed in the IR spectrum of **3** (coordinating C=O and non-coordinating C=O oriented out of the cavity). By comparison of the IR spectra, it can be assumed that **2** may have the same polymeric structure as **3** in the solid state.

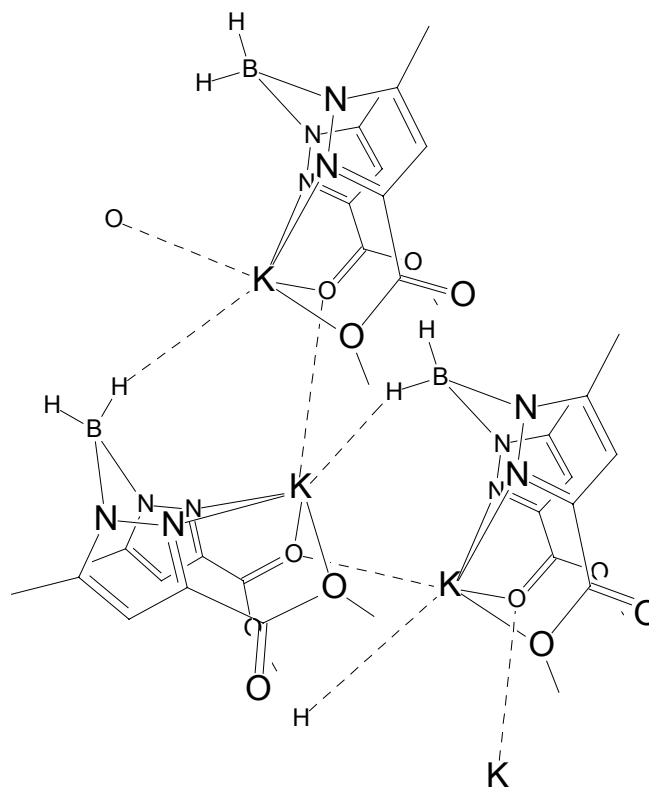
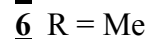
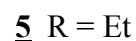
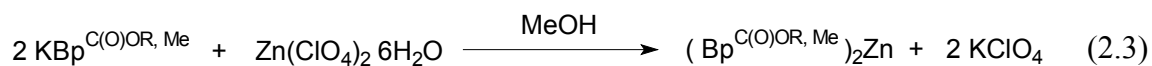


Figure 2.1. Schematic drawing of the polymeric structure of $\text{KBp}^{\text{C(O)OMe,Me}}$ **3**.

2.1.3. Bis-dihydrobis(3-carboxyalkyl-5-methyl)pyrazolylborate zinc complexes $(\text{Bp}^{\text{C(O)OR,Me}})_2\text{Zn}$

The coordination behaviour of the new $\text{Bp}^{\text{C(O)OR,Me}}$ ligands towards zinc was studied by reaction of **2** and **3** with several zinc salts. Thus, with zinc perchlorate the coordinatively saturated $(\text{Bp}^{\text{C(O)OR,Me}})_2\text{Zn}$ complexes **5** and **6** were obtained, as shown in equation 2.3.



The IR and ^1H NMR data of **5** and **6** are summarized in table 2.2 for a better comparison with those of the free ligands (Table 2.1). Thus, the IR B-H and C=O vibrations are found at higher wavenumbers and the ^1H NMR $\text{CH}(\text{pz})$ and $\text{CH}_3(\text{pz})$ resonances are shifted towards low field.

Table 2.2. Selected IR vibrations (cm^{-1} , in KBr) and ^1H NMR resonances (ppm, in CDCl_3) of **5** and **6**.

	ν (B-H) (cm^{-1})	ν (C=O) (cm^{-1})	δ [CH(pz)] (ppm)	δ [CH ₃ (pz)] (ppm)
5	2484, 2444	1731	6.47	2.44
6	2486, 2463	1738, 1716	6.53	2.47

The crystal structures of **5** and **6** confirmed that two $\text{Bp}^{\text{C(O)OR,Me}}$ are coordinating in a bidentate fashion to one zinc ion. As shown in figure 2.2, all ester carbonyls are pointed at the zinc ion, but only one is interacting with it. This interaction could be also detected as a weak C=O vibration band at 1716 cm^{-1} in the IR spectrum of **6**.

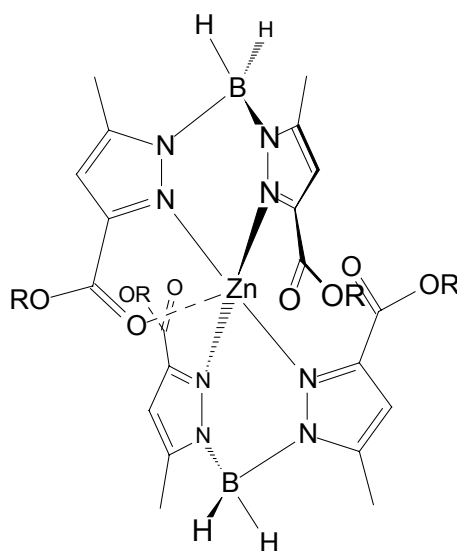


Figure 2.2. Schematic drawing of the structure of $(\text{Bp}^{\text{C(O)OR,Me}})_2\text{Zn}$ **5** (R = Et) and **6** (R = Me).

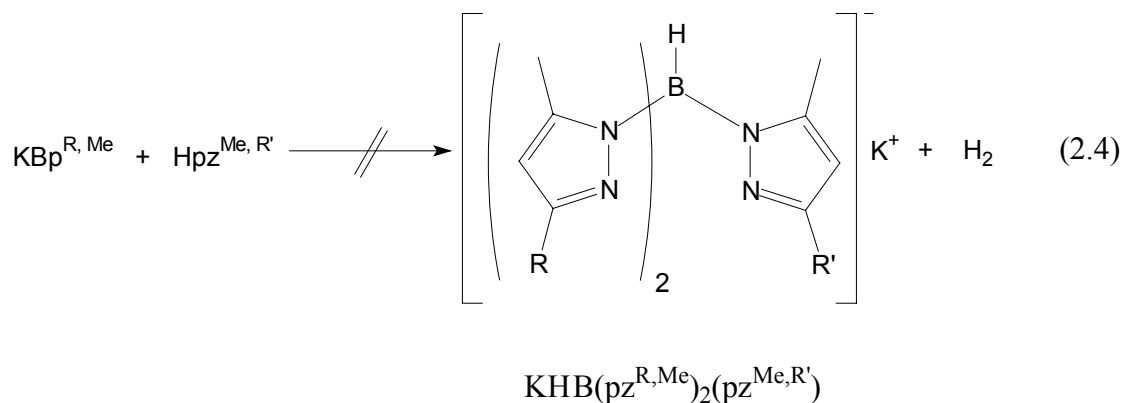
The reaction of $\text{KBp}^{\text{C(O)OEt,Me}}$ with zinc chloride in methanol also gave rise to the methyl ester substituted bis-ligand complex **6**, instead of the expected ethyl ester substituted complex **5**. Such a transesterification process has already been reported by Carrano to be catalysed by a binuclear zinc hydroxo complex of $\text{Tp}^{\text{C(O)OEt, Me}}$ in methanolic solution.⁵⁸

2.1.4. Modifications: hydrolysis and heteroscorpionates

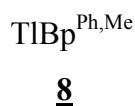
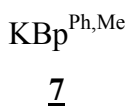
The ultimate aim of this work was to obtain water soluble ligands able to support zinc complexes appropriate for the functional modeling chemistry of zinc enzymes in aqueous solution. Keeping this in mind, the ester substituted compounds **1**, **2**, **3** and **4** were subjected to hydrolysis under mild conditions in order to prepare the corresponding carboxylic acid substituted compounds. Unfortunately, the B-N bond was cleaved first under the conditions required for the desired hydrolysis of the ester groups, being the carboxylic acid substituted pyrazole $\text{Hpz}^{\text{Me,C(O)OH}}$ the only product isolable from the reaction.

The ester substituted bis(pyrazol-1-yl)borates **2** and **3** were also tested as precursors of novel N_3 -heteroscorpionates. Asymmetric hydrotris(pyrazol-1-yl)borates or N_3 -heteroscorpionates of general formula $[\text{HB}(\text{pz})_2(\text{pz}^*)]^-$, where $\text{pz} \neq \text{pz}^*$, have already been obtained by reaction of a Bp ligand with one equivalent of a differently substituted pyrazole (pz^*) at high temperature.⁷⁴ Besides them, N_2O and, more rarely, N_2S -heteroscorpionates able to support monomeric tetrahedral zinc complexes relevant to the modeling of carboxypeptidase B, thermolysin, peptide deformylase, T7 lysozyme and cobalamin methionine synthase, have been synthesized by insertion of CO_2 and Ph_2CS respectively into the B-H bond of several $\text{Bp}^{\text{R,R'}}\text{Zn}$ -halides.^{75,76,77} Furthermore, our group has recently succeeded in the synthesis of a series of novel N_2S -heteroscorpionate ligands making use of the thermolysis reaction of unsubstituted KTp in the presence of different thioimidazoles.⁷⁸

In the present work, various dihydrobis(pyrazol-1-yl)borates ($\text{Bp}^{\text{R,Me}}$), including **2** and **3**, have been reacted with different pyrazoles ($\text{Hpz}^{\text{Me,R'}}$) according to equation 2.4, in order to synthesize ester substituted heteroscorpionates of formula $[\text{HB}(\text{pz}^{\text{R,Me}})_2(\text{pz}^{\text{Me,R'}})]^-$. However, none of all the possibilities for the reaction depicted below, either under melting conditions or in solution, was found to give rise to a carboxyester substituted N_3 -heteroscorpionate.



The starting materials, $\text{KBp}^{\text{R, Me}}$ and $\text{Hpz}^{\text{Me, R}'}$, were synthesized as described in the literature except of $\text{KBp}^{\text{Ph, Me}}$, for which no synthesis could be found. However, $\text{KBp}^{\text{Ph, Me}}$ **7** could be easily prepared under melting conditions and purified by metathesis with TlNO_3 in aqueous THF as the thallium salt **8**.



While the $\text{Tp}^{\text{Ph, Me}}\text{Zn}$ complexes have been intensively studied in the last years, no zinc chemistry of $\text{Bp}^{\text{Ph, Me}}$ has been described before. Therefore, **7** was reacted with several zinc salts. Thus, with zinc salts of poorly coordinating counter ions, i.e. perchlorate, sulfate, the bis-ligand complex $(\text{Bp}^{\text{Ph, Me}})_2\text{Zn}$ **9** always resulted, while with a zinc salt of a strongly coordinating counter ion such as chloride, the expected zinc chloride complex **10** was isolated in crystalline form. As shown in figure 2.3, the structure determination of **10** reveals that a methanol molecule is also coordinating to zinc.

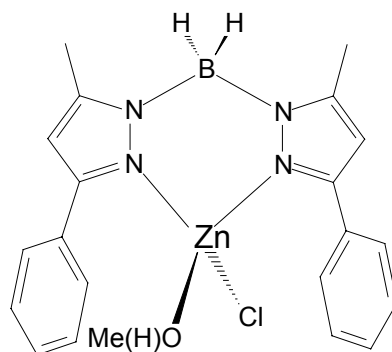


Figure 2.3. Schematic drawing of the structure of $(\text{Bp}^{\text{Ph,Me}})\text{Zn}(\text{Cl})(\text{MeOH})$ **10**.

The spectroscopic data of **7**, **8**, **9** and **10** can be compared to those of $\text{KTp}^{\text{Ph,Me}}$ in table 2.3. Just like for any bis(pyrazol-1-yl)borate, the IR B-H vibrations and the ^1H NMR resonances of **7** are at lower wavenumbers and lower field than those of its homologue tris(pyrazol-1-yl)borate $\text{KTp}^{\text{Ph,Me}}$. A characteristic feature of bis(pyrazol-1-yl)borates is also the complex B-H stretching pattern observed in the IR spectra of **7**, **8**, **9** and **10**.^{79,80,81} The ^1H NMR spectrum of **10** suggests that it may undergo spontaneous decomposition in deuterated chloroform.

Table 2.3. Selected IR vibrations (cm^{-1} , in KBr) and ^1H NMR proton resonances (ppm) of $\text{KTp}^{\text{Ph,Me}}$ (in CDCl_3), **7** (in d^4 -MeOD), **8** (in d^6 -DMSO), **9** (in CDCl_3) and **10** (in CDCl_3).

	ν (B-H) (cm^{-1})	δ [$\text{CH}(\text{pz})$] (ppm)	δ [$\text{CH}_3(\text{pz})$] (ppm)
$\text{KTp}^{\text{Ph,Me}}$	2525	6.26	2.31
7	2430, 2378, 2301, 2269	6.11	2.06
8	2440, 2389, 2290, 2244, 2203	6.22	2.33
9	2477, 2435	5.92	2.23
10	2473, 2390, 2336, 2280	6.16, 5.92	2.45, 2.23

2.2. Pyridyl substituted ligands $\text{Tp}^{4'\text{Py,Me}}$ and $\text{Tp}^{4'(6'\text{Me})\text{Py,Me}}$

It is well known that the structure and reactivity of Tp based model complexes $\text{Tp}^{\text{R,Me}}\text{Zn}$ can be not only sterically influenced by the bulky substituents (R) in the 3-position of the pyrazoles, but also electronically, as already shown by the hydrophobic effect of the aromatic rings on the nucleophilicity of $\text{Tp}^{\text{Cum,Me}}\text{ZnOH}$. Despite its importance, only few papers dealing with the electronic effect of functional groups attached to Tp can be found in the literature, that of Carrano on the carboxyester substituted system $\text{Tp}^{\text{C(O)OEt,Me}}$ being the latest example.

First efforts in this field were made by Graham, who prepared Tp ligands bearing electron withdrawing substituents such as perfluoromethyl groups.⁸² Later, Dias showed that the fluoroalkyl substituents exhibit donor qualities toward the metal ion buried into the cavity as well as toward external metals.⁸³ Ward prepared Tp ligands with 2'-pyridyl substituents in the 3-position of the pyrazoles, which were shown to act as perfect tripods encapsulating lanthanide(III) and actinide(III) ions.⁸⁴ With first-row transition metal dications, however, the ligand was shown to act no longer as an encapsulating tripod, since each bidentate pyrazolyl arm coordinates to a different metal ion generating tetrameric complexes of type $(\text{M}_4\text{L}_4)^{4+}$.⁸⁵ In order to avoid this, our group prepared Tp ligands with 3'-pyridyl substituents in the 3-position of the pyrazoles.⁵⁹ Tripodal $\text{Tp}^{3'\text{Py,Me}}\text{Zn}$ complexes relevant to the modeling of oligomeric zinc enzymes such as phospholipase C, alkaline phosphatase and P1 nuclease could be isolated.^{86, 87} Furthermore, a labile substrate such as H_3O_2^- could be stabilized through intermolecular interactions of hydrophilic nature with the pyridyl nitrogens and the solvent molecules.⁸⁷ Lately, Ward has isolated the potassium and thallium salts of the monosubstituted hydro-tris(3-(4'-pyridyl)pyrazol-1-yl)borate $\text{Tp}^{4'\text{Py}}$.⁸⁸

Now, we have considered it necessary to further exploit the ability of pyridyl substituted Tp ligands to become involved in hydrogen bonding interactions with the solvent molecules in order to reach the desired solubility in water. Thus, in an effort to place the pyridyl nitrogens in a more accessible position for the solvent molecules, the new 4'-pyridyl substituted ligands $\text{Tp}^{4'\text{Py,Me}}$ and $\text{Tp}^{4'(6'\text{Me})\text{Py,Me}}$ have been prepared.

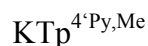
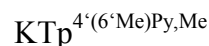
The following section 2.2.1 covers the synthesis of the new ligands $\text{Tp}^{4'\text{Py,Me}}$ and $\text{Tp}^{4'(6'\text{Me})\text{Py,Me}}$. The versatile coordination behaviour of $\text{Tp}^{4'\text{Py,Me}}$ towards zinc is revealed

in several zinc complexes described in sections 2.2.2 and 2.2.3. The ability of $\text{Tp}^{4\text{Py,Me}}$ to stabilize zinc coordination to small neutral co-ligands is demonstrated in the novel complexes $[\text{Tp}^{4\text{Py,Me}}\text{Zn}\cdot\text{OH}_2]\text{ClO}_4$ and $[\text{Tp}^{4\text{Py,Me}}\text{Zn}\cdot\text{HOME}]\text{ClO}_4$ described in section 2.2.4. A $\text{Tp}^{4\text{Py,Me}}\text{ZnOH}$ complex is used as Brønsted base and nucleophilic species in order to model various enzymatic reactions. Finally, the catalytic activity of the aqua complex $[\text{Tp}^{4\text{Py,Me}}\text{Zn}\cdot\text{OH}_2]\cdot\text{ClO}_4$ in several hydrolytic cleavages is studied.

2.2.1. Potassium hydrotris(3-(4'-pyridyl)-5-methyl)pyrazolylborate and potassium hydrotris(3-(4'-(6'-methyl)-pyridyl)-5-methyl)pyrazolylborate, $\text{KTp}^{4\text{Py,Me}}$ and $\text{KTp}^{4(6\text{Me})\text{Py,Me}}$

The syntheses of $\text{KTp}^{4\text{Py,Me}}$ **11** and $\text{KTp}^{4(6\text{Me})\text{Py,Me}}$ **12** followed well established literature procedures.⁵⁹ The β -diketones 4'-pyridyl-butan-2,4-dione and 4'-(6'-methyl)-pyridyl-butan-2,4-dione were synthesized by the Claisen acylation of acetone with ethyl isonicotinate and ethyl 2-methylisonicotinate respectively.⁸⁹ Ethyl isonicotinate was commercially available but ethyl 2-methylisonicotinate had to be prepared following a two step synthesis described in literature.⁹⁰ First, permanganate oxidation of 2,4-lutidine followed by acidification with sulphuric acid gave a mixture of methylpyridinecarboxylic acids. Second, HCl-catalysed esterification of this mixture in ethanol under water-free conditions gave ethyl 4-methyl-2-pyridinecarboxylate and the desired ethyl 2-methylisonicotinate, which could be separated by fractional distillation in a Vigreux column.

After recrystallization from petroleum ether, the β -diketones were reacted with hydrazine hydrate, as described by Gough and King,⁹¹ to obtain the pyrazoles $\text{Hpz}^{\text{Me,4Py}}$ and $\text{Hpz}^{\text{Me,4(6Me)Py}}$. They precipitated from the reaction solutions as crystalline powders and, in contrast to that required for the synthesis of 3'-pyridyl substituted Tp ligands,⁹² they were used without further purification in the melting reaction. Thus, $\text{KTp}^{4\text{Py,Me}}$ **11** and $\text{KTp}^{4(6\text{Me})\text{Py,Me}}$ **12** could be obtained in 50 and 40 % yield respectively. It is to note that, in order to improve the yields, an excess of the pyrazole (4:1 molar ratio of pyrazole to KBH_4) was always used and the melting mixture was kept at 200 °C for three hours, even though a strong hydrogen evolution was already observed at 160 °C.

**11****12**

11 and **12** are insoluble in non-polar solvents such as diethyl ether and toluene, as well as in chloroform, but soluble in polar solvents such as DMSO, acetonitrile and methanol. Their solubility in water was tested in comparison to their analogues $\text{KTp}^{3\text{'Py,Me}}$ and $\text{KTp}^{3\text{'(6'Me)Py,Me}}$, being shown that all four pyridyl substituted Tp ligands are soluble in aqueous methanol but only the new $\text{KTp}^{4\text{'Py,Me}}$ (**11**) is soluble in water. A survey of the literature showed that $\text{KTp}^{4\text{'Py,Me}}$ represents the first example of water soluble Tp ligand able to build a hydrophobic cavity around zinc.

Selected IR and ^1H NMR data of **11** and **12** are summarized in table 2.4 for a better comparison with those of the zinc complexes described in the following sections. The most characteristic feature of **11** and **12** is the sharp B-H vibration band observed in their IR spectra.

Table 2.4. Selected IR vibrations (cm^{-1} , in KBr) and ^1H NMR proton resonances (ppm, in d^6 -DMSO) of **11** and **12**.

	$\nu(\text{B-H})$ (cm^{-1})	δ [$\text{CH}(\text{pz})$] (ppm)	δ [$\text{CH}_3(\text{pz})$] (ppm)
<u>11</u>	2446	6.44	2.02
<u>12</u>	2486	6.41	1.99

$\text{KTp}^{4\text{'Py,Me}}$ and $\text{KTp}^{4\text{'(6'Me)Py,Me}}$ could be crystallized from acetonitrile as large crystals, but only the crystal structure analysis of $\text{KTp}^{4\text{'Py,Me}}$ provided a reliable structural characterization. As shown in figure 2.4, $\text{KTp}^{4\text{'Py,Me}}$ is a coordination polymer, in which the potassium cation is six-coordinated to three nitrogens belonging to the same Tp ligand and to three other nitrogens belonging to the pyridine substituents of different neighbouring KTp units. No pyridyl nitrogen remains uncoordinated, since two pyridine rings are bridging KTp units inside one-dimensional chains and the third one is linking parallel chains to each other.

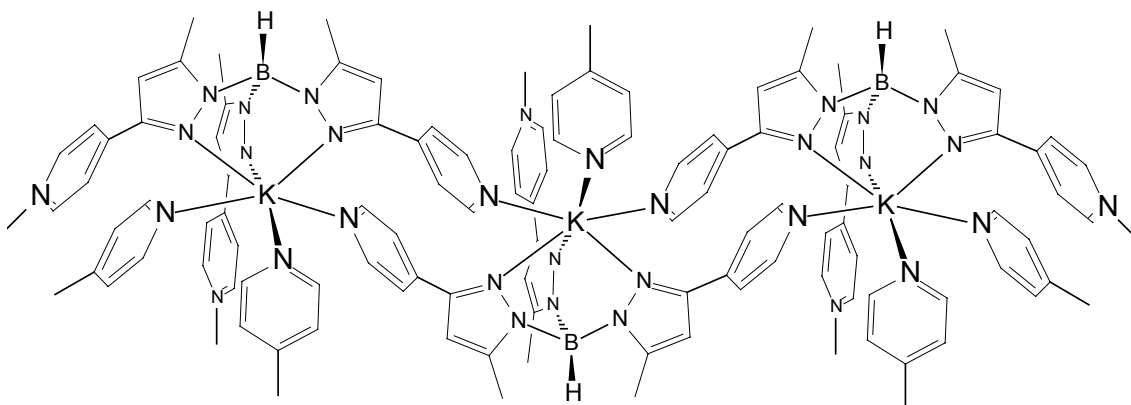


Figure 2.4. Schematic drawing of the polymeric structure of $\text{KTp}^{4\text{Py,Me}}$ **11**.

2.2.2. Hydrotris(3-(4'-pyridyl)-5-methyl)pyrazolylborate zinc halides $\text{Tp}^{4\text{Py,Me}}\text{Zn-Hal}$

The simplest ligand $\text{Tp}^{4\text{Py,Me}}$ was chosen to synthesize the halide complexes $\text{Tp}^{4\text{Py,Me}}\text{Zn-Hal}$, where Hal denotes Cl, Br and I in **13**, **14** and **15** respectively. They were prepared by the reaction of the potassium salt **11** with ZnCl_2 , ZnBr_2 or ZnI_2 in a methanol/dichloromethane solution. After filtration of precipitated KCl, KBr or KI and partial evaporation of the solvent, a colourless powder was deposited and spectroscopically identified as the desired product $\text{Tp}^{4\text{Py,Me}}\text{Zn-Hal}$.

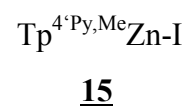
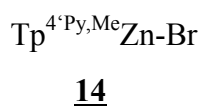
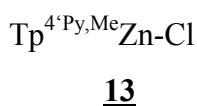


Table 2.5. Selected IR vibrations (cm^{-1} , in KBr) and ^1H NMR proton resonances (ppm, in $\text{d}^6\text{-DMSO}$) of **13**, **14** and **15**.

	$\nu(\text{B-H})$ (cm^{-1})	δ [$\text{CH}(\text{pz})$] (ppm)	δ [$\text{CH}_3(\text{pz})$] (ppm)
13	2553, 2496	6.65, 6.44	2.54, 2.02
14	2557, 2499	6.63, 6.46	2.53, 2.07
15	2557, 2491	6.63, 6.46	2.54, 2.00

As shown in table 2.5, two well separated B-H vibration bands can be observed in the IR spectra of **13**, **14** and **15**, one of higher energy at 2557 cm^{-1} coinciding with those found for $\text{Tp}^{3\text{Py,Me}}\text{Zn-Hal}$ complexes ($2551\text{-}2557 \text{ cm}^{-1}$),⁶⁰ and one of lower energy, but

still at 50 cm^{-1} higher wave number than that of $\text{KTp}^{4\text{'Py,Me}}$ (Table 2.4). The B-H vibration band of higher energy appears about 30 cm^{-1} higher than those of electron rich substituted $\text{Tp}^{\text{R,Me}}\text{Zn-Hal}$ complexes ($\text{R} = t\text{Bu, Cum}$), thereby giving an indication of a possible polar influence of the pyridyl substituents. The B-H vibration band of lower energy suggests the presence of a second type of Tp ligand with the negative charge more located on the BH function. A similar set of B-H vibrations has been reported before to be observed in the IR spectra of several $\text{Tp}^{\text{R,R'}}\text{M-X}$ complexes, in which Tp coordinates simultaneously in a tridentate and in a bidentate mode attending to steric demands of other ligands (X) attached to the metal ion.^{93, 94} Bidentate coordination of Tp towards zinc is very rare but not unprecedented, since in our group it has already been observed for $\text{Tp}^{\text{R,Me}}\text{Zn-amino acid complexes}$.^{95, 96}

Even though the $\text{Tp}^{4\text{'Py,Me}}\text{Zn-Hal}$ complexes **13**, **14** and **15** crystallized always as white needles inappropriate for a structure determination that could support their IR spectra, the structure of the potassium salt **11** (Figure 2.4) suggests that pyridyl coordination to neighbouring zinc ions could be strongly stabilized through stacking interactions between the aromatic rings causing the displacement of a pyrazolyl arm out of the coordination sphere of zinc. Accordingly, in the ^1H NMR spectra of **13**, **14** and **15** two well separated resonances for the protons $\text{CH}_3(\text{pz})$, $\text{CH}(\text{pz})$ and $\text{CHpy}(3',5')$ confirm the existence of chemically non-equivalent pyrazolyl arms. A similar set of resonances has already been observed in the ^1H NMR spectra of $\text{Tp}^{3\text{'Py,Me}}\text{ZnOH}$ in CDCl_3 at low temperatures,⁶⁰ and structurally demonstrated to be due to the ability of a pyridyl substituent of the Tp ligand to coordinate to a neighbouring $\text{Tp}^{3\text{'Py,Me}}\text{Zn}$ unit in order to form dimeric species.

2.2.3. Hydrotris(3-(4'-pyridyl)-5-methyl)pyrazolylborate zinc acetate $\text{Tp}^{4\text{'Py,Me}}\text{Zn-OC(O)CH}_3$ and nitrate $\text{Tp}^{4\text{'Py,Me}}\text{Zn-ONO}_2$

A critical step in the mechanism of action of carbonic anhydrase involves the formation of a bicarbonate intermediate,⁹⁷ the interaction between the metal center and the bicarbonate ligand playing an essential role in determining the efficiency of the catalytic cycle. While metal bicarbonate complexes are rare and specifically zinc bicarbonate complexes are unstable with respect to loss of CO_2 ,⁹⁸ several acetate and

nitrate complexes have been proposed to correlate with the coordination trend of analogous bicarbonate complexes.^{99, 100, 101}

Now, the new acetate and nitrate complexes, **16** and **17**, have been synthesized by direct addition of $\text{Zn}(\text{OAc})_2 \cdot 2\text{H}_2\text{O}$ and $\text{Zn}(\text{NO}_3)_2 \cdot 6\text{H}_2\text{O}$, respectively, to a solution of $\text{KTp}^{4\text{Py,Me}}$ in methanol/dichloromethane. Upon rapid evaporation of the solvent, powders were deposited and spectroscopically identified as the desired products.



16



17

Even though in the IR spectrum of **16** the antisymmetric C=O vibration band appears to overlap with that of the aromatic rings at 1608 cm^{-1} , the broad peak found at 1.51 ppm in its ^1H NMR, which is typically assigned to the methyl group of a zinc coordinated acetate ligand, is enough evidence for the formation of the acetate complex **16**. Additionally, the proton resonances of $\text{CH}(\text{pz})$ and $\text{CH}_3(\text{pz})$ (Table 2.6) are shifted to low field compared to those of the ligand **11** (Table 2.4). Regarding to **17**, its ^1H NMR spectrum in d^6 -DMSO resembles those of the halide complexes **13**, **14** and **15** (Table 2.5), in which two sets of proton resonances suggest the existence of chemically non-equivalent pyrazolyl arms.

Table 2.6. Selected IR vibrations (cm^{-1} , in KBr) and ^1H NMR proton resonances (ppm, in d^6 -DMSO) of **16** and **17**.

	$\nu(\text{B-H}) (\text{cm}^{-1})$	$\delta [\text{CH}(\text{pz})] (\text{ppm})$	$\delta [\text{CH}_3(\text{pz})] (\text{ppm})$
16	2558	6.64	2.56
17	2550	6.62, 6.45	2.55, 2.01

The already known tendency of a zinc coordinated acetate to be monodentate was confirmed in the monomeric structure of **16**, (See section 3.5). The hydrophilic character of the ligand system is also showed by the fact that a pyridyl nitrogen is hydrogen bound to a co-crystallized methanol molecule. In contrast to the monomeric structure of the acetate complex, the nitrate complex **17** consists of zigzag-shaped one-dimensional chains, as shown in figure 2.5. Thus, one pyridyl nitrogen is always involved in coordination to a neighbouring zinc ion, which is further coordinated by a bidentate nitrate ligand. It should be accepted that such a bidentate nitrate coordination

is favoured here in order to complete an approximately octahedral coordination sphere around zinc.¹⁰¹ According to the ^1H NMR spectrum of **17**, in which non-equivalent pyrazolyl arms can be clearly distinguished, oligomerization resulting from the coordination of one pyridyl nitrogen of each $\text{Tp}^{4\text{Py,Me}}$ ligand to a neighbouring $\text{Tp}^{4\text{Py,Me}}\text{Zn}$ unit must remain in solution. However, the fact that the intensity ratio between the peaks of both types of pyrazoles is not 2:1 (see section 4.2.16), leads us to suspect that a monomer-oligomer equilibrium, in which the monomeric form of **17** is favoured, must be occurring in solution.

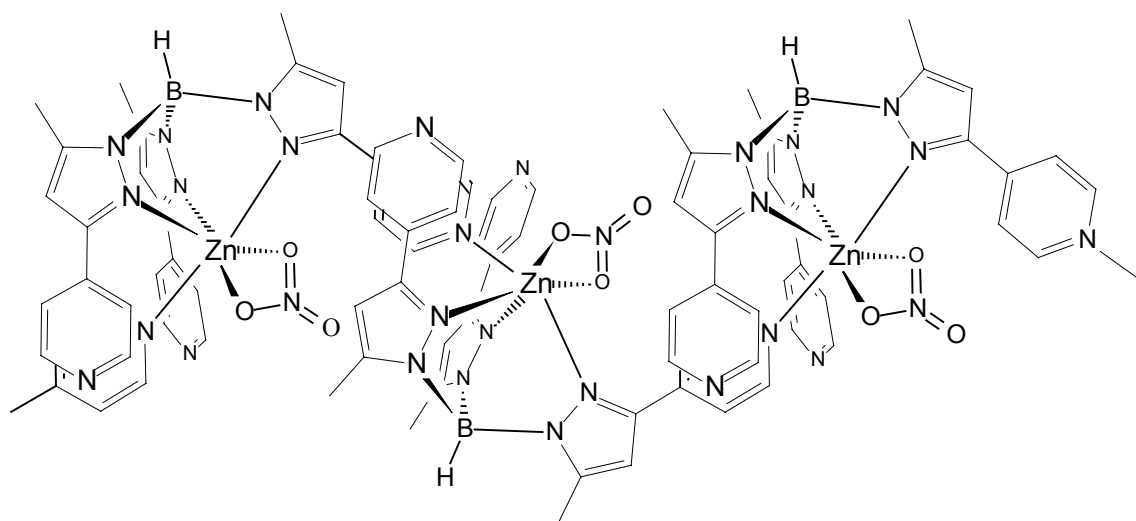
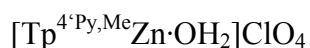
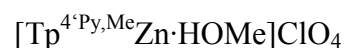


Figure 2.5. Schematic drawing of the polymeric structure of $\text{Tp}^{4\text{Py,Me}}\text{Zn-ONO}_2$ **17**.

2.2.4. Hydrotris(3-(4'-pyridyl)-5-methyl)pyrazolylborate zinc aqua and methanol complexes, $[\text{Tp}^{4\text{Py,Me}}\text{Zn}\cdot\text{OH}_2]\text{ClO}_4$ and $[\text{Tp}^{4\text{Py,Me}}\text{Zn}\cdot\text{HOMe}]\text{ClO}_4$

As already mentioned in chapter 1, the resting state of the active site of most zinc-metalloenzymes can be generally represented by a tetrahedral Zn(II) ion attached to the protein backbone by three amino acid residues, with the fourth site being occupied by a water molecule.⁴ In the case of liver alcohol dehydrogenase (LADH), the displacement of this water molecule to give a tetrahedral zinc-alcohol intermediate has been postulated to be a critical step in the mechanism of action of this enzyme (See scheme 1.1).¹⁰² Since only few examples of mononuclear tetrahedral zinc aqua and alcohol

complexes can be found in literature, it was attempted now to prepare the novel Tp based aqua and methanol complexes **18** and **19**. Prior attempts to synthesize a Tp based zinc aqua species by protonation of the corresponding hydroxo complex with protic reagents (HA) have always resulted in coordination of the counterion (A^-) to zinc or hydrolytic destruction of the Tp ligand,³⁷ except for $[Tp^{tBu,Me}ZnOH_2][HOB(C_6F_5)_3]$.¹⁰³

**18****19**

The aqua complex **18** was synthesized by the reaction of $KTp^{4Py,Me}$ with $Zn(ClO_4)\cdot 6H_2O$ in a dichloromethane/methanol/water mixture. Crystals of good quality for a X-ray analysis were deposited in the reaction solution at 5°C. The same reaction in the absence of water led to the rapid precipitation of a white powder, which could be spectroscopically identified as the methanol complex **19**. After several days, the remaining **19** still dissolved in the reaction solution was deposited as colourless crystals suitable for a structure determination.

In the IR spectra of **18** and **19** (Table 2.7), the B-H vibration band is found at higher wavenumber than that of $KTp^{4Py,Me}$ (Table 2.4), giving an indication of Tp coordination to zinc, and the strong absorption at 1093 and 1094 cm^{-1} , respectively, reveals the presence of a perchlorate counterion. Besides the broad O-H vibration band, at 3515 and 3428 cm^{-1} respectively, which is ascribed to water contained in the solid sample, an O-H vibration band at 3121 cm^{-1} for **18** and at 3572 cm^{-1} for **19** reveals the existence of either the water or the methanol complex. The low $\nu(O-H)$ stretching frequency belonging to the zinc bound water molecule in **18** leads us to suspect that it may be involved in strong H-bonding interactions. Previously, an O-H absorption at 3150 cm^{-1} in the IR spectrum of the pyrazolylbis(thioimidazolyl)borate zinc ethanol complex $\{[(pz^{Ph,Me})Bm^{o-An}]Zn\cdot HOEt\}\cdot (ClO_4)\cdot EtOH$ ¹⁰⁴ has been assigned to the zinc bound ethanol molecule, which is involved in strong H-bonding interactions with the solvent.

Similar to the observations for the halide and nitrate complexes described in sections 2.2.2 and 2.2.3, the ¹H NMR spectra of **18** and **19** in d^6 -DMSO show two sets of proton resonances belonging to chemically non-equivalent pyrazolyl groups. Therefore, the polymerisation by pyridyl coordination observed in the crystal structure of

$\text{Tp}^{4\text{Py,Me}}\text{Zn-ONO}_2$ (Figure 2.5) was to be expected for **18** and **19**. The $\text{CH}_3(\text{OMe})$ resonance of the zinc bound methanol appears at 3.34 ppm in the ^1H NMR spectrum of **19**. However, as already reported for previous $\text{Tp}^{\text{R,Me}}\text{Zn-aqua}^{87,105}$ and $\text{Tm}^{\text{R}}\text{Zn-alcohol}^{106}$ complexes, Tm^{R} denoting a tris(imidazolyl)borate ligand, the OH signal belonging to the aqua or methanol ligand could not be detected in the ^1H NMR spectrum of either **18** or **19**.

Table 2.7. Selected IR vibrations (cm^{-1} , in KBr) and ^1H NMR proton resonances (ppm, in d^6 -DMSO) of **18** and **19**.

	$\nu(\text{O-H})$ (cm^{-1})	$\nu(\text{B-H})$ (cm^{-1})	$\nu(\text{Cl=O})$ (cm^{-1})	δ [$\text{CH}(\text{pz})$] (ppm)	δ [$\text{CH}_3(\text{pz})$] (ppm)
18	3515, 3121	2567	1093	6.63, 6.46	2.55, 2.00
19	3572, 3428	2574	1094	6.62, 6.45	2.55, 2.01

The structure determinations of **18** and **19** confirmed that one pyridyl nitrogen of each $\text{Tp}^{4\text{Py,Me}}$ ligand coordinates to a neighbouring $\text{Tp}^{4\text{Py,Me}}\text{Zn}$ unit, thereby generating dimeric species (Figure 2.6) instead of polymeric chains, as in the case of **17** (Figure 2.5). A significant part of the force linking the two $\text{Tp}^{4\text{Py,Me}}\text{Zn}$ units comes from a stacking interaction between the two aromatic pyridine rings which connect two halves of the dimer across a center of symmetry. The zinc ion is five-coordinated in a slightly distorted trigonal-bipyramidal environment, the Zn-N(py) distances being much shorter than those found before for $\text{Tp}^{3\text{Py,Me}}\text{Zn-Hal}^{60}$. The axis of the trigonal bipyramid is defined by the zinc ion, the oxygen donor of the neutral aqua or methanol ligand and the nitrogen donor of a pyrazole. The distance to zinc of the pyrazole nitrogen in the axial position is much longer than that of the pyrazole nitrogens in the equatorial positions, but still in the range of those found before in the crystal structure of $(\text{Tp}^{3\text{Py,Me}}\text{Zn})_2(\text{O}_2\text{H}_3)\text{ClO}_4$ and $(\text{Tp}^{\text{Pic,Me}}\text{Zn})_2(\text{O}_2\text{H}_3)\text{ClO}_4^{87}$. The Zn-O distance of 2.17 Å in the aqua complex **18** is significantly longer than those found for the tetrahedral aqua complexes $[\text{Tp}^{t\text{Bu,Me}}\text{Zn}\cdot\text{OH}_2][\text{HOB}(\text{C}_6\text{F}_5)_3]^{103}$ (1.93 Å) and $[(\text{X}_6\text{R}_3\text{ImR}_3)\text{Zn}(\text{OH}_2)_2](\text{ClO}_4)_2^{30}$ (1.97 Å), ($\text{X}_6\text{R}_3\text{ImR}_3$) being a tris(imidazolyl)calixarene ligand, but in the range of those found for the recently reported trigonal pyramidal $[(\text{TriMIm})\text{Zn}\cdot\text{OH}_2]^{2+ 31}$ (2.13 Å) and for the trigonal bipyramidal $[(\text{tren})\text{Zn}\cdot\text{OH}_2](\text{ClO}_4)_2^{107}$ (2.12 Å).

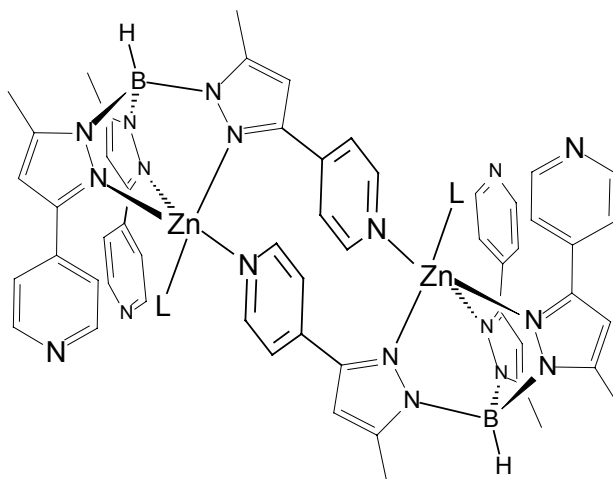


Figure 2.6. Schematic drawing of the dimeric structure of $[\text{Tp}^{4\text{-Py,Me}}\text{Zn}\cdot\text{L}]\text{ClO}_4$ ($\text{L} = \text{OH}_2$) **18** and ($\text{L} = \text{HOME}$) **19**. The two perchlorate counterions have been omitted for clarity.

A more detailed structural description of **18** and **19** will be given in chapter 3, but it is pertinent to note here that in **18** the zinc bound water molecule participates in an intermolecular H-bonding network in which the pyridine nitrogens and solvent molecules are also involved. Similarly, the zinc bound water ligand at the active site of carbonic anhydrase participates in a H-bonding network involving additional water molecules which mediate a proton shuttle to His-64, prior to proton transfer to the surroundings.¹⁰⁸

2.2.5. Hydrotris(3-(4'-pyridyl)-5-methyl)pyrazolylborate zinc hydroxide $\text{Tp}^{4\text{-Py,Me}}\text{Zn}\text{-OH}$

The modeling of hydrolytic zinc enzymes with Tp based zinc complexes involves the use of the corresponding $\text{TpZn}\text{-OH}$ species. Therefore, the preparation and use of the zinc hydroxo complex of $\text{Tp}^{4\text{-Py,Me}}$ was one of the main purposes of the synthesis of this ligand. Following our standard procedure for the preparation of $\text{Tp}^{\text{R,Me}}\text{Zn}\text{-OH}$ compounds,⁴⁷ $\text{KTp}^{4\text{-Py,Me}}$ was treated successively with $\text{Zn}(\text{ClO}_4)\cdot 6\text{H}_2\text{O}$ and an excess of KOH to obtain the hydroxo complex **20**. It is important to remember that the analogous pyridyl substituted complexes $\text{Tp}^{3\text{-Py,Me}}\text{Zn}\text{-OH}$ and $\text{Tp}^{3\text{-(6'-Me)Py,Me}}\text{Zn}\text{-OH}$ ⁶⁰ have been already reported to be not as inert as $\text{Tp}^{t\text{-Bu,Me}}\text{Zn}\text{-OH}$,⁴⁴ $\text{Tp}^{\text{Ph,Me}}\text{Zn}\text{-OH}$ ¹⁰⁹ or

$\text{Tp}^{\text{Cum,Me}}\text{Zn-OH}$,⁴⁷ but to share the thermal lability of the $\text{Tp}^{\text{R}}\text{Zn-OH}$ complexes without alkyl substituents in the 5 position of the pyrazoles toward dismutation into $(\text{Tp}^{\text{R}})_2\text{Zn}$ and Zn(OH)_2 .^{110,44} Therefore, in order to avoid thermal dismutation of **20** the temperature of the solution was carefully kept under 10°C during the reaction.



20

In the ¹H NMR spectrum of **20** in d⁶-DMSO, a pattern of resonances similar to that observed for the aqua and methanol complexes (Table 2.7) leads us to suspect that **20** may also exist as a dimer in solution (Figure 2.6). Specifically, the proton resonances of $\text{CH}_3(\text{pz})$, $\text{CH}(\text{pz})$ and $\text{CHpy}(2',6')$ are arranged in pairs at 2.55 / 2.01 ppm, 6.62 / 6.44 ppm and 8.73 / 8.41 ppm. A signal for the OH group could not be detected in the ¹H NMR spectrum of **20**, but the OH ligand could be identified by a sharp band at 3633 cm⁻¹ in the IR spectrum. The B-H band, at 2551 cm⁻¹, is found to be at 100 cm⁻¹ higher wave number than that of $\text{KTp}^{4\text{Py,Me}}$ (Table 2.4).

When the reaction of $\text{KTp}^{4\text{Py,Me}}$ with $\text{Zn(ClO}_4)_2 \cdot 6\text{H}_2\text{O}$ and KOH was carried out at room temperature, the ¹H NMR spectrum of the isolated product showed no obvious difference to that of **20** but, in addition to a B-H vibration at 2555 cm⁻¹, a broad B-H band centered at 2459 cm⁻¹ could be detected in the IR spectrum. If the solution was allowed to evaporate slowly at room temperature a white solid, which was identified as Zn(OH)_2 , precipitated indicating that partial dismutation of a hydroxo species into the bis(ligand) complex $(\text{Tp}^{4\text{Py,Me}})_2\text{Zn}$ and Zn(OH)_2 was occurring in the solution. Furthermore, after filtration of Zn(OH)_2 , colourless crystals of **21** suitable for a structure determination were deposited from the clear solution.



21

As shown in figure 2.7, **21** was revealed to consist of trimers in which a $(\text{Tp}^{4\text{Py,Me}})_2\text{Zn}$ complex, resulting from the partial dismutation of the zinc hydroxo complex **20**, is linked by two of its six pyrazolyl arms to two neighbouring $\text{Tp}^{4\text{Py,Me}}\text{Zn-OH}$ units. In contrast to the strong stacking interactions between bridging pyridyl rings that stabilize the dimeric structures of **18** and **19**, in **21** none of both bridging pyridyl

rings is interacting with any aromatic ring, but still strongly bound to the neighbouring zinc ion. Weak stacking interactions can however be assumed to exist between the pyridine and the pyrazole rings of the four remaining pyrazolyl arms of $(\text{Tp}^{4\text{Py,Me}})_2\text{Zn}$ as a result of the intertwining of both Tp ligands (See section 3.9). Regarding to the apical $\text{Tp}^{4\text{Py,Me}}\text{Zn-OH}$ units, a distance of 2.80 Å between a pyrazole nitrogen and zinc suggests the partial detachment of the Tp ligand from zinc as a consequence of the additional coordination of a neighbouring pyridine. The resulting highly unsymmetrical coordination environment around zinc could be described as trigonal bipyramidal with the roughly linear N(py)-Zn-N(pz) array involving the distant pyrazole nitrogen.

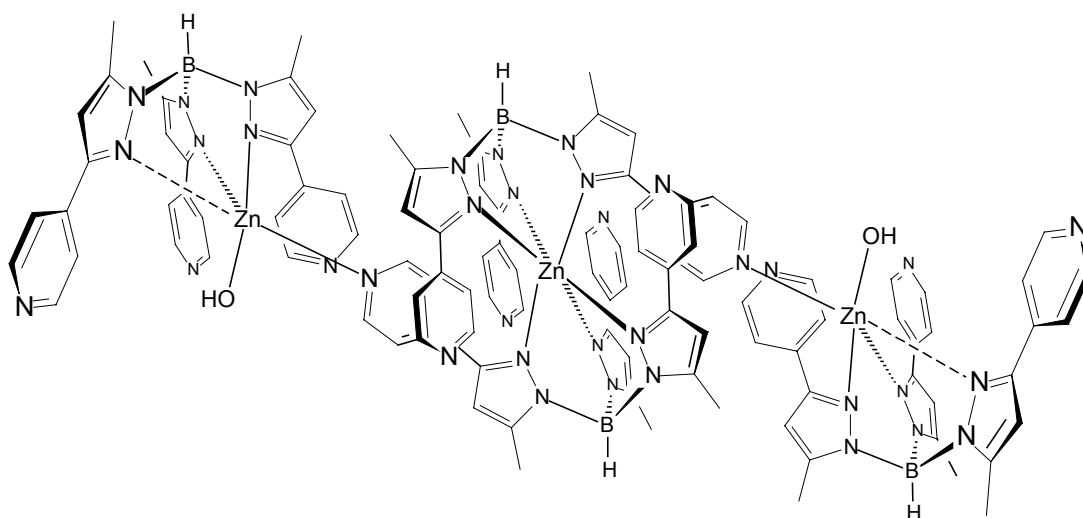


Figure 2.7. Trimeric structure of $[(\text{Tp}^{4\text{Py,Me}})_2\text{Zn}][\text{Tp}^{4\text{Py,Me}}\text{Zn-OH}]_2$ **21**.

The spectroscopic data support the crystal structure of **21**. Thus, in its IR spectrum the $\nu(\text{B-H})$ stretching frequency of the $(\text{Tp}^{4\text{Py,Me}})_2\text{Zn}$ entity, at 2555 cm^{-1} , is about 100 cm^{-1} higher than that belonging to the partially detached Tp ligand of the $\text{Tp}^{4\text{Py,Me}}\text{Zn-OH}$ units, at 2459 cm^{-1} . In the ^1H NMR spectrum of **21**, four signals can be found for each type of proton ($\text{CH}_3(\text{pz})$, $\text{CH}(\text{pz})$, $\text{CHpy}(3',5')$ and $\text{CHpy}(2',6')$). In the range for $\text{CH}(\text{pz})$, two singlets of identical intensity at 6.44 and 6.62 ppm belong to the $\text{CH}(\text{pz})$ protons of the $(\text{Tp}^{4\text{Py,Me}})_2\text{Zn}$ and $\text{Tp}^{4\text{Py,Me}}\text{Zn-OH}$ entities respectively. Additionally, two singlets of less intensity (one fourth of those at 6.44 and 6.62 ppm) are found at 6.55 and 6.70 ppm. The singlet at 6.55 ppm can be assigned to the $\text{CH}(\text{pz})$ protons of the bridging pyrazolyl groups of $(\text{Tp}^{4\text{Py,Me}})_2\text{Zn}$, and that at 6.70 ppm to those of the partially detached pyrazolyl groups of $\text{Tp}^{4\text{Py,Me}}\text{Zn-OH}$.

2.2.6. Heterocumulene insertions

The functional modeling of carbonic anhydrase (CA) has involved detailed structural and mechanistic analyses as well as theoretical calculations based on the insertion reactions of CO₂ and related heterocumulenes such as CS₂, isothiocyanates and isocyanates into the Zn-OH function of electron rich Tp^{R,Me}Zn-OH complexes.^{53,111} In this way, a four-centre mechanism in which the nucleophilic zinc bound OH is the leaving group and the transformation of CO₂ to bicarbonate proceeds via the bidentate to the monodentate attachment of the bicarbonate ligand could be well established for the carbonic anhydrase catalysed hydration of CO₂.⁴⁹

Besides this, studies on methanolic solutions of Tp^{R,Me}Zn-OH complexes have shown that the corresponding alkoxide Tp^{R,Me}Zn-OMe exists in the alcoholic solution as an equilibrium component in very small quantities.^{50,112} Additionally, some alkylation reactions with methyl iodide have demonstrated that Tp^{R,Me}Zn-alkoxides are stronger nucleophiles than the corresponding Tp^{R,Me}Zn-hydroxides.⁵⁰ Therefore, in the CO₂ insertion reactions with Tp^{R,Me}Zn-OH complexes in alcoholic solutions, in which a zinc bound alkyl carbonate Tp^{R,Me}Zn-OC(O)OR is produced, a Tp^{R,Me}Zn-OR intermediate is to be considered as the nucleophilic species attacking CO₂, despite its extremely low concentration in the Tp^{R,Me}Zn-OH/ROH mixture.

In our group, CO₂ insertions in the presence of water into a more polar system such as Tp^{3Py,Me}Zn-OH had already been found to lead to the methylcarbonate complex Tp^{3Py,Me}Zn-OC(O)OMe.¹¹³ In order to provide more information in this regard, insertion reactions of CO₂ and CS₂ into the Zn-OH function of the polar Tp^{4Py,Me}Zn-OH have been now carried out in the presence of water.

For this purpose, CO₂ was bubbled through a clear solution of the hydroxo complex **20** in dichloromethane/methanol/water. The temperature of the solution was carefully kept under 10°C in order to avoid the formation of the bis(ligand) complex (Tp^{4Py,Me})₂Zn and to improve the solubility of CO₂. Allowing the solution to stand over night at 5°C, the product **22** was precipitated in the form of colourless crystals.



In the IR spectrum, a broad band at 1607 cm^{-1} can be assigned to the asymmetric C=O vibration of the methylcarbonate ligand, according to the values observed previously for alkylcarbonate complexes.^{47,50} In contrast to the other zinc complexes of the polar $\text{Tp}^{4\text{Py,Me}}$ ligand, **22** was revealed to have a very good solubility in chloroform. In its ^1H NMR spectrum in CDCl_3 a singlet at 2.82 ppm can be assigned to the $\text{CH}_3(\text{OMe})$ protons of the methylcarbonate ligand by comparison with that found at 2.70 ppm for the homologous complex $\text{Tp}^{3\text{Py,Me}}\text{Zn-OC(O)OMe}$. Further spectroscopic details can be found in table 2.8, at the end of this section.

The existence of different types of pyrazoles in the zinc coordinated $\text{Tp}^{4\text{Py,Me}}$ ligand suggested by the ^1H NMR spectrum of **22** (Table 2.8) was confirmed by a crystal structure determination. Thus, as shown in figure 2.8, **22** consists of a methylcarbonate and a chloride complex strongly linked to each other through a pyridyl ring, similarly to the case of **21** (Figure 2.7). On one hand, the expected methylcarbonate complex $\text{Tp}^{4\text{Py,Me}}\text{Zn-OC(O)OMe}$ could be already predicted from the singlet at 2.82 ppm observed in the ^1H NMR spectrum of **22**. On the other hand, the unexpected chloride complex $\text{Tp}^{4\text{Py,Me}}\text{Zn-Cl}$ may be a result of the reaction between $\text{Tp}^{4\text{Py,Me}}\text{Zn-OH}$ and traces of HCl often found in dichloromethane. The pyridine coordination to neighbouring zinc ions commonly displayed by pyridyl substituted Tp systems is also taking place in **22**, this time generating one-dimensional chains instead of the dimers observed for the homologous complex $\text{Tp}^{3\text{Py,Me}}\text{Zn-OC(O)OMe}$.¹¹³

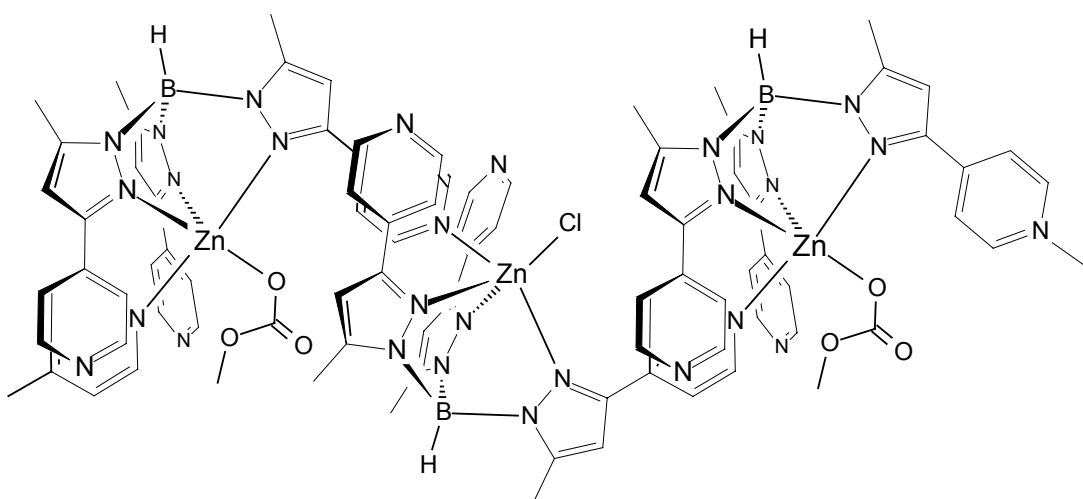
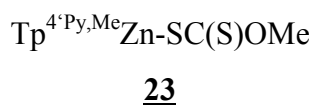


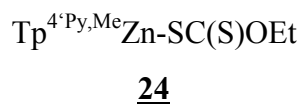
Figure 2.8. Polymeric structure of $[\text{Tp}^{4\text{Py,Me}}\text{Zn-OC(O)OMe}][\text{Tp}^{4\text{Py,Me}}\text{Zn-Cl}]$ **22**.

Keeping in mind that the insertion of heterocumulenes (CX_2) proceeds by an approach of the heteroatom (X) to zinc in order to bind CX_2 in a four-center intermediate, and considering that the sulphur atoms of CS_2 bind stronger to zinc than the oxygen atoms of CO_2 , the reaction of CS_2 with $Tp^{4Py,Me}Zn-OH$ in an alcoholic solution (ROH) to generate a xanthogenate complex $Tp^{4Py,Me}Zn-SC(S)OR$ could be expected to be easy. In fact, after stirring a mixture of the hydroxo complex **20** with an excess of CS_2 in a dichloromethane/methanol/water solution, the expected xanthogenate complex **23** was found to be the only product formed in the reaction.



As shown in table 2.8, a sharp vibration band at 1208 cm^{-1} in the IR spectrum of **23** can be assigned to the C=S bond, and a singlet at 3.17 ppm in its 1H NMR spectrum to the OMe group of the methylxanthogenate ligand. The latter is found to be at lower field than that of the methylcarbonate ligand of **22**, which appears at 2.82 ppm, but still at higher field than that of free methanol, typically found at 3.41 ppm. Furthermore, the $CH_3(OMe)$ proton resonances of **22** and **23** are at lower field than those found for $Tp^{R,Me}Zn-XC(X)OMe$ complexes of phenyl, cumenyl and *t*-butyl substituted Tp ligands, according to a less hydrophobic environment around the methylcarbonate/methylxanthogenate ligand in **22** and **23**.

When the reaction of the hydroxo complex **20** with CS_2 was performed in a dichloromethane/ethanol/water solution, the expected ethylxanthogenate complex **24** was obtained in quantitative yields. **24** could not be obtained in a pure form but it was characterized by IR and 1H -NMR.



In the 1H NMR spectrum of **24** the OEt group of the ethylxanthogenate ligand can be identified by a triplet and a quadruplet at 0.90 and 3.50 ppm respectively, shifted to high field compared to those of free ethanol, typically found at 1.19 and 3.59 ppm.

Table 2.8. Selected IR vibrations (cm^{-1} , in KBr) and ^1H NMR proton resonances (ppm, in CDCl_3) of **22** (OR = OMe), **23** (OR = OMe) and **24** (OR = OEt).

	$\nu(\text{B-H})$ (cm^{-1})	$\nu(\text{C=X})$ (cm^{-1})	δ [$\text{CH}(\text{pz})$] (ppm)	δ [$\text{CH}_2(\text{OR})$] (ppm)	δ [$\text{CH}_3(\text{OR})$] (ppm)	δ [$\text{CH}_3(\text{pz})$] (ppm)
22	2555	1699	6.30, 5.85	-	2.82	2.56, 2.50
23	2562	1207	6.30	-	3.17	2.59
24	2556	-	6.31	3.49	0.90	2.59

2.2.7. Brønsted base properties of $\text{Tp}^{4\text{Py,Me}}\text{Zn-OH}$ **20**

In section 2.2.6, the reactivity of alcoholic solutions of the hydroxo complex **20** in terms of heterocumulene insertions has been demonstrated. Now, the reactivity of **20** as a Brønsted base towards deprotonation of substances with acidic character, such as *p*-nitrophenol (HONit) and β -ketoalcohols ($\text{CH}_3\text{C}(\text{O})\text{CHC}(\text{OH})\text{R}$) is studied.

It has been already explained that the formation of an alkylcarbonate or alkylxanthogenate species like **22**, **23** or **24** is assumed to proceed via a simple alkoxide complex TpZn-OR ($\text{R} = \text{Me, Et}$), which is very labile toward hydrolysis and hence not isolable in the presence of water. However, very stable alkoxide complexes can be easily generated upon reaction of TpZn-OH with phenols and fluorinated alcohols.^{114, 115} For example, $\text{Tp}^{\text{R,Me}}\text{Zn-ONit}$ complexes have been obtained by the facile reaction of $\text{Tp}^{\text{R,Me}}\text{Zn-OH}$ with *p*-nitrophenol and have been revealed to be a powerful tool for the functional modeling of ester cleavage.¹¹⁶ Now, the new *p*-nitrophenolate complex **25** has been prepared by reaction of $\text{Tp}^{4\text{Py,Me}}\text{Zn-OH}$ with *p*-nitrophenol in methanol/dichloromethane/water.



25

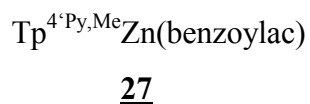
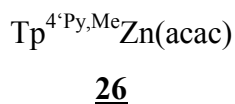
The *p*-nitrophenolate ligand of **25** was spectroscopically identified by two IR bands at 1584 and 1304 cm^{-1} , which correspond to the asymmetric and symmetric N=O vibrations of the nitro group, and by a ^1H NMR resonance at 5.88 ppm, which belongs to the $\text{CHph}(2,6)$ protons of its phenyl ring. The $\text{CHph}(3,5)$ resonance is found at 7.51 ppm, being overlapped with the $\text{CHpy}(3',5')$ resonance of the $\text{Tp}^{4\text{Py,Me}}$ ligand. The above described spectroscopic data are in accord with those reported before for the ONit

ligand of aromatically substituted $\text{Tp}^{\text{R,Me}}\text{Zn-ONit}$ complexes,¹¹⁴ while those of the $\text{Tp}^{4\text{Py,Me}}$ ligand, which are summarized in table 2.9 at the end of this section, are similar to those found for the xanthogenates **23** and **24** (Table 2.8).

Although no evidence of dimerization can be found in the IR and ^1H NMR spectra of **25**, it is not certain that it exists as a monomer in the solid state since a crystal structure determination is not available and, furthermore, the homologous $\text{Tp}^{3\text{Py,Me}}\text{Zn-ONit}$ has been reported to form dimeric species similar to **18** and **19**.⁹² However, the full spectroscopic characterization of **25** provides a very valuable information for the identification of the products resulting from the cleavage reactions studied in following sections.

TpZn -hydroxamate and TpZn -ketoalcoholate complexes have served as “*transition state analogues*” of zinc containing metalloproteases like collagenases and thermolysin, closely resembling the immediate environment of the zinc ion in the enzyme-inhibitor complex.¹¹⁷ These “*transition state analogues*” are significantly stabilized through the chelating attachment of hydroxamates and ketoalcoholates to zinc, enforcing pentacoordination around it even in zinc complexes of the highly sterically impeded $\text{Tp}^{\text{Cum,Me}}$ system.¹¹⁸

Such a chelating effect was expected to avoid the formation of dimeric species, typically stabilized for pyridyl substituted Tp systems, in the case of the new acetylacetonate and benzoylacetonate complexes, **26** and **27**. These β -ketoenolate complexes were easily prepared by the reaction of **20** with acetylacetone (MeC(O)CHC(OH)Me) and benzoylacetone (MeC(O)CHC(OH)Ph) respectively in a methanol/dichloromethane solution.



In the ^1H NMR spectra of **26** and **27** in CDCl_3 , the resonances of the β -ketoenolate ligands are typically high field shifted owing to the ring current effect of the $\text{Tp}^{4\text{Py,Me}}$ ligand. Specifically, the $\text{CH}_3(\text{MeC(O)})$ resonance is found at 1.14 and 1.13 ppm, and the $\text{CH}(\text{C(O)CHC(O)})$ resonance at 5.02 and 5.62 ppm, for **26** and **27** respectively. Other spectroscopic details concerning the $\text{Tp}^{4\text{Py,Me}}$ ligand have been summarized in table 2.9.

The structure determination of **27** revealed the chelating attachment of the benzoylacetone ligand, similar to that reported for other β -ketoenolates.^{118, 119} This impedes the further coordination of a neighbouring pyridine to zinc, and monomeric species are formed in the solid state, as shown in figure 2.9. The coordination geometry of zinc can be described as distorted square pyramidal and the ZnO_2C_3 chelate ring as virtually planar. From the spectroscopic data, the acetylacetonate ligand in **26** can be proposed to coordinate to zinc also in a chelating form generating monomeric species similar to benzoylacetone in **27**.

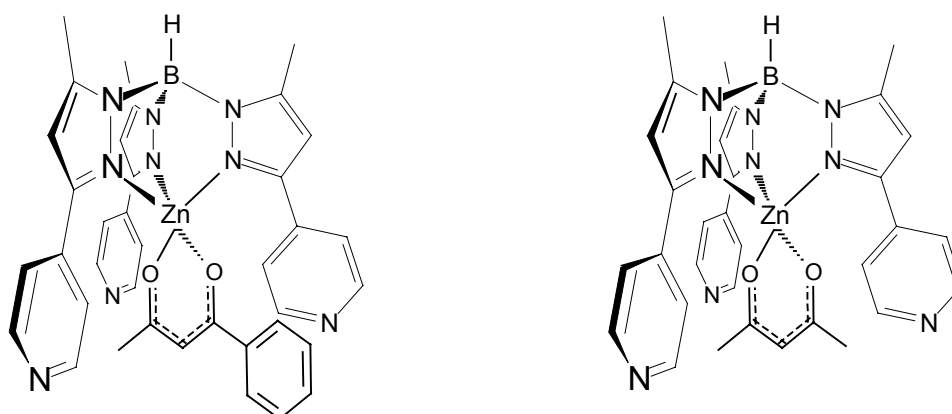


Figure 2.9. Schematic drawing of the structure of $\text{Tp}^{4\text{Py,Me}}\text{Zn}(\text{benzoylac})$ **27** (left), and of the proposed structure for $\text{Tp}^{4\text{Py,Me}}\text{Zn}(\text{acac})$ **26** (right).

Table 2.9. Selected IR vibrations (cm^{-1} , in KBr) and ^1H NMR proton resonances (ppm, in CDCl_3) of **25**, **26** and **27**.

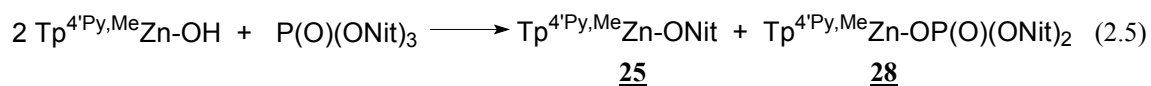
	$\nu(\text{B-H})$ (cm^{-1})	δ [$\text{CH}(\text{pz})$] (ppm)	δ [$\text{CH}_3(\text{pz})$] (ppm)
25	2559	6.43	2.62
26	2549	6.30	2.55
27	2549	6.31	2.57

2.2.8. Hydrolytic properties of $\text{Tp}^{4\text{Py,Me}}\text{Zn-OH}$ **20**

An extensive amount of work on the modeling of hydrolytic zinc enzymes by means of functionalised coordination compounds of zinc¹⁹ together with the underlying biochemical studies have contributed to establish that the active species in the cleavage reactions catalysed by hydrolytic zinc enzymes is a highly nucleophilic Zn-OH

function, which results from the deprotonation of a zinc bound water molecule at physiological pH. Our own group's contributions to this field include studies on $\text{Tp}^{\text{R,Me}}\text{Zn-OH}$ promoted cleavage of esters, amides, pyrocarbonates, organophosphates, pyrophosphates, sulfonatophosphates and nucleotide derivatives.⁴⁹ The work described in this section will be centered in the hydrolytic activity of the novel hydroxo complex $\text{Tp}^{4\text{Py,Me}}\text{Zn-OH}$ towards three activated substrates, namely tris(*p*-nitrophenyl)phosphate, P(O)(ONit)_3 , *p*-nitrophenylacetate, $\text{CH}_3\text{C(O)ONit}$, and trifluoroacetamide, $\text{CF}_3\text{C(O)NH}_2$, in another effort of functional modeling representative hydrolytic zinc enzymes such as alkaline phosphatase, carboxypeptidase A and, currently emerging as major targets for drug design, metallo β -lactamases and matrix metalloproteinases.^{120, 121, 122}

The P-O bond of the *p*-nitrophenyl and sugar substituted phosphotriesters has been already shown to undergo hydrolysis in the presence of $\text{Tp}^{\text{R,Me}}\text{Zn-OH}$ complexes.^{123, 68} Now, the ease of hydrolytic P-O cleavage of the highly activated tris(*p*-nitrophenyl)phosphate has once more been evidenced by the rapid reaction of one equivalent of P(O)(ONit)_3 with two equivalents of the hydroxo complex **20** in a methanol/dichloromethane mixture to produce one equivalent of the nitrophenolate complex **25**, which has been described in the previous section, and one equivalent of the new tris(*p*-nitrophenyl)phosphate complex **28**, as shown in equation 2.5. Even though the reaction solution turned yellow immediately indicating the prompt formation of **25**, the quantitative hydrolysis of P(O)(ONit)_3 needed two hours to be completed, and no further hydrolysis of the bis(*p*-nitrophenyl)phosphate complex **28** could be observed by prolonging the reaction time.



The products of hydrolysis could be easily separated and spectroscopically identified. The nitrophenolate complex **25** has already been described in section 2.2.7. The bis(*p*-nitrophenyl)phosphate complex **28** was also accessible by reaction of **20** with HOP(O)(ONit)_2 in a methanol/dichloromethane solution. Thus, after volatiles were removed and the raw product was washed with chloroform a light yellow powder, which could be spectroscopically identified as **28**, was obtained. In its ¹H NMR

lactams could be cleaved by means of electron rich $\text{Tp}^{\text{R,Me}}\text{Zn-OH}$ complexes.¹²⁶ In the present work, the reaction of the hydroxo complex **20** with $\text{CF}_3\text{C(O)NH}_2$ was hoped to give the corresponding hydrolysis products but, instead of that, the trifluoroacetamide complex **29** resulting from the deprotonation of the amide function was the only isolated product. Likewise, the corresponding trifluoroacetamide complex has been already found to be the only product of the reaction of $\text{CF}_3\text{C(O)NH}_2$ with several $\text{Tp}^{\text{R,Me}}\text{Zn-OH}$ complexes ($\text{R}=\text{Ph}$, Cum and $2'\text{Fu}$).^{126, 129}



29

Complex **29** is characterized by a B-H vibration at 2559 cm^{-1} and a C=O vibration at 1679 cm^{-1} , which is in the same range than those found for $\text{Tp}^{\text{Ph,Me}}\text{Zn-NHC(O)CF}_3$ ⁵² and $\text{Tp}^{2'\text{Fu,Me}}\text{Zn-NHC(O)CF}_3$,¹²⁹ at 1686 cm^{-1} and 1690 cm^{-1} respectively. Its NH proton gives rise to a NMR signal at 5.05 ppm in CDCl_3 , and the ^{19}F resonance of the CF_3 group occurs at -76.03 ppm . Crystals of **29** appropriate for a structure determination could not be grown.

2.2.9. Hydrolytic properties of $[\text{Tp}^{4\text{Py,Me}}\text{Zn}\cdot\text{OH}_2]\text{ClO}_4$ **18**

As shown in section 2.2.4, the novel aqua complex $[\text{Tp}^{4\text{Py,Me}}\text{Zn}\cdot\text{OH}_2]\text{ClO}_4$ has been revealed to possess remarkable structural similarities with the resting state of relevant zinc metalloenzymes, such as carbonic anhydrase II (CA II). Specifically, the Zn-O bond distance in $[\text{Tp}^{4\text{Py,Me}}\text{Zn}\cdot\text{OH}_2]\text{ClO}_4$ (2.17 \AA) is in the range of that found for the zinc bound water molecule in the active site of CA II crystallized at pH 6 (2.05 \AA). The latter is found to be strongly hydrogen bound to a threonine residue and to two water molecules, one of which is called “deep water” due to its very short distance from the zinc bound aqua ligand.⁹ Also this feature finds analogy in the intermolecular H-bonding network present in the crystal structure of $[\text{Tp}^{4\text{Py,Me}}\text{Zn}\cdot\text{OH}_2]\text{ClO}_4$, in which the zinc bound water molecule, the pyridine nitrogens of the $\text{Tp}^{4\text{Py,Me}}$ system and different solvent molecules are involved (See chapter 3).

Likewise, the molecular structure of Parkin’s mononuclear zinc aqua complex $[\text{Tp}^{t\text{Bu,Me}}\text{Zn}(\text{OH}_2)][\text{HOB}(\text{C}_6\text{F}_5)_3]$, which is accessible by protonation of $\text{Tp}^{t\text{Bu,Me}}\text{Zn-OH}$

using $(\text{C}_6\text{F}_5)_3\text{B}(\text{OH}_2)$ as an acid, reveals that this complex actually exists as a hydrogen-bonded ion pair, with a short $\text{O}\cdots\text{O}$ separation of 2.48 Å between the zinc bound water and the counterion $[\text{HOB}(\text{C}_6\text{F}_5)_3]^-$.¹⁰³ However, to our knowledge only one functional study on the reactivity of $[\text{Tp}^{t\text{Bu},\text{Me}}\text{Zn}(\text{OH}_2)][\text{HOB}(\text{C}_6\text{F}_5)_3]$ towards CO_2 in comparison with the structurally characterized $\text{Tp}^{t\text{Bu},\text{Me}}\text{Zn}-\text{OH}$ was undertaken in order to demonstrate that the catalytic hydration of CO_2 by carbonic anhydrase requires deprotonation of the coordinated water molecule.¹⁰⁵

More recently, the zinc aqua complex $[\text{Tp}^{\text{C}(\text{O})\text{OEt},\text{Me}}\text{Zn}\cdot(\text{OH}_2)_3]\text{ClO}_4$ could be stabilized through intramolecular hydrogen interactions between the carbonyl oxygens of the $\text{Tp}^{\text{C}(\text{O})\text{OEt},\text{Me}}$ ligand and the zinc bound water molecules, but no crystal structure was published.⁵⁸ These water molecules have been affirmed to be easily displaced by bidentate ligands such as amino acids, although no specific details of these reactivity studies have been provided to date.⁵⁷

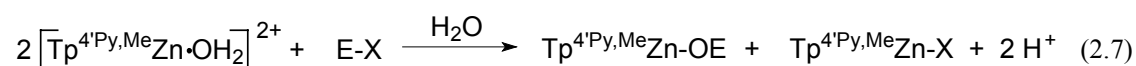
More interesting is the fact that the metal aqua complexes of the carboxyester substituted $\text{Tp}^{\text{C}(\text{O})\text{OEt},\text{Me}}$ ligand are very soluble in polar solvents such as methanol, although not in water. Now, polar zinc complexes could be also isolated with the water soluble $\text{Tp}^{4\text{Py},\text{Me}}$ ligand, providing a unique opportunity to study the TpZn chemistry under more natural conditions than those demanded by the hydrophobic *t*-butyl, phenyl and cumenyl substituted $\text{Tp}^{\text{R},\text{Me}}\text{Zn}-\text{OH}$ complexes, which however have afforded the most valuable information on the biological role of zinc. Thus, the solution studies on the reactivity of such hydrophobic complexes for the modeling of zinc containing hydrolytic enzymes have always been performed in nonaqueous solvents because the molecular species involved, such as $\text{Tp}^{\text{R},\text{Me}}\text{Zn}-\text{OH}$, are immiscible with water, and hence water cannot be introduced as a reagent. For this reason the reactions are stoichiometric rather than catalytic and there is no turnover involving the regeneration of the reactive species $\text{Tp}^{\text{R},\text{Me}}\text{Zn}-\text{OH}$.

The only example of functional studies with TpZn model complexes under relatively polar conditions are the kinetic studies on the hydrolytic cleavage of (2,3-isopropylidene-5-methyl-ribose)bis(*p*-nitrophenyl)phosphate by $\text{Tp}^{\text{Ph},\text{Me}}\text{Zn}-\text{OH}$, $\text{Tp}^{\text{Cum},\text{Me}}\text{Zn}-\text{OH}$, $\text{Tp}^{3\text{Py},\text{Me}}\text{Zn}-\text{OH}$ and $\text{Tp}^{\text{Pic},\text{Me}}\text{Zn}-\text{OH}$ in chloroform/acetonitrile mixtures, containing a maximum of 50 % acetonitrile.⁹² An enhancement of the reaction

rates is observed in 50 % acetonitrile, indicating that an increase in the polarity of the solution favours the formation of the polar intermediate to the final products. Much higher hydrolysis rates have been obtained, however, with other zinc model complexes which allow to carry out such reactivity studies in aqueous solution.¹³⁰

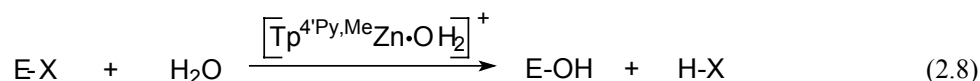
In the present work, $[\text{Tp}^{4\text{Py,Me}}\text{Zn}\cdot\text{OH}_2]\text{ClO}_4$ has been reacted with several phosphotriesters and carboxyesters in 25 % DMSO aqueous solutions, hoping to promote not only the stoichiometric but also the catalytic cleavage of the substrates.

On the one hand, if only stoichiometric amounts of substrate (E-X) were observed to be hydrolysed in the presence of $[\text{Tp}^{4\text{Py,Me}}\text{Zn}\cdot\text{OH}_2]\text{ClO}_4$, the reaction depicted in equation 2.7 could be proposed in accordance with that generally found in $\text{Tp}^{\text{R,Me}}\text{Zn}\cdot\text{OH}$ promoted hydrolyses.¹¹⁶ In this case, the products would bind strongly to the $\text{Tp}^{4\text{Py,Me}}\text{Zn}$ unit and $[\text{Tp}^{4\text{Py,Me}}\text{Zn}\cdot\text{OH}_2]\text{ClO}_4$ could not be regenerated.



E	X	SUBSTRATE
P(O)(OR) ₂	OR'	phosphotriester
RC(O)	OR'	carboxyester

On the other hand, if an excess of E-X was observed to be hydrolysed in the presence of only catalytic amounts of $[\text{Tp}^{4\text{Py,Me}}\text{Zn}\cdot\text{OH}_2]\text{ClO}_4$, it would mean that the aqua species is somehow regenerated for the further nucleophilic cleavage of substrate. In this case, the final products of hydrolysis would not bind to zinc and the reaction would occur catalytically (Equation 2.8).



With this in mind, the hydrolysis of several phosphotriesters and carboxyesters in the presence of firstly stoichiometric and secondly catalytic amounts of $[\text{Tp}^{4\text{Py,Me}}\text{Zn}\cdot\text{OH}_2]\text{ClO}_4$ was studied. For the stoichiometric reactions, two equivalents of the aqua complex **18** and one equivalent of the substrate were mixed in a NMR tube containing a d⁶-DMSO/D₂O (75:25) mixture. The reaction was monitored by ³¹P NMR

spectroscopy if the substrate was a phosphotriester, and by ^1H NMR spectroscopy if the substrate was a carboxyester. For the catalytic reactions, one equivalent of **18** and four equivalents of the substrate (unless otherwise noted) were mixed in d^6 -DMSO/ D_2O (75:25), and the reaction was monitored by ^1H NMR spectroscopy. In this case, a buffer was added to the reaction mixture in order to maintain the pH near 7. For every experiment, background hydrolysis in the absence of the aqua complex was also recorded. The hydrolyses of phosphotriesters and carboxyesters are discussed in sections 2.2.9.1 and 2.2.9.2 respectively.

2.2.9.1. Hydrolysis of phosphotriesters by **18**

The hydrolysis in the presence of stoichiometric amounts of **18** was studied for three phosphotriesters $\text{P}(\text{O})(\text{OR})_3$: triphenylphosphate $\text{P}(\text{O})(\text{OPh})_3$, tris(*o*-dichlorophenyl)phosphate $\text{P}(\text{O})(\text{oClPh})_3$ and tris(*p*-nitrophenyl)phosphate $\text{P}(\text{O})(\text{ONit})_3$.

In the case of triphenylphosphate, the resonance at -16.72 ppm belonging to $\text{P}(\text{O})(\text{OPh})_3$ did not change in time, and a new small one, which could be assigned to one of the three possible products of hydrolysis $(\text{OH})\text{P}(\text{O})(\text{OPh})_2$, $(\text{O}^-)\text{P}(\text{O})(\text{OPh})_2$ or $\text{Tp}^{4\text{Py,Me}}\text{Zn-OP}(\text{O})(\text{OPh})_2$, appeared at -11.95 ppm. According to ^{31}P NMR, only 5 % of $\text{P}(\text{O})(\text{OPh})_3$ was hydrolysed after 7 days.

In the case of tris(*o*-dichlorophenyl)phosphate, the resonance at -22.32 ppm belonging to $\text{P}(\text{O})(\text{oClPh})_3$ decreased with time, and a new one at -12.95 ppm, which could be assigned to one of the three possible products of hydrolysis $(\text{OH})\text{P}(\text{O})(\text{oClPh})_2$, $(\text{O}^-)\text{P}(\text{O})(\text{oClPh})_2$ or $\text{Tp}^{4\text{Py,Me}}\text{Zn-OP}(\text{O})(\text{oClPh})_2$, increased with time. According to ^{31}P NMR, 90 % of $\text{P}(\text{O})(\text{oClPh})_3$ was hydrolysed after 6 days.

In the case of tris(*p*-nitrophenyl)phosphate, the resonance at -20.00 ppm belonging to $\text{P}(\text{O})(\text{ONit})_3$ decreased with time, and a new one at -13.75 ppm, which could be assigned to one of the three possible products of hydrolysis $(\text{OH})\text{P}(\text{O})(\text{ONit})_2$, $(\text{O}^-)\text{P}(\text{O})(\text{ONit})_2$ or $\text{Tp}^{4\text{Py,Me}}\text{Zn-OP}(\text{O})(\text{ONit})_2$, increased with time. According to ^{31}P NMR, 100 % of $\text{P}(\text{O})(\text{ONit})_3$ was hydrolysed after 15 minutes.

In conclusion, the reactivity of the aqua complex **18** can be compared to that of the hydroxo complex $\text{Tp}^{3\text{Py,Me}}\text{Zn-OH}$, which has been reported to hydrolyse only 5 % of

P(O)(OPh)_3 in 16 hours.⁹² However, the hydrolysis of the highly activated tris(*p*-nitrophenyl)phosphate by **18** in the presence of water is very fast and indeed comparable to that obtained with $\text{Tp}^{4\text{Py,Me}}\text{Zn-OH}$ in methanol/dichloromethane (Section 2.2.8). Therefore, the aqua complex **18** can be used as an appropriate nucleophile for the hydrolytic P-O cleavage of certain activated phosphotriesters, such as tris(*p*-nitrophenyl)phosphate, in aqueous solution.

A complete identification of the products of hydrolysis could be achieved by ^1H NMR spectroscopy. With this purpose, the ^1H NMR spectrum of the product mixture obtained in the reaction of P(O)(ONit)_3 with **18** was recorded after no more substrate was detected by ^{31}P NMR. Figure 2.10 shows only the low-field range of the ^1H NMR spectrum, in which the signals corresponding to the *p*-nitrophenyl groups (ONit) of two different hydrolysis products and those of the $\text{Tp}^{4\text{Py,Me}}$ ligand are clearly distinguished.

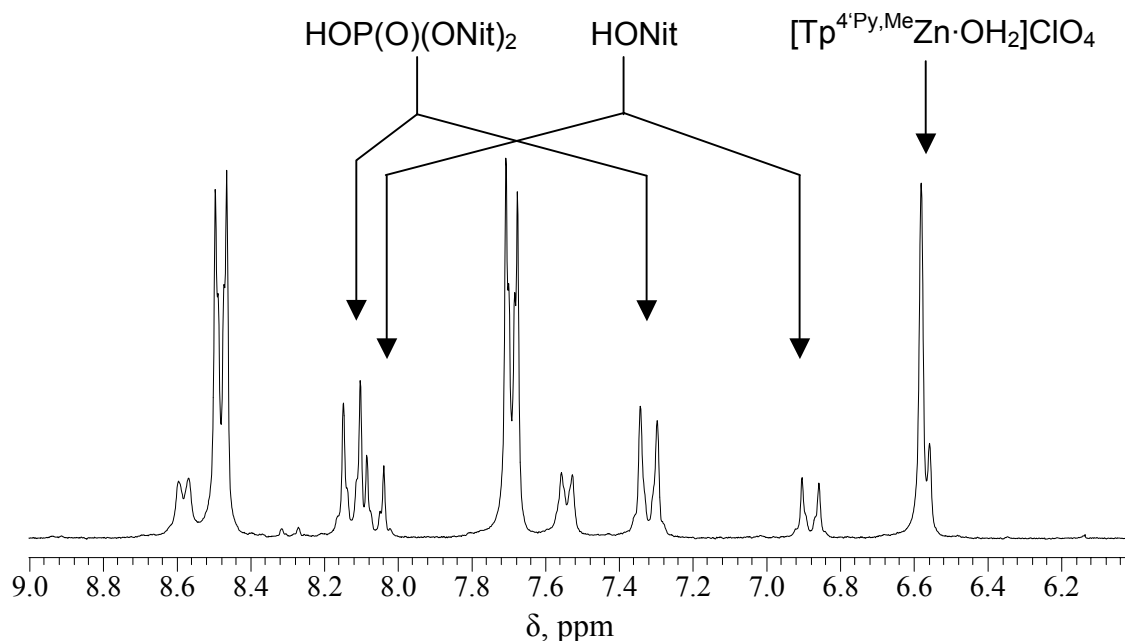


Fig. 2.10. ^1H NMR spectrum of the product mixture obtained from the hydrolysis of tris(*p*-nitrophenyl)phosphate by **18** in $\text{d}^6\text{-DMSO/D}_2\text{O}$ (75:25) at 310 K.

By comparison with the proton resonances given in table 2.10, the hydrolysis products can be identified as free *p*-nitrophenol, HONit, and bis(*p*-nitrophenyl)phosphate, HOP(O)(ONit)_2 . For example, the doublet centered at 6.9 ppm in the ^1H NMR spectrum of figure 2.10 can be assigned to the $\text{CH}_{\text{ph}(2,6)}$ protons of the

p-nitrophenyl ring of HONit, and the doublet at 7.3 ppm, to those of HOP(O)(ONit)₂. Additionally, the resonances of the pyridyl and pyrazolyl CH protons of the Tp^{4'Py,Me} system coincide with those of the aqua complex **18**, given in table 2.11. For example, the two signals at 6.56 and 6.58 ppm in the ¹H NMR spectrum of figure 2.10 can be assigned to the pyrazolyl CH protons of [Tp^{4'Py,Me}Zn·OH₂]ClO₄.

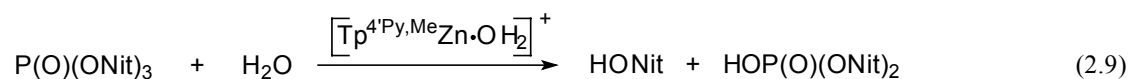
Table 2.10. ¹H NMR resonances of the *p*-nitrophenyl protons of HONit and HOP(O)(ONit)₂ in d⁶-DMSO/D₂O (75:25).

	HONit	HOP(O)(ONit) ₂
δ [CH _{ph} (2,6)] (ppm)	6.86-6.93	7.30-7.35
δ [CH _{ph} (3,5)] (ppm)	8.04-8.10	8.12-8.17

Table 2.11. ¹H NMR resonances of [Tp^{4'Py,Me}Zn·OH₂]ClO₄ in d⁶-DMSO/D₂O (75:25).

	δ [CH(pz)] (ppm)	δ [CH _{py} (3',5')] (ppm)	δ [CH _{py} (2',6')] (ppm)
18	6.56, 6.58	7.56-7.58, 7.66-7.68	8.44-8.47, 8.53-8.55

In conclusion, it has been demonstrated that the products of the hydrolysis of P(O)(ONit)₃ by [Tp^{4'Py,Me}Zn·OH₂]ClO₄ in aqueous solution are not binding to the Tp^{4'Py,Me}Zn unit, thereby allowing the regeneration of the nucleophilic species for the further cleavage of substrate. Therefore, the hydrolysis can be proposed to occur according to reaction 2.9.



In order to probe the catalytic activity of the aqua complex, an excess of P(O)(ONit)₃ was employed in the reaction with **18** in the presence of water. In a first experiment, two equivalents of P(O)(ONit)₃ were mixed with one equivalent of **18** in d⁶-DMSO/D₂O (75:25) and the reaction was followed by ¹H NMR spectroscopy. As shown in figure 2.11, the intensity of the signals corresponding to P(O)(ONit)₃ decreased with time, while those of the hydrolysis products, HONit and HOP(O)(ONit)₂, increased with time.

The hydrolysis of P(O)(ONit)_3 to HONit and HOP(O)(ONit)_2 was completed after 90 minutes. Contrary to expectation, the proton resonances of the $\text{Tp}^{4\text{Py,Me}}$ system, marked with the symbol (*) in figure 2.11, are shifted to low field and, therefore, they can not be assigned to those of the aqua complex **18**, given in table 2.11. This may be due to the formation of an excess of the acid HOP(O)(ONit)_2 which implies a decrease in the pH of the solution. This results in the hydrolytic cleavage of the B-N bond of the $\text{Tp}^{4\text{Py,Me}}$ ligand and, therefore, in the destruction of the aqua complex **18**.

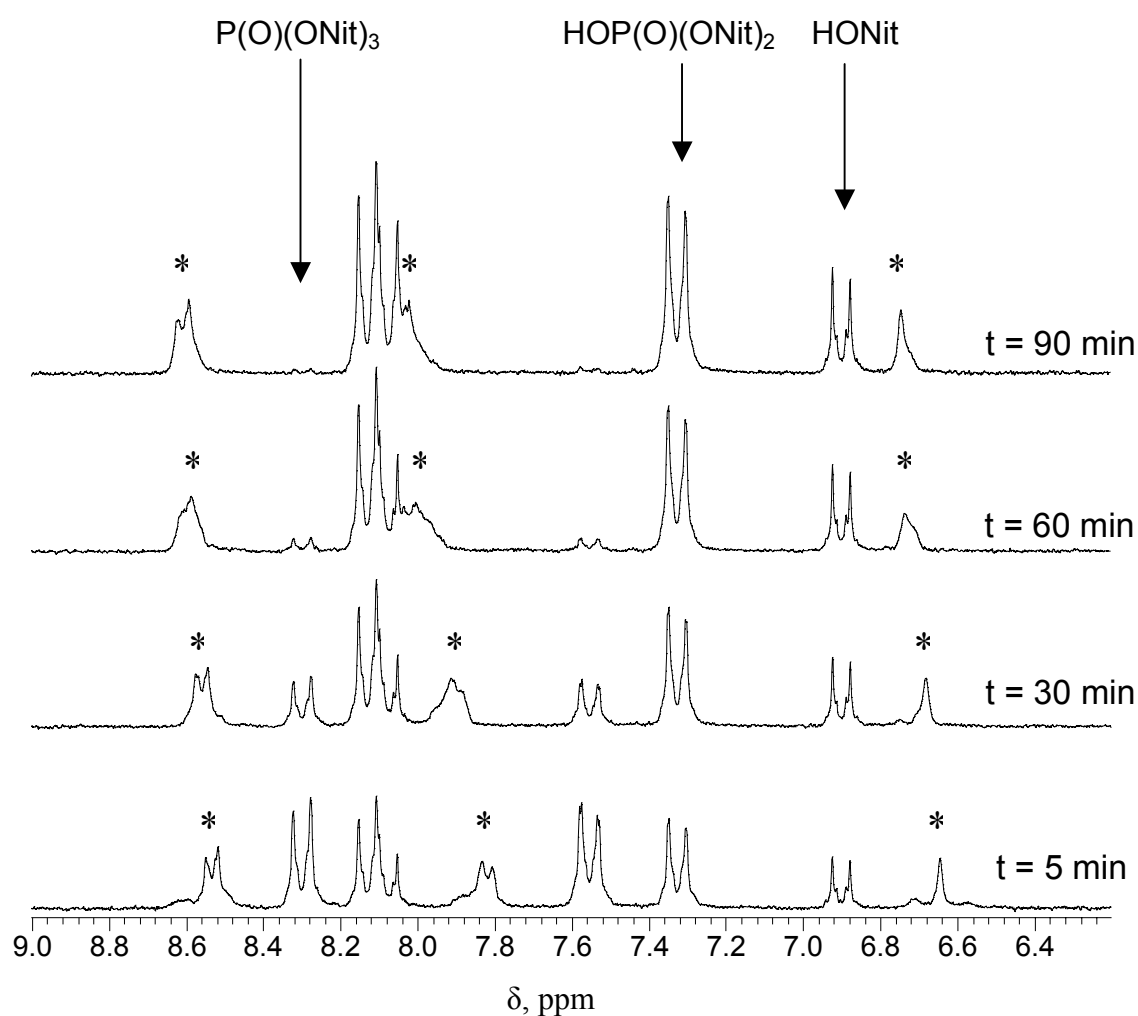


Fig. 2.11. Aromatic range of the ^1H NMR spectra of the product mixtures found at different times in the hydrolysis of 2 equivalents of P(O)(ONit)_3 with 1 equivalent of **18**. The spectra were measured in $\text{d}^6\text{-DMSO/D}_2\text{O}$ (75:25) at 310 K.

In order to avoid the decrease of pH due to the formation of the acid HOP(O)(ONit)_2 , which is suspected to be responsible for the hydrolytic destruction of **18**, the commercially available buffer 3-morpholinopropanesulfonic acid (MOPS, $\text{pK}_a = 7.2$) was added to the reaction mixture in a 5-fold excess with respect to the substrate concentration. Then, in a second experiment, four equivalents of P(O)(ONit)_3 were mixed with one equivalent of **18** in a d^6 -DMSO/ D_2O (75:25) solution containing 20 equivalents of MOPS, and the reaction was followed by ^1H NMR spectroscopy.

As shown in figure 2.12, the intensity of the signals corresponding to P(O)(ONit)_3 decreased with time, while the signals of the hydrolysis products, HONit and HOP(O)(ONit)_2 , increased with time. Furthermore, the hydrolysis of the four equivalents of P(O)(ONit)_3 was completed after 51 minutes, and therefore, the reaction was much faster than in the absence of MOPS (See figure 2.11). Furthermore, the proton resonances of the $\text{Tp}^{4\text{Py,Me}}$ system remain unshifted and are in agreement with those given in table 2.11 for the aqua complex **18**. For example, the signal centered at 6.57 ppm in the ^1H NMR spectrum of figure 2.12 can be assigned to the pyrazolyl CH protons of **18**. Additionally, background hydrolysis of P(O)(ONit)_3 due to MOPS was measured in the absence of **18** and shown to be negligible.

In conclusion, not only stoichiometric amounts, but a 4-fold excess of P(O)(ONit)_3 can be hydrolysed by $[\text{Tp}^{4\text{Py,Me}}\text{Zn}\cdot\text{OH}_2]\text{ClO}_4$ in aqueous solution. The immediate inhibition due to strong binding of the cleavage products to the $\text{Tp}^{4\text{Py,Me}}\text{Zn}$ unit, which generally occurs in the hydrolyses promoted by $\text{Tp}^{\text{R,Me}}\text{Zn}\cdot\text{OH}$, has been avoided. As a consequence, the nucleophilic species is regenerated after every reaction, thereby allowing the catalytic hydrolysis of the substrate.

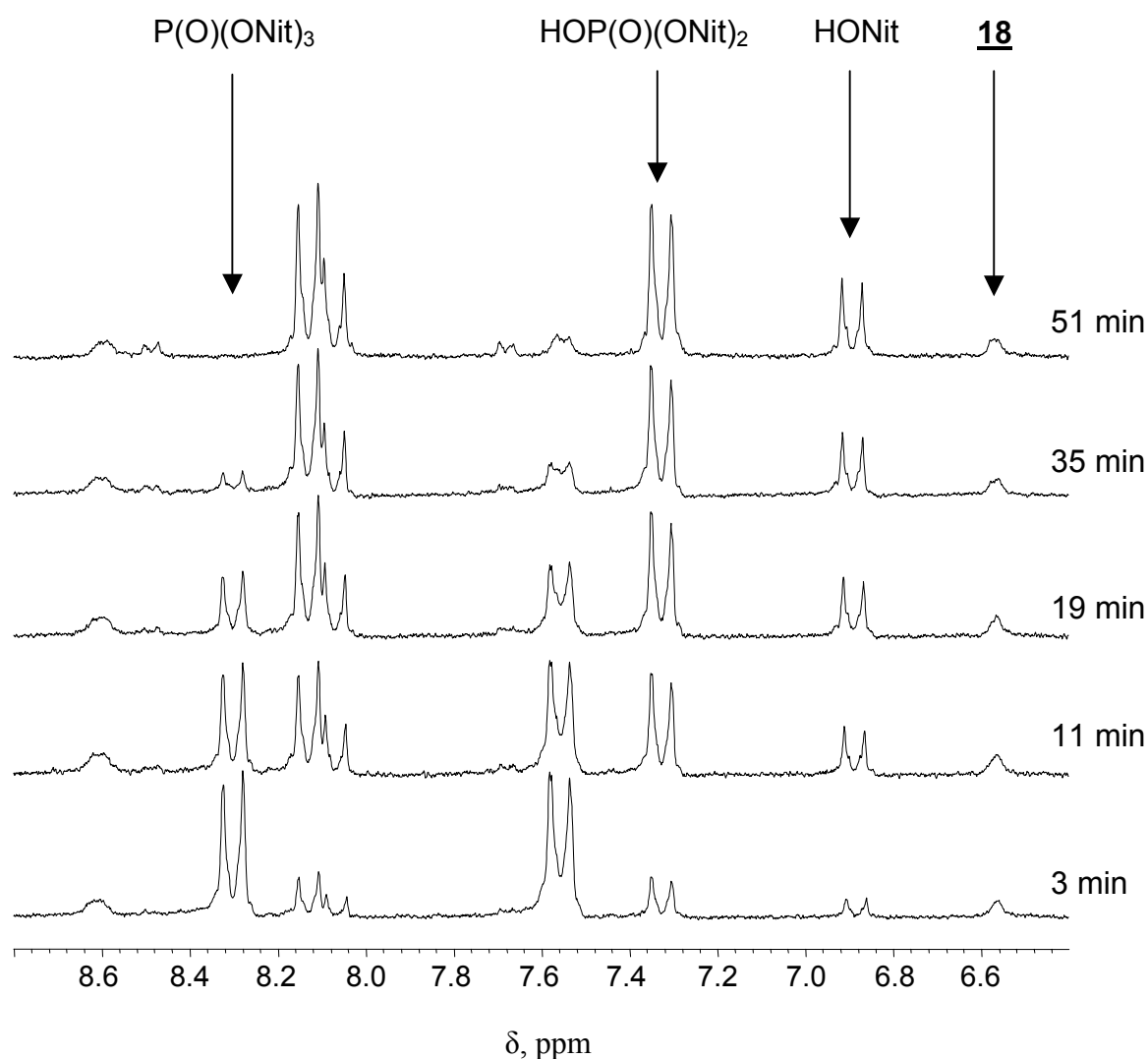


Fig. 2.12. Aromatic range of the ^1H NMR spectra of the product mixtures found at different times in the hydrolysis of 4 equivalents of $\text{P}(\text{O})(\text{ONit})_3$ with 1 equivalent of **18** in the presence of MOPS. The spectra were measured in $\text{d}^6\text{-DMSO}/\text{D}_2\text{O}$ (75:25) at 310 K.

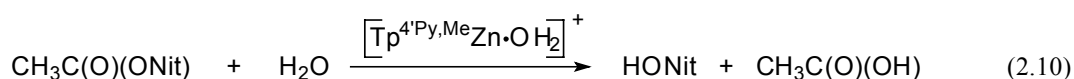
2.2.9.2. Hydrolysis of carboxyesters by **18**

In analogy to phosphoester hydrolysis, described in the previous section, the hydrolysis of carboxyesters was studied in the presence of firstly stoichiometric and secondly catalytic amounts of $[\text{Tp}^{4\text{Py,Me}}\text{Zn}\cdot\text{OH}_2]\text{ClO}_4$.

Firstly, the hydrolysis in the presence of stoichiometric amounts of the aqua complex **18** was studied for three carboxyesters $RC(O)(OR')$: β -butyrolactone, *p*-nitrophenylacetate $CH_3C(O)(ONit)$ and trifluoro(*p*-nitrophenyl)acetate $CF_3C(O)(ONit)$. The reaction of two equivalents of **18** with one equivalent of the corresponding $RC(O)(OR')$ in d^6 -DMSO containing 25 % D_2O was monitored by 1H NMR spectroscopy. In the case of β -butyrolactone, no hydrolysis could be observed after 7 days. In the case of *p*-nitrophenylacetate, the set of doublets belonging to $CH_3C(O)(ONit)$, at 7.35-7.39 and 8.23-8.28 ppm, disappeared with time and a new set at 6.86-6.93 and 8.04-8.10 ppm, corresponding to the generated HONit, emerged with time. According to the 1H NMR spectra, 100 % of $CH_3C(O)(ONit)$ was hydrolysed after 5 days. The reaction with trifluoro(*p*-nitrophenyl)acetate could not be followed by 1H NMR spectroscopy because the proton resonances of $CF_3C(O)(ONit)$ and the generated HONit have the same chemical shifts. However, in the ^{19}F NMR spectrum of the reaction mixture, the signal of $CF_3C(O)(ONit)$ at -74.95 ppm could not be detected and an intensive signal at -73.64 ppm could be assigned to the hydrolysis product $CF_3C(O)(OH)$.

In the case of *p*-nitrophenylacetate, the products of hydrolysis could be spectroscopically identified as free *p*-nitrophenol, HONit, and acetic acid, $CH_3C(O)(OH)$. Furthermore, the signals belonging to the aqua complex **18** could be clearly distinguished in the 1H NMR spectrum of the product mixture after the hydrolysis was completed. In contrast, if $Tp^{4Py,Me}Zn-OH$ was used as the nucleophilic species, the products of hydrolysis were the corresponding zinc complexes $Tp^{4Py,Me}Zn-ONit$ (**25**) and $Tp^{4Py,Me}Zn-OC(O)CH_3$ (**16**), as already explained in section 2.2.8.

In conclusion, $[Tp^{4Py,Me}Zn \cdot OH_2]ClO_4$ has been demonstrated to be nucleophilic enough to promote the hydrolysis of certain activated carboxyesters, such as *p*-nitrophenylacetate in aqueous DMSO. As expected, the C(O)-O bond of $CH_3C(O)(ONit)$ is less susceptible to hydrolytic cleavage than the P-O bond of $P(O)(ONit)_3$. Finally, the products of the hydrolysis of $CH_3C(O)(ONit)$ by $[Tp^{4Py,Me}Zn \cdot OH_2]ClO_4$ are not bound to the $Tp^{4Py,Me}Zn$ unit, thereby allowing the regeneration of the nucleophilic species for further cleavage of the substrate. Therefore, the hydrolysis can be proposed to occur according to equation 2.10.



Secondly, an excess of $\text{CH}_3\text{C}(\text{O})(\text{ONit})$ was reacted with the aqua complex **18**, in order to probe the catalytic activity of the latter. Thus, four equivalents of $\text{CH}_3\text{C}(\text{O})(\text{ONit})$ were mixed with one equivalent of $[\text{Tp}^{4\text{Py,Me}}\text{Zn}\cdot\text{OH}_2]\text{ClO}_4$ in a d^6 -DMSO/D₂O (75:25) solution containing 20 equivalents of MOPS, and the reaction was followed by ¹H NMR spectroscopy. Background hydrolysis due to MOPS was measured in the absence of $[\text{Tp}^{4\text{Py,Me}}\text{Zn}\cdot\text{OH}_2]\text{ClO}_4$ and observed to be negligible. The pH of the solution, before the reactants were mixed and after the reaction was finished, remained neutral within acceptable limits.

As shown in figure 2.13, the intensity of the signals corresponding to $\text{CH}_3\text{C}(\text{O})(\text{ONit})$ decreased with time, while the intensity of the signals of the hydrolysis product HONit increased with time. Only 50 % of $\text{CH}_3\text{C}(\text{O})(\text{ONit})$ was hydrolysed after 20 days, and no further hydrolysis could be achieved by prolonging the reaction time, even though the signals of $[\text{Tp}^{4\text{Py,Me}}\text{Zn}\cdot\text{OH}_2]\text{ClO}_4$ remained almost unshifted. Therefore, it can be concluded that this hydrolysis cannot be called catalytic.

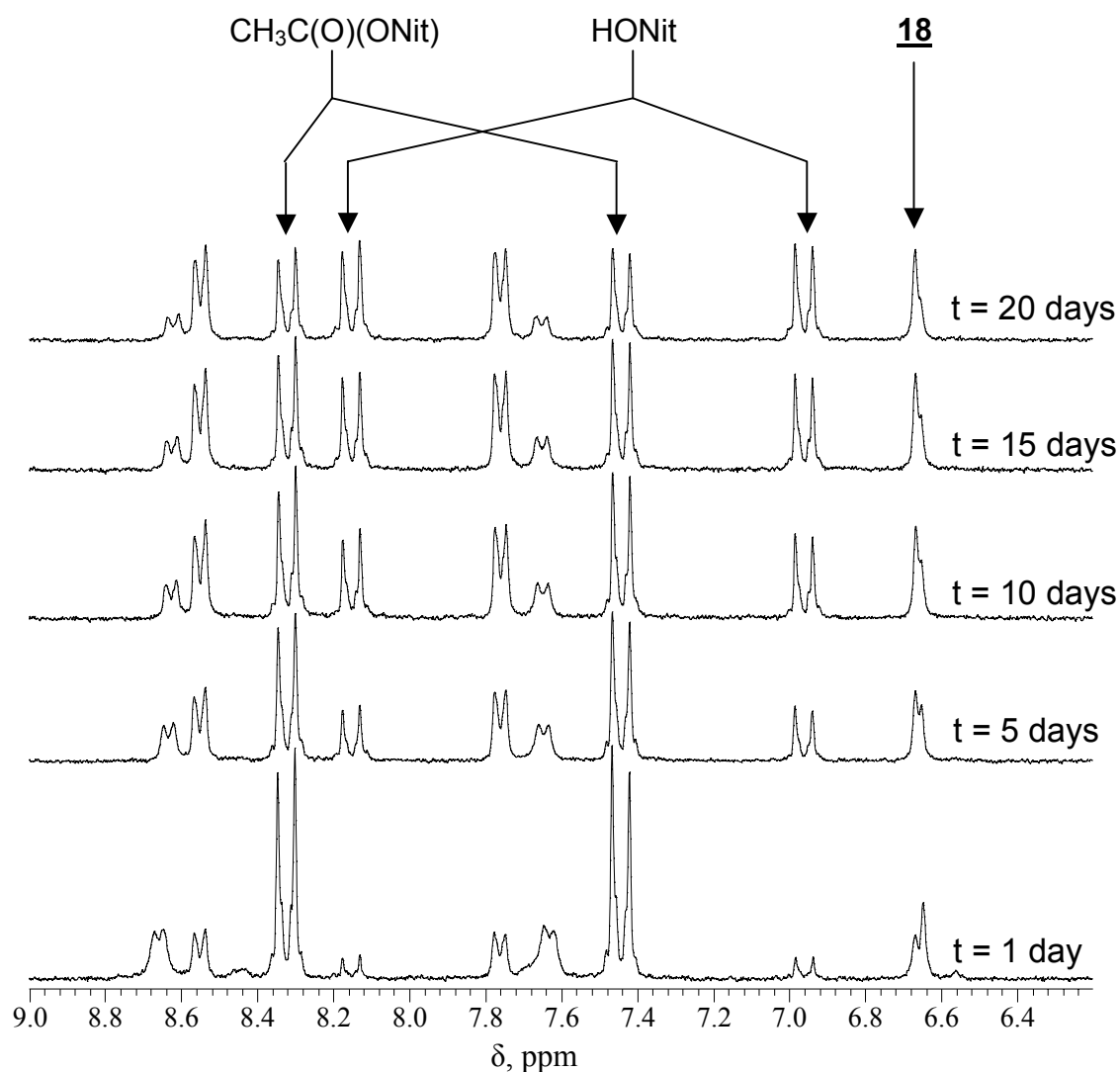
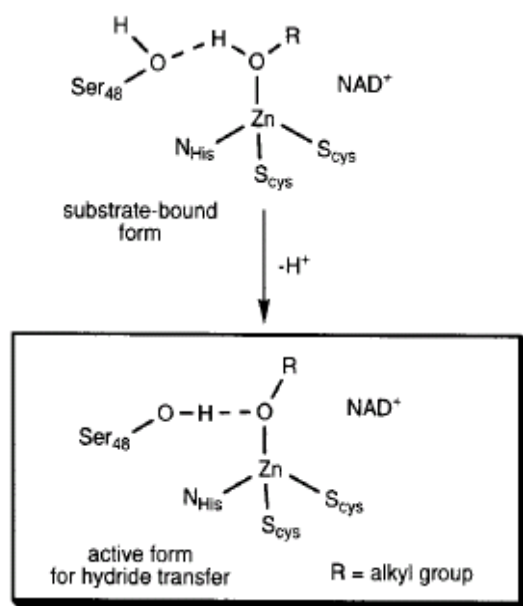


Fig. 2.13. Aromatic range of the ^1H NMR spectra of the product mixtures found at different times in the hydrolysis of 4 equivalents of $\text{CH}_3\text{C}(\text{O})(\text{ONit})$ with 1 equivalent of **18** in the presence of MOPS. The spectra were measured in d^6 -DMSO/ D_2O (75:25) at 310 K.

2.3. Carboxamide substituted ligands $\text{Tp}^{\text{C}(\text{O})\text{NHR,Me}}$

The zinc containing enzyme liver alcohol dehydrogenase (LADH) catalyses the two-electron oxidation of an alcohol to an aldehyde or ketone, coupled with reduction of NAD^+ to NADH .¹³¹ A key step in the mechanistic pathway of this oxidation is the formation of a zinc alkoxide species, via displacement of a zinc-bound water molecule, which is suggested to be the active moiety for hydride transfer to NAD^+ , a chemical

reaction that yields the oxidized alcohol product and NADH. Several alkoxide and alcohol complexes exhibiting structural and functional similarities to the proposed zinc alkoxide active form of LADH have been reported by Parkin^{112, 132} and our group.^{114, 133} The presence of a hydrophobic cavity around the metal ion has been postulated to contribute to the stabilization of such complexes. However, in the active site of LADH a serine residue (Ser₄₈) has been proposed to interact with the zinc bound alkoxide species via a strong hydrogen bond with the alkoxide oxygen, stabilizing it and influencing its chemistry (Scheme 2.1).¹³⁴

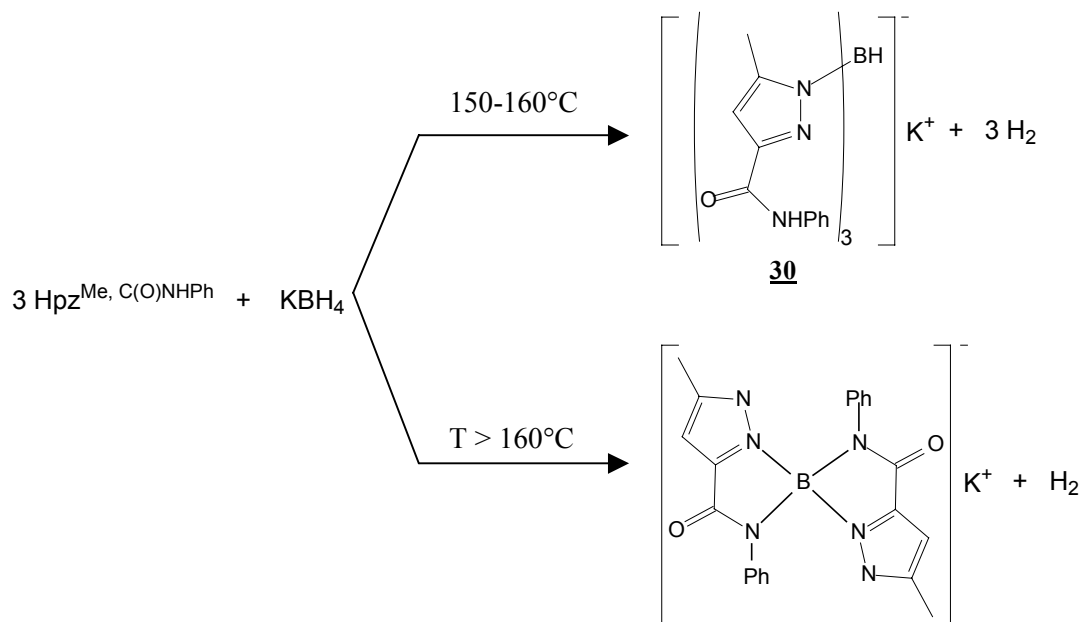


Scheme 2.1. Hydrogen bonding interactions in LADH involving Ser₄₈.

This aspect could be effectively modelled by Berreau^{135, 136} with dipyriddy–thiolate ligands containing pendant amides which can act as H-bonding donors. The enhanced stability of their zinc alkoxide complexes (**IV**) with respect to hydrolysis underlines the importance of H-bonding in influencing the reactivity of substrates bound to the metal ion. A further example of tripodal ligands placing H-bonding groups near the metal center are the tris(2-aminoethyl)amine based ligands of Borovik,^{63, 137} which contain three urea groups appended from a central amine nitrogen via ethylene spacers (**V**). A series of monomeric complexes with terminal hydroxo ligands inside the protective hydrogen bond cavity formed by the urea substituents, as well as an impressive range of manganese and iron-oxo complexes could be stabilized through strong intramolecular

$\text{Hpz}^{\text{Me,C(O)OEt}}$. Second, hydrolysis of this carboxyester substituted pyrazole gave the corresponding carboxylic acid substituted pyrazole $\text{Hpz}^{\text{Me,C(O)OH}}$. This was further reacted with thionyl chloride to obtain its tricyclic anhydride, 2-7-dimethyl-dipyrazolo[1,5-a;1'-5'-a]pyrazine-4,9-dione. Third, by reaction of the diketopiperazine with phenyl and tolyl amine in refluxing toluene, the corresponding carboxamide substituted pyrazoles $\text{Hpz}^{\text{Me,C(O)NHPH}}$ and $\text{Hpz}^{\text{Me,C(O)NHTol}}$ could be synthesized in very good yields.

By the melting reaction with KBH_4 only $\text{Hpz}^{\text{Me,C(O)NHPH}}$ could be converted to the desired hydrotris(3-phenylcarboxamide-5-methyl)pyrazolylborate $\text{KTp}^{\text{C(O)NHPH, Me}}$ **30**. After washing with acetonitrile and recrystallization from methanol/dichloromethane, $\text{KTp}^{\text{C(O)NHPH, Me}}$ could be isolated in 11 % yield. In order to improve the yield, an excess of the pyrazole (4:1 molar ratio of pyrazole to KBH_4) was always used and the melting mixture was kept at 150-160 °C for three hours. At higher temperatures, the deprotonation of the carboxamide NH function was found to be favoured and the potassium bis((3-methyl-5-phenylcarboxamide)pyrazol-1-yl)borate was obtained as the only product of the melting reaction (Scheme 2.2).



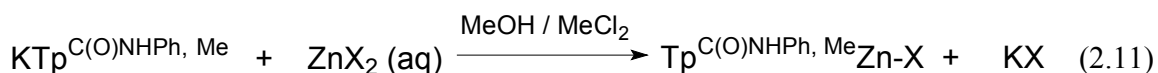
Scheme 2.2. Synthesis of $\text{KTp}^{\text{C(O)NHPH, Me}}$ **30**.

The new $\text{KTp}^{\text{C(O)NHPH, Me}}$ is insoluble in non-polar solvents such as toluene and chloroform, as well as in polar solvents such as acetonitrile and water. It is, however,

very soluble in alcohols such as methanol and ethanol as well as in alcohol/water mixtures. It is characterized by a B-H vibration band at 2470 cm^{-1} , a C=O vibration band at 1653 cm^{-1} and a N-H vibration band at 3365 cm^{-1} , which is in the range of N-monosubstituted carboxyamides. Its NH proton gives rise to a NMR signal at 9.25 ppm in d^6 -DMSO. Additionally, the $\text{CH}_3(\text{pz})$ and $\text{CH}(\text{pz})$ proton resonances appear at 2.01 and 6.46 ppm, respectively. **30** could be obtained in a crystalline form but its crystal structure analysis did not provide a reliable structural characterization.

2.3.2. Hydrotris(3-phenylcarboxamide-5-methyl)pyrazolylborate zinc complexes $\text{Tp}^{\text{C(O)NHPH, Me}}\text{Zn-X}$ ($\text{X} = \text{Cl}, \text{ONO}_2$ and OC(O)CH_3)

The coordination behaviour of the new $\text{Tp}^{\text{C(O)NHPH, Me}}$ ligand towards zinc was studied by reaction of **30** with several zinc salts, as shown in equation 2.11. Thus, the chloride, nitrate and acetate complexes **31**, **32** and **33** could be obtained in crystalline form by rapid evaporation of the solvent.



30

31 X = Cl

32 X = ONO_2

33 X = OC(O)CH_3

The most characteristic spectroscopic features of **31**, **32** and **33** are given in table 2.12. In comparison with **30**, the CH and CH_3 proton resonances are shifted towards low field and the IR B-H vibration band is found at higher wavenumbers. However, the IR N-H vibration band is found at lower wavenumber, thereby indicating that it may be involved in H-bonding interactions. Complexes **31**, **32** and **33** crystallized always as white needles inappropriate for a crystal structure determination.

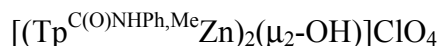
Table 2.12. Selected IR vibrations (cm^{-1} , in KBr) and ^1H NMR proton resonances (ppm, in CDCl_3) of **31**, **32** and **33**.

	ν (B-H) (cm^{-1})	ν (C=O) (cm^{-1})	ν (N-H) (cm^{-1})	δ [NH] (ppm)	δ [CH(pz)] (ppm)	δ [CH_3 (pz)] (ppm)
31	2511	1648	3315	8.89	6.80	2.53
32	2566	1648	3282	9.80	6.54	2.39
33	2573	-	3307	8.95	6.69	2.52, 2.39

The complex IR stretching pattern found in the 1650-1450 cm^{-1} spectral range for all three complexes **31**, **32** and **33** (for more details, see experimental section) is generally observed for N-monosubstituted carboxyamides as a consequence of the numerous association modes of a carboxyamide function by means of H-bonding interactions.¹³⁸ This makes it difficult to identify of the carboxylate group belonging to the acetate ligand in the IR spectrum of **33**. However, a broad peak at 1.75 ppm in its ^1H NMR spectrum can be clearly assigned to the CH_3 protons of the zinc coordinated acetate ligand.

2.3.3. Bis(hydrotris(3-phenylcarboxyamide-5-methyl)pyrazolylborate zinc hydroxide perchlorate $[(\text{Tp}^{\text{C(O)NHPH,Me}}\text{Zn})_2(\mu_2\text{-OH})]\text{ClO}_4$

In an effort to synthesize a mononuclear zinc aqua complex with the new ligand $\text{Tp}^{\text{C(O)NHPH,Me}}$, **30** was reacted with $\text{Zn}(\text{ClO}_4)\cdot 6\text{H}_2\text{O}$ in a mixture of methanol and dichloromethane at room temperature. Crystals precipitated from the reaction solution which were identified as the hydroxide bridged binuclear complex **34**.



34

In the IR spectrum of **34**, the B-H vibration band (2565 cm^{-1}) is found at higher wavenumbers than that of $\text{KTp}^{\text{C(O)NHPH,Me}}$ **30**, giving an indication of Tp coordination to zinc, and an absorption at 1107 cm^{-1} is found in the same position as that of the perchlorate counterion of the hydroxide bridged complex $[(\text{Tp}^{2\text{Fu,Me}}\text{Zn})_2(\mu_2\text{-OH})]\text{ClO}_4$,¹²⁹ revealing the presence of a perchlorate counterion. In the ^1H NMR spectrum of **34**, the CH and CH_3 proton resonances are shifted towards low field if compared to **30**, while the CH resonances belonging to the phenyl groups of the phenylcarboxyamides are strongly shifted towards high field. This is generally observed for binuclear zinc complexes of aromatically substituted Tp ligands.⁴⁷ The strong high-field shifts can be considered a consequence of ring current effects resulting from the intertwining of the phenyl groups of opposing $\text{Tp}^{\text{C(O)NHPH,Me}}$ ligands. A comparison of the phenylcarboxyamide proton resonances of **30** and **34** can be found in table 2.13.

Table 2.13. ^1H NMR resonances corresponding to the phenylcarboxamide substituents of **30** (ppm, in d^6 -DMSO) and **34** (ppm, in CDCl_3).

	δ [$\text{CH}_{\text{ph}(4)}$] (ppm)	δ [$\text{CH}_{\text{ph}(3,5)}$] (ppm)	δ [$\text{CH}_{\text{ph}(2,6)}$] (ppm)	δ [NH] (ppm)
30	7.01, m	7.27, m	7.64, d	9.25, b
34		6.78, m	7.07, m	9.29, b

The crystal structure of **34** confirmed that two $\text{Tp}^{\text{C}(\text{O})\text{NHPH,Me}}\text{Zn}$ units are bridged by a single hydroxide anion, thereby generating a binuclear species in the solid state (Figure 2.14). Accordingly, one perchlorate counterion is found outside the coordination sphere of zinc. It was also revealed the existence of a series of secondary interactions of hydrophobic and hydrophilic nature, involving the phenylcarboxamide groups, the zinc centers and the bridging hydroxide. It can be predicted that they will influence the chemistry of $\text{Tp}^{\text{C}(\text{O})\text{NHPH,Me}}$ based zinc complexes as they do in the active sites of zinc metalloenzymes, providing a better modeling of the latter.

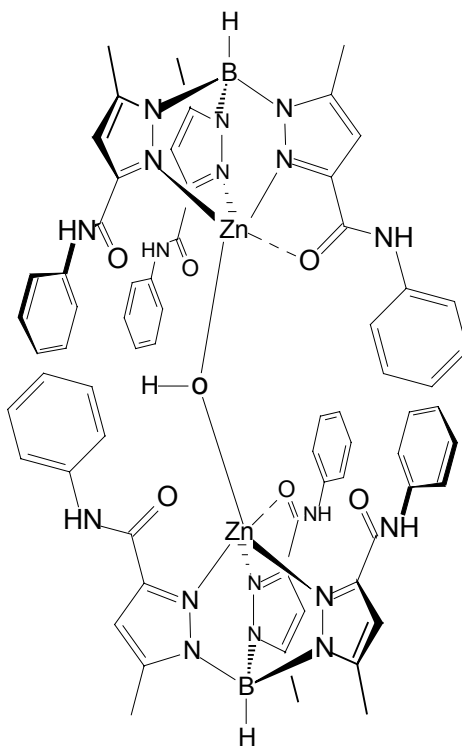


Figure 2.14. Schematic drawing of the structure of the binuclear hydroxo bridged $[(\text{Tp}^{\text{C}(\text{O})\text{NHPH,Me}}\text{Zn})_2(\mu_2\text{-OH})]\text{ClO}_4$ **34**. The perchlorate counterion has been omitted.

3. Structure determinations

The following complexes were characterized by single crystal X-ray diffraction: $\text{KBp}^{\text{C(O)OMe,Me}}$ **3**, $(\text{Bp}^{\text{C(O)OEt,Me}})_2\text{Zn}$ **5**, $(\text{Bp}^{\text{C(O)OMe,Me}})_2\text{Zn}$ **6**, $(\text{Bp}^{\text{Ph,Me}})\text{Zn}(\text{Cl})(\text{MeOH})$ **10**, $\text{KTp}^{4\text{Py,Me}}$ **11**, $\text{Tp}^{4\text{Py,Me}}\text{Zn-OC(O)CH}_3$ **16**, $\text{Tp}^{4\text{Py,Me}}\text{Zn-ONO}_2$ **17**, $[\text{Tp}^{4\text{Py,Me}}\text{Zn-OH}_2]\text{ClO}_4$ **18**, $[\text{Tp}^{4\text{Py,Me}}\text{Zn-HOMe}]\text{ClO}_4$ **19**, $[(\text{Tp}^{4\text{Py,Me}})_2\text{Zn}][\text{Tp}^{4\text{Py,Me}}\text{Zn-OH}]_2$ **21**, $[\text{Tp}^{4\text{Py,Me}}\text{Zn-OC(O)OMe}][\text{Tp}^{4\text{Py,Me}}\text{Zn-Cl}]$ **22**, $\text{Tp}^{4\text{Py,Me}}\text{Zn}(\text{benzoylac})$ **27** and $[(\text{Tp}^{\text{C(O)NHPh,Me}}\text{Zn})_2(\mu_2\text{-OH})]\text{ClO}_4$ **34**.

The structures were solved by direct or Patterson methods. The positions of the heaviest atoms such as Zn, K or Cl and the majority of the positions of the O, N and C atoms could be found. The positions of the remaining atoms were determined by difference Fourier syntheses. All non-hydrogen atoms were refined anisotropically. Unless otherwise noted, the hydrogen atoms were isotropically refined after the "riding model" concept, the distances of the hydrogen atoms being fixed as follows: CH = 96 pm (methyl, methylene), CH = 98 pm (methyne), CH = 93 pm (aromatic) and O-H = 96 pm. The hydrogen atoms were included with fixed distances and isotropic temperature factors 1.2 times those of their attached atoms (1.5 in methyl groups). An exact listing of the crystallographic data as well as the tables of the atomic parameters and the temperature factors can be found in chapter 4 together with the ORTEP drawings of the structures.

3.1. Potassium dihydrobis(3-carboxymethyl-5-methyl)pyrazolylborate $\text{KBp}^{\text{C(O)OMe,Me}}$ **3**

Colourless crystals of **3** suitable for X-ray diffraction were obtained by slowly cooling down a saturated toluene/methanol (90:10) solution. Complex **3** belongs to the monoclinic crystal system, space group P2(1). Its molecular structure was solved by direct methods and refined to a final R index of 0.060. The single-crystal X-ray diffraction study on **3** revealed a one-dimensional polymeric structure resulting from

close contacts between the potassium ion and the pyrazolyl nitrogens, some oxygens of the ester groups and one hydrogen of the BH₂ function. Specifically, each potassium ion is coordinated to two nitrogens and two oxygens of one Bp^{C(O)OMe,Me} ligand. Further coordination to one nitrogen, one oxygen and one hydrogen belonging to three neighbouring ligand units result in a seven-coordinated potassium center of very low symmetry. The structure of **3** is shown in figure 3.1, where the complete coordination sphere around K(1) is detailed.

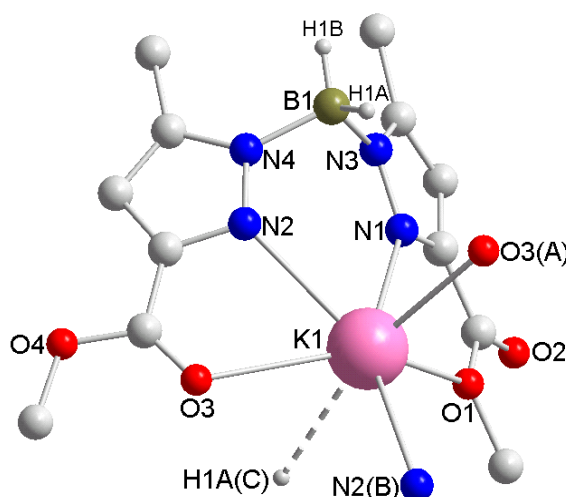


Figure 3.1. Interactions around the potassium ion and atom labelling scheme for KBp^{C(O)OMe,Me} **3**.

Table 3.1 lists the bonding parameters around potassium. The K(1)-N bond distances for the nitrogens N(1) and N(2) average 2.79 Å and the K(1)-O bond distances for O(1) and O(3), 2.91 Å. Additionally, the K(1)-O3(A) bond distance of 2.74 Å reveals a stronger coordination to the carbonyl oxygen of a second Bp^{C(O)OMe,Me} ligand, and the K(1)-H1A(C) bond distance of 2.72 Å is indicative of a 3-center-2-electron K...H-B interaction with a third ligand unit. The resulting coordination around K(1) can be described as a highly distorted pentagonal bipyramid with a K(1)-N2(B) bond of 3.09 Å, which is very long but still not out of range for the coordination to a further Bp^{C(O)OMe,Me} unit. The apical positions of the pentagonal bipyramid are occupied by the carbonyl oxygen O3(A) and the hydrogen H1A(C) of two different ligand units. The O3(A)-K(1)-H1A(C) angle is 165.3°. The carboxyester functionalities of the ligand are coplanar with the pyrazolyl rings, while the latter are forming an angle of 108.5° with

each other. The N(1)-K(1)-O(1) and N(2)-K(1)-O(3) angles of 57.0 and 57.6° respectively are very small for a five-membered chelate ring. Thus, the potassium ion is deviated 0.90 Å from the plane defined by N(1), N(2), O(3) and O(1) in direction to O3(A). Further bond angles of complex **3** are listed in table 3.1.

Table 3.1. Selected bond lengths [Å] and angles [°] of KBp^{C(O)OMe,Me} **3**.

Bond	[Å]	Angle	[°]
K(1)-O(3)A	2.742(4)	O(3)A-K(1)-N(1)	79.28(13)
K(1)-N(1)	2.791(5)	O(3)A-K(1)-N(2)	93.47(12)
K(1)-N(2)	2.799(4)	N(1)-K(1)-N(2)	70.72(13)
K(1)-O(1)	2.836(4)	O(3)A-K(1)-O(1)	95.90(13)
K(1)-O(3)	2.974(4)	N(1)-K(1)-O(1)	56.96(13)
K(1)-N(2)B	3.088(4)	N(2)-K(1)-O(1)	123.66(13)
		O(3)A-K(1)-O(3)	123.62(10)
		N(1)-K(1)-O(3)	122.78(12)
		N(2)-K(1)-O(3)	57.56(12)
		O(1)-K(1)-O(3)	140.39(13)
		O(3)A-K(1)-N(2)B	85.24(13)
		N(1)-K(1)-N(2)B	153.76(13)
		N(2)-K(1)-N(2)B	131.77(7)
		O(1)-K(1)-N(2)B	104.36(12)
		O(3)-K(1)-N(2)B	83.44(11)

In addition to the coordination to K(1) through N(1), N(2), O(1) and O(3), each Bp^{C(O)OMe,Me} anion is bound to three further potassium ions, thereby creating zig-zag shaped one-dimensional chains, as shown in figure 3.2. This occurs via the pyrazolyl nitrogen N(2), the carbonyl oxygen O(3) and the H(1A) of the BH₂ function.

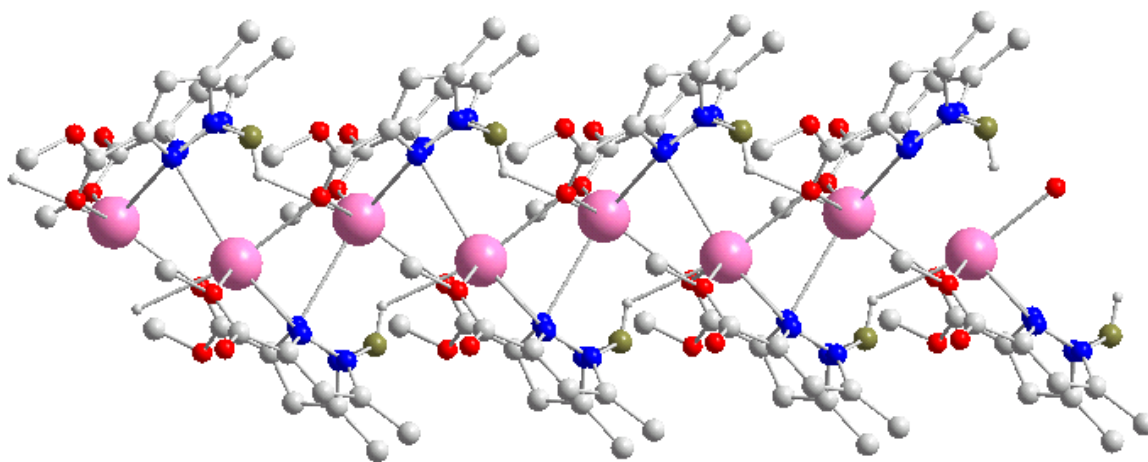
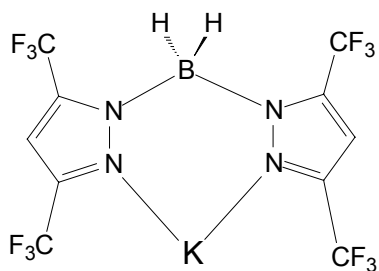
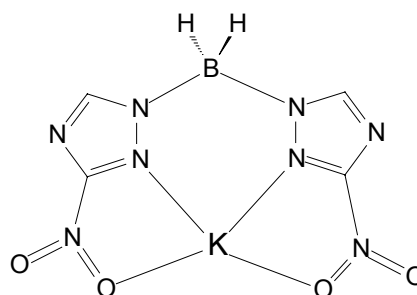


Figure 3.2. Atomic arrangements along one-dimensional chains in $\text{KBp}^{\text{C(O)OMe,Me}}$ **3**.

Although most new pyrazolylborate ligands are synthesized initially as potassium salts, there still exist only a small number of structure determinations for such salts.^{139,140,141,142,143} These include the perfluorinated $[\text{H}_2\text{B}(3,5\text{-(CF}_3)_2\text{Pz})_2]\text{K}$ (**VII**),¹⁴³ which shows a polymeric structure with K-N bond distances marginally shorter than the K(1)-N2(B) bond of 3.09 Å in **3**, and K \cdots H separations of 2.77 Å. Additionally, in the recently reported dihydrobis(triazolyl)borate complex $[\text{H}_2\text{B}((3\text{-NO}_2)\text{Tz})_2]\text{K}$ (**VIII**)¹⁴⁴ the bonding mode of the nitro functionalities, averaging K-O bond distances of 3.16 Å, can be compared to that of the carboxyester groups in **3**.



VII



VIII

3.2. Bis-dihydrobis(3-carboxyalkyl-5-methyl)pyrazolylborate zinc complexes (Bp^{C(O)OR,Me})₂Zn 5 (R = Et) and 6 (R = Me)

Colourless crystals of 5 and 6 suitable for X-ray diffraction were obtained by slowly evaporating the solvent of a saturated ethanol/dichloromethane and methanol/dichloromethane solution, respectively. Complex 5 belongs to the triclinic crystal system, space group P-1, and 6 to the monoclinic crystal system, space group P2(1)/c. The molecular structure of 5 was solved by direct methods and refined to a final R index of 0.071, and that of 6 was solved by Patterson methods and refined to a final R index of 0.068. Both complexes crystallize as discrete molecules with four nitrogen atoms belonging to two Bp^{C(O)OR,Me} anions coordinated to the zinc ion in a distorted tetrahedral geometry. For complex 5, a disorder for the methyl carbon C(18) was observed. The structures of 5 and 6 are shown in figure 3.3.

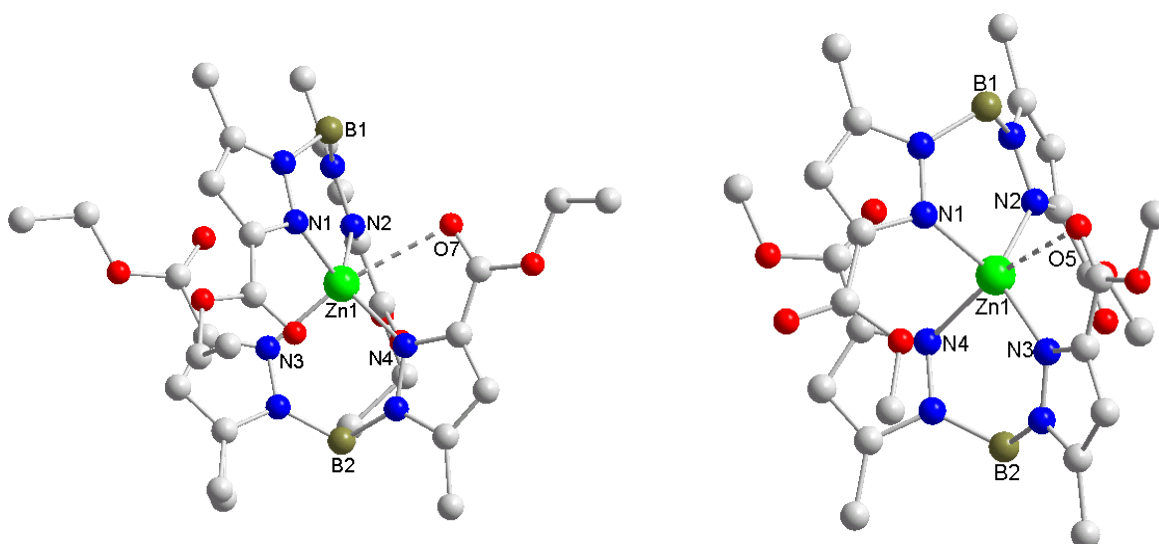


Figure 3.3. Molecular structures of (Bp^{C(O)OEt,Me})₂Zn 5 (left) and (Bp^{C(O)OMe,Me})₂Zn 6 (right).

Selected bond lengths and angles are listed in tables 3.2 and 3.3, for 5 and 6 respectively. In complex 5, the Zn(1)-N bond distances for the nitrogens N(4), N(2) and N(1) range from 2.00 to 2.05 Å. In contrast, the Zn(1)-N(3) bond distance, of 2.10 Å, is significantly longer. Nearly identical Zn(1)-N bond distances are observed for complex 6. The shorter Zn(1)-N bond distances can be compared to those found in the tetrahedral complexes [H₂B(3,5-(CH₃)₂Pz)₂]₂Zn (2.01-2.02 Å) and [H₂B(3,5-(CF₃)₂Pz)₂]₂Zn (2.01-

2.04 Å) described by Dias.¹⁴³ However, the longer Zn(1)-N(3) bond distance is only slightly shorter than those found in the octahedral complex [HB(3,5-(CH₃)₂Pz)₃]₂Zn (2.15-2.19 Å).¹⁴⁵

Table 3.2. Selected bond lengths [Å] and angles [°] of (Bp^{C(O)OEt,Me})₂Zn **5**.

Bond	[Å]	Angle	[°]
Zn(1)-N(4)	2.002(4)	N(4)-Zn(1)-N(2)	126.38(17)
Zn(1)-N(2)	2.008(4)	N(4)-Zn(1)-N(1)	122.01(16)
Zn(1)-N(1)	2.048(4)	N(2)-Zn(1)-N(1)	97.86(15)
Zn(1)-N(3)	2.104(4)	N(4)-Zn(1)-N(3)	97.03(16)
		N(2)-Zn(1)-N(3)	112.17(17)
		N(1)-Zn(1)-N(3)	98.27(16)

Table 3.3. Selected bond lengths [Å] and angles [°] of (Bp^{C(O)OMe,Me})₂Zn **6**.

Bond	[Å]	Angle	[°]
Zn(1)-N(3)	1.998(5)	N(3)-Zn(1)-N(2)	127.51(19)
Zn(1)-N(2)	2.018(5)	N(3)-Zn(1)-N(1)	122.27(18)
Zn(1)-N(1)	2.054(4)	N(2)-Zn(1)-N(1)	98.36(17)
Zn(1)-N(4)	2.104(5)	N(3)-Zn(1)-N(4)	94.88(18)
		N(2)-Zn(1)-N(4)	111.31(18)
		N(1)-Zn(1)-N(4)	98.91(17)

Additionally to the coordination to the nitrogen atoms, the zinc ion shows a slight tendency to become involved in a weak interaction with one of the carbonyl oxygens. This is not so much expressed in the bond distances Zn(1)-O(7) of 2.84 Å and Zn(1)-O(5) of 2.76 Å, for **5** and **6** respectively, but in the N(3)-Zn(1)-O(7) and N(4)-Zn(1)-O(5) angles of 161.4° and 158.3°. For example, in the binuclear hydroxo bridged complex [(Tp^{C(O)OEt,Me}Zn)₂(μ₂-OH)]ClO₄ described by Carrano,⁵⁸ each zinc ion shows a rather stronger interaction with one of the ester carbonyls of the opposite ligand (2.58 Å), so that the coordination geometry around zinc can be described as distorted trigonal bipyramidal. In complexes **5** and **6**, this interaction leads to a distortion of the tetrahedral geometry, as expressed by the deviations of maximal 16.9° and 18.0°, for **5**

and **6** respectively, from the 109.5° angle expected for an idealized tetrahedral geometry. The dihedral angle formed between the planes defined by Zn(1), N(1), N(2) and by Zn(1), N(3), N(4) is 83.3° and 84.2° , for **5** and **6** respectively, so that the two $\text{Bp}^{\text{C(O)OR,Me}}$ anions binding zinc are not completely perpendicular to each other.

In complexes **5** and **6**, the $\text{Zn}(\text{N-N})_2\text{B}$ units adopt a significantly distorted boat conformation, flattened at the Zn end. This distortion can better be viewed in figure 3.4, where the substituents on the pyrazole rings have been omitted, except of the ester group involved in the coordination to zinc. Thus, the planes defined by N(1), N(2), N(5), N(6) and by Zn(1), N(1), N(2) form an angle of 179.5° and 177.0° , in **5** and **6** respectively, and the planes defined by N(3), N(4), N(7), N(8) and by Zn(1), N(3), N(4) form an angle of 176.7° and 175.7° . Minor distortions from the boat conformation have been found for the tetrahedral complex $[\text{H}_2\text{B}(3,5\text{-}(\text{CH}_3)_2\text{Pz})_2]_2\text{Zn}$ (165.3°) and for its perfluorinated analogue $[\text{H}_2\text{B}(3,5\text{-}(\text{CF}_3)_2\text{Pz})_2]_2\text{Zn}$ (165.9°).¹⁴³ This may be attributed to a bigger steric effect of the carboxyester groups and the demands of the interaction with the carbonyl oxygen O(7) and O(5) in **5** and **6** respectively. As a consequence, the $\text{Zn}(1)\cdots\text{B}$ distances average 3.32 \AA for both complexes, thereby being out of the bonding range for a 3-center-2-electron $\text{Zn}\cdots\text{H}\cdots\text{B}$ interaction.

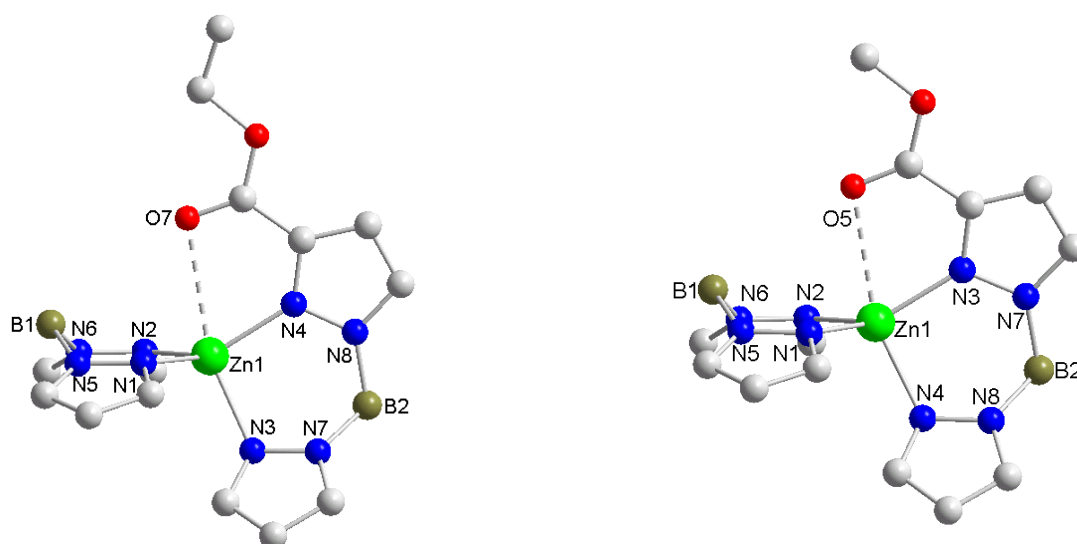


Figure 3.4. View of the distorted boat conformation in $\text{Bp}^{\text{C(O)OEt,Me}}$ **5** (left) and in $\text{Bp}^{\text{C(O)OMe,Me}}$ **6** (right). The substituents on the pyrazole rings have been omitted for clarity.

3.3. Dihydrobis(3-phenyl-5-methyl)pyrazolylborate zinc chloride methanol $(\text{Bp}^{\text{Ph,Me}})\text{Zn}(\text{Cl})(\text{MeOH})$ **10**

Colourless crystals of **10** were obtained by cooling to -20°C a saturated methanol/dichloromethane solution. Complex **10** belongs to the monoclinic crystal system, space group $P2(1)/c$. Its molecular structure was solved by direct methods and refined to a final R index of 0.061. The single-crystal X-ray diffraction study on **10** reveals a tetrahedral coordination geometry around the zinc ion with two pyrazolyl nitrogen donors of $\text{Bp}^{\text{Ph,Me}}$, and with one oxygen of a methanol molecule and one chloride anion occupying the two remaining coordination sites. In the asymmetric unit two methanol molecules are found in addition to one molecule of complex **10**. The structure of **10** is shown in figure 3.5, and selected bond lengths and angles are listed in table 3.4.

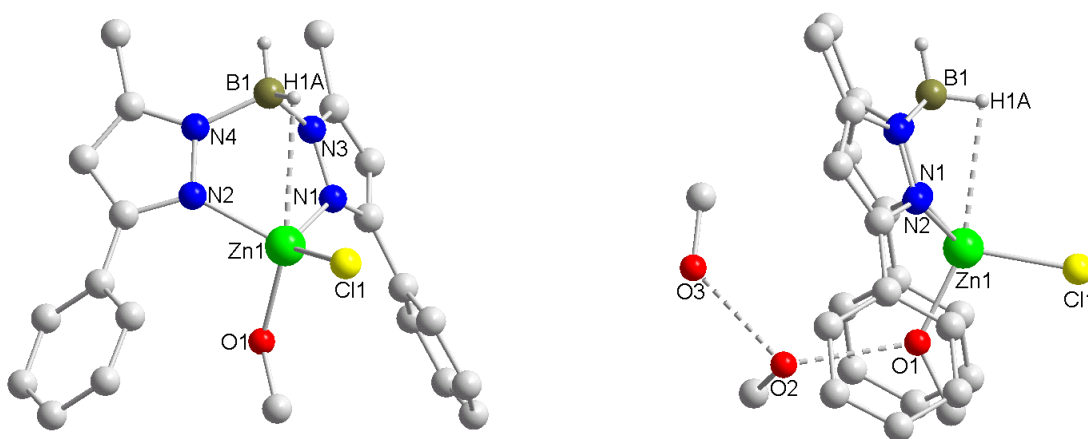


Figure 3.5. Molecular structure of $(\text{Bp}^{\text{Ph,Me}})\text{Zn}(\text{Cl})(\text{MeOH})$ **10** (left), and H-bonding network found in the asymmetric unit of **10** (right). Only the hydrogens on boron are shown.

The $\text{Zn}(1)\text{-N}$ and $\text{Zn}(1)\text{-O}(1)$ bond distances are both 1.99 \AA , while the $\text{Zn}(1)\text{-Cl}(1)$ bond distance of 2.21 \AA is significantly longer, as expected for a chloride ligand. The $\text{O}(1)\text{-Zn}(1)\text{-Cl}(1)$ and the average $\text{O}(1)\text{-Zn}(1)\text{-N}$ bond angles are 105.4° and 103.8° , deviating only slightly from the 109.5° angle expected for an idealized tetrahedral geometry, however the average $\text{Cl}(1)\text{-Zn}(1)\text{-N}$ angle is significantly widened to 120.9° . This distortion may be attributed to a weak 3-center-2-electron $\text{Zn}(1)\cdots\text{H}(1\text{A})\text{-B}(1)$ interaction with a $\text{Zn}(1)\cdots\text{B}(1)$ distance of 2.98 \AA , which forces the $\text{Zn}(\text{N-N})_2\text{B}$ unit of

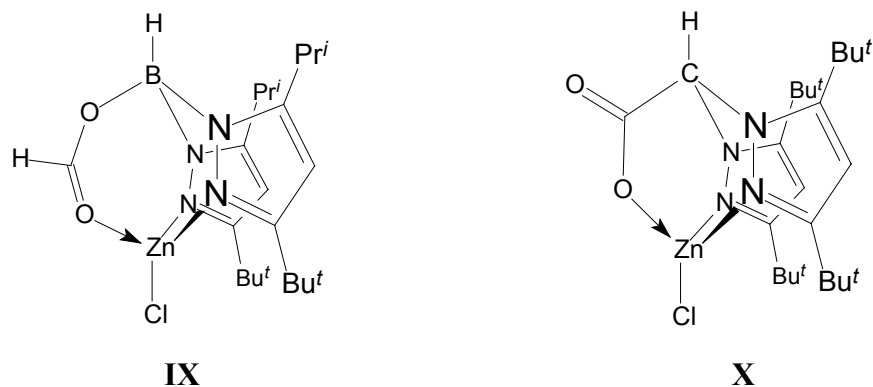
the Bp^{Ph,Me} ligand into the characteristic boat conformation. The angle between the planes defined by N(1), N(2), N(3), N(4) and by Zn(1), N(1), N(2) is 152.8° and, therefore, much smaller than those found in complexes **5** and **6**.

Table 3.4. Selected bond lengths [Å] and angles [°] of (Bp^{Ph,Me})Zn(Cl)(MeOH) **10**.

Bond	[Å]	Angle	[°]
Zn(1)-N(1)	1.987(4)	N(1)-Zn(1)-O(1)	104.38(18)
Zn(1)-O(1)	1.989(4)	N(1)-Zn(1)-N(2)	99.80(18)
Zn(1)-N(2)	1.996(4)	O(1)-Zn(1)-N(2)	103.30(17)
Zn(1)-Cl(1)	2.2060(18)	N(1)-Zn(1)-Cl(1)	118.95(14)
		O(1)-Zn(1)-Cl(1)	105.44(13)
		N(2)-Zn(1)-Cl(1)	122.75(14)

As shown in figure 3.5 (right), the methanol ligand is embedded between the two aromatic phenyl rings of Bp^{Ph,Me}. It is attached to a second methanol molecule by a hydrogen bond, which in turn is hydrogen bonded to another methanol molecule present in the asymmetric unit, with O(1)⋯O(2) and O(2)⋯O(3) distances of 2.57 and 2.66 Å, respectively. These and the Zn(1)-O(1) bond distance of 1.99 Å are only marginally shorter than the Zn-O and O⋯O distances reported for several tetrahedral alcohol complexes [Tm^RZn(HOR)]⁺(HOR),^{106, 146} Tm^R denoting a tris(thioimidazolyl)borate ligand, and the pyrazolylbis(thioimidazolyl)borate zinc ethanol complex {[pz^{Ph,Me})Bm^{o-An}]Zn·HOEt}·(ClO₄)·EtOH.¹⁰⁴ The latter is considered the best structural model of liver alcohol dehydrogenase since it reproduces the essential structural features of the enzymatic situation.

Tetrahedral zinc complexes with two pyrazolyl nitrogens, one alcohol oxygen and one halide coordinating to zinc have not been reported before. Usual are the halide zinc complexes of heteroscorpionate ligands which bind to the zinc ion in a facially tridentate N₂O manner, as exemplified by complexes **IX**⁷⁶ and **X**.¹⁴⁷ In comparison with **10**, the tetrahedral geometry around zinc is distorted to a greater extent due to the bite angle of the tripodal ligand. Thus, deviations of 20.4° and 21.9° from the 109.5° angle expected for an idealized tetrahedral geometry have been reported for **IX** and **X** respectively.



3.4. Potassium hydrotris(3-(4'-pyridyl)-5-methyl)pyrazolylborate $\text{KTp}^{4\text{Py,Me}}$ **11**

Colourless crystals of **11** suitable for X-ray diffraction were obtained by slowly cooling down a saturated acetonitrile solution. Complex **11** belongs to the monoclinic crystal system, space group $P2(1)/c$. Its molecular structure was solved by Patterson methods and refined to a final R index of 0.068. The single-crystal X-ray diffraction study on **11** revealed a three-dimensional polymeric structure resulting from the coordination of potassium to three pyrazolyl nitrogens of a $\text{Tp}^{4\text{Py,Me}}$ ligand and three pyridyl nitrogens belonging to neighbouring $\text{KTp}^{4\text{Py,Me}}$ units. Thus, each potassium ion is six-coordinated in an octahedral coordination geometry, as shown in figure 3.6.

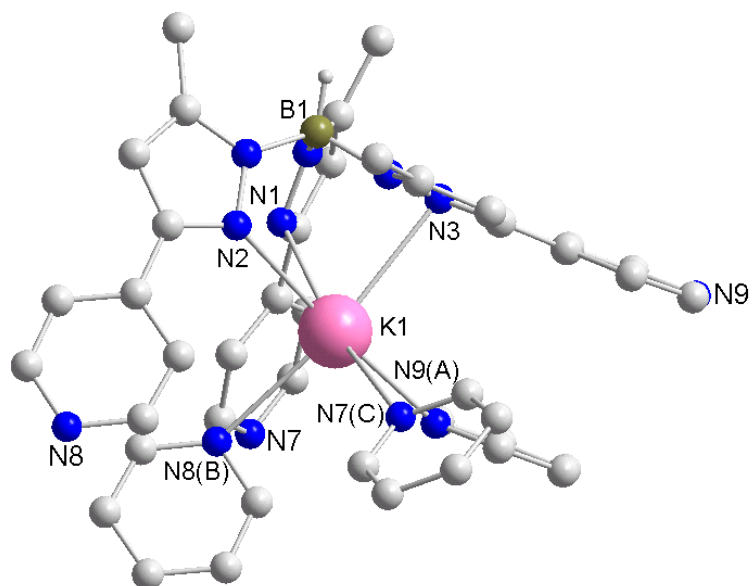


Figure 3.6. Potassium coordination geometry and atom labelling scheme for $\text{KTp}^{4\text{Py,Me}}$

11.

In addition to one molecule of complex **11**, one non-coordinating acetonitrile molecule is present in the asymmetric unit. Selected bond lengths of **11** are given in table 3.5.

Table 3.5. Selected bond lengths [\AA] of $\text{KTp}^{4\text{Py,Me}}$ **11**.

Bond	[\AA]
K(1)-N(9)A	2.802(4)
K(1)-N(2)	2.810(3)
K(1)-N(8)B	2.869(3)
K(1)-N(1)	2.897(3)
K(1)-N(3)	3.022(3)
K(1)-N(7)C	3.152(4)

In complex **11**, the K(1)-N bond distances for the pyrazolyl nitrogens N(1) and N(2) average 2.85 \AA , while the K(1)-N(3) bond distance of 3.02 \AA is significantly longer, although not out of the bonding range,^{148,149} indicating an unsymmetrical binding of the $\text{Tp}^{4\text{Py,Me}}$ ligand to the potassium ion. The K(1)-N bond distances for the pyridyl nitrogens N(9)A, N(8)B and N(7)C show a wider spread about the average value of 2.94 \AA , the K(1)-N(7)C distance marking the extreme (3.15 \AA). The resulting coordination geometry of the six-coordinated K(1) can be described as octahedral to a good approximation. The deviations of the bond angles of **11** from those of a regular octahedron are given in table 3.6.¹⁵⁰ The average deviation is 10.3°.

Table 3.6. Deviation of the measured angles [$^\circ$] in **11** (measd) from the regular octahedral coordination geometry (O_h).

Angle	measd	O_h	Δ
N(9)A-K(1)-N(2)	172.67(11)	180	7.33
N(8)B-K(1)-N(3)	160.89(10)	180	19.11
N(1)-K(1)-N(7)C	166.91(10)	180	13.09
N(9)A-K(1)-N(8)B	90.42(11)	90	0.42
N(9)A-K(1)-N(1)	104.17(11)	90	14.17

N(9)A-K(1)-N(3)	88.49(10)	90	1.51
N(9)A-K(1)-N(7)C	84.33(12)	90	5.67
N(2)-K(1)-N(8)B	92.85(9)	90	2.85
N(2)-K(1)-N(1)	68.89(9)	90	21.11
N(2)-K(1)-N(3)	86.28(8)	90	3.72
N(2)-K(1)-N(7)C	102.10(10)	90	12.10
N(8)B-K(1)-N(1)	97.93(10)	90	7.93
N(8)B-K(1)-N(7)C	91.87(10)	90	1.87
N(1)-K(1)-N(3)	63.95(8)	90	26.05
N(3)-K(1)-N(7)C	106.99(10)	90	16.99

In complex **11**, the coordination of each potassium ion to three pyridyl nitrogens belonging to different $\text{KTp}^{4\text{Py,Me}}$ neighbours results in a three-dimensional coordination polymer. Thus, no pyridyl nitrogen of the $\text{Tp}^{4\text{Py,Me}}$ ligand remains uncoordinated, since N(8) and N(9) are bridging $\text{KTp}^{4\text{Py,Me}}$ units inside zig-zag shaped one-dimensional chains and N(7) is linking parallel chains to each other. A fragment of chain is shown in figure 3.7.

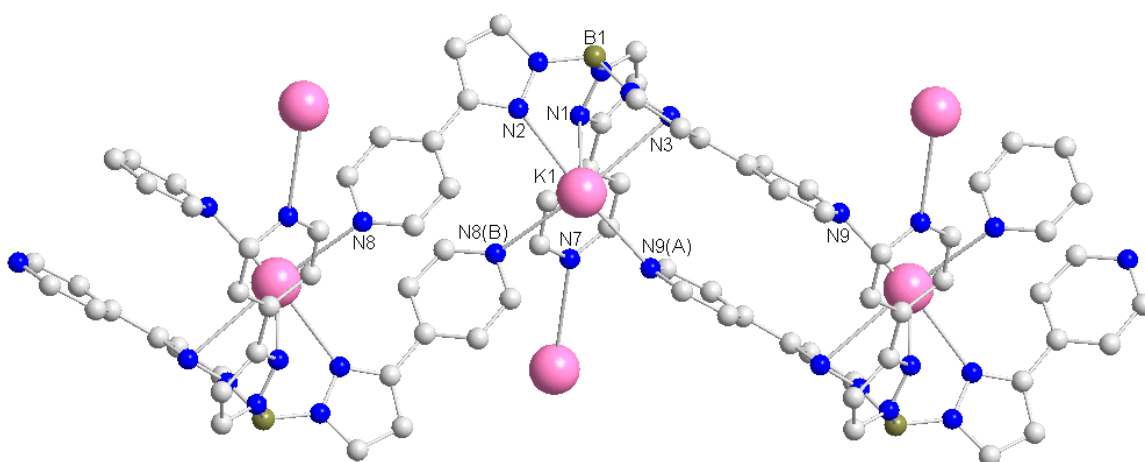


Figure 3.7. Atomic arrangements along zig-zag shaped one-dimensional chains in $\text{KTp}^{4\text{Py,Me}}$ **11**. The methyl groups in the 5-position of the pyrazoles have been omitted for clarity.

A significant part of the force linking adjacent $\text{KTp}^{4\text{Py,Me}}$ units inside the chains comes from a strong stacking interaction between the bridging pyridine rings.¹⁵¹ Specifically, the pair of bridging pyridine rings containing N(8) and N(8)B are parallel and separated from each other by an interplanar distance of 4.01 Å. Likewise, the pair of parallel bridging pyridyl rings containing N(9) and N(9)A are separated from each other by an interplanar distance of 3.92 Å.

Only few papers on structurally characterized potassium complexes of Tp ligands can be found in the literature.^{59,139,142} For example, the pyridyl substituted $\text{KTp}^{3\text{Py,Me}}$ and $\text{KTp}^{3(6\text{Me})\text{Py,Me}}$ have already been characterized in our group,⁵⁹ and show a pyridine coordination to the potassium ion similar to that found in complex **11**. The K-N bond distances reported for the coordinating pyridine nitrogens range from 2.90 to 3.06 Å. However, the coordination geometry around the potassium ion in these complexes is not exactly the same as in complex **11**.

3.5. Hydrotris (3-(4'-pyridyl)-5-methyl)pyrazolylborate zinc acetate $\text{Tp}^{4\text{Py,Me}}\text{Zn-OC(O)CH}_3$ **16**

Colourless crystals of **16** suitable for X-ray diffraction were obtained by slowly cooling down a saturated methanol solution. Complex **16** crystallizes in layers in the monoclinic crystal system, space group P2(1)/c. Its molecular structure was solved by Patterson methods and refined to a final R index of 0.058. As shown in figure 3.8, discrete molecules of **16** result from the coordination of the zinc center to three pyrazolyl nitrogens of one $\text{Tp}^{4\text{Py,Me}}$ and two oxygens of one acetate, which coordinates in an anisobidentate mode. In addition to one molecule of complex **16**, one methanol molecule is present in the asymmetric unit. Selected bond lengths and angles of **16** are listed in table 3.7.

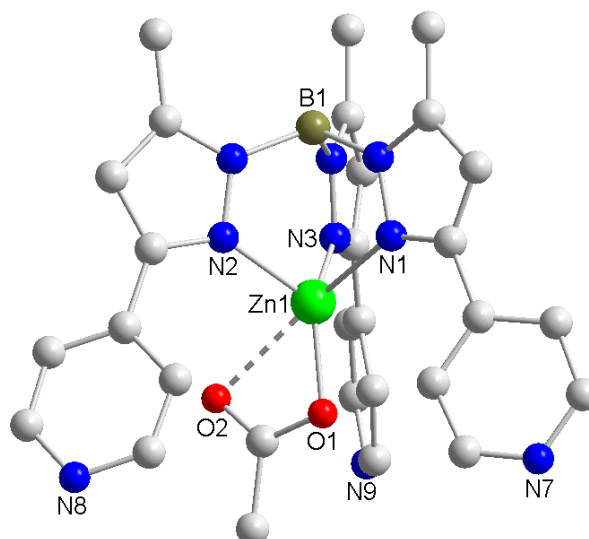


Figure 3.8. Molecular structure of $\text{Tp}^{4\text{-Py,Me}}\text{Zn-OC(O)CH}_3$ **16**.

Table 3.7. Selected bond lengths [\AA] and angles [$^\circ$] of $\text{Tp}^{4\text{-Py,Me}}\text{Zn-OC(O)CH}_3$ **16**.

Bond	[\AA]	Angle	[$^\circ$]
Zn(1)-O(1)	1.919(3)	O(1)-Zn(1)-N(3)	128.17(11)
Zn(1)-N(3)	2.018(3)	O(1)-Zn(1)-N(2)	124.07(13)
Zn(1)-N(2)	2.018(3)	N(3)-Zn(1)-N(2)	97.86(11)
Zn(1)-N(1)	2.108(3)	O(1)-Zn(1)-N(1)	114.19(11)
Zn(1)-O(2)	2.534(3)	N(3)-Zn(1)-N(1)	93.28(12)
		N(2)-Zn(1)-N(1)	89.12(10)
		O(1)-Zn(1)-O(2)	57.30(11)
		N(3)-Zn(1)-O(2)	98.46(11)
		N(2)-Zn(1)-O(2)	90.00(11)
		N(1)-Zn(1)-O(2)	168.24(10)

The Zn(1)-N bond distances for the nitrogens N(2) and N(3) are identical, while the Zn(1)-N(1) distance of 2.108 \AA is slightly longer. The asymmetry in the bonding of the acetate ligand to zinc, with Zn(1)-O bond distances of 1.92 and 2.53 \AA for O(1) and O(2) respectively, indicates the localization of its negative charge on O(1). Similar bond distances have been observed in other Tp based zinc acetate complexes like $\text{Tp}^{2\text{-Fu,Me}}\text{Zn-OC(O)CH}_3$ ¹²⁹ and $\text{Tp}^{3\text{-(6-Me)Py,Me}}\text{Zn-OC(O)CH}_3\cdot\text{B(OH)}_3$.⁹² For example, in $\text{Tp}^{2\text{-Fu,Me}}\text{Zn-OC(O)CH}_3$, the Zn-N bond distances range from 2.04 to 2.09 \AA and the

Zn-O bond distances, from 1.92 to 2.53 Å. In contrast, the acetate ligand of $\text{Tp}^{\text{tBu}}\text{Zn-OC(O)CH}_3$ binds zinc with substantially different Zn-O distances for both oxygen donors (1.86 and 2.95 Å).¹⁴⁵

In complex **16**, the coordination geometry around the five-coordinate Zn(1) ion can be described as highly distorted trigonal bipyramidal, the apical positions being occupied by N(1) and O(2). Five-coordinate zinc complexes can adopt a wide variety of geometries between a trigonal-bipyramid (TBP) and a square-pyramid (SP). Various procedures have been described to quantify the deviations of five-coordinate species from the ideal TBP or SP geometries.^{152,153} The simplest method uses a function of the two largest bonding angles at zinc, namely τ . The value of τ can vary from 1.00, for an ideal TBP, to 0.00, for an ideal SP. In complex **16**, a value of 0.67 has been calculated for τ , indicating a high deviation from the idealized trigonal bipyramidal geometry.

Tripodal zinc acetate complexes have generally served as models of bicarbonate coordination towards zinc in the enzyme human carbonic anhydrase II (HCA II).¹⁰¹ In fact, a comparison of the structure of **16** with that of the bicarbonate form of HCA II (Thr200[®]His200)¹⁵⁴ showed structural analogies between the binding mode of acetate in **16** and the binding mode of bicarbonate in the enzyme. The bonding parameters around the zinc center are shown in figure 3.9. The bicarbonate anion in HCA II(Thr200[®]His200) exhibits the same near-monodentate coordination mode as the acetate anion in the model complex **16**, with a weak second interaction of 2.5 Å between a bicarbonate oxygen and the zinc(II) ion.

However, important differences can be found in the interplanar angle between the best fit plane of the acetate ion (or bicarbonate ion in the enzyme), formed by O(1), O(2), C(29), and the plane defined by the zinc center and the two oxygen donors. This angle is near 0° in complex **16** and 34° in HCA II. This is known to be due to the hydrogen-bond interactions of the bicarbonate anion with a nearby Thr199 residue in the active site of HCA II, which do not occur in the model complex.

Finally, the hydrophilic character of the $\text{Tp}^{4\text{Py,Me}}$ ligand in complex **16** is shown by the fact that a pyridyl nitrogen is involved in a hydrogen bond to the co-crystallized methanol molecule. Specifically, N(7) is hydrogen bound to the methanol oxygen with a N(7)⋯O(3) bond distance of 2.83 Å.

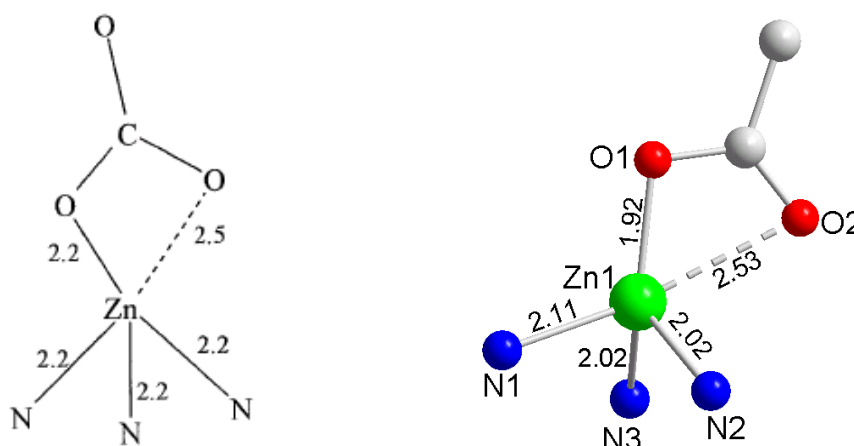


Figure 3.9. Coordination geometry of zinc in HCA II (Thr200[®]His200)¹⁵⁴ (left) and in $\text{Tp}^{4\text{Py,Me}}\text{Zn-OC(O)CH}_3$ **16** (right).

3.6. Hydrotris (3-(4'-pyridyl)-5-methyl)pyrazolylborate zinc nitrate $\text{Tp}^{4\text{Py,Me}}\text{Zn-ONO}_2$ **17**

Colourless crystals of **17** suitable for X-ray diffraction were obtained by slowly cooling down a saturated chloroform/methanol solution. Complex **17** belongs to the monoclinic crystal system, space group P2(1)/n. Its molecular structure was solved by direct methods and refined to a final R index of 0.052. The single-crystal X-ray diffraction study on **17** revealed a one-dimensional polymeric structure resulting from the coordination of one pyridyl nitrogen of each $\text{Tp}^{4\text{Py,Me}}$ ligand to a neighbouring zinc ion. Thus, each zinc ion is six-coordinated to three pyrazolyl nitrogens of one $\text{Tp}^{4\text{Py,Me}}$, two oxygens of one nitrate, which coordinates in a bidentate mode, and one pyridyl nitrogen belonging to an adjacent $\text{Tp}^{4\text{Py,Me}}\text{Zn-ONO}_2$ unit. The structure of **17** is shown in figure 3.10, and selected bond lengths and angles are listed in table 3.8.

In complex **17**, the Zn(1)-N bond distances for the pyrazolyl nitrogens N(1), N(2) and N(3) range from 2.10 to 2.26 Å, being significantly longer than those found in complex **16**, but very similar to those reported for several octahedral complexes of type $(\text{Tp})_2\text{Zn}$.^{145, 155} For example, in $(\text{Tp}^{2\text{Fu,Me}})_2\text{Zn}$ ¹²⁹ and $(\text{Tp}^{3\text{Py,Me}})_2\text{Zn}$,⁶⁰ the Zn-N bond distances for the pyrazolyl nitrogens range from 2.12 to 2.26 Å, and from 2.23 to 2.27 Å, respectively.

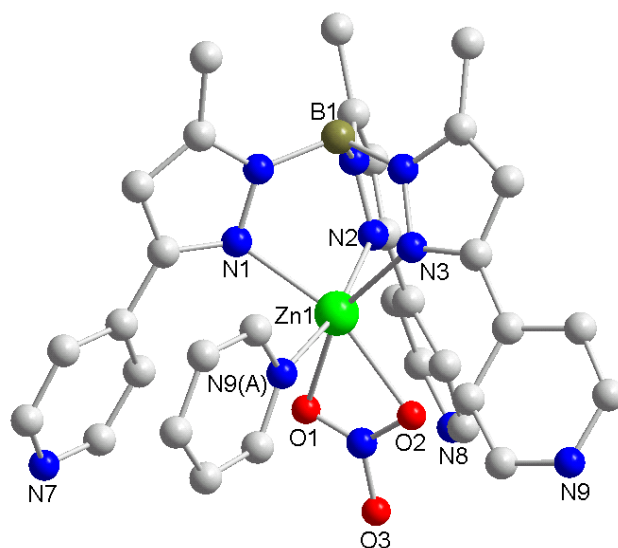


Figure 3.10. Zinc coordination geometry and atom labelling scheme for $\text{Tp}^{4\text{-Py,Me}}\text{Zn-ONO}_2$ **17**.

Table 3.8. Selected bond lengths [Å] and angles [°] of $\text{Tp}^{4\text{-Py,Me}}\text{Zn-ONO}_2$ **17**.

Bond	[Å]	Angle	[°]
Zn(1)-N(3)	2.102(3)	N(3)-Zn(1)-N(1)	99.56(12)
Zn(1)-N(1)	2.126(3)	N(3)-Zn(1)-O(1)	154.92(14)
Zn(1)-O(1)	2.189(4)	N(1)-Zn(1)-O(1)	105.41(14)
Zn(1)-O(2)	2.200(3)	N(3)-Zn(1)-O(2)	98.29(12)
Zn(1)-N(9)A	2.250(3)	N(1)-Zn(1)-O(2)	161.12(13)
Zn(1)-N(2)	2.263(3)	O(1)-Zn(1)-O(2)	57.22(13)
		N(3)-Zn(1)-N(9)A	93.56(11)
		N(1)-Zn(1)-N(9)A	84.02(11)
		O(1)-Zn(1)-N(9)A	91.39(12)
		O(2)-Zn(1)-N(9)A	88.77(11)
		N(3)-Zn(1)-N(2)	86.22(11)
		N(1)-Zn(1)-N(2)	84.72(12)
		O(1)-Zn(1)-N(2)	93.65(12)
		O(2)-Zn(1)-N(2)	102.60(12)
		N(9)A-Zn(1)-N(2)	168.54(11)

Regarding to the nitrate ligand in **17**, the Zn(1)-O bond distances of 2.19 and 2.20 Å, for O(1) and O(2) respectively, are nearly identical. It is known that a nitrate anion can bind to a single metal center by three different coordination modes, namely bidentate, anisobidentate and unidentate, which can be classified according to the geometrical criteria summarized in figure 3.11 and table 3.9.¹⁵⁶

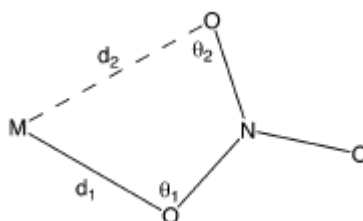
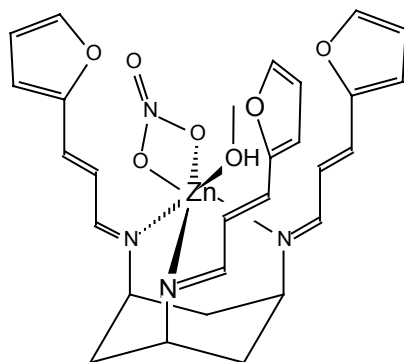


Figure 3.11. Geometrical parameters used for assigning nitrate coordination modes.

Table 3.9. Criteria for assigning nitrate coordination modes.

	unidentate	anisobidentate	bidentate
d_2-d_1 [Å]	>0.6	0.3-0.6	<0.3
$\theta_1-\theta_2$ [°]	>28	14-28	<14

On the basis of these criteria, previous studies on $\text{TpZn}(\text{NO}_3)$ and $[\text{PimZn}(\text{NO}_3)]^+$ complexes, Pim denoting a neutral tris(imidazolyl)phosphine, have demonstrated the preference of nitrate for unidentate and anisobidentate coordination towards zinc in complexes based on these types of tripodal ligands.^{99, 100} In contrast, the nitrate ligand in **17** binds zinc in a clearly bidentate mode, with a value of d_2-d_1 near 0 Å and a $\theta_1-\theta_2$ value of 1.5°, θ_1 and θ_2 corresponding to the angles N(10)-O(1)-Zn(1) and N(10)-O(2)-Zn(1) respectively. This can be compared to the octahedral complex $[(\text{fr-protach})\text{Zn}(\eta^2\text{-O}_2\text{NO})(\text{MeOH})]^+$ (**XI**),¹⁰¹ which contains a bidentate nitrate ligand and a methanol ligand. In complex **XI**, the tendency of nitrate to coordinate in a bidentate fashion to zinc is favoured by coordination of a solvent molecule to give the zinc ion a near-octahedral coordination geometry. Similarly, in complex **17** the bidentate coordination of nitrate to zinc is favoured by coordination of a pyridyl nitrogen belonging to a neighbouring $\text{Tp}^{4\text{Py,Me}}\text{Zn-ONO}_2$ unit. Thus, the resulting coordination sphere around the six-coordinated Zn(1) can be described as near-octahedral, with an average deviation of the bond angles of 10.6° from those of a regular octahedron.



XI

As shown in figure 3.12, pyridyl coordination to a neighbouring zinc ion results in the formation of a zigzag-shaped one-dimensional polymer, which is partially stabilized through a stacking interaction between the bridging pyridine ring containing N9(A) and the non-bridging pyridine ring containing N(7). The interplanar distance is 3.74 Å and the slip angle 12.5°.

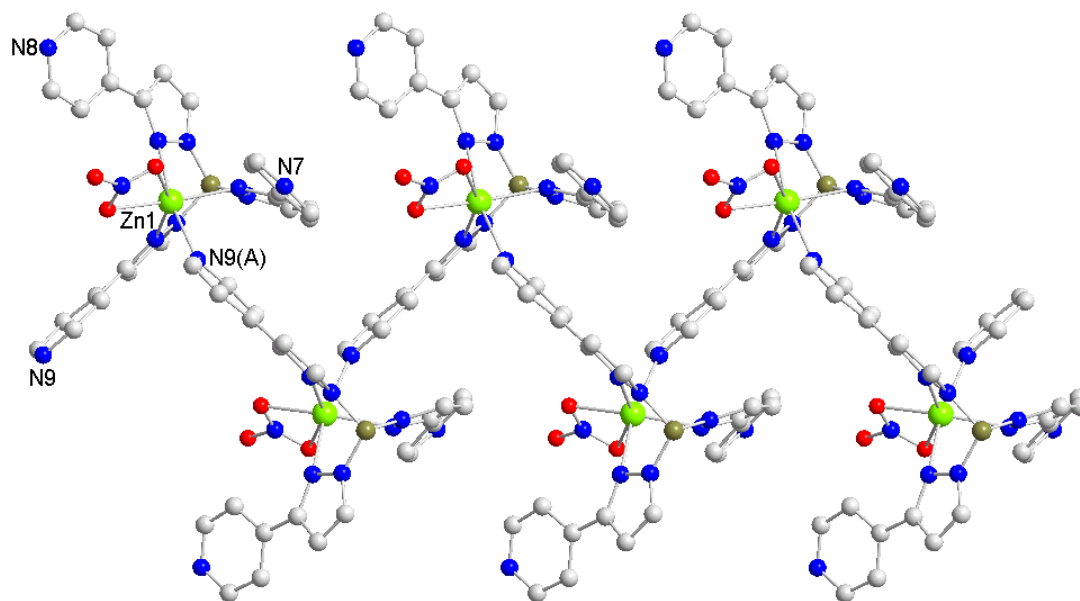


Figure 3.12. Atomic arrangements along zig-zag shaped one-dimensional chains in $\text{Tp}^{4\text{-Py,Me}}\text{Zn-ONO}_2$ **17**. The methyl groups in the 5-position of the pyrazoles have been omitted for clarity.

3.7. Hydrotris(3-(4'-pyridyl)-5-methyl)pyrazolylborate zinc aqua complex [Tp^{4'Py,Me}Zn·OH₂]₂ClO₄ **18**

Colourless crystals of **18** suitable for X-ray diffraction were obtained by slowly cooling down a saturated dichloromethane/methanol/water solution. Complex **18** belongs to the monoclinic crystal system, space group P2(1)/c. Its molecular structure was solved by direct methods and refined to a final R index of 0.081. The single-crystal X-ray diffraction study revealed that **18** forms dimeric molecules in the solid state, the dimerization resulting from the coordination of one pyridyl nitrogen of each Tp^{4'Py,Me} ligand to the opposing zinc ion. Thus, each zinc ion is coordinated to three pyrazolyl nitrogens of one Tp^{4'Py,Me} ligand, the oxygen donor of one neutral aqua ligand and one pyridyl nitrogen of an adjacent [Tp^{4'Py,Me}Zn·OH₂]⁺ unit. In figure 3.13, the two independent molecules of **18** present in the asymmetric unit are shown. Additionally, two perchlorate anions, four water molecules, two methanol molecules and one dichloromethane molecule are found in the asymmetric unit. Two highly distorted solvent molecules (one methanol and one dichloromethane) as well as three water molecules were treated as a diffused contribution using the program SQUEEZE (Platon Library).¹⁵⁷ The determined and calculated density and absorption coefficients include the solvent molecules but individual atoms do not appear in the atom list.

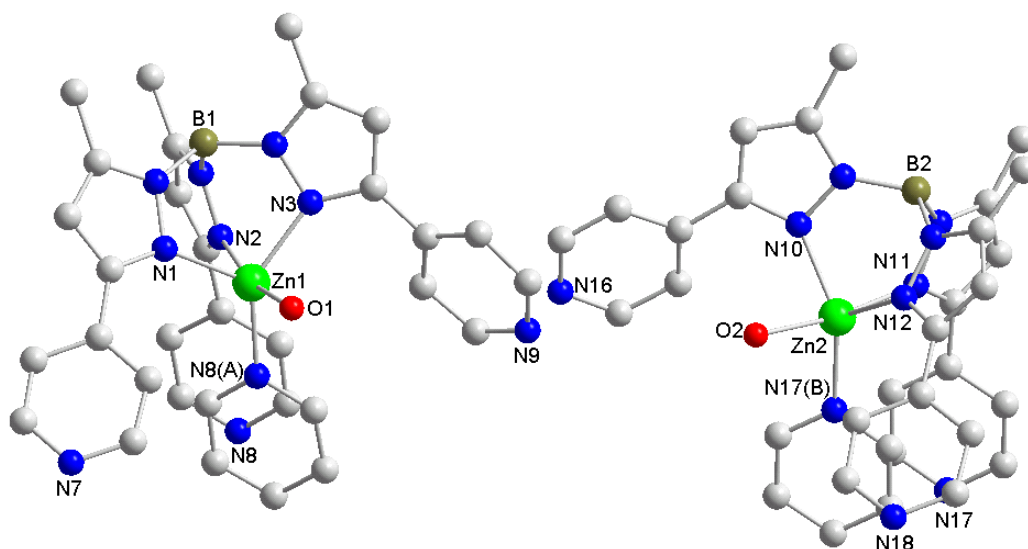


Figure 3.13. Structure of the two independent molecules of [Tp^{4'Py,Me}Zn·OH₂]₂ClO₄ **18** present in the asymmetric unit. The perchlorate anions and the solvent molecules have been omitted for clarity.

In complex **18**, the coordination geometry around the five-coordinate Zn(1) and Zn(2) ions can be described as highly distorted trigonal bipyramidal, the axis of the bipyramid being defined by the nitrogen donor of a pyrazole, the zinc ion and the oxygen donor of the neutral aqua ligand, i.e. N(2)-Zn(1)-O(1) and N(11)-Zn(2)-O(2) respectively. The deviation from the idealized trigonal bipyramidal geometry is well expressed in the τ value of 0.53 and 0.48 for Zn(1) and Zn(2) respectively. Selected bond lengths and angles are listed in tables 3.10 and 3.11.

Table 3.10. Selected bond lengths [\AA] of $[\text{Tp}^{4\text{Py,Me}}\text{Zn}\cdot\text{OH}_2]\text{ClO}_4$ **18**.

Bond	[\AA]	Bond	[\AA]
Zn(1)-N(8)A	2.005(5)	Zn(2)-N(17)B	2.011(5)
Zn(1)-N(3)	2.025(5)	Zn(2)-N(12)	2.024(5)
Zn(1)-N(1)	2.031(5)	Zn(2)-N(10)	2.060(5)
Zn(1)-O(1)	2.168(4)	Zn(2)-O(2)	2.139(4)
Zn(1)-N(2)	2.352(5)	Zn(2)-N(11)	2.278(5)

Table 3.11. Selected bond angles [$^\circ$] of $[\text{Tp}^{4\text{Py,Me}}\text{Zn}\cdot\text{OH}_2]\text{ClO}_4$ **18**.

Angle	[$^\circ$]	Angle	[$^\circ$]
N(8)-Zn(1)-N(3)	137.2(2)	N(17)-Zn(2)-N(12)	116.8(2)
N(8)-Zn(1)-N(1)	119.29(19)	N(17)-Zn(2)-N(10)	142.9(2)
N(3)-Zn(1)-N(1)	103.36(19)	N(12)-Zn(2)-N(10)	100.13(19)
N(8)-Zn(1)-O(1)	92.35(16)	N(17)-Zn(2)-O(2)	91.82(17)
N(3)-Zn(1)-O(1)	87.57(17)	N(12)-Zn(2)-O(2)	96.08(16)
N(1)-Zn(1)-O(1)	94.37(17)	N(10)-Zn(2)-O(2)	87.24(16)
N(8)-Zn(1)-N(2)	95.95(17)	N(17)-Zn(2)-N(11)	93.56(17)
N(3)-Zn(1)-N(2)	81.51(17)	N(12)-Zn(2)-N(11)	86.84(17)
N(1)-Zn(1)-N(2)	87.77(17)	N(10)-Zn(2)-N(11)	84.85(17)
O(1)-Zn(1)-N(2)	169.07(15)	O(2)-Zn(2)-N(11)	171.94(16)

The Zn-N bond distances for the pyrazolyl nitrogens in equatorial positions, N(1), N(3) in the case of Zn(1) and N(10), N(12) in the case of Zn(2), are nearly identical ($2.04 \pm 0.02 \text{ \AA}$). In contrast, the Zn(1)-N(2) and Zn(2)-N(11) bond distances involving

the axial pyrazolyl nitrogens are significantly longer (2.35 and 2.28 Å respectively). This asymmetry in the bonding of the $\text{Tp}^{4\text{Py,Me}}$ ligand to zinc has already been observed in the binuclear complexes $(\text{Tp}^{3\text{Py,Me}}\text{Zn})_2(\text{O}_2\text{H}_3)\text{ClO}_4$ and $(\text{Tp}^{\text{Pic,Me}}\text{Zn})_2(\text{O}_2\text{H}_3)\text{ClO}_4$.⁸⁷ In these complexes, each zinc ion is also five-coordinated in a slightly distorted trigonal bipyramidal geometry due to attachment of one pyridyl nitrogen. The equatorial pyrazolyl nitrogens are attached at normal distances (2.01-2.05 Å), while the axial pyrazolyl nitrogens are found at 2.31-2.49 Å. Additionally, a long Zn-N bond of 2.29 and 2.39 Å, for $(\text{Tp}^{3\text{Py,Me}}\text{Zn})_2(\text{O}_2\text{H}_3)\text{ClO}_4$ and $(\text{Tp}^{\text{Pic,Me}}\text{Zn})_2(\text{O}_2\text{H}_3)\text{ClO}_4$ respectively, involves the pyridine nitrogen occupying one apex of the bipyramid. In contrast, in complex **18** much shorter bond distances have been found for the coordinating pyridine nitrogens, which occupy equatorial positions (Zn(1)-N(8)A and Zn(2)-N(17)B of 2.01 Å).

Regarding to the aqua ligand in **18**, the Zn-O bond distances of 2.14 and 2.17 Å, for Zn(1) and Zn(2) respectively, are significantly longer than those found for the tetrahedral aqua complexes $[\text{Tp}^{t\text{Bu,Me}}\text{Zn}\cdot\text{OH}_2][\text{HOB}(\text{C}_6\text{F}_5)_3]^{103}$ (1.93 Å) and $[(\text{X}_6\text{R}_3\text{ImR}_3)\text{Zn}(\text{OH}_2)_2](\text{ClO}_4)_2^{30}$ (1.97 Å), ($\text{X}_6\text{R}_3\text{ImR}_3$) being a tris(imidazolyl)-calixarene ligand, but in the range of those found for the recently reported trigonal pyramidal $[(\text{TriMIm})\text{Zn}\cdot\text{OH}_2]^{2+}$ ³¹ (2.13 Å) and for the trigonal bipyramidal $[(\text{tren})\text{Zn}\cdot\text{OH}_2](\text{ClO}_4)_2^{107}$ (2.12 Å).

As shown in figure 3.14, the pyridyl coordination to a neighbouring zinc ion occurring in complex **18** results in the formation of dimeric molecules in the solid state instead of polymeric chains, as in the case of **17** (Figure 3.12). Thus, two $[\text{Tp}^{4\text{Py,Me}}\text{Zn}\cdot\text{OH}_2]^+$ units are held together by one pair of bridges, which involves the pyridine ring containing N(8) and its symmetrically equivalent, the center of the dimer residing upon a center of inversion. A significant part of the force linking the two $[\text{Tp}^{4\text{Py,Me}}\text{Zn}\cdot\text{OH}_2]^+$ units comes from a strong stacking interaction between the bridging pyridine rings which are separated by an interplanar distance of 3.73 Å with a slip angle of 0.02°. In the second molecule present in the asymmetric unit, the bridging pyridine containing N(17) is also stacked on its symmetrically equivalent of an opposing $[\text{Tp}^{4\text{Py,Me}}\text{Zn}\cdot\text{OH}_2]^+$ unit, with an interplanar distance of 3.57 Å and a slip angle of 0.03°. The linking pattern provided by the two pyridyl groups stacked across a center of symmetry closely resembles that in the zinc halide complexes of $\text{Tp}^{3\text{Py,Me}}$.⁶⁰

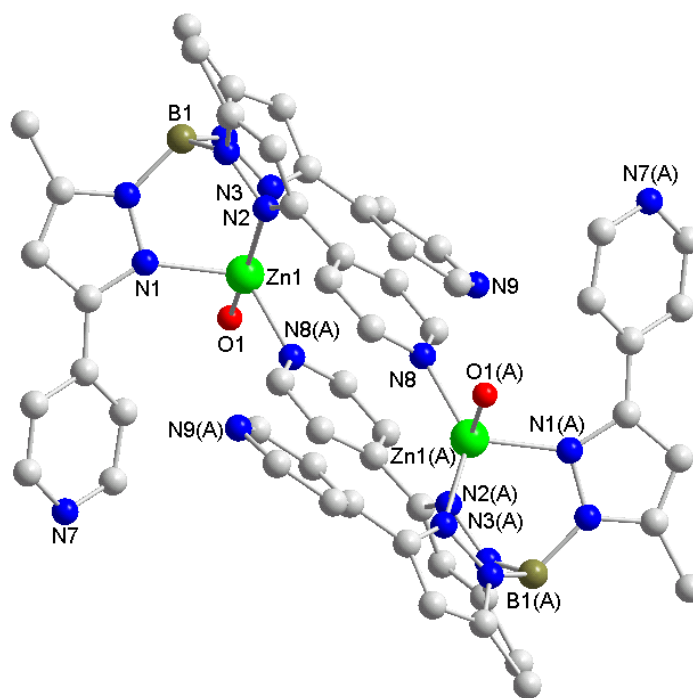


Figure 3.14. Dimeric unit related to Zn(1) in $[\text{Tp}^{4\text{-Py,Me}}\text{Zn}\cdot\text{OH}_2]\text{ClO}_4$ **18**.

The novel aqua complex **18** possesses remarkable structural similarities with the resting state of relevant zinc metalloenzymes, such as carbonic anhydrase II (CA II). Specifically, the Zn-O bond distance for the aqua ligand (2.14-2.17 Å) is only slightly longer than that found for the zinc bound water molecule in the active site of CA II crystallized at pH 6 (2.05 Å). The latter is found to be strongly hydrogen bound to a threonine residue ($\text{O}\cdots\text{O}$ 2.69 Å) and to two water molecules, one of which is called “deep water” due to its very short distance from the zinc bound aqua ligand ($\text{O}\cdots\text{O}$ 2.43 Å).⁹ Also this feature finds analogy in the intermolecular H-bonding network present in the crystal structure of **18**, in which the zinc bound water molecule, the pyridine nitrogens of the $\text{Tp}^{4\text{-Py,Me}}$ system and different solvent molecules are involved (Figure 3.15).

Table 3.12. $\text{O}\cdots\text{O}$ distances [Å] for the H-bonding interactions found in the asymmetric unit of $[\text{Tp}^{4\text{-Py,Me}}\text{Zn}\cdot\text{OH}_2]\text{ClO}_4$ **18**.

Bond	[Å]
$\text{O}(1)\cdots\text{O}(12)$	2.69
$\text{O}(2)\cdots\text{O}(11)$	2.65
$\text{O}(11)\cdots\text{N}(9)$	2.80

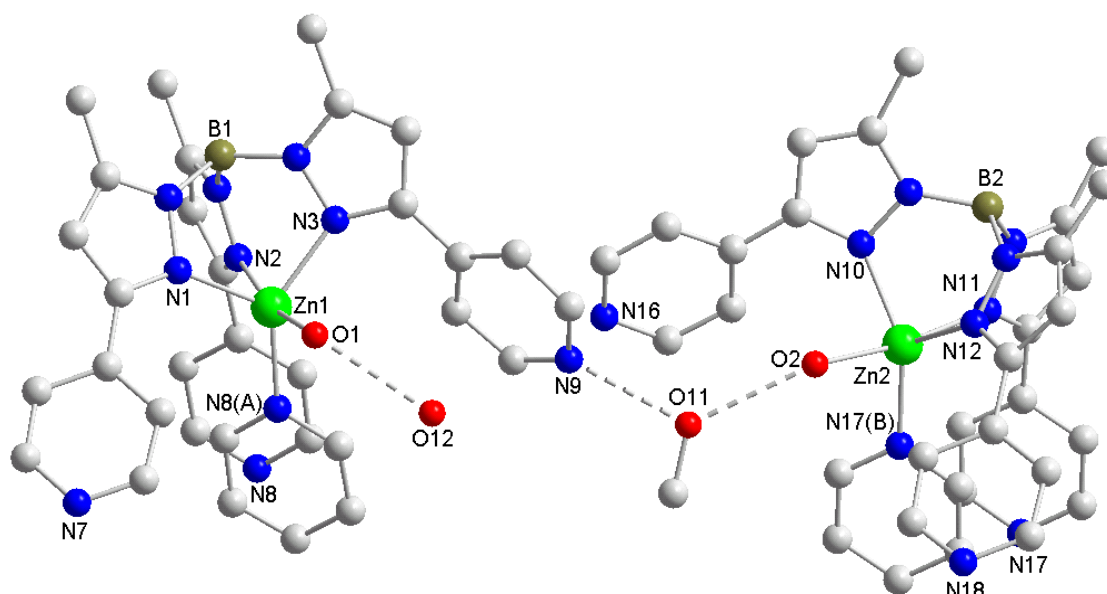


Figure 3.15. Hydrogen bonding network found in the asymmetric unit of $[\text{Tp}^{4\text{-Py,Me}}\text{Zn}\cdot\text{OH}_2]\text{ClO}_4$ **18**.

3.8. Hydrotris(3-(4'-pyridyl)-5-methyl)pyrazolylborate zinc methanol complex $[\text{Tp}^{4\text{-Py,Me}}\text{Zn}\cdot\text{HOME}]\text{ClO}_4$ **19**

Colourless crystals of **19** suitable for X-ray diffraction were obtained by slowly cooling down a saturated dichloromethane/methanol solution. Complex **19** belongs to the triclinic crystal system, space group P-1. Its molecular structure was solved by direct methods and refined to a final R index of 0.053. The structure determination of **19** confirmed that it differs from complex **18** only in the identity of the neutral ligand binding zinc, both compounds showing similar molecular structures despite crystallizing in different space groups. Figure 3.16 shows that **19**, just like **18**, can be described as composed in the solid state of dimers held together across a center of symmetry by one pyridyl substituent. Each zinc ion is five-coordinated to the three pyrazole nitrogens of one $\text{Tp}^{4\text{-Py,Me}}$ ligand and the oxygen donor of one neutral methanol ligand, in addition to one pyridine nitrogen, which is part of a neighbouring $[\text{Tp}^{4\text{-Py,Me}}\text{Zn}\cdot\text{HOME}]^+$ unit.

One molecule of $[\text{Tp}^{4\text{-Py,Me}}\text{Zn}\cdot\text{HOME}]^+$ and one highly distorted perchlorate counterion are present in the asymmetric unit of **19**. The Cl(1) atom was refined in two

positions, each with 50% occupancy. Additionally, two water molecules, six highly distorted methanol molecules and one dichloromethane molecule were found in the asymmetric unit. They were treated as a diffused contribution using the program SQUEEZE (Platon Library). The determined and calculated density and absorption coefficients include the solvent molecules but individual atoms do not appear in the atom list.

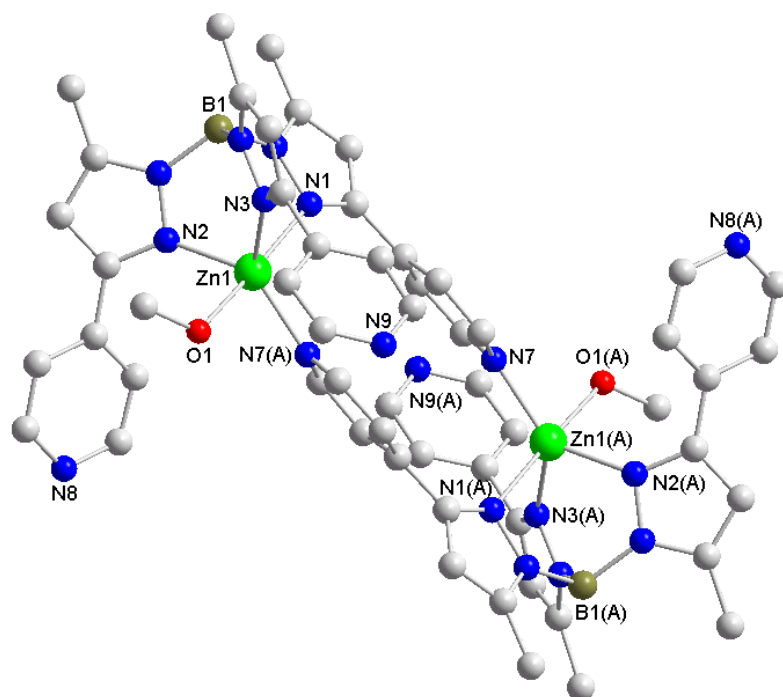


Figure 3.16. Dimeric unit of $[\text{Tp}^{4\text{Py,Me}}\text{Zn}\cdot\text{HOME}]\text{ClO}_4$ **19**. The two perchlorate anions have been omitted for clarity.

In complex **19**, the coordination polyhedron around the five-coordinate Zn(1) ion can be described as a rather regular trigonal bipyramid ($\tau = 0.70$), with the axis N(1)-Zn(1)-O(1) being defined by the nitrogen donor of a pyrazole, the zinc ion and the oxygen donor of the neutral methanol ligand. The equatorial plane is defined by the pyrazole nitrogens N(2) and N(3) of one $\text{Tp}^{4\text{Py,Me}}$ ligand, and the pyridine nitrogen N(7)A of the opposite $[\text{Tp}^{4\text{Py,Me}}\text{Zn}\cdot\text{HOME}]^+$ unit. The Zn(1) ion lies out of this plane with a root-mean-square deviation from the plane of 0.06 Å in direction to N(1). Nearly negligible deviations from the equatorial plane have also been observed for Zn(1) and Zn(2) in

complex **18**. Further bond angles and selected bond lengths of complex **19** are listed in table 3.13.

Table 3.13. Selected bond lengths [\AA] and angles [$^\circ$] of $[\text{Tp}^{4\text{Py,Me}}\text{Zn}\cdot\text{HOMe}]\text{ClO}_4$ **19**.

Bond	[\AA]	Angle	[$^\circ$]
Zn(1)-N(7)A	2.034(2)	N(7)A-Zn(1)-N(2)	131.95(9)
Zn(1)-N(2)	2.047(2)	N(7)A-Zn(1)-N(3)	129.01(9)
Zn(1)-N(3)	2.047(2)	N(2)-Zn(1)-N(3)	98.78(10)
Zn(1)-O(1)	2.185(2)	N(7)A-Zn(1)-O(1)	84.65(9)
Zn(1)-N(1)	2.210(2)	N(2)-Zn(1)-O(1)	90.91(9)
		N(3)-Zn(1)-O(1)	90.65(10)
		N(7)A-Zn(1)-N(1)	98.83(9)
		N(2)-Zn(1)-N(1)	90.40(9)
		N(3)-Zn(1)-N(1)	83.33(9)
		O(1)-Zn(1)-N(1)	173.97(9)

The bond distances around Zn(1) are cleanly grouped into three short ones for the equatorial and two long ones for the axial ligands. In analogy to complex **18**, the equatorial pyrazolyl nitrogens N(2) and N(3) are attached at a distance of 2.05 \AA , while the axial pyrazolyl nitrogen N(1) is attached at 2.21 \AA . The Zn(1)-N7(A) bond distance for the bridging pyridine is almost identical to the average value of 2.01 \AA given for complex **18**, but much shorter than those reported for the dimeric zinc halide complexes of $\text{Tp}^{3\text{Py,Me}}$.⁶⁰ For example, in $\text{Tp}^{3\text{Py,Me}}\text{Zn-I}$ the large size of the iodide ligand results in an extremely long Zn-N bond distance for the bridging pyridine nitrogen of ca. 3.03 \AA . The coordination geometry around the zinc ion can no longer be described as trigonal bipyramidal, but as distorted pseudotetrahedral, which can be compared to the atomic arrangement in the initial stage of a $\text{S}_{\text{N}}2$ substitution at a tetrahedral zinc(II) center.¹¹⁶

Regarding to the methanol ligand in **19**, the Zn(1)-O(1) bond distance of 2.18 \AA is significantly longer than those reported for several tetrahedral alcohol complexes based on sulphur rich tripodal ligands, such as $[\text{Tm}^{\text{R}}\text{Zn}(\text{HOR})]^+(\text{HOR})$,^{106, 158} Tm^{R} denoting a tris(thioimidazolyl)borate (ca. 2.00 \AA), and the pyrazolylbis(thioimidazolyl)borate zinc

ethanol complex $\{[(pz^{Ph,Me})Bm^{o-An}]Zn \cdot HOEt\} \cdot (ClO_4) \cdot EtOH$ (1.97 Å).¹⁰⁴ However, the Zn(1)-O(1) bond distance is only marginally longer than those observed for the aqua ligand in complex **18**, and in the range of that reported for the trigonal bipyramidal $[(tren)Zn \cdot HOME](ClO_4)$ (BPh₄) (2.11 Å).¹⁵⁹

In complex **19**, two $[Tp^{4Py,Me}Zn \cdot HOME]^+$ units are held together by one pair of bridges involving the pyridine ring with N(7) and its symmetry equivalent, as already shown in figure 3.16. There exist a strong stacking interaction between the two parallel pyridine rings, which are separated by an interplanar distance of 3.52 Å. More interestingly, a second pyridine ring of each $Tp^{4Py,Me}$ ligand is involved in a hydrogen bond to the methanol ligand of a neighbouring $[Tp^{4Py,Me}Zn \cdot HOME]^+$ unit, thereby generating double chains (Figure 3.17). These H-bonding interactions were established clearly by locating the hydroxyl hydrogen atom H(2) in the difference Fourier maps. Thus, the N(8)B \cdots H(2) bond distance is 1.99 Å. In addition to this hydrogen bonding interaction, there is a stacking interaction between the two symmetrically equivalent pyridine rings containing N(8) and N8(B), with an interplanar distance of 3.76 Å and a slip angle of 0.04°.

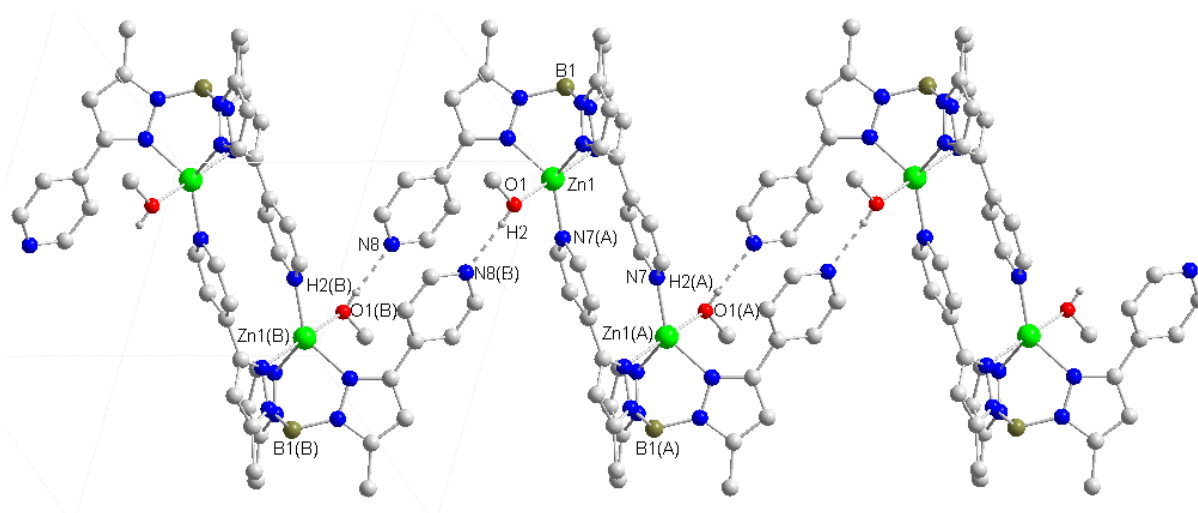


Figure 3.17. Atomic arrangements along zig-zag shaped one-dimensional chains in $[Tp^{4Py,Me}Zn \cdot HOME]ClO_4$ **19**. Only the hydroxyl hydrogen H(2) of the methanol ligand is shown.

3.9. Bis (hydrotris (3-(4'-pyridyl)-5-methyl)pyrazolylborate)-zinc-bis (hydrotris (3-(4'-pyridyl)-5-methyl)pyrazolylborate zinc hydroxide) [(Tp^{4'Py,Me})₂Zn][Tp^{4'Py,Me}Zn-OH]₂ **21**

Colourless crystals of **21** suitable for X-ray diffraction were obtained by slowly evaporating the solvent of a saturated dichloromethane/methanol solution. Complex **21** belongs to the monoclinic crystal system, space group C2/c. Its structure was solved by direct methods and refined to a final R index of 0.060. The single-crystal X-ray diffraction study revealed that **21** forms trimers in the solid state consisting of one (Tp^{4'Py,Me})₂Zn unit linked by two of its six pyridylpyrazolyl groups to two neighbouring Tp^{4'Py,Me}Zn-OH units. The molecular structure of **21** is shown in figure 3.18. In addition to one half molecule of **21**, the asymmetric unit contains one water molecule and two dichloromethane molecules, one of them being partially shared by two unit cells. The zinc ion of the (Tp^{4'Py,Me})₂Zn unit is coordinated to six pyrazolyl nitrogens in an octahedral coordination geometry. The zinc ions of the Tp^{4'Py,Me}Zn-OH units are coordinated to three pyrazolyl nitrogens of one Tp^{4'Py,Me} ligand, one pyridyl nitrogen of the adjacent (Tp^{4'Py,Me})₂Zn unit and one hydroxide anion.

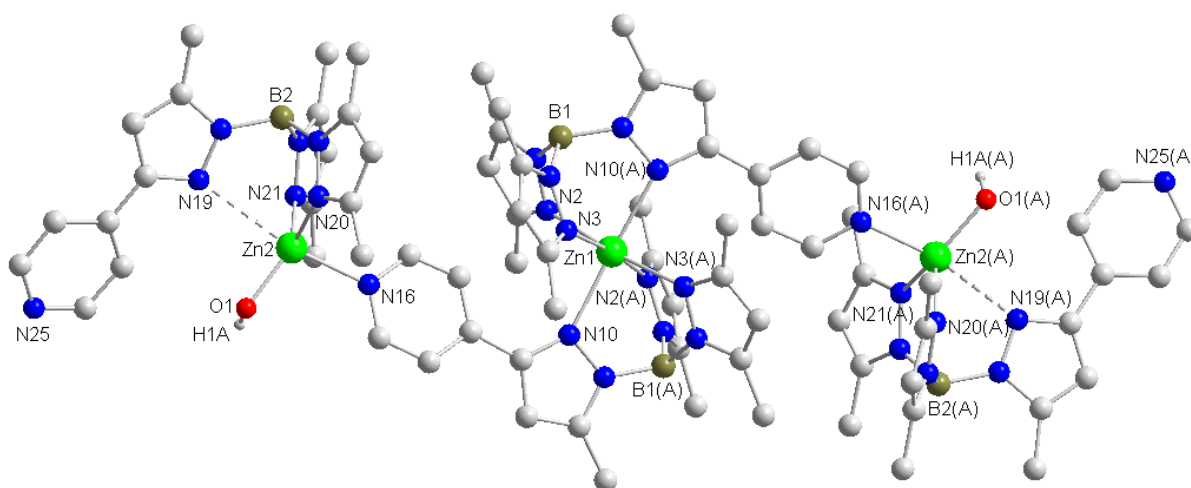


Figure 3.18. Solid state structure of [(Tp^{4'Py,Me})₂Zn][Tp^{4'Py,Me}Zn-OH]₂ **21**. The pyridyl substituents on the pyrazole rings which are not involved in the coordination to zinc have been omitted for clarity. Only the hydroxyl hydrogens, H(1A) and H1A(A), are shown.

Selected bonding parameters for Zn(1) are listed in table 3.14. The coordination geometry of the six-coordinated Zn(1) can be described as octahedral to a good approximation. The average deviation of the bond angles from those of a regular octahedron is 4.2°. The Zn(1)-N bond distances for the pyrazolyl nitrogens range from 2.19 to 2.29 Å, being very similar to those reported for several octahedral (Tp)₂Zn complexes.^{145, 160} For example, in (Tp^{2-Fu,Me})₂Zn¹²⁹ and (Tp^{3-Py,Me})₂Zn,⁶⁰ the Zn-N bond distances range from 2.12 to 2.26 Å, and from 2.23 to 2.27 Å, respectively.

Table 3.14. Selected bond lengths [Å] and angles [°] of Zn(1) in complex **21**.

Bond	[Å]	Angle	[°]
Zn(1)-N(3)	2.186(3)	N(3)-Zn(1)-N(3)A	97.30(17)
Zn(1)-N(3)A	2.186(3)	N(3)-Zn(1)-N(2)A	172.34(12)
Zn(1)-N(2)A	2.214(3)	N(3)A-Zn(1)-N(2)A	88.16(12)
Zn(1)-N(2)	2.214(3)	N(3)-Zn(1)-N(2)	88.16(12)
Zn(1)-N(10)A	2.285(3)	N(3)A-Zn(1)-N(2)	172.34(12)
Zn(1)-N(10)	2.285(3)	N(2)A-Zn(1)-N(2)	86.93(17)
		N(3)-Zn(1)-N(10)A	89.13(11)
		N(3)A-Zn(1)-N(10)A	85.71(11)
		N(2)A-Zn(1)-N(10)A	96.65(11)
		N(2)-Zn(1)-N(10)A	89.02(11)
		N(3)-Zn(1)-N(10)	85.71(11)
		N(3)A-Zn(1)-N(10)	89.13(11)
		N(2)A-Zn(1)-N(10)	89.02(11)
		N(2)-Zn(1)-N(10)	96.65(11)
		N(10)A-Zn(1)-N(10)	172.20(16)

Figure 3.19 shows how the six pyridylpyrazolyl groups are intertwined in a propellerlike fashion. There are stacking interactions between the pyrazolyl and the pyridyl rings of both opposing Tp^{4-Py,Me} ligands, with an average interplanar distance of 3.93 Å and an average slip angle of 31.2°. The stacking interaction is weaker for the bridging pyridines containing N(16) and N16(A), which are separated from the closest

pyrazolyl ring (that with N(3) and N3(A) respectively) by an interplanar distance of 4.09 Å and a slip angle of 39.0°.

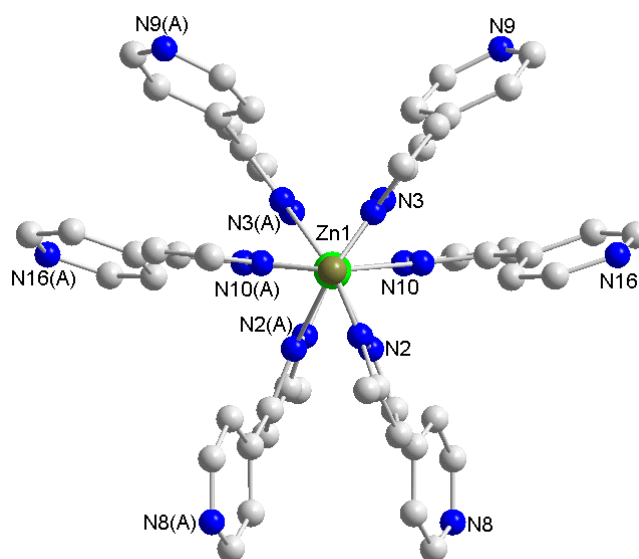


Figure 3.19. Perspective view along the B(1)-Zn(1)-B1(A) axis of the $(\text{Tp}^{4\text{Py,Me}})_2\text{Zn}$ unit in **21**. Only the pyrazolyl nitrogens coordinating to zinc and the pyridyl nitrogens have been labelled.

Regarding the $\text{Tp}^{4\text{Py,Me}}\text{Zn-OH}$ units (Figure 3.20), selected bonding parameters for Zn(2) are listed in table 3.15. The average Zn(2)-N bond distance of 2.04 Å for the pyrazolyl nitrogens N(20) and N(21) is in the normal range, while a distance of 2.80 Å between the pyrazolyl nitrogen N(19) and Zn(2) suggests the partial detachment of the $\text{Tp}^{4\text{Py,Me}}$ ligand from zinc. This is not unprecedented since Zn-N bond distances of 3.09 and 2.96 Å have been reported before for one nitrogen donor of the Tp ligand in $\text{Tp}^{\text{Cum,Me}}\text{Zn-OP(O)(OPh)}_2$ ¹⁶¹ and $\text{Tp}^{\text{Ph,Me}}\text{Zn-(p-nitroanilido-leucine)}$,⁶⁹ respectively. In complex **21**, the highly unsymmetrical binding of $\text{Tp}^{4\text{Py,Me}}$ to Zn(2), with one Zn-N(pyrazole) bond much longer than the other two, is a consequence of the additional coordination of a neighbouring pyridine through its nitrogen donor N(16). The resulting highly unsymmetrical coordination geometry around Zn(2) can be described as intermediate between a flattened tetrahedron with N(16) at the apex, and an elongated trigonal bipyramid with N(16) at the short and N(19) at the long apex, forming a N(16)-Zn-N(19) angle of 165.7°.

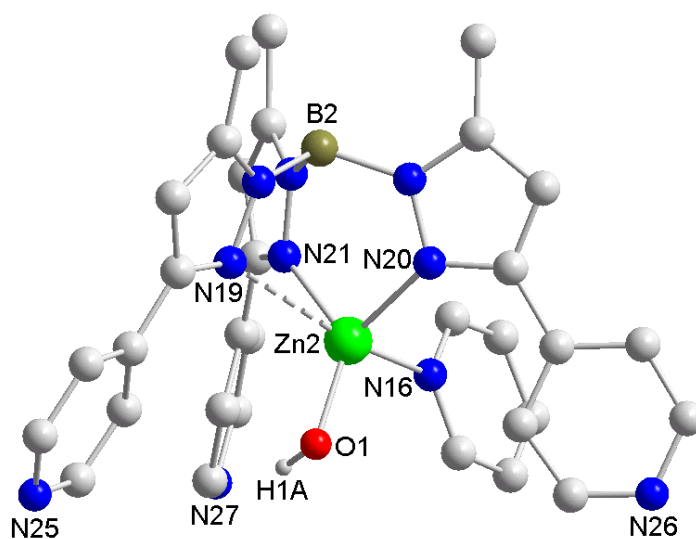


Figure 3.20. Zinc coordination geometry and atom labelling scheme of the $\text{Tp}^{4\text{-Py,Me}}\text{Zn-OH}$ unit in **21**.

Table 3.15. Selected bond lengths [\AA] and angles [$^\circ$] of Zn(2) in complex **21**.

Bond	[\AA]	Angle	[$^\circ$]
Zn(2)-O(1)	1.874(3)	O(1)-Zn(2)-N(21)	131.39(13)
Zn(2)-N(21)	2.039(3)	O(1)-Zn(2)-N(20)	122.01(13)
Zn(2)-N(20)	2.048(3)	N(21)-Zn(2)-N(20)	100.21(13)
Zn(2)-N(16)	2.118(3)	O(1)-Zn(2)-N(16)	103.13(13)
Zn(2) \cdots N(19)	2.805(3)	N(21)-Zn(2)-N(16)	93.93(13)
		N(20)-Zn(2)-N(16)	96.57(13)
		O(1)-Zn(2)-N(19)	89.06(13)
		N(19)-Zn(2)-N(16)	165.74(13)
		N(20)-Zn(2)-N(19)	82.84(13)
		N(19)-Zn(2)-N(21)	72.25(13)

3.10. Hydrotris(3-(4'-pyridyl)-5-methyl)pyrazolylborate)-zinc-methylcarbonate-Hydrotris(3-(4'-pyridyl)-5-methyl)pyrazolylborate)-zinc-chloride
[Tp^{4'Py,Me}Zn-OC(O)OMe][Tp^{4'Py,Me}Zn-Cl] 22

Colourless crystals of 22 suitable for X-ray diffraction were obtained by cooling to 5°C a saturated dichloromethane/methanol/water solution. Complex 22 belongs to the monoclinic crystal system, space group C2/c. Its structure was solved by direct methods and refined to a final R index of 0.072. The single-crystal X-ray diffraction study revealed that 22 forms one-dimensional polymers consisting of one methylcarbonate complex Tp^{4'Py,Me}Zn-OC(O)OMe and one chloride complex Tp^{4'Py,Me}Zn-Cl, linked to each other through pyridyl nitrogen donors. The zinc ions in Tp^{4'Py,Me}Zn-OC(O)OMe and Tp^{4'Py,Me}Zn-Cl are coordinated to three pyrazolyl nitrogens of one Tp^{4'Py,Me} ligand, one pyridyl nitrogen of an adjacent Tp^{4'Py,Me}Zn unit and either one methylcarbonate or one chloride anion, respectively. The asymmetric unit of complex 22 is shown in figure 3.21. In addition to one molecule of 22, two water molecules were found in the asymmetric unit and treated as a diffused contribution using the program SQUEEZE (Platon Library). The determined and calculated density and absorption coefficients include the water molecules but individual atoms do not appear in the atom list. Selected bond lengths and angles of 34 are listed in tables 3.16 and 3.17.

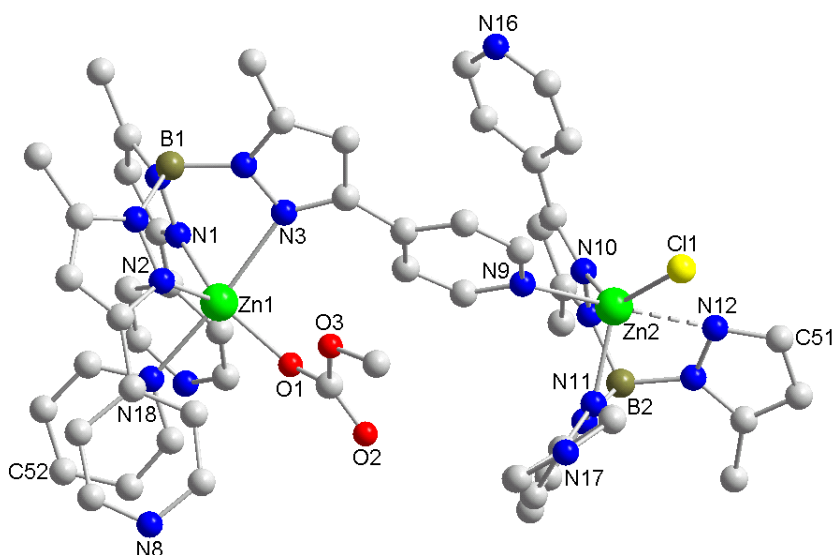


Figure 3.21. Structure of the symmetrically independent unit of [Tp^{4'Py,Me}Zn-OC(O)OMe][Tp^{4'Py,Me}Zn-Cl] in complex 22.

Table 3.16. Selected bond lengths [\AA] of $[\text{Tp}^{4\text{Py,Me}}\text{Zn-OC(O)OMe}][\text{Tp}^{4\text{Py,Me}}\text{Zn-Cl}]$ **22**.

Bond	[\AA]	Bond	[\AA]
Zn(1)-O(1)	1.930(3)	Zn(2)-N(11)	2.035(4)
Zn(1)-N(2)	2.038(4)	Zn(2)-N(10)	2.050(4)
Zn(1)-N(1)	2.070(4)	Zn(2)-N(9)	2.181(4)
Zn(1)-N(18)	2.192(4)	Zn(2)-Cl(1)	2.285(4)
Zn(1)-N(3)	2.300(4)	Zn(2)-N(12)	2.575(4)

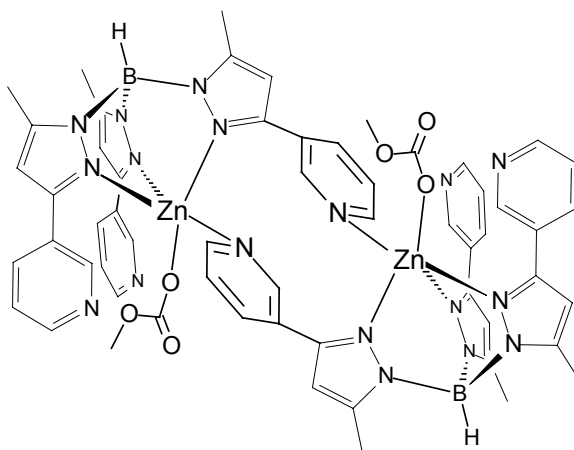
Table 3.17. Selected bond angles [$^\circ$] of $[\text{Tp}^{4\text{Py,Me}}\text{Zn-OC(O)OMe}][\text{Tp}^{4\text{Py,Me}}\text{Zn-Cl}]$ **22**.

Angle	[$^\circ$]	Angle	[$^\circ$]
O(1)-Zn(1)-N(2)	130.06(16)	N(11)-Zn(2)-N(10)	99.55(15)
O(1)-Zn(1)-N(1)	132.33(15)	N(11)-Zn(2)-N(9)	95.25(14)
N(2)-Zn(1)-N(1)	97.60(15)	N(10)-Zn(2)-N(9)	95.40(15)
O(1)-Zn(1)-N(18)	88.54(14)	N(11)-Zn(2)-Cl(1)	122.58(16)
N(2)-Zn(1)-N(18)	92.55(15)	N(10)-Zn(2)-Cl(1)	135.21(15)
N(1)-Zn(1)-N(18)	90.77(14)	N(9)-Zn(2)-Cl(1)	95.16(12)
O(1)-Zn(1)-N(3)	96.40(13)	Cl(1)-Zn(2)-N(12)	90.26(15)
N(2)-Zn(1)-N(3)	89.31(14)	N(11)-Zn(2)-N(12)	85.57(2)
N(1)-Zn(1)-N(3)	81.04(14)	N(10)-Zn(2)-N(12)	77.55(2)
N(18)-Zn(1)-N(3)	171.77(13)	N(9)-Zn(2)-N(12)	173.03(15)

The coordination geometry around the five-coordinated Zn(1) ion can be described as highly distorted trigonal bipyramidal, with a τ value of 0.65.^{152,153} The Zn-N bond distances for the pyrazolyl nitrogens N(1) and N(2) in equatorial positions are in the normal range, while the Zn(1)-N(3) bond distance of 2.30 \AA involving the pyrazolyl nitrogen located on one apex of the bipyramid is significantly longer. This asymmetry in the bonding of the $\text{Tp}^{4\text{Py,Me}}$ ligand to zinc has already been observed in the aqua and methanol complexes **18** and **19**. The second apex of the bipyramid is occupied by the pyridine nitrogen N(18) of a neighbouring $\text{Tp}^{4\text{Py,Me}}\text{Zn-Cl}$ unit, the N(3)-Zn(1)-N(18) bond angle being 171.8 $^\circ$. The equatorial plane is defined by the pyrazole nitrogens N(1) and N(2), and the oxygen donor O(1) of the methylcarbonate ligand. The Zn(1) ion is in this plane, with a root-mean-square deviation of only 0.01 \AA in direction to N(18).

The methylcarbonate ligand coordinates in an unidentate mode, with the carbonyl oxygen O(2) oriented out of the coordination sphere of Zn(1). This and the Zn(1)-O(1) bond distance of 1.93 Å can be compared to that reported before for $\text{Tp}^{\text{Ph,Me}}\text{Zn-OC(O)OMe}$ and $\text{Tp}^{\text{Cum,Me}}\text{Zn-OC(O)OMe}$ (1.89-1.92 Å).^{47,50} However, in contrast to these tetrahedral $\text{TpZn-alkylcarbonate}$ complexes, the long Zn(1)⋯O(3) separation of 3.03 Å in **22** indicates that there is no interaction with the oxygen ion of the –OMe group.

In the analogous complex $\text{Tp}^{3\text{Py,Me}}\text{Zn-OC(O)OMe}$ (**XII**),¹¹³ the coordination geometry around zinc and the binding mode of the methylcarbonate ligand, with a Zn-O bond distance of 1.93 Å and a Zn⋯O separation of 2.94 Å for the oxygen ion of the –OMe group, are nearly identical to those observed in **22**. However, the pyridyl coordination to a neighbouring zinc ion occurring in complex **XII** results in the formation of dimeric molecules in the solid state instead of polymeric chains, as in the case of **22** (See figure 3.22 at the end of this section).



XII

Regarding the $\text{Tp}^{4\text{Py,Me}}\text{Zn-Cl}$ unit, the Zn(2)-Cl(1) bond distance of 2.29 Å is in the normal range, but the Zn(2)-N(12) distance of 2.57 Å for one pyrazolyl nitrogen suggests the partial detachment of the $\text{Tp}^{4\text{Py,Me}}$ ligand from zinc, as already observed in complex **21**. The resulting highly unsymmetrical coordination geometry around Zn(2) can be described as distorted trigonal bipyramidal, with a τ value of 0.60.^{152,153} As shown in figure 3.21, the axis of the bipyramid is defined by the nitrogen donor N(9) of one pyrazole, the zinc ion Zn(2) and the pyridyl nitrogen donor N(12) of the adjacent

$\text{Tp}^{4\text{Py,Me}}\text{Zn-OC(O)OMe}$ unit, the N(9)-Zn(2)-N(12) bond angle being 173.0° . The equatorial plane is defined by the pyrazole nitrogens N(10) and N(11), and the chloride anion Cl(1). The Zn(2) ion is 0.20 \AA deviated from this plane in direction to N(9).

The polymeric structure of **22** is shown in figure 3.22. Weak stacking interactions involving the bridging pyridine rings with N(9) and N(18) contribute to the stabilization of the polymeric structure. Specifically, the bridging pyridine with N(9) and the non-bridging pyridine containing N(16) are separated by an interplanar distance of 4.13 \AA and a slip angle of 33.8° ; and the bridging pyridine with N(18) and the non-bridging pyridine containing N(8) are separated by an interplanar distance of 4.12 \AA and a slip angle of 28.8° .

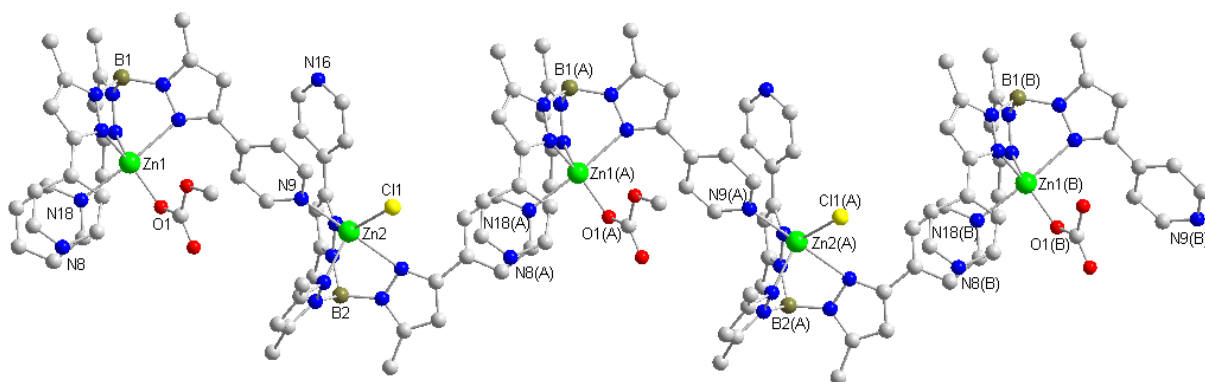


Figure 3.22. Atomic arrangements along the zig-zag shaped chains in $[\text{Tp}^{4\text{Py,Me}}\text{Zn-OC(O)OMe}][\text{Tp}^{4\text{Py,Me}}\text{Zn-Cl}]$ **22**. Only the bridging pyridyl rings involved in the coordination to zinc, and those interacting with them are shown.

3.11. Hydrotris(3-(4'-pyridyl)-5-methyl)pyrazolylborate zinc benzoylacetate $\text{Tp}^{4\text{Py,Me}}\text{Zn}(\text{benzoylac})$ **27**

Colourless crystals of **27** suitable for X-ray diffraction were obtained by slowly evaporating the solvent of a saturated acetonitrile/dichloromethane solution. Complex **27** forms rhombic crystals belonging to the monoclinic crystal system, space group $P2(1)/n$. Its structure was solved by direct methods and refined to a final R index of 0.060. As shown in figure 3.23, discrete molecules of **27** result from the coordination of three pyrazolyl nitrogen atoms of one $\text{Tp}^{4\text{Py,Me}}$ ligand and of two oxygen atoms of one

benzoylacetate ligand to the zinc center. In addition to one molecule of complex **27**, one dichloromethane molecule is present in the asymmetric unit. Selected bond lengths and angles of **27** are listed in table 3.18.

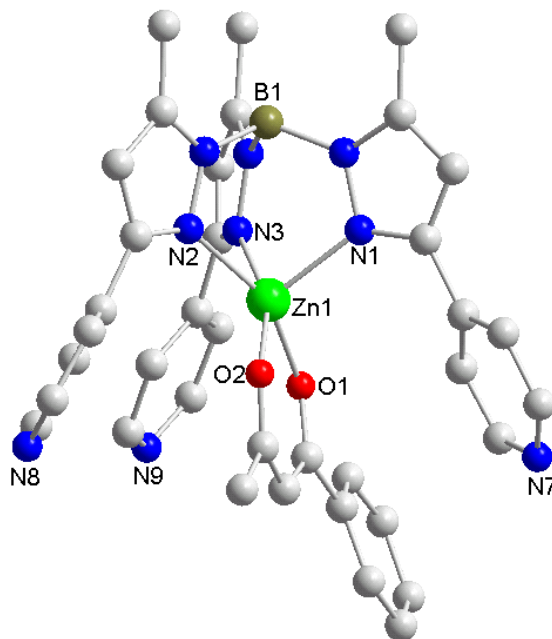


Figure 3.23. Molecular structure of $\text{Tp}^{4\text{Py,Me}}\text{Zn}(\text{benzoylac})$ **27**.

Table 3.18. Selected bond lengths [\AA] and angles [$^\circ$] of $\text{Tp}^{4\text{Py,Me}}\text{Zn}(\text{benzoylac})$ **27**.

Bond	[\AA]	Angle	[$^\circ$]
Zn(1)-O(1)	1.992(2)	O(1)-Zn(1)-O(2)	89.64(10)
Zn(1)-O(2)	2.008(3)	O(1)-Zn(1)-N(1)	111.26(11)
Zn(1)-N(1)	2.062(3)	O(2)-Zn(1)-N(1)	105.33(11)
Zn(1)-N(3)	2.132(3)	O(1)-Zn(1)-N(3)	91.87(10)
Zn(1)-N(2)	2.144(3)	O(2)-Zn(1)-N(3)	160.55(11)
		N(1)-Zn(1)-N(3)	92.17(11)
		O(1)-Zn(1)-N(2)	155.69(11)
		O(2)-Zn(1)-N(2)	87.10(10)
		N(1)-Zn(1)-N(2)	92.81(10)
		N(3)-Zn(1)-N(2)	83.57(11)

The coordination geometry of Zn(1) can be described as square pyramidal to a good approximation, with a τ value of 0.08. The two oxygen donors, O(1) and O(2), of the

diketonate ligand and two pyrazolyl nitrogen donors of the $\text{Tp}^{4\text{Py,Me}}$ ligand comprise the N_2O_2 basal plane, while the axial coordination position is occupied by N(1), with a Zn(1)-N(1) bond distance of 2.06 Å. The zinc ion is displaced from the N_2O_2 basal plane towards the apical N(1) by 0.38 Å.

The benzoylacetone ligand binds to zinc in a symmetric manner with Zn(1)-O bond distances of 1.99 and 2.01 Å. The ZnO_2C_3 chelate ring is almost ideally planar, with a mean deviation from the plane of 0.04 Å. Its C-O and C-C bond lengths as usual point to its delocalised nature. The chelating attachment of the benzoylacetone ligand in complex **27** is similar to that reported for other β -ketoenolates,^{51,96,118} avoiding the further coordination of a neighbouring pyridine to zinc, so that monomeric species can be formed. The orientation of the β -diketonate ring with respect to the aromatic pyridyl rings of the $\text{Tp}^{4\text{Py,Me}}$ ligand suggests some stacking interactions between them, thereby providing an ‘exit’ for the voluminous phenyl substituent of the benzoylacetone ligand from the inner pocket of the molecule.

Complex **27** shows the same characteristics as the $\text{TpZn}(\beta\text{-ketoenolate})$ complexes described in the literature. The Zn-O bond lengths, the shape and the orientation of the benzoylacetone ligand correspond to those in other related complexes. Minor differences appear in the coordination geometry around zinc, being square-pyramidal in complex **27** and, for example, intermediate between distorted trigonal bipyramidal and square-pyramidal in the complex $\text{Tp}^{\text{Cum,Me}}\text{Zn}(\text{cumoylac})$.¹¹⁸

3.12. Bis(hydrotris-(3-phenylamide-5-methylpyrazol-1-yl)borate zinc)(μ_2 -hydroxide) perchlorate $[(\text{Tp}^{\text{C(O)NHPH,Me}}\text{Zn})_2(\mu_2\text{-OH})]\text{ClO}_4$ **34**

Colourless crystals of **34** suitable for X-ray diffraction were obtained by slowly evaporating the solvent of a saturated dichloromethane/methanol solution. Complex **34** belongs to the monoclinic crystal system, space group C2/c. Its molecular structure was solved by direct methods and refined to a final R index of 0.096. In complex **34**, two $[\text{Tp}^{\text{C(O)NHPH,Me}}\text{Zn}]^+$ units are bridged by a single hydroxide anion, thereby generating binuclear species in the solid state, as shown in figure 3.24. In addition to one molecule of **34** and one perchlorate counterion, in the asymmetric unit were found one water molecule and two highly distorted methanol and dichloromethane molecules. These

were treated as a diffused contribution using the program SQUEEZE (Platon Library). The determined and calculated density and absorption coefficients include the solvent molecules but individual atoms do not appear in the atom list. Selected bonding parameters around Zn(1) and Zn(2) are listed separately in tables 3.19 and 3.20.

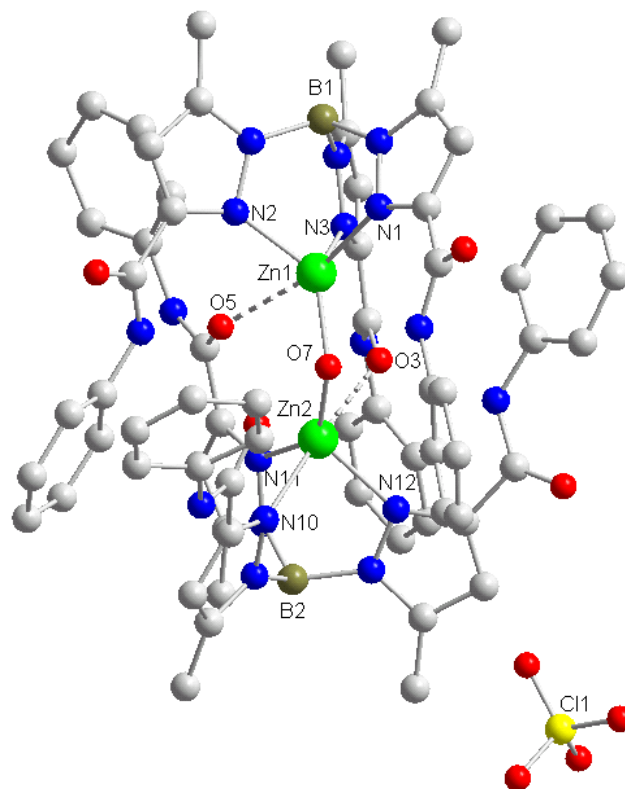


Figure 3.24. Structure of $[(\text{Tp}^{\text{C(O)NHPH,Me}}\text{Zn})_2(\mu_2\text{-OH})]\text{ClO}_4$ **34**.

Table 3.19. Selected bond lengths [\AA] and angles [$^\circ$] of Zn(1) in complex **34**.

Bond	[\AA]	Angle	[$^\circ$]
Zn(1)-O(7)	1.885(5)	O(7)-Zn(1)-N(2)	127.9(2)
Zn(1)-N(2)	1.975(7)	O(7)-Zn(1)-N(3)	127.8(3)
Zn(1)-N(3)	1.997(7)	N(2)-Zn(1)-N(3)	96.1(3)
Zn(1)-N(1)	2.108(7)	O(7)-Zn(1)-N(1)	111.1(2)
Zn(1)-O(5)	2.768(6)	N(2)-Zn(1)-N(1)	88.9(3)
		N(3)-Zn(1)-N(1)	94.0(3)
		N(1)-Zn(1)-O(5)	165.2(3)
		O(5)-Zn(1)-N(2)	80.1(3)

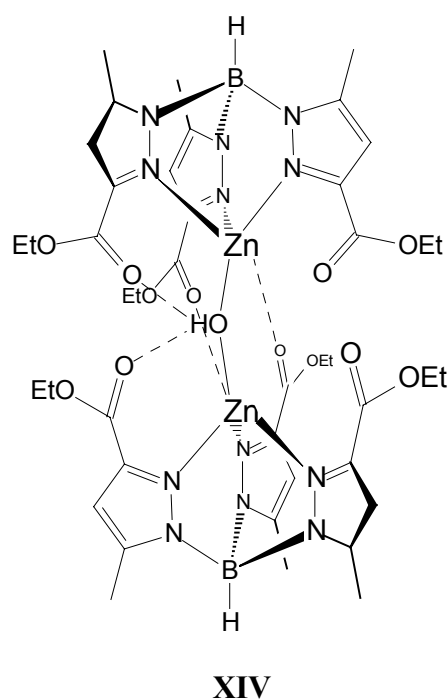
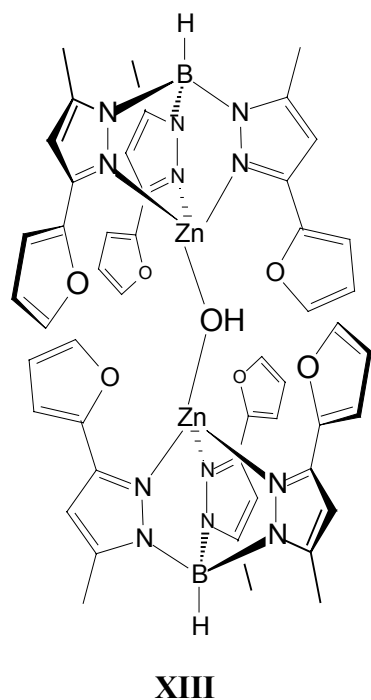
O(5)-Zn(1)-N(3)	77.5(3)
O(5)-Zn(1)-O(7)	83.56(3)

Table 3.20. Selected bond lengths [Å] and angles [°] of Zn(2) in complex **34**.

Bond	[Å]	Angle	[°]
Zn(2)-O(7)	1.901(5)	O(7)-Zn(2)-N(11)	137.7(3)
Zn(2)-N(11)	1.964(7)	O(7)-Zn(2)-N(12)	121.8(2)
Zn(2)-N(12)	2.044(7)	N(11)-Zn(2)-N(12)	98.8(3)
Zn(2)-N(10)	2.124(6)	O(7)-Zn(2)-N(10)	103.9(2)
Zn(2)-O(3)	2.400(5)	N(11)-Zn(2)-N(10)	88.3(3)
		N(12)-Zn(2)-N(10)	87.2(2)
		O(7)-Zn(2)-O(3)	85.04(19)
		N(11)-Zn(2)-O(3)	85.5(2)
		N(12)-Zn(2)-O(3)	87.4(2)
		N(10)-Zn(2)-O(3)	171.1(2)

In complex **34**, the coordination geometry of both zinc centres, Zn(1) and Zn(2), can be described as distorted trigonal bipyramidal, the axis of the bipyramid being defined by one of the carbonyl oxygens of the opposite $\text{Tp}^{\text{C(O)NHPH,Me}}$ ligand, the zinc ion and the nitrogen donor of a pyrazole, i.e. N(1)-Zn(1)-O(5) and N(10)-Zn(2)-O(3). The deviation from the idealized trigonal bipyramidal geometry is well expressed in the τ value of 0.62 and 0.56 for Zn(1) and Zn(2) respectively. The Zn-N bond distances for the pyrazolyl nitrogens are grouped into two short ones for the equatorial and a longer one for the axial nitrogen. The equatorial pyrazolyl nitrogens N(2), N(3) and N(11), N(12) are attached at an average distance of 1.98 and 2.00 Å to Zn(1) and Zn(2), respectively, while the axial pyrazolyl nitrogens, N(1) and N(10), are attached at 2.11 and 2.12 Å. The interaction with one of the amide carbonyls of the opposite $\text{Tp}^{\text{C(O)NHPH,Me}}$ ligand is much stronger for Zn(2), with a Zn(2)-O(3) bond distance of 2.40 Å, than for Zn(1), with a Zn(1)-O(5) bond distance of 2.77 Å.

The O(7) donor of the bridging hydroxide binds to Zn(1) and Zn(2) in a rather symmetrically form, with an average Zn-O(7) bond length of 1.89 Å. This is only slightly longer than the values reported for the relevant mononuclear hydroxo complexes $\text{Tp}^{\text{tBu,Me}}\text{ZnOH}$ and $\text{Tp}^{\text{Cum,Me}}\text{ZnOH}$ (ca. 1.85 Å),^{43,47} and shorter than that found for further binuclear hydroxo bridged complexes characterized in our group. For example, bond distances of 1.94 and 1.95 Å have been given for the bridging hydroxide in complex $[(\text{Tp}^{2\text{Fu,Me}}\text{Zn})_2(\mu_2\text{-OH})]\text{ClO}_4$ (**XIII**).¹²⁹ The same values have been reported for complex $[(\text{TriMImZn})_2(\mu_2\text{-OH})]^{3+}$,³¹ where TriMIm denotes a tris(imidazolyl) benzene ligand. In this case, the steric demands of the TriMIm ligand enforces zinc into a square pyramidal coordination sphere requiring that the single oxygen bridge involves a wide Zn-O-Zn angle (160.0°). In **34** the Zn(1)-O(7)-Zn(2) bond angle is 120.3° and the Zn(1)⋯Zn(2) separation 3.28 Å. In the binuclear hydroxo bridged complex **XIV**,⁵⁸ the bonding parameters of the hydroxo bridge (average Zn-O(H) bond distance of 1.87 Å and Zn-O(H)-Zn bond angle of 134.4°) are very similar to those found in **34**. Furthermore, the carbonyl oxygens of the ester groups in **XIV** are directed to the center of the binding cavity strongly interacting with zinc (Zn-O = 2.58 Å), similarly to that occurring in **34**.



In complex **XIV**, the hydroxyl hydrogen is bonded to two ester carbonyl moieties with O \cdots O distances of 2.90 and 2.84 Å. This feature finds also analogy in the intramolecular H-bonding network present in the crystal structure of **34**, in which the bridging hydroxide is linked to the amide oxygen O(4) with a O(7) \cdots O(4) distance of 2.59 Å (Figure 3.25). Further hydrogen interactions involve nearby C=O and NH groups of both opposing Tp^{C(O)NHPh,Me} ligands. Specifically, O(3) is hydrogen bonded to N(18) with a O(3) \cdots N(18) distance of 2.88 Å, and O(5) is hydrogen bonded to N(8) with a O(5) \cdots N(8) distance of 2.90 Å. Additionally, the phenyl rings of the carboxamide functions are intertwined, having stacking interactions with the pyrazolyl rings of the opposing Tp^{C(O)NHPh,Me} ligand. Specifically, the phenyl ring which contains C(17) is separated from the pyrazolyl ring which contains N(10) by an interplanar distance of 3.83 Å and a slip angle of 6.6°; the phenyl ring which contains C(28) is separated from the pyrazolyl ring which contains N(11) by an interplanar distance of 3.64 Å and a slip angle of 6.5°; and the phenyl ring which contains C(61) is separated from the pyrazolyl ring which contains N(1) by an interplanar distance of 3.90 Å and a slip angle of 8.6°.

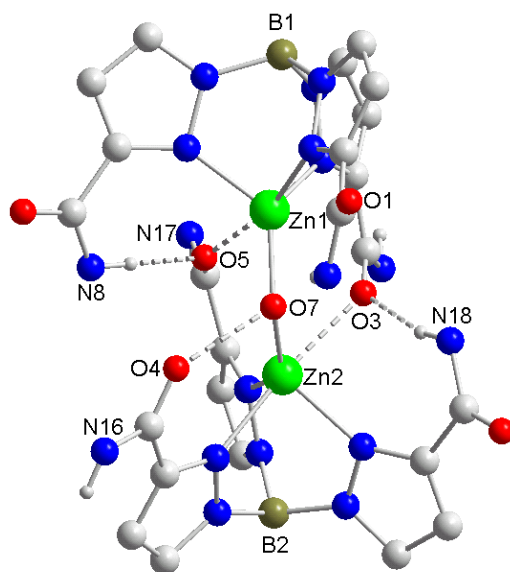


Figure 3.25. Intramolecular H-bonding network in complex **34**. For clarity, the methyl and the phenyl substituents have been omitted, and only some of the atoms involved in the H-bonding network have been labelled.

4. Experimental section

4.1. General

All manipulations were performed under a pure nitrogen atmosphere using Standard-Schlenk technique, unless otherwise indicated. All reagents were obtained commercially and used without further purification. The solvents were supplied in analytical qualities and dried under reflux with the following drying agents: CaH₂ for dichloromethane or chloroform, Na-K-alloy for diethyl ether, hexane and toluene, and Mg for methanol.

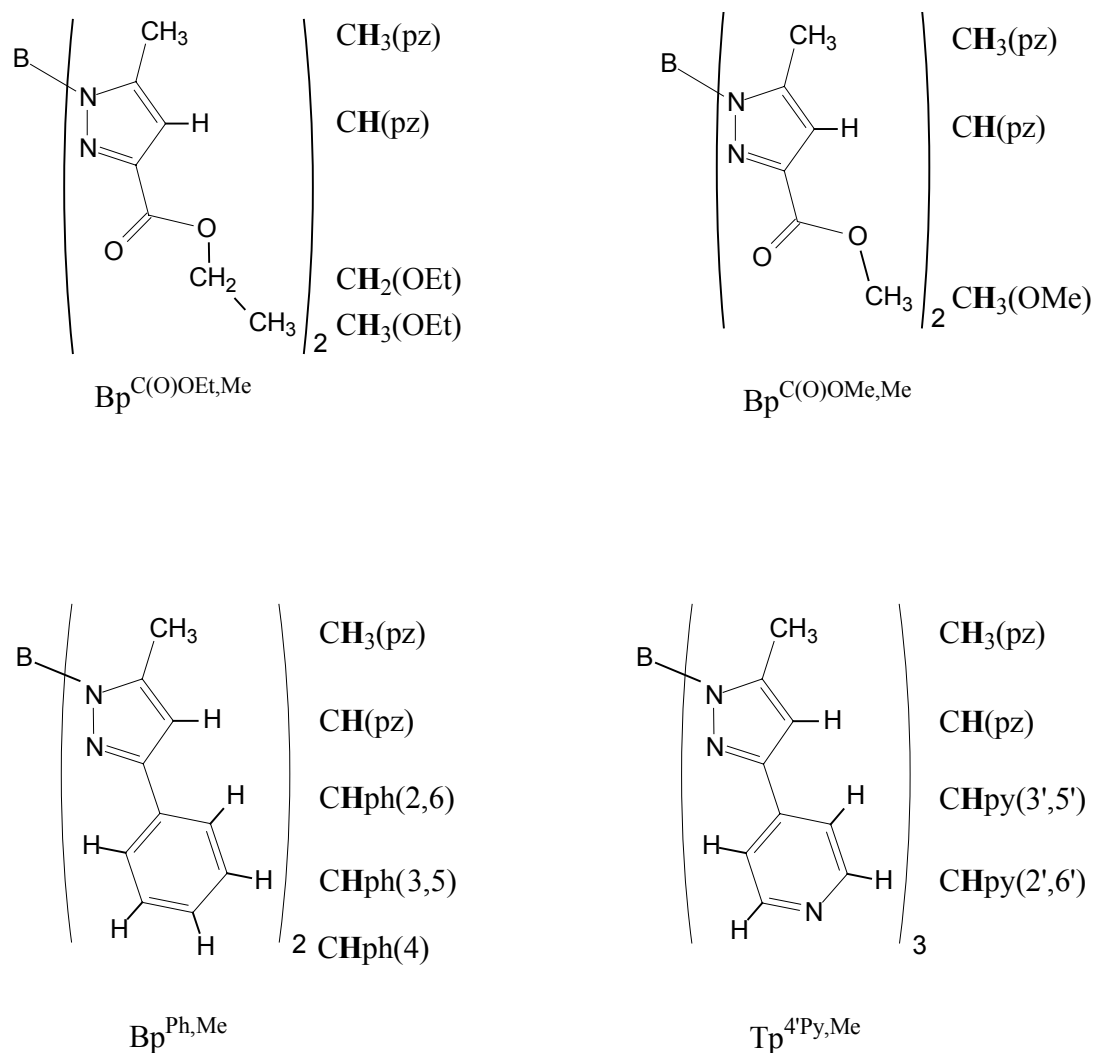
The following starting compounds were prepared according to the literature procedures: ethyl 2,4-diketopentanoate,¹⁶² (3-methyl-5-carboxyethyl)pyrazole,⁵⁷ methyl 2,4-diketopentanoate,¹⁶³ (3-methyl-5-carboxymethyl)pyrazole,¹⁶⁴ potassium hydrotris(3-carboxyethyl-5-methyl)pyrazolylborate (**1**),⁵⁷ ethyl 2-methylisonicotinate,⁹⁰ 4'-pyridylbutan-2,4-dione,⁸⁹ 4'-(6'-methyl)-pyridylbutan-2,4-dione,⁸⁹ (3-(4'-pyridyl)-5-methyl)pyrazole,^{91,165} (3-(4'-(6'-methyl)-pyridyl)-5-methyl)pyrazole,^{91,165} 3,5-dimethylpyrazole,¹⁶⁶ (3-methyl-5-phenyl)pyrazole,¹⁶⁵ (3-methyl-5-carboxylic acid)pyrazole,¹⁶⁷ 2-7-dimethyl-dipyrazolo[1,5-a;1'-5'-a]pyrazine-4,9-dione¹⁶⁸ and (3-methyl-5-phenylcarboxamide)pyrazole.¹⁶⁸

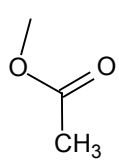
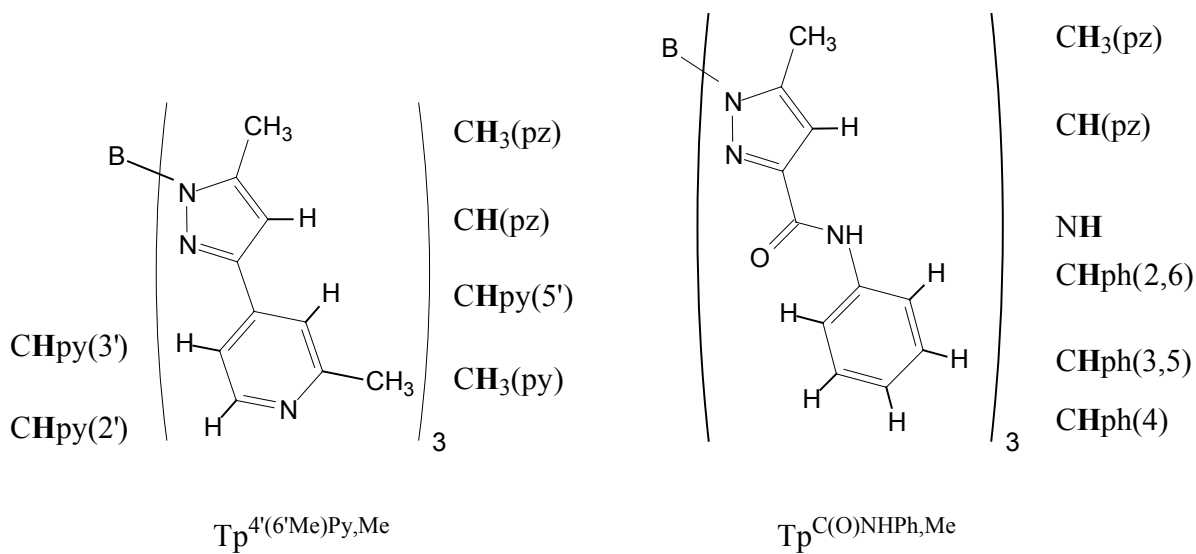
The NMR spectra were recorded on a Bruker-DPX-200 instrument with Fourier-Transform technique. Either a proton signal of the solvent or of tetramethylsilane was used as internal standard for the calibration of the ¹H NMR spectra. For the calibration of the ¹³C NMR spectra, the ¹³C-signal of the solvent was used as internal standard. The signal of CFCl₃ was used for the calibration of the ¹⁹F NMR spectra as internal standard. The signal of H₃PO₄ (85%) was used as external standard for the calibration of the ³¹P NMR spectra. Unless otherwise noted all NMR spectra were recorded at 300 K.

The IR spectra were obtained using a Bruker-IFS-25 spectrometer with Fourier-Transform technique. Elemental analyses were performed by the analytical laboratory of the Chemical Laboratory of the University of Freiburg using a Perkin-Elmer-

Analyzer 240 or a VarioEl from Elementaranalysen-Systeme GmbH. The determination of the zinc content succeeded by complexometric titration with EDTA using commercially available indicator buffer tablets (Merck). Decomposition of the complexes succeeded in concentrated nitric acid. The melting points were measured on a MEL-TEMP hot stage apparatus.

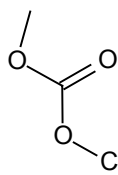
The assignment of the ^1H NMR signals for the pyrazolylborate ligands and for the coligands in compounds **22**, **23**, **24**, **25**, **26**, **27** and **28** is as follows:





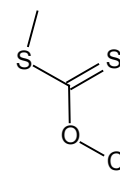
$\text{CH}_3(\text{OAc})$

OAc



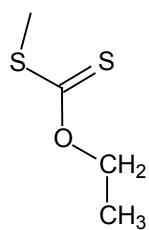
$\text{CH}_3(\text{OMe})$

OC(O)OMe



$\text{CH}_3(\text{OMe})$

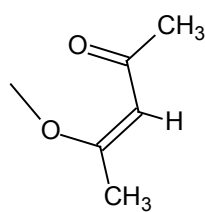
SC(S)OMe



$\text{CH}_2(\text{OEt})$

$\text{CH}_3(\text{OEt})$

SC(S)OEt

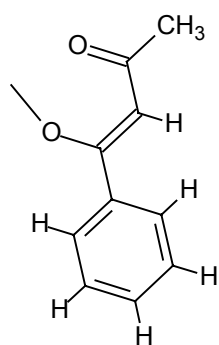


$\text{CH}_3(\text{MeC(O)})$

$\text{CH}(\text{C(O)CHC(O)})$

$\text{CH}_3(\text{MeC(O)})$

acac



$\text{CH}_3(\text{MeC(O)})$

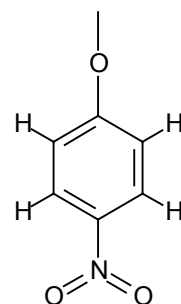
$\text{CH}(\text{C(O)CHC(O)})$

$\text{CHph}(2,6)$

$\text{CHph}(3,5)$

$\text{CHph}(4)$

benzoylac



$\text{CHph}(2,6)$

$\text{CHph}(3,5)$

ONit

4.2. Syntheses

4.2.1. Potassium dihydrobis(3-carboxyethyl-5-methyl)pyrazolylborate



1.71 g (31.70 mmol) of KBH_4 were added to a solution of 12.24 g (79.39 mmol) of (3-methyl-5-carboxyethyl)pyrazole⁵⁷ in 150 ml of toluene. The mixture was stirred under reflux in an oil bath at 120°C. After 2 h, a white powder precipitated but the mixture was kept reacting for 2 days, until the hydrogen evolution ceased. After cooling to room temperature, the white precipitate was filtered off, washing 3 times with 5 ml of toluene each to eliminate impurities of unreacted pyrazole, and 1 time with 5 ml of water to eliminate traces of KBH_4 . The solid was dried in vacuo to yield 9.65 g (85 %) of 2 as a white powder, m.p. 188°C.

$\text{C}_{14}\text{H}_{20}\text{BKN}_4\text{O}_4 \cdot \text{H}_2\text{O}$	Calc.:	C 44.69	H 5.89	N 14.89
(358.25 + 18.02)	Found:	C 45.28	H 5.29	N 14.63

IR (KBr, cm^{-1}) 3446 (water) b, 2989 m, 2976 m, 2933 w, 2903 w, 2451 (B-H) m, 2424 (B-H) m, 1719 (C=O) vs, 1703 (C=O) vs, 1532 w, 1484 m, 1445 m, 1419 m, 1393 m, 1346 w, 1259 s, 1229 s, 1187 vs, 1164 s, 1120 m, 1092 m, 1036 m, 1005 w, 981 w, 907 w, 840 w, 807 w, 779 s, 630 w.

$^1\text{H-NMR}$ (CDCl₃) 1.26 [t, $^3\text{J} = 7.1$ Hz, 6H, $\text{CH}_3(\text{OEt})$], 1.65 [b, 2H, H_2O], 2.33 [s, 6H, $\text{CH}_3(\text{pz})$], 4.16 [q, $^3\text{J} = 7.1$ Hz, 4H, $\text{CH}_2(\text{OEt})$], 6.31 [s, 2H, $\text{CH}(\text{pz})$].

$^{13}\text{C-NMR}$ (CDCl₃ + 2 dr. CD₃OD) 12.1 [$\text{CH}_3(\text{pz})$], 13.7 [$\text{CH}_3(\text{OEt})$], 59.9 [$\text{CH}_2(\text{OEt})$], 106.4 [pz(4)], 141.6 [pz(5)], 144.1 [pz(3)], 164.7 [C(O)].

4.2.2. Potassium dihydrobis(3-carboxymethyl-5-methyl)pyrazolylborate



1.07 g (19.83 mmol) of KBH_4 were added to a solution of 6.95 g (49.59 mmol) of (3-methyl-5-carboxymethyl)pyrazole¹⁶⁴ in 150 ml of toluene. The mixture was stirred under reflux in an oil bath at 120°C. After 2 h, a white powder precipitated but the mixture was kept reacting for 2 days, until the hydrogen evolution ceased. After cooling to room temperature, the white precipitate was filtered off, washing 3 times with 5 ml of toluene each to eliminate impurities of unreacted pyrazole. The residue was recrystallized from toluene/methanol (90:10) to yield 3.99 g (61 %) of colourless **3**, m.p. 242°C.

$\text{C}_{12}\text{H}_{16}\text{BKN}_4\text{O}_4$	Calc.:	C 43.65	H 4.88	N 16.97
(330.19)	Found:	C 43.01	H 4.81	N 17.22

IR (KBr, cm^{-1}) 3419 (water) b, 3025 w, 2954 w, 2852 w, 2446 (B-H) m, 2402 (B-H) w, 1717 (C=O) vs, 1705 (C=O) s, 1532 w, 1473 m, 1450 m, 1426 m, 1415 m, 1377 w, 1365 w, 1349w, 1253 s, 1217 w, 1196 s, 1166 vs, 1120 m, 1026 m, 983 w, 896 w, 811 w, 777 s, 623 w.

$^1\text{H-NMR}$ (CDCl₃ + 2 dr. CD₃OD) 2.27 [s, 6H, CH₃(pz)], 3.70 [s, 6H, CH₃(OMe)], 6.27 [s, 2H, CH(pz)].

$^{13}\text{C-NMR}$ (CDCl₃ + 2 dr. CD₃OD) 12.3 [CH₃(pz)], 51.0 [CH₃(OMe)], 106.6 [pz(4)], 141.3 [pz(5)], 144.3 [pz(3)], 165.1 [C(O)].

4.2.3. Thallium dihydrobis(3-carboxymethyl-5-methyl)pyrazolylborate



To a clear solution of 1.62 g (4.90 mmol) of **3** in 50 ml of dimethylformamide was dropped with stirring a solution of 1.44 g (5.40 mmol) of TINO_3 in 10 ml of water over

a period of 30 min. A white powder precipitated immediately, but the mixture was kept reacting for 6 h. The precipitate was filtered off, washed 1 time with 5 ml of warm water to eliminate traces of unreacted TlNO_3 , and dried in vacuo to yield 2.11 g (87 %) of **4** as a white powder, m.p. 230°C.

$\text{C}_{12}\text{H}_{16}\text{BN}_4\text{O}_4\text{Tl} \cdot \text{H}_2\text{O}$ (495.47 + 18.02)	Calc.:	C 28.07	H 3.53	N 10.91
	Found:	C 27.50	H 3.16	N 10.60

IR (KBr, cm^{-1}) 3432 (water) b, 2962 m, 2444 (B-H) m, 1734 (C=O) vs, 1700 w, 1684 w, 1652 w, 1558 w, 1540 w, 1506 w, 1451 m, 1412 m, 1363 w, 1261 s, 1245 s, 1199 m, 1160 m, 1111 s, 1027 s, 945 w, 887 w, 808 s, 774 m, 625 w.

$^1\text{H-NMR}$ (CDCl_3) 1.60 [b, 2H, H_2O], 2.37 [s, 6H, $\text{CH}_3(\text{pz})$], 3.86 [s, 6H, $\text{CH}_3(\text{OMe})$], 6.37 [s, 2H, $\text{CH}(\text{pz})$].

$^{13}\text{C-NMR}$ ($\text{CDCl}_3 + 2 \text{ dr. CD}_3\text{OD}$) 11.7 [$\text{CH}_3(\text{pz})$], 51.0 [$\text{CH}_3(\text{OMe})$], 107.0 [$\text{pz}(4)$], 141.4 [$\text{pz}(5)$], 144.8 [$\text{pz}(3)$], 164.4 [$\text{C}(\text{O})$].

4.2.4. Bis-dihydrobis(3-carboxyethyl-5-methyl)pyrazolylborate zinc



A solution of 330 mg (0.89 mmol) of $\text{Zn}(\text{ClO}_4)_2 \cdot 6\text{H}_2\text{O}$ in 5 ml of methanol was dropped with stirring to a solution of 577 mg (1.61 mmol) of **2** in 30 ml of methanol over a period of 5 min. A slurry of KClO_4 precipitated immediately, but the mixture was kept reacting for 2 h. Then KClO_4 was filtered off and the filtrate was evaporated to dryness in vacuo. The residue was dissolved in 10 ml of ethanol/dichloromethane (1:1) and the clear solution was slowly evaporated at room temperature to yield after 1 day 527 mg (93 %) of **5** as colourless crystals, m.p. 146°C.

$\text{C}_{28}\text{H}_{40}\text{B}_2\text{N}_8\text{O}_8\text{Zn} \cdot \text{H}_2\text{O}$ (703.68 + 18.02)	Calc.:	C 46.60	H 5.87	N 15.53
	Found:	C 46.56	H 5.75	N 15.35

IR (KBr, cm^{-1}) 3433 (water) b, 3140 w, 2979 m, 2935 w, 2906 w, 2484 (B-H) m, 2444 (B-H) m, 1731 (C=O) vs, 1534 m, 1490 w, 1440 s, 1377 m, 1361 w, 1294 w, 1252 s, 1207 m, 1173 vs, 1114 s, 1043 s, 988 w, 897 w, 864 w, 843 w, 819 w, 773 s, 721 w, 674 w, 616 w.

$^1\text{H-NMR}$ (CDCl_3) 0.96 [t, $^3\text{J} = 7.1$, 12H, $\text{CH}_3(\text{OEt})$], 1.55 [b, 2H, H_2O], 2.44 [s, 12H, $\text{CH}_3(\text{pz})$], 3.87 [q, $^3\text{J} = 7.1$, 8H, $\text{CH}_2(\text{OEt})$], 6.47 [s, 4H, $\text{CH}(\text{pz})$].

4.2.5. Bis-dihydrobis(3-carboxymethyl-5-methyl)pyrazolylborate zinc



A solution of 172 mg (0.46 mmol) of $\text{Zn}(\text{ClO}_4)_2 \cdot 6\text{H}_2\text{O}$ in 5 ml of methanol was dropped with stirring to a solution of 277 mg (0.84 mmol) of 3 in 20 ml of methanol over a period of 5 min. A slurry of KClO_4 precipitated immediately, but the mixture was kept reacting for 6 h. Then KClO_4 was filtered off and the clear filtrate was concentrated in vacuo until a crystalline product started to precipitate. The solution was heated until the solid redissolved and kept at 5°C overnight to yield 245 mg (90 %) of 6 as colourless crystals, m.p. 162°C .

$\text{C}_{24}\text{H}_{32}\text{B}_2\text{N}_8\text{O}_8\text{Zn}$	Calc.:	C 44.51	H 4.98	N 17.30	Zn 10.10
(647.58)	Found:	C 43.76	H 4.75	N 16.76	Zn 9.88

IR (KBr, cm^{-1}) 3148 w, 3136 w, 2955 w, 2933 w, 2486 (B-H) m, 2463 (B-H) m, 1738 (C=O) vs, 1716 (C=O) s, 1536 m, 1487 w, 1452 s, 1373 w, 1355 w, 1277 m, 1249 s, 1167 s, 1117 s, 1040 m, 988 w, 959 w, 881 w, 837 w, 813 s, 782 m, 769 m, 674 w, 613 w.

$^1\text{H-NMR}$ (CDCl_3) 2.47 [s, 12H, $\text{CH}_3(\text{pz})$], 3.36 [s, 12H, $\text{CH}_3(\text{OMe})$], 6.53 [s, 4H, $\text{CH}(\text{pz})$].

4.2.6. Potassium dihydrobis(3-phenyl-5-methyl)pyrazolylborate $\text{KBp}^{\text{Ph,Me}}$ **7**

3.52 g (22.25 mmol) of (3-methyl-5-phenyl)pyrazole¹⁶⁵ and 522 mg (9.67 mmol) of KBH_4 were mixed with stirring in a three-necked 50 ml flask equipped with an immersing thermometer. The temperature of the mixture was slowly increased to 130°C over a period of 30 min. At 120°C the mixture melted and the gas evolution became brisk. The melt was kept stirring at 130°C until no more hydrogen was evolved (ca. 2 h), and then slowly cooled to room temperature. The resulting glassy residue was carefully powdered and suspended in 20 ml of toluene in an ultrasound bath, in order to remove impurities of unreacted pyrazole. The mixture was filtered, washing 1 time with 5 ml of toluene and 1 time with 5 ml of petroleum ether ($30\text{-}50^\circ\text{C}$). The colourless residue was recrystallized from 15 ml of acetonitrile at -20°C . 886 mg (25 %) of **7** resulted as a colorless powder, m.p. 220°C . Cocrystallized acetonitrile could not be removed by prolonged pumping.

$\text{C}_{20}\text{H}_{20}\text{BKN}_4 \cdot \text{CH}_3\text{CN}$	Calc.:	C 64.87	H 5.69	N 17.19
(366.31 + 41.05)	Found:	C 65.04	H 5.61	N 16.75

IR (KBr , cm^{-1}) 3055 w, 2967 w, 2930 w, 2855 w, 2430 (B-H) w, 2378 (B-H) m, 2301 (B-H) w, 2269 (B-H) w, 1602 w, 1540 m, 1508 m, 1469 m, 1450 m, 1413 m, 1345 m, 1214 s, 1174 vs, 1114 m, 1084 w, 1068 w, 1014 w, 985 w, 961 w, 886 w, 799 m, 771 s, 693 s, 633 w.

$^1\text{H-NMR}$ (CD_3OD) 1.92 [s, 3H, $\text{CH}_3(\text{CH}_3\text{CN})$], 2.06 [s, 6H, $\text{CH}_3(\text{pz})$], 6.11 [s, 2H, $\text{CH}(\text{pz})$], 7.09 [m, 2H, $\text{CHph}(4)$], 7.23 [m, 4H, $\text{CHph}(3,5)$], 7.66 [d, $^3\text{J} = 8.3$ Hz, 4H, $\text{CHph}(2,6)$].

$^1\text{H-NMR}$ (CD_3CN)	2.36 [s, 6H, $\text{CH}_3(\text{pz})$], 6.22 [s, 2H, $\text{CH}(\text{pz})$], 7.21 [m, 2H, $\text{CHph}(4)$], 7.31 [m, 4H, $\text{CHph}(3,5)$], 7.71 [m, 4H, $\text{CHph}(2,6)$].
$^{13}\text{C-NMR}$ (CD_3CN)	13.3 [$\text{CH}_3(\text{pz})$], 102.5 [$\text{pz}(4)$], 126.1 [$\text{ph}(3,5)$], 127.2 [$\text{ph}(4)$], 129.4 [$\text{ph}(2,6)$], 136.7 [$\text{ph}(1)$], 145.0 [$\text{pz}(5)$], 150.6 [$\text{pz}(3)$].

4.2.7. Thallium dihydrobis(3-phenyl-5-methyl)pyrazolylborate $\text{TlBp}^{\text{Ph,Me}}$ **8**

To a clear solution of 276 mg (0.75 mmol) of **7** in 20 ml of tetrahydrofuran was dropped with stirring a solution of 220 mg (0.83 mmol) of TlNO_3 in 5 ml of water over a period of 5 min. A white powder precipitated immediately, but the mixture was kept reacting overnight. The precipitate was filtered off, washed 1 time with 5 ml of warm water to eliminate traces of unreacted TlNO_3 , and dried in vacuo to yield 356 mg (89 %) of **8** as a colourless powder, m.p. 248°C .

$\text{C}_{20}\text{H}_{20}\text{BN}_4\text{Tl}$	Calc.:	C 45.19	H 3.79	N 10.54
(531.60)	Found:	C 45.14	H 3.97	N 10.39

IR (KBr, cm^{-1}) 3037 w, 2927 w, 2440 (B-H) m, 2389 (B-H) w, 2290 (B-H) w, 2244 (B-H) m, 2203 (B-H) w, 1600 w, 1535 w, 1504 w, 1470 m, 1451 m, 1428 w, 1410 m, 1384 w, 1352 w, 1261 w, 1218 w, 1178 m, 1162 s, 1108 m, 1085 m, 1024 w, 966 m, 914 w, 881 m, 790 w, 764 vs, 696 s, 651 w, 629 w, 607 w.

$^1\text{H-NMR}$ (DMSO-d_6 , 310 K) 2.33 [s, 6H, $\text{CH}_3(\text{pz})$], 6.22 [s, 2H, $\text{CH}(\text{pz})$], 7.17 [m, 2H, $\text{CHph}(4)$], 7.31 [m, 4H, $\text{CHph}(3,5)$], 7.69 [d, $^3\text{J} = 7.8$ Hz, 4H, $\text{CHph}(2,6)$].

^{13}C -NMR (DMSO- d_6 , 310 K) 12.6 [$\text{CH}_3(\text{pz})$], 101.7 [$\text{pz}(4)$], 125.0 [$\text{ph}(3,5)$], 126.1 [$\text{ph}(4)$], 128.3 [$\text{ph}(2,6)$], 135.0 [$\text{ph}(1)$], 143.5 [$\text{pz}(5)$], 149.0 [$\text{pz}(3)$].

4.2.8. Bis-dihydrobis(3-phenyl-5-methyl)pyrazolylborate zinc ($\text{Bp}^{\text{Ph,Me}}\text{)}_2\text{Zn}$ **9**

A solution of 307 mg (0.82 mmol) of $\text{Zn}(\text{ClO}_4)_2 \cdot 6\text{H}_2\text{O}$ in 5 ml of methanol was dropped with stirring to a solution of 550 mg (1.50 mmol) of **7** in 30 ml of methanol/dichloromethane (1:1) over a period of 5 min. A slurry of KClO_4 precipitated immediately, but the mixture was kept reacting for 6 h. Then KClO_4 was filtered off and the clear filtrate was slowly evaporated at room temperature to yield after 2 days 324 mg (60 %) of **9** as colourless needles, m.p. 182°C.

$\text{C}_{40}\text{H}_{40}\text{B}_2\text{N}_8\text{Zn} \cdot \text{H}_2\text{O}$	Calc.:	C 65.11	H 5.74	N 15.19
(719.82 + 18.02)	Found:	C 65.24	H 5.72	N 15.16

IR (KBr, cm^{-1}) 3450 (water) b, 3124 w, 3058 w, 2962 w, 2927 w, 2477 (B-H) m, 2435 (B-H) m, 1541 m, 1502 m, 1482 m, 1435 s, 1418 m, 1378 w, 1357 m, 1191 m, 1161 s, 1120 m, 1107 s, 1092 w, 1070 w, 1029 w, 983 m, 911 w, 879 w, 804 w, 760 vs, 693 s, 629 w, 607 w.

^1H -NMR (CDCl_3) 1.53 [b, 2H, H_2O], 2.23 [s, 12H, $\text{CH}_3(\text{pz})$], 5.92 [s, 4H, $\text{CH}(\text{pz})$], 7.12 [m, 20H, $\text{CHph}(2,3,4,5,6)$].

^{13}C -NMR (CDCl_3) 13.1 [$\text{CH}_3(\text{pz})$], 105.4 [$\text{pz}(4)$], 127.2 [$\text{ph}(3,5)$], 127.5 [$\text{ph}(4)$], 128.0 [$\text{ph}(2,6)$], 131.8 [$\text{ph}(1)$], 146.2 [$\text{pz}(5)$], 153.8 [$\text{pz}(3)$].

4.2.9. Dihydrobis(3-phenyl-5-methyl)pyrazolylborate zinc chloride methanol

$(\text{Bp}^{\text{Ph,Me}})\text{Zn}(\text{Cl})(\text{MeOH})$ **10**

A solution of 160 mg (1.17 mmol) of ZnCl_2 in 5 ml of methanol was dropped to a solution of 392 mg (1.07 mmol) of **7** in 20 ml of methanol/dichloromethane (1:1) over a period of 5 min. After 6 h of stirring small amounts of a cloudy precipitate were removed by filtration and the clear filtrate was concentrated in vacuo to a volume of 10 ml. Storing at -20°C overnight precipitated 266 mg (54 %) of **10** as colourless crystals, m.p. 140°C .

$\text{C}_{21}\text{H}_{24}\text{BClN}_4\text{OZn}$ (460.10)	Calc.:	C 54.82	H 5.26	N 12.18	Zn 14.21
	Found:	C 54.13	H 5.15	N 12.36	Zn 13.72

IR (KBr, cm^{-1})	3059 m, 2928 m, 2473 (B-H) s, 2390 (B-H) m, 2336 (B-H) m, 2280 (B-H) w, 1608 w, 1540 s, 1503 s, 1483 m, 1438 s, 1421 m, 1380 w, 1363 s, 1220 w, 1163 vs, 1118 vs, 1097 m, 1072 w, 1030 w, 1011 w, 985 s, 920 w, 887 w, 805 m, 765 vs, 698 s, 628 m, 613 m.
-----------------------------	--

$^1\text{H-NMR}$ (DMSO- d_6 , 310 K)	2.39 [s, 6H, $\text{CH}_3(\text{pz})$], 3.17 [s, 3H, $\text{CH}_3(\text{MeOH})$], 6.41 [s, 2H, $\text{CH}(\text{pz})$], 7.35 [m, 6H, $\text{CH}_{\text{ph}}(3,4,5)$], 7.74 [m, 4H, $\text{CH}_{\text{ph}}(2,6)$].
--	--

4.2.10. Potassium hydrotris(3-(4'-pyridyl)-5-methyl)pyrazolylborate

$\text{KTp}^{4'\text{Py,Me}}$ **11**

A mixture of 6.28 g (39.44 mmol) of (3-(4'-pyridyl)-5-methyl)pyrazole^{91,165} and 532 mg (9.86 mmol) of KBH_4 was stirred in a three-necked 100 ml flask equipped with an immersing thermometer. The temperature was slowly increased to 200°C over a period of 30 min. At $140\text{--}160^\circ\text{C}$ the mixture melted and the gas evolution became brisk. The melt was kept stirring at 200°C until it started to turn brown (ca. 3 h) and then slowly cooled to room temperature. The resulting glassy residue was carefully powdered and

refluxed in 100 ml of toluene for 30 min, in order to remove impurities of unreacted pyrazole. The mixture was filtered hot and the light brown residue was washed 3 times with 5 ml of boiling toluene each and 1 time with 5 ml of petroleum ether (30-50°C). Recrystallization from 50 ml of acetonitrile at -20°C yielded after 1 day 2.59 g (50 %) of **11** as colourless crystals, m.p. 328°C.

$C_{27}H_{25}BKN_9$	Calc.:	C 61.72	H 4.80	N 23.99
(525.46)	Found:	C 61.23	H 4.85	N 23.87

IR (KBr, cm^{-1}) 3121 w, 3035 w, 2980 w, 2929 w, 2857 w, 2446 (B-H) m, 1605 vs, 1555 w, 1540 m, 1511 m, 1464 w, 1432 s, 1348 s, 1307 m, 1219 m, 1194 s, 1175 s, 1158 m, 1070 s, 1054 s, 994 s, 966 m, 833 s, 807 s, 779 s, 703 w, 660 w, 638 m, 536 m.

1H -NMR (DMSO- d_6 , 310 K) 2.02 [s, 9H, CH_3 (pz)], 6.44 [s, 3H, CH (pz)], 7.58 [dd, $^3J = 4.5$ Hz, $^4J = 1.5$ Hz, 6H, $CH_{py}(3',5')$], 8.42 [dd, $^3J = 4.5$ Hz, $^4J = 1.5$ Hz, 6H, $CH_{py}(2',6')$].

^{13}C -NMR (DMSO- d_6 , 310 K) 11.8 [CH_3 (pz)], 102.8 [pz(4)], 119.0 [$py(3',5')$], 142.4 [$py(4')$], 144.4 [pz(5)], 146.0 [pz(3)], 149.5 [$py(2',6')$].

4.2.11. Potassium hydrotris(3-(4'-(6'-methyl)pyridyl)-5-methyl)pyrazolylborate



2.66 g (15.35 mmol) of (3-(4'-(6'-methyl)-pyridyl)-5-methyl)pyrazole^{91,165} and 207 mg (3.84 mmol) of KBH_4 were mixed with stirring in a three-necked 50 ml flask equipped with an immersing thermometer. The temperature was slowly increased to 200°C over a period of 30 min. The melt was kept stirring at 200°C until it started to turn brown (ca. 3 h) and then slowly cooled to room temperature. The resulting glassy residue was carefully powdered and refluxed in 50 ml of toluene for 30 min, in order to remove impurities of unreacted pyrazole. The mixture was filtered hot and the light

brown residue was washed 3 times with 5 ml of boiling toluene each and 1 time with 5 ml of petroleum ether (30-50°C). Recrystallization from 50 ml of undried acetonitrile at -20°C yielded 871 mg (40 %) of **12** as colourless crystals, m.p. 319°C (dec.).

$C_{30}H_{31}BKN_9 \cdot H_2O$ (567.54 + 18.02)	Calc.:	C 61.54	H 5.68	N 21.53
	Found:	C 61.05	H 5.76	N 21.33

IR (KBr, cm^{-1}) 3192 (water) b, 2956 w, 2920 w, 2486 (B-H) w, 1612 vs, 1557 m, 1540 s, 1503 w, 1468 m, 1446 m, 1418 s, 1382 w, 1325 s, 1286 m, 1195 s, 1160 m, 1089 w, 1072 s, 1038 w, 1002 m, 977 m, 860 s, 835 m, 775 s, 702 w, 663 w, 644 m, 554 w, 508 w, 446 w.

1H -NMR (DMSO- d_6 , 310 K) 1.99 [s, 9H, CH_3 (pz)], 2.41 [s, 9H, CH_3 (py)], 6.41 [s, 3H, CH (pz)], 7.38 [d, $^3J = 5.1$ Hz, 3H, CH py(3')], 7.45 [s, 3H, CH py(5')], 8.28 [d, $^3J = 5.1$ Hz, 3H, CH py(2')].

^{13}C -NMR (DMSO- d_6 , 310 K) 10.1 [CH_3 (pz)], 22.3 [CH_3 (py)], 101.1 [pz(4)], 114.7 [py(3')], 116.4 [py(5')], 141.0 [py(4')], 142.6 [py(2')], 144.4 [py(6')], 147.1 [pz(5)], 155.9 [pz(3)].

4.2.12. Hydrotris(3-(4'-pyridyl)-5-methyl)pyrazolylborate zinc chloride

$Tp^{4'Py,Me}Zn-Cl$ **13**

A solution of 46 mg (0.33 mmol) of $ZnCl_2$ in 5 ml of methanol was dropped within 5 min to a solution of 160 mg (0.30 mmol) of **11** in 20 ml of methanol/dichloromethane (1:1). After 6 h of stirring small amounts of a cloudy precipitate were removed by filtration and the clear filtrate was slowly evaporated at room temperature to yield after 2 days 116 mg (65 %) of **13** as colourless needles, m.p. 238°C.

$C_{27}H_{25}BClN_9Zn \cdot 1.5 H_2O$ (587.21 + 27.02)	Calc.:	C 52.80	H 4.59	N 20.52
	Found:	C 52.63	H 4.48	N 20.66

IR (KBr, cm ⁻¹)	3420 (water) b, 3066 w, 3032 w, 2973 w, 2929 w, 2553 (B-H) w, 2496 (B-H) w, 1619 s, 1606 m, 1541 s, 1521 w, 1506 w, 1474 s, 1437 m, 1369 m, 1346 m, 1310 w, 1220 s, 1178 w, 1129 m, 1081 s, 1064 m, 1026 m, 991 w, 963 s, 828 s, 786 w, 743 w, 709 w, 690 w, 663 m, 634 w, 539 w, 486 w.
¹ H-NMR (DMSO-d ₆ , 310 K)	2.02 [s, 6H, CH ₃ (pz)], 2.54 [s, 3H, CH ₃ (pz)], 6.44 [s, 2H, CH(pz)], 6.65 [s, 1H, CH(pz)], 7.58 [d, ³ J = 6.0 Hz, 4H, CHpy(3',5')], 7.70 [d, ³ J = 5.5 Hz, 2H, CHpy(3',5')], 8.41 [d, ³ J = 6.0 Hz, 4H, CHpy(2',6')], 8.59 [d, ³ J = 6.0 Hz, 2H, CHpy(2',6')].

4.2.13. Hydrotris(3-(4'-pyridyl)-5-methyl)pyrazolylborate zinc bromide

TP^{4Py,Me}Zn-Br 14

A solution of 150 mg (0.67 mmol) of ZnBr₂ in 10 ml of methanol/dichloromethane (1:1) was dropped with stirring to a solution of 318 mg (0.61 mmol) of 11 in 20 ml of methanol/dichloromethane (1:1) over a period of 30 min. A white solid precipitated immediately, but the mixture was kept reacting for 6 h. Then the solvent was removed in vacuo and the residue was dissolved in chloroform/methanol (90:10) under reflux. Storing at 5°C over 2 days precipitated 298 mg (78 %) of 14 as colourless needles, m.p. 252°C.

C ₂₇ H ₂₅ BBrN ₉ Zn	Calc.:	C 51.34	H 3.99	N 19.96	Zn 10.35
(631.66)	Found:	C 50.77	H 4.11	N 19.53	Zn 10.07

IR (KBr, cm ⁻¹)	3123 w, 3060 w, 3035 w, 2964 w, 2927 w, 2856 w, 2557 (B-H) w, 2499 (B-H) w, 1621 vs, 1546 m, 1509 m, 1474 w, 1438 s, 1371 m, 1347 m, 1314 w, 1221 m, 1178 s, 1065 s, 1026 m, 991 m, 963 w, 838 m, 812 w, 790 m, 756 w, 716 w, 635 m, 551 w.
-----------------------------	---

$^1\text{H-NMR}$ (DMSO- d_6 , 310 K) 2.07 [s, 1.5H, $\text{CH}_3(\text{pz})$], 2.53 [s, 7.5H, $\text{CH}_3(\text{pz})$], 6.46 [s, 0.5H, $\text{CH}(\text{pz})$], 6.63 [s, 2.5H, $\text{CH}(\text{pz})$], 7.61 [m, 6H, $\text{CHpy}(3',5')$], 8.42 [d, $^3\text{J} = 5.3$ Hz, 1H, $\text{CHpy}(2',6')$], 8.62 [d, $^3\text{J} = 4.9$ Hz, 5H, $\text{CHpy}(2',6')$].

4.2.14. Hydrotris(3-(4'-pyridyl)-5-methyl)pyrazolylborate zinc iodide

$\text{Tp}^{4\text{Py,Me}}\text{Zn-I}$ **15**

The preparation of **15** was analogous to that of **14**, but with ZnI_2 (127 mg, 0.40 mmol). Recrystallization from chloroform/methanol (90:10) at 5°C yielded 184 mg (75%) of **15** as colourless needles, m.p. 226°C .

$\text{C}_{27}\text{H}_{25}\text{BIN}_9\text{Zn}$	Calc.:	C 47.78	H 3.71	N 18.57	Zn 9.64
(678.66)	Found:	C 47.09	H 3.83	N 19.00	Zn 9.32

IR (KBr, cm^{-1}) 3031 w, 2964 w, 2928 w, 2557 (B-H) w, 2491 (B-H) w, 1617 s, 1542 s, 1521 w, 1507 w, 1474 w, 1436 s, 1367 m, 1345 m, 1309 w, 1219 m, 1179 s, 1128 w, 1064 s, 1024 m, 990 m, 962 w, 829 m, 793 s, 710 w, 635 m, 552 w.

$^1\text{H-NMR}$ (DMSO- d_6 , 310 K) 2.00 [s, 1.5H, $\text{CH}_3(\text{pz})$], 2.54 [s, 7.5H, $\text{CH}_3(\text{pz})$], 6.46 [s, 0.5H, $\text{CH}(\text{pz})$], 6.63 [s, 2.5H, $\text{CH}(\text{pz})$], 7.56 [m, 6H, $\text{CHpy}(3',5')$], 8.41 [d, $^3\text{J} = 6.0$ Hz, 1H, $\text{CHpy}(2',6')$], 8.72 [dd, $^3\text{J} = 4.6$ Hz, $^4\text{J} = 1.4$ Hz, 5H, $\text{CHpy}(2',6')$].

4.2.15. Hydrotris(3-(4'-pyridyl)-5-methyl)pyrazolylborate zinc acetate

$\text{Tp}^{4\text{Py,Me}}\text{Zn-OC(O)CH}_3$ **16**

A solution of 174 mg (0.79 mmol) of $\text{Zn(OAc)}_2 \cdot 2\text{H}_2\text{O}$ in 5 ml of methanol was dropped within 5 min to a solution of 379 mg (0.72 mmol) of **11** in 20 ml of methanol/dichloromethane (1:1). After 6 h of stirring small amounts of a cloudy

precipitate were removed by filtration and the clear filtrate was evaporated to dryness in vacuo. Recrystallization from 15 ml of methanol at 5°C yielded after 1 day 401 mg (91 %) of **16** as large crystals, m.p. 242°C.

$C_{29}H_{28}BN_9O_2Zn$	Calc.:	C 57.03	H 4.62	N 20.64
(610.80)	Found:	C 56.49	H 4.82	N 20.42

IR (KBr, cm^{-1}) 3122 w, 3075 w, 3041 w, 2980 w, 2928 w, 2816 w, 2558 (B-H) m, 1608 vs, 1543 s, 1505 w, 1474 w, 1436 s, 1406 w, 1371 m, 1347 m, 1332 w, 1311 w, 1220 w, 1171 s, 1130 w, 1102 w, 1064 s, 1033 m, 991 m, 935 w, 860 w, 829 s, 792 s, 774 m, 699 m, 687 w, 658 w, 636 m, 543 w, 503 w.

1H -NMR (DMSO- d_6 , 310 K) 1.51 [b, 3H, $CH_3(OAc)$], 2.56 [s, 9H, $CH_3(pz)$], 6.64 [s, 3H, $CH(pz)$], 7.60 [dd, $^3J = 4.6$ Hz, $^4J = 1.4$ Hz, 6H, $CHpy(3',5')$], 8.60 [d, $^3J = 6.0$ Hz, 6H, $CHpy(2',6')$].

4.2.16. Hydrotris(3-(4'-pyridyl)-5-methyl)pyrazolylborate zinc nitrate

$Tp^{4'Py,Me}Zn-ONO_2$ **17**

A solution of 146 mg (0.49 mmol) of $Zn(NO_3)_2 \cdot 6H_2O$ in 5 ml of methanol was dropped within 5 min to a solution of 234 mg (0.45 mmol) of **11** in 20 ml of methanol. A white solid precipitated immediately, but the mixture was kept stirring for 6 h. Then the solvent was removed in vacuo and the residue was dissolved in chloroform/methanol (90:10) under reflux. Storing at 5°C over 5 days precipitated 188 mg (69 %) of **17** as colourless crystals, m.p. 210°C (dec.).

$C_{27}H_{25}BN_{10}O_3Zn \cdot H_2O$	Calc.:	C 51.33	H 4.31	N 22.17
(613.76 + 18.02)	Found:	C 51.47	H 4.01	N 22.05

IR (KBr, cm^{-1}) 3414 (water) b, 3145 m, 3075 w, 3031 w, 2989 w, 2963 w, 2924 w, 2550 (B-H) m, 1613 s, 1548 s, 1509 vs, 1475 m, 1430 vs, 1384 s, 1363 m, 1346 m, 1306 m, 1281 vs, 1222 m, 1194 s, 1128 w, 1074 s, 1063 s, 1026 w, 1015 m, 993 w, 982 m, 886 w, 831 w, 812 s, 795 s, 743 w, 705 m, 687 w, 664 w, 637 m, 540 m.

$^1\text{H-NMR}$ (DMSO- d_6 , 310 K) 2.01 [s, 1.5H, $\text{CH}_3(\text{pz})$], 2.55 [s, 7.5H, $\text{CH}_3(\text{pz})$], 6.45 [s, 0.5H, $\text{CH}(\text{pz})$], 6.62 [s, 2.5H, $\text{CH}(\text{pz})$], 7.56 [m, 6H, $\text{CHpy}(3',5')$], 8.41 [d, $^3J = 5.7$ Hz, 1H, $\text{CHpy}(2',6')$], 8.72 [d, $^3J = 5.9$ Hz, 5H, $\text{CHpy}(2',6')$].

4.2.17. Hydrotris(3-(4'-pyridyl)-5-methyl)pyrazolylborate zinc aqua complex $[\text{Tp}^{4'\text{Py,Me}}\text{Zn}\cdot\text{OH}_2]\text{ClO}_4$ **18**

165 mg (0.31 mmol) of **11** were dissolved in 20 ml of methanol/dichloromethane (1:1), and 128 mg (0.34 mmol) of $\text{Zn}(\text{ClO}_4)_2\cdot 6\text{H}_2\text{O}$ in 5 ml H_2O were added dropwise. The mixture was stirred for 2 h at room temperature and then the precipitated KClO_4 was filtered off. The filtrate was concentrated in vacuo to one half of the initial volume and then slowly evaporated at room temperature to yield after 1 day 151 mg (72 %) of **18** as colourless crystals, m.p. 300°C . Cocrystallized water could not be completely removed by prolonged pumping.

$\text{C}_{27}\text{H}_{27}\text{BClN}_9\text{O}_5\text{Zn}\cdot\text{H}_2\text{O}$	Calc.:	C 47.19	H 4.25	N 18.34
(669.22 + 18.02)	Found:	C 47.01	H 4.15	N 18.19

IR (KBr, cm^{-1}) 3515 (water) b, 3121 (O-H) s, 3061 w, 2971 w, 2933 w, 2567 (B-H) m, 1622 s, 1611 s, 1544 s, 1512 w, 1476 w, 1441 s, 1370 m, 1346 m, 1312 w, 1193 m, 1178 s, 1093 (Cl=O) vs, 1064 vs, 992 m, 830 m, 815 s, 784 s, 717 w, 637 m, 623 m, 559 w.

$^1\text{H-NMR}$ (DMSO- d_6 , 310 K) 2.00 [s, 1.5H, $\text{CH}_3(\text{pz})$], 2.55 [s, 7.5H, $\text{CH}_3(\text{pz})$], 6.46 [s, 0.5H, $\text{CH}(\text{pz})$], 6.63 [s, 2.5H, $\text{CH}(\text{pz})$], 7.67 [m, 6H, $\text{CHpy}(3',5')$], 8.53 [d, $^3J = 6.0$ Hz, 1H, $\text{CHpy}(2',6')$], 8.84 [d, $^3J = 5.9$ Hz, 5H, $\text{CHpy}(2',6')$].

$^{13}\text{C-NMR}$ (DMSO- d_6 , 310 K) 12.2 [$\text{CH}_3(\text{pz})$], 106.1 [pz(4)], 119.1 [py(4')], 121.9 [py(3',5')], 139.0 [pz(5)], 146.8 [pz(3)], 149.8 [py(2',6')].

4.2.18. Hydrotris(3-(4'-pyridyl)-5-methyl)pyrazolylborate zinc methanol complex [Tp^{4'Py,Me}Zn·HOMe]ClO₄ **19**

210 mg (0.40 mmol) of **11** were dissolved in 30 ml of methanol/dichloromethane (1:1), and 163 mg (0.44 mmol) of $\text{Zn}(\text{ClO}_4)_2 \cdot 6\text{H}_2\text{O}$ in 5 ml methanol were added dropwise over a period of 10 min. A slurry of KClO_4 precipitated immediately. It was filtered off and the clear filtrate was stirred for 6 h. After this time large amounts of a colourless solid had precipitated. The precipitate was filtered off and dried in vacuo to yield 180 mg (66 %) of **19** as a colourless powder, m.p. 284°C. The mother liquor was concentrated in vacuo to ca. 20 ml and kept at 5°C overnight to yield 10 mg (4 %) of **19** as X-ray quality crystals.

$\text{C}_{28}\text{H}_{29}\text{BClN}_9\text{O}_5\text{Zn} \cdot \text{H}_2\text{O}$	Calc.:	C 47.96	H 4.46	N 17.98
(683.25 + 18.02)	Found:	C 47.75	H 4.36	N 17.60

IR (KBr, cm^{-1}) 3572 (O-H) m, 3428 (water) b, 3131 w, 3068 w, 2971 w, 2930 w, 2574 (B-H) m, 1623 s, 1610 s, 1544 s, 1508 w, 1472 w, 1439 s, 1429 s, 1371 m, 1346 m, 1318 w, 1194 m, 1176 s, 1094 (Cl=O) vs, 1078 vs, 991 m, 841 m, 816 m, 790 s, 719 w, 707 w, 695 w, 624 m, 570 w, 552 w.

$^1\text{H-NMR}$ (DMSO- d_6 , 310 K) 2.01 [s, 1.5H, $\text{CH}_3(\text{pz})$], 2.55 [s, 7.5H, $\text{CH}_3(\text{pz})$], 3.34 [s, 3H, $\text{CH}_3(\text{HOMe})$], 6.45 [s, 0.5H, $\text{CH}(\text{pz})$], 6.62 [s, 2.5H, $\text{CH}(\text{pz})$], 7.56 [m, 6H, $\text{CHpy}(3',5')$], 8.41 [d, $^3J = 5.9$ Hz, 1H, $\text{CHpy}(2',6')$], 8.73 [d, $^3J = 5.9$ Hz, 5H, $\text{CHpy}(2',6')$].

$^{13}\text{C-NMR}$ (DMSO- d_6 , 310 K) 12.3 [$\text{CH}_3(\text{pz})$], 48.5 [$\text{CH}_3(\text{MeOH})$], 106.3 [pz(4)], 119.3 [py(4')], 122.0 [py(3',5')], 139.1 [pz(5)], 147.0 [pz(3)], 150.0 [py(2',6')].

4.2.19. Hydrotris(3-(4'-pyridyl)-5-methyl)pyrazolylborate zinc hydroxide

$\text{Tp}^{4'\text{Py,Me}}\text{Zn-OH}$ **20**

To a suspension of 229 mg (0.34 mmol) of **18** in 20 ml of methanol/dichloromethane (1:1), was added water until a clear solution formed (ca. 5 ml). This solution was cooled to 5-10°C in an ice bath and treated with 34.6 mg (0.62 mmol) of KOH dissolved in 10 ml of methanol/dichloromethane (1:1). After 2 h of stirring the precipitated KClO_4 was filtered off. The filtrate was concentrated in vacuo until a colourless solid started to precipitate. Storing at 5°C over 2 days yielded 142 mg (73 %) of **20** as a colourless powder, m.p. 296°C. **20** was found to be very hygroscopic.

$\text{C}_{27}\text{H}_{26}\text{BN}_9\text{OZn} \cdot 2 \text{H}_2\text{O}$	Calc.:	C 53.62	H 5.00	N 20.84
(568.76 + 36.03)	Found:	C 53.68	H 4.81	N 21.07

IR (KBr, cm^{-1}) 3633 (O-H) w, 3394 (water) b, 3119 w, 3035 s, 2974 w, 2929 w, 2857 w, 2551 (B-H) w, 1605 s, 1543 m, 1511 m, 1465 w, 1432 s, 1368 w, 1346 m, 1306 m, 1220 w, 1181 s, 1129 w, 1069 m, 1019 w, 992 m, 967 w, 831 m, 785 s, 700 m, 664 w, 639 m, 536 m.

$^1\text{H-NMR}$ (DMSO- d_6 , 310 K) 2.01 [s, 6H, $\text{CH}_3(\text{pz})$], 2.55 [s, 3H, $\text{CH}_3(\text{pz})$], 6.44 [s, 2H, $\text{CH}(\text{pz})$], 6.62 [s, 1H, $\text{CH}(\text{pz})$], 7.56 [m, 6H,

CHpy(3',5')), 8.41 [d, $^3J = 5.6$ Hz, 4H, CHpy(2',6')],
8.73 [d, $^3J = 5.3$ Hz, 2H, CHpy(2',6')].

**4.2.20. Bis (hydrotris (3-(4'-pyridyl)-5-methyl)pyrazolylborate) zinc-bis
(hydrotris(3-(4'-pyridyl)-5-methyl)pyrazolylborate zinc hydroxide)
[(Tp^{4'Py,Me})₂Zn][Tp^{4'Py,Me}Zn-OH]₂ 21**

The synthesis described in 4.1.19 was performed at room temperature. After filtration of the precipitated KClO₄ the solvent was slowly evaporated. Precipitated Zn(OH)₂ was removed twice by filtration. After 2 days 20 mg of 21 had precipitated in the form of colourless crystals, m.p. 176°C. The crystals were analysed without removing the co-crystallized solvent molecules before.

C ₁₀₈ H ₁₀₂ B ₄ N ₃₆ O ₂ Zn ₃ · 2 H ₂ O · 2 CH ₂ Cl ₂	Calc.:	C 55.43	H 4.74	N 21.15
(2175.65 + 36.03 + 171.88)	Found:	C 55.12	H 5.28	N 20.75

IR (KBr, cm⁻¹) 3407 (water) vs, 2956 w, 2925 w, 2854 w, 2555 (B-H) w, 2459 (B-H) w, 1606 vs, 1544 m, 1513 w, 1465 w, 1433 s, 1369 w, 1347 m, 1307 m, 1222 w, 1181 s, 1129 w, 1065 s, 1026 m, 992 m, 966 w, 832 m, 787 s, 700 m, 638 m, 536 m.

¹H-NMR (DMSO-d₆, 310 K) 2.02 [s, 14H, CH₃(pz)], 2.08 [s, 4H, CH₃(pz)], 2.16 [s, 4H, CH₃(pz)], 2.55 [s, 14H, CH₃(pz)], 5.74 [s, 4H, CH₂Cl₂], 6.44 [s, 5H, CH(pz)], 6.55 [s, 1H, CH(pz)], 6.62 [s, 5H, CH(pz)], 6.70 [s, 1H, CH(pz)], 7.56 [m, 20H, CHpy(3',5')], 7.63 [d, $^3J = 6.2$ Hz, 2H, CHpy(3',5')], 7.74 [d, $^3J = 6.2$ Hz, 2H, CHpy(3',5')], 8.41 [d, $^3J = 5.9$ Hz, 10H, CHpy(2',6')], 8.48 [d, $^3J = 6.2$ Hz, 2H, CHpy(2',6')], 8.59 [d, $^3J = 6.2$ Hz, 2H, CHpy(2',6')], 8.73 [d, $^3J = 4.9$ Hz, 10H, CHpy(2',6')].

**4.2.21. Hydrotris(3-(4'-pyridyl)-5-methyl)pyrazolylborate)-zinc-methylcarbonate-
Hydrotris(3-(4'-pyridyl)-5-methyl)pyrazolylborate)-zinc-chloride**
[Tp^{4'Py,Me}Zn-OC(O)OMe][Tp^{4'Py,Me}Zn-Cl] 22

223 mg (0.39 mmol) of **20** were dissolved in 50 ml of methanol/dichloromethane/water (1:1:0.5). The solution was cooled to 5-10°C in an ice bath and slowly evaporated to half of the initial volume by passing a stream of CO₂ through it over a period of 4 h. Small amounts of a white precipitate were removed by filtration and the clear filtrate was kept at 5°C overnight to yield 10 mg (2 %) of **22** as colourless crystals, m.p. 238°C. They were separated by decantation and analysed by single-crystal X-ray diffraction, IR and ¹H-NMR spectroscopy. The mother liquor was concentrated to 5 ml under a slow stream of CO₂, the remaining solvent was removed with a syringe, and the colourless residue was dried in vacuo to yield 58 mg of analytically impure **22**.

IR (KBr, cm⁻¹) 3421 (water) b, 3126 w, 3073 w, 3035 w, 2964 w, 2928 w, 2559 (B-H) w, 1606 b, 1545 m, 1512 w, 1467 w, 1434 vs, 1370 w, 1348 m, 1222 w, 1179 vs, 1066 s, 1028 w, 992 w, 965 w, 832 m, 793 s, 743 w, 700 m, 637 m, 538 m.

¹H-NMR (CDCl₃) 2.50 [s, 12H, CH₃(pz)], 2.56 [s, 6H, CH₃(pz)], 2.82 [s, 3H, CH₃(OMe)], 5.85 [s, 2H, CH(pz)], 6.30 [s, 4H, CH(pz)], 6.36 [dd, ³J = 4.7 Hz, ⁴J = 1.7 Hz, 4H, CHpy(3',5')], 7.45 [d, ³J = 6.2 Hz, 6H, CHpy(3',5')], 7.53 [dd, ³J = 4.4 Hz, ⁴J = 1.6 Hz, 4H, CHpy(3',5')], 7.74 [dd, ³J = 4.6 Hz, ⁴J = 1.6 Hz, 4H, CHpy(2',6')], 8.59 [d, ³J = 5.2 Hz, 8H, CHpy(2',6')].

**4.2.22. Hydrotris(3-(4'-pyridyl)-5-methyl)pyrazolylborate) zinc methyl
dithiocarbonate [Tp^{4'Py,Me}Zn-SC(S)OMe] 23**

To a solution of 352 mg (0.62 mmol) of **20** in 30 ml of methanol/dichloromethane/water (1:1:0.5), which was cooled to 5-10°C in an ice bath, were added dropwise 371 μ l (470 mg, 6.18 mmol) of CS₂ over a period of 30 min. After 6 h of stirring all volatiles were removed in vacuo and the residue was taken up in 10 ml of chloroform. After 30 min of stirring the mixture was filtered and the filtrate was evaporated to dryness in vacuo to yield 289 mg (71 %) of **23** as a colourless powder, m.p. 218°C.

C₂₉H₂₈BN₉OS₂Zn
(658.93)

Calc.: C 52.86 H 4.28 N 19.13 S 9.73 Zn 9.92
Found: C 52.32 H 4.42 N 20.11 S 8.96 Zn 9.48

IR (KBr, cm⁻¹)

3420 (water) b, 3138 w, 3029 w, 2985 w, 2927 w, 2853 w, 2562 (B-H) m, 1606 s, 1545 s, 1504 w, 1472 w, 1438 s, 1370 m, 1346 m, 1309 w, 1207 s, 1193 s, 1181 s, 1155 w, 1100 w, 1066 vs, 990 m, 959 w, 861 w, 828 s, 799 s, 782 w, 698 m, 637 m, 550 w, 536 w, 463 w.

¹H-NMR (CDCl₃)

2.59 [s, 9H, CH₃(pz)], 3.17 [s, 3H, CH₃(OMe)], 6.30 [s, 3H, CH(pz)], 7.52 [dd, ³J = 4.4 Hz, ⁴J = 1.6 Hz, 6H, CHpy(3',5')], 8.60 [dd, ³J = 4.4 Hz, ⁴J = 1.6 Hz, 6H, CHpy(2',6')].

4.2.23. Hydrotris(3-(4'-pyridyl)-5-methyl)pyrazolylborate) zinc ethyl dithiocarbonate [Tp^{4'Py,Me}Zn-SC(S)OEt] **24**

To a solution of 368 mg (0.65 mmol) of **20** in 50 ml of ethanol/dichloromethane/water (1:1:0.5), which was cooled to 5-10°C in an ice bath, were added dropwise 388 μ l (492 mg, 6.48 mmol) of CS₂ over a period of 30 min. After 12 h of stirring all volatiles were removed in vacuo, and the residue was recrystallized from 15 ml of acetonitrile/dichloromethane (1:1) at 5°C to yield after 2 days 296 mg (68 %) of **24** as a colourless powder, m.p. 224°C. **24** could not be obtained in a pure form but it was characterized by IR and ¹H-NMR.

IR (KBr, cm^{-1}) 3410 (water) b, 3029 w, 2968 w, 2926 w, 2556 (B-H) m, 1606 m 1543 m, 1505 w, 1471 w, 1438 s, 1371 m, 1346 m, 1310 w, 1177 vs, 1108 m, 1066 s, 1052 s, 990 m, 859 w, 827 m, 793 vs, 715 w, 697 w, 664 w, 636 w.

$^1\text{H-NMR}$ (CDCl_3) 0.90 [t, $^3\text{J} = 7.0$ Hz, 3H, $\text{CH}_3(\text{OEt})$], 2.59 [s, 9H, $\text{CH}_3(\text{pz})$], 3.49 [q, $^3\text{J} = 7.0$ Hz, 2H, $\text{CH}_2(\text{OEt})$], 6.31 [s, 3H, $\text{CH}(\text{pz})$], 7.54 [dd, $^3\text{J} = 4.5$ Hz, $^4\text{J} = 1.6$ Hz, 6H, $\text{CHpy}(3',5')$], 8.60 [dd, $^3\text{J} = 4.5$ Hz, $^4\text{J} = 1.6$ Hz, 6H, $\text{CHpy}(2',6')$].

4.2.24. Hydrotris(3-(4'-pyridyl)-5-methyl)pyrazolylborate) zinc *p*-nitrophenolate $\text{Tp}^{4\text{Py,Me}}\text{Zn-ONit}$ **25**

To a solution of 278 mg (0.49 mmol) of **20** in 30 ml of methanol/dichloromethane /water (1:1:0.5), which was cooled to 5-10°C in an ice bath, was added dropwise a solution of 68 mg (0.49 mmol) of *p*-nitrophenol in 5 ml of methanol. After 6 h of stirring all volatiles were removed in vacuo and the residue was recrystallized from 15 ml of methanol/dichloromethane (1:2) at -20°C to yield 314 mg (93 %) of **25** as a light yellow powder, m.p. 254°C (dec.).

$\text{C}_{33}\text{H}_{29}\text{BN}_{10}\text{O}_3\text{Zn} \cdot \text{H}_2\text{O}$	Calc.:	C 55.99	H 4.41	N 19.79
(689.86 + 18.02)	Found:	C 56.15	H 4.42	N 19.74

IR (KBr, cm^{-1}) 3411 (water) b, 3034 w, 2929 w, 2559 (B-H) w, 1607 m, 1584 (N=O) s, 1544 m, 1494 m, 1434 m, 1370 w, 1347 w, 1334 w, 1304 (N=O) vs, 1219 w, 1176 s, 1109 m, 1066 m, 991 w, 829 m, 790 m, 758 w, 700 w, 656 w, 635 m, 544 w, 498 w.

$^1\text{H-NMR}$ (CDCl_3) 1.66 [b, 2H, H_2O], 2.62 [s, 9H, $\text{CH}_3(\text{pz})$], 5.88 [d, $^3\text{J} = 9.1$ Hz, 2H, $\text{CHph}(2,6)$], 6.43 [s, 3H, $\text{CH}(\text{pz})$], 7.51 [m,

8H, CHpy(3',5'), CHph(3,5)], 8.41 [dd, $^3J = 4.5$ Hz, $^4J = 1.4$ Hz, 6H, CHpy(2',6')].

4.2.25. Hydrotris(3-(4'-pyridyl)-5-methyl)pyrazolylborate) zinc acetylacetonate Tp^{4'Py,Me}Zn(acac) **26**

To a solution of 506 mg (0.89 mmol) of **20** in 30 ml of methanol/dichloromethane (1:1), which was cooled to 5-10°C in an ice bath, were added dropwise 101 µl (98 mg, 0.98 mmol) of acetylacetonate over a period of 5 min. After 6 h of stirring all volatiles were removed in vacuo and the residue was recrystallized from 15 ml of acetonitrile/dichloromethane (1:1) at 5°C to yield after 2 days 504 mg (87 %) of **26** as a light yellow powder, m.p. 230°C.

C ₃₂ H ₃₂ BN ₉ O ₂ Zn (650.86)	Calc.:	C 59.05	H 4.96	N 19.37	Zn 10.05
	Found:	C 58.58	H 5.53	N 18.51	Zn 9.91

IR (KBr, cm ⁻¹)	3378 (water) b, 3122 m, 3029 s, 2966 s, 2927 m, 2549 (B-H) s, 1610 vs, 1543 s, 1517 s, 1439 vs, 1314 m, 1263 s, 1218 m, 1177 vs, 1104 m, 1065 s, 1018 m, 990 s, 956 w, 926 m, 859 w, 828 s, 782 vs, 713 m, 695 m, 637 s, 546 m, 496 w, 438 w, 411 m.
-----------------------------	--

¹ H-NMR (CDCl ₃)	1.14 [s, 6H, CH ₃ (MeC(O))], 2.55 [s, 9H, CH ₃ (pz)], 5.02 [s, 1H, CH(C(O)CHC(O))] 6.30 [s, 3H, CH(pz)], 7.39 [dd, $^3J = 4.6$ Hz, $^4J = 1.4$ Hz, 6H, CHpy(3',5')], 8.52 [dd, $^3J = 4.6$ Hz, $^4J = 1.4$ Hz, 6H, CHpy(2',6')].
---	--

4.2.26. Hydrotris(3-(4'-pyridyl)-5-methyl)pyrazolylborate) zinc benzoylacetonate Tp^{4'Py,Me}Zn(benzoylac) **27**

To a solution of 407 mg (0.71 mmol) of **20** in 25 ml of methanol/dichloromethane (1:1), which was cooled to 5-10°C in an ice bath, was added dropwise a solution of 116

mg (0.71 mmol) of benzoylacetone in 5 ml of dichloromethane. After 6 h of stirring all volatiles were removed in vacuo, and the residue was recrystallized from 15 ml of acetonitrile/dichloromethane (1:1) at 5°C to yield after 2 days 479 mg (94 %) of **27** as colourless crystals, m.p. 211°C (dec.). Co-crystallized dichloromethane could not be completely removed by prolonged pumping.

$C_{37}H_{34}BN_9O_2Zn \cdot 0.25 CH_2Cl_2$	Calc.:	C 60.92	H 4.77	N 17.16
(712.94 + 21.49)	Found:	C 61.12	H 4.97	N 17.10

IR (KBr, cm^{-1}) 3420 (water) b, 3134 w, 3067 w, 3032 w, 2984 w, 2928 m, 2549 (B-H) m, 1607 vs, 1594 vs, 1566 vs, 1543 vs, 1513 vs, 1485 s, 1450 s, 1388 vs, 1348 w, 1307 m, 1284 m, 1222 m, 1175 s, 1130 w, 1106 w, 1070 s, 1028 w, 990 s, 955 w, 829 s, 804 w, 784 s, 712 s, 691 m, 664 w, 637 s, 579 w, 550 m, 489 w, 427 w.

1H -NMR ($CDCl_3$) 1.13 [s, 3H, $CH_3(MeC(O))$], 2.57 [s, 9H, $CH_3(pz)$], 5.29 [s, 0.5H, CH_2Cl_2], 5.62 [s, 1H, $CH(C(O)CHC(O))$] 6.31 [s, 3H, $CH(pz)$], 7.01 [m, 2H, $CHph(2,6)$], 7.14 [m, 2H, $CHph(3,5)$], 7.32 [m, 1H, $CHph(4)$], 7.40 [dd, $^3J = 4.5$ Hz, $^4J = 1.5$ Hz, 6H, $CHpy(3',5')$], 8.39 [dd, $^3J = 4.5$ Hz, $^4J = 1.5$ Hz, 6H, $CHpy(2',6')$].

4.2.27. Hydrotris(3-(4'-pyridyl)-5-methyl)pyrazolylborate) zinc bis(*p*-nitrophenyl)phosphate $Tp^{4'Py,Me}Zn-OP(O)(ONit)_2$ **28**

To a solution of 278 mg (0.49 mmol) of **20** in 25 ml of methanol/dichloromethane (1:1), which was cooled to 5-10°C in an ice bath, was added dropwise a solution of 183 mg (0.54 mmol) of $HOP(O)(ONit)_2$ in 10 ml of methanol. After 2 h of stirring all volatiles were removed in vacuo, and the raw product was suspended in 5 ml of chloroform. Then the suspension was filtered and the clear filtrate was evaporated to dryness in vacuo to yield 134 mg (31 %) of **28** as a light yellow powder, m.p. 231°C. **28**

could not be obtained in a pure form but it was characterized by IR, $^1\text{H-NMR}$ and $^{31}\text{P-NMR}$ spectroscopy.

IR (KBr, cm^{-1})	3386 (water) b, 3113 w, 3081 w, 2566 (B-H) w, 1621 m, 1610 m, 1591 (N=O) m, 1548 w, 1515 s, 1490 s, 1438 m, 1373 w, 1346 (N=O) vs, 1298 m, 1258 m, 1224 s, 1179 m, 1110 b, 1066 m, 1020 w, 992 w, 900 b, 851 m, 836 w, 793 m, 761 w, 750 m, 715 w, 689 w, 641 m, 620 w, 544 m, 498 w, 447 w.
$^1\text{H-NMR}$ (CDCl_3)	2.60 [s, 9H, $\text{CH}_3(\text{pz})$], 6.40 [s, 3H, $\text{CH}(\text{pz})$], 6.85 [d, $^3\text{J} = 8.9$ Hz, 4H, $\text{CHph}(2,6)$], 7.52 [d, $^3\text{J} = 5.9$ Hz, 6H, $\text{CHpy}(3',5')$], 7.98 [d, $^3\text{J} = 9.1$ Hz, 4H, $\text{CHph}(3,5)$], 8.61 [d, $^3\text{J} = 5.7$ Hz, 6H, $\text{CHpy}(2',6')$].
$^{31}\text{P-NMR}$ (CDCl_3)	-16.9 [s, 1P]

4.2.28. Hydrotris(3-(4'-pyridyl)-5-methyl)pyrazolylborate) zinc trifluoroacetamidate $\text{Tp}^{4'\text{Py,Me}}\text{Zn-NHC(O)CF}_3$ **29**

To a solution of 397 mg (0.70 mmol) of **20** in 30 ml of methanol/dichloromethane (2:1), which was cooled to 5-10°C in an ice bath, was added dropwise a solution of 79 mg (0.70 mmol) of trifluoroacetamide in 5 ml of methanol. After 6 h of stirring all volatiles were removed in vacuo, and the residue was recrystallized from 15 ml of chloroform at room temperature to yield after 2 days 343 mg (74 %) of **29** as a colourless powder, m.p. 207°C (dec.).

$\text{C}_{29}\text{H}_{26}\text{BF}_3\text{N}_{10}\text{OZn} \cdot 0.25 \text{CHCl}_3$	Calc.: C 50.65	H 3.81	N 20.19	Zn 9.43
(663.79 + 29.84)	Found: C 49.88	H 3.93	N 19.68	Zn 9.00

IR (KBr, cm^{-1})	3416 (N-H) m, 3133 w, 3070 w, 3034 w, 2977 w, 2929 w, 2859 w, 2559 (B-H) w, 1679 (C=O) s, 1607 m, 1544
-----------------------------	--

m, 1509 w, 1463 m, 1440 s, 1372 m, 1348 m, 1312 w, 1256 w, 1221 w, 1176 vs, 1145 m, 1067 s, 1028 w, 991 m, 964 w, 830 m, 792 m, 744 w, 721 w, 701 w, 660 w, 637 m, 550 w, 516 w, 496 w.

¹H-NMR (CDCl₃) 2.58 [s, 9H, CH₃(pz)], 5.05 [b, 1H, NH], 6.34 [s, 3H, CH(pz)], 7.39 [d, ³J = 5.9 Hz, 6H, CHpy(3',5')], 8.60 [d, ³J = 5.8 Hz, 6H, CHpy(2',6')].

¹H-NMR (CD₂Cl₂) 2.58 [s, 9H, CH₃(pz)], 6.36 [s, 3H, CH(pz)], 7.31 [s, 0.25H, CHCl₃], 7.41 [m, 6H, CHpy(3',5')], 8.56 [m, 6H, CHpy(2',6')].

¹⁹F-NMR (CDCl₃) -76.03 [CF₃]

4.2.29. Potassium hydrotris(3-phenylcarboxamide-5-methyl)pyrazolylborate KTp^{C(O)NPh,Me} **30**

A mixture of 3.29 g (16.35 mmol) of (3-methyl-5-phenylcarboxamide)pyrazole¹⁶⁸ and 221 mg (4.09 mmol) of KBH₄ was stirred in a three-necked 50 ml flask equipped with an immersing thermometer. The temperature was slowly increased to 150°C over a period of 30 min, temperature at which the mixture melted. The melt was kept stirring at 150°C until no more hydrogen was evolved (ca. 2 h) and then heated to 160°C for 30 min. After it was cooled to room temperature, the resulting glassy residue was carefully powdered and refluxed in 30 ml of acetonitrile for 30 min, in order to remove impurities of unreacted pyrazole. The mixture was filtered hot and the residue was washed 3 times with 5 ml of boiling acetonitrile each and 1 time with 2 ml of water. Recrystallization from 40 ml of methanol/dichloromethane (1:2) at -20°C yielded after 2 days 300 mg (11 %) of **30** as large crystals, m.p. 250°C.

C ₃₃ H ₃₁ BN ₉ O ₃ K · H ₂ O	Calc.:	C 59.19	H 4.97	N 18.83
(651.58 + 18.02)	Found:	C 59.43	H 5.14	N 18.44

IR (KBr, cm^{-1})	3365 (N-H) s, 3309 b, 3129 w, 3056 w, 2959 w, 2929 w, 2470 (B-H) m, 1653 (C=O) vs, 1597 s, 1530 vs, 1497 s, 1445 s, 1429 s, 1376 w, 1345 m, 1315 s, 1241 m, 1189 vs, 1119 w, 1073 s, 1029 w, 1012 w, 982 w, 915 w, 881 m, 826 m, 807 w, 751 s, 692 s, 652 m, 578 m, 508 m, 445 w.
$^1\text{H-NMR}$ (DMSO- d_6 , 310 K)	2.01 [s, 9H, $\text{CH}_3(\text{pz})$], 6.46 [s, 3H, $\text{CH}(\text{pz})$], 7.01 [m, 3H, $\text{CHph}(4)$], 7.27 [m, 6H, $\text{CHph}(3,5)$], 7.64 [d, $^3J = 7.6$ Hz, 6H, $\text{CHph}(2,6)$], 9.25 [s, 3H, NH].
$^{13}\text{C-NMR}$ (DMSO- d_6 , 310 K)	11.8 [$\text{CH}_3(\text{pz})$], 105.0 [$\text{pz}(4)$], 119.4 [$\text{ph}(2,6)$], 122.9 [$\text{ph}(4)$], 128.4 [$\text{ph}(3,5)$], 138.7 [$\text{ph}(1)$], 144.3 [$\text{pz}(5)$], 145.2 [$\text{pz}(3)$], 161.2 [$\text{C}(\text{O})$].

4.2.30. Hydrotris(3-phenylcarboxamide-5-methyl)pyrazolylborate zinc chloride
 $\text{Tp}^{\text{C}(\text{O})\text{NHPh,Me}_3}\text{Zn-Cl}$ **31**

A solution of 22 mg (0.16 mmol) of ZnCl_2 in 2 ml of methanol was added dropwise to a solution of 96 mg (0.15 mmol) of **30** in 10 ml of methanol/dichloromethane (1:1). After 3 h of stirring small amounts of a cloudy precipitate were removed by filtration and the clear filtrate was slowly evaporated at room temperature to yield after 1 day 91 mg (87 %) of **31** as colourless needles, m.p. 216°C .

$\text{C}_{33}\text{H}_{31}\text{BClN}_9\text{O}_3\text{Zn} \cdot \text{H}_2\text{O}$	Calc.:	C 54.20	H 4.55	N 17.05
(713.32 + 18.02)	Found:	C 53.74	H 4.66	N 17.05

IR (KBr, cm^{-1})	3315 (N-H) s, 3266 s, 3152 w, 3117 m, 3060 w, 2966 w, 2930 w, 2511 (B-H) w, 1648 (C=O) s, 1598 vs, 1564 s, 1533 vs, 1499 m, 1478 w, 1452 s, 1429 s, 1375 w, 1319 s, 1276 w, 1245 m, 1180 vs, 1130 w, 1085 w, 1067 m,
-----------------------------	--

1025 m, 985 w, 887 m, 829 m, 815 m, 769 m, 753 s,
691 m, 648 m, 591 w, 509 m.

$^1\text{H-NMR}$ (CDCl_3) 1.57 [b, 2H, H_2O], 2.53 [s, 9H, $\text{CH}_3(\text{pz})$], 6.80 [s, 3H, $\text{CH}(\text{pz})$], 7.14 [m, 3H, $\text{CHph}(4)$], 7.33 [m, 6H, $\text{CHph}(3,5)$], 7.74 [d, $^3\text{J} = 7.8$ Hz, 6H, $\text{CHph}(2,6)$], 8.89 [s, 3H, NH].

4.2.31. Hydrotris(3-phenylcarboxamide-5-methyl)pyrazolylborate zinc nitrate $\text{Tp}^{\text{C(O)NHPH,Me}}\text{Zn-ONO}_2$ **32**

A solution of 50 mg (0.17 mmol) of $\text{Zn}(\text{NO}_3)_2 \cdot 6\text{H}_2\text{O}$ in 5 ml of methanol was added dropwise to a solution of 100 mg (0.15 mmol) of **30** in 10 ml of methanol. After 3 h of stirring small amounts of a cloudy precipitate were removed by filtration and the clear filtrate was evaporated to dryness in vacuo. Recrystallization from 10 ml of methanol/dichloromethane (1:1) at 5°C yielded 87 mg (77 %) of **32** as a white powder, m.p. 190°C.

$\text{C}_{33}\text{H}_{31}\text{BN}_{10}\text{O}_6\text{Zn}$	Calc.:	C 53.57	H 4.22	N 18.93	Zn 8.84
(739.87)	Found:	C 52.93	H 4.31	N 19.01	Zn 8.49

IR (KBr, cm^{-1}) 3282 b, 3134 m, 2566 (B-H) w, 1648 (C=O) b, 1601 s, 1553 s, 1534 s, 1497 m, 1451 s, 1431 s, 1384 vs, 1354 s, 1318 s, 1250 w, 1178 s, 1065 m, 1040 w, 989 w, 916 w, 887 w, 828 w, 753 m, 691 m, 642 w, 590 w, 510 w.

$^1\text{H-NMR}$ (CDCl_3) 2.39 [s, 9H, $\text{CH}_3(\text{pz})$], 6.54 [s, 3H, $\text{CH}(\text{pz})$], 6.76 [m, 9H, $\text{CHph}(3,4,5)$], 7.03 [d, $^3\text{J} = 8.2$ Hz, 6H, $\text{CHph}(2,6)$], 9.80 [s, 3H, NH].

4.2.32. Hydrotris(3-phenylcarboxamide-5-methyl)pyrazolylborate zinc acetate



A solution of 35 mg (0.16 mmol) of $\text{Zn(OAc)}_2 \cdot 2\text{H}_2\text{O}$ in 2 ml of methanol was added dropwise to a solution of 94 mg (0.14 mmol) of **30** in 10 ml of methanol/dichloromethane (2:1). After 3 h of stirring small amounts of a cloudy precipitate were removed by filtration and the clear filtrate was slowly evaporated at room temperature to yield after 1 day 93 mg (88 %) of **33** as colourless crystals, m.p. 216°C.

$\text{C}_{35}\text{H}_{34}\text{BN}_9\text{O}_5\text{Zn}$ (736.91)	Calc.:	C 57.05	H 4.65	N 17.11	Zn 8.87
	Found:	C 56.29	H 4.75	N 16.84	Zn 8.65
IR (KBr, cm^{-1})	3307 (N-H) s, 3131 w, 2930 w, 2573 (B-H) m, 1683 m, 1650 s, 1600 s, 1553 s, 1535 s, 1500 m, 1478 w, 1452 m, 1435 m, 1378 m, 1347 w, 1318 s, 1248 m, 1179 vs, 1131 w, 1070 s, 1038 m, 987 w, 937 w, 923 w, 890 m, 815 m, 759 s, 748 s, 692 s, 667 w, 646 m, 607 w, 587 w, 573 w, 511 m, 455 w.				
$^1\text{H-NMR}$ (CDCl_3)	1.75 [s, 3H, $\text{CH}_3(\text{OAc})$], 2.39 [s, 3H, $\text{CH}_3(\text{pz})$], 2.52 [s, 6H, $\text{CH}_3(\text{pz})$], 6.69 [m, 5H, $\text{CH}(\text{pz})$, $\text{CHph}(4)$], 7.08 [m, 5H, $\text{CHph}(2,3,4,5,6)$], 7.28 [m, 4H, $\text{CHph}(3,5)$], 7.67 [d, $^3\text{J} = 7.6$ Hz, 4H, $\text{CHph}(2,6)$], 8.95 [b, 3H, NH].				

4.2.33. Bis(hydrotris(3-phenylcarboxamide-5-methyl)pyrazolylborate zinc



A solution of 84 mg (0.22 mmol) of $\text{Zn(ClO}_4)_2 \cdot 6\text{H}_2\text{O}$ in 2 ml of methanol was added dropwise to a solution of 133 mg (0.20 mmol) of **30** in 10 ml of methanol/dichloromethane (1:1). After 3 h of stirring the precipitated KClO_4 was

removed by filtration and the clear filtrate was slowly evaporated at room temperature to yield after 1 day 111 mg (74 %) of **34** as colourless crystals, m.p. 218°C.

$C_{66}H_{63}B_2ClN_{18}O_{11}Zn_2 \cdot H_2O$	Calc.:	C 53.20	H 4.40	N 16.92
(1472.19 + 18.02)	Found:	C 52.84	H 4.67	N 16.34

IR (KBr, cm^{-1}) 3298 b, 3137 w, 3061 w, 2967 w, 2931 w, 2565 (B-H) w, 1646 b, 1601 s, 1552 s, 1534 s, 1498 m, 1479 w, 1451 s, 1431 s, 1377 w, 1347 w, 1318 s, 1249 m, 1177 s, 1121 m, 1107 (Cl=O) m, 1065 s, 1040 w, 887 m, 832 w, 770 s, 752 s, 692 s, 642 m, 591 m, 512 m.

1H -NMR ($CDCl_3$) 1.55 [b, 2H, H_2O], 2.43 [s, 18H, $CH_3(pz)$], 6.54 [s, 6H, $CH(pz)$], 6.78 [m, 18H, $CH_{ph}(3,4,5)$], 7.07 [m, 12H, $CH_{ph}(2,6)$], 9.29 [b, 6H, NH]

^{13}C -NMR ($CDCl_3$) 12.8 [$CH_3(pz)$], 108.0 [$pz(4)$], 120.6 [$ph(2,6)$], 124.5 [$ph(4)$], 128.1 [$ph(3,5)$], 136.3 [$ph(1)$], 146.6 [$pz(5)$], 146.7 [$pz(3)$], 158.9 [$C(O)$].

4.3. X-Ray single crystal determinations

The single-crystal X-ray diffraction data of the complexes were collected with a Smart-CCD diffractometer of Bruker AXS using Mo-K α radiation. None of the crystals showed any significant intensity loss throughout the data collections. The collected data were processed by SAINT,¹⁶⁹ in which the decay and Lorentz-Polarisation corrections were applied. The absorption corrections were applied to the data by using the SADABS program.¹⁷⁰ The structures were solved by direct or Patterson methods using SHELXS-97¹⁷¹ to find out the positions of the heavy atoms. The other non-hydrogen atoms were located by Fourier syntheses and refined using SHELXL-97.¹⁷² The PLATON program¹⁷³ was used to search for higher symmetry. The least squares refinements were performed using all independent reflections by the full matrix on F². The hydrogen atoms were positioned at calculated sites (with C-H 0.96 Å) and were constrained to ride on their linked atoms with isotropic thermal parameters of 1.5 times the factor of the methyl groups and 1.2 times the factor of the other groups. The R-indexes and goodness of Fit (Goof) are defined by the equations given below, where n is the number of the reflections and p is the number of parameters.

$$w = 1 / [\sigma^2(F_0^2) + (aP)^2 + bP] \text{ with } P = (F_0^2 + 2F_c^2)/3 \quad (4.1)$$

$$wR_2 = [\sum [w(F_0^2 - F_c^2)^2] / \sum [w(F_0^2)^2]]^{1/2} \quad (4.2)$$

$$R1 = \sum |F_0 - F_c| / \sum F_0 \quad (4.3)$$

$$\text{Goof} = [\sum [w(F_0^2 - F_c^2)^2] / (n-p)]^{1/2} \quad (4.4)$$

The crystal data are given in tables 4.1 – 4.7. The complete positional and thermal parameters are listed in tables 4.8 – 4.20. The ORTEP drawings of the structures, generated using the XP program,¹⁷⁴ are shown in figures 4.1 – 4.13.

Table 4.1. Crystallographic data for **3** and **5**.

	3	5
Empirical formula	C ₁₂ H ₁₆ BKN ₄ O ₄	C ₂₈ H ₄₀ B ₂ N ₈ O ₈ Zn
Formula weight	330.20	703.67
Crystal size [mm]	0.48 x 0.38 x 0.03	0.18 x 0.13 x 0.09
Crystal colour	colourless	colourless
Space group	P2(1)	P-1
Z	2	2
a [Å]	12.051(3)	10.3832(19)
b [Å]	6.0828(13)	13.788(3)
c [Å]	12.201(3)	13.936(3)
α[°]	90	93.445(3)
β[°]	117.141(4)	108.628(3)
γ[°]	90	107.741(3)
Volume [Å ³]	795.9(3)	1773.1(6)
d (calc.) [g/cm ³]	1.378	1.318
μ(MoKα) [mm ⁻¹]	0.355	0.749
Temperature [K]	293(2)	296(2)
Θ-range [°]	1.88 to 30.14	1.57 to 28.87
Index ranges	-14<=h<=16 -7<=k<=8 -16<=l<=11	-13<=h<=13 -18<=k<=18 -18<=l<=18
Absorption correction	SADABS	SADABS
Reflections collected	4804	32254
Independent reflections	3528[R(int) = 0.0367]	8283[R(int) = 0.0641]
Reflections observed [I>2σ(I)]	2202	4354
Reflections refined	3528	8283
Parameters	200	425
Goodness-of-fit	1.011	1.043
Final R indices [I>2σ(I)]	R1 = 0.0603, wR2 = 0.1340	R1 = 0.0714, wR2 = 0.1849
Final R indices (all data)	R1 = 0.1112, wR2 = 0.1803	R1 = 0.1436, wR2 = 0.2505
Largest diff. peak and hole [e.Å ⁻³]	0.691 -0.676	0.947 -0.614

Table 4.2. Crystallographic data for **6** and **10**.

	6	10
Empirical formula	C ₂₄ H ₃₂ B ₂ N ₈ O ₈ Zn	C ₂₁ H ₂₃ BClN ₄ OZn · 2 CH ₃ OH
Formula weight	647.57	459.09 + 64.08
Crystal size [mm]	0.19 x 0.12 x 0.07	0.23 x 0.17 x 0.10
Crystal colour	colourless	colourless
Space group	P2(1)/c	P2(1)/c
Z	4	4
a [Å]	10.264(2)	12.424(4)
b [Å]	22.302(4)	10.234(3)
c [Å]	13.283(3)	21.353(6)
α[°]	90	90
β[°]	102.065(4)	95.145(5)
γ[°]	90	90
Volume [Å ³]	2973.6(10)	2704.0(14)
d (calc.) [g/cm ³]	1.446	1.285
μ(MoKα) [mm ⁻¹]	0.886	1.036
Temperature [K]	296(2)	293(2)
Θ-range [°]	1.81 to 30.12	1.65 to 28.74
Index ranges	-14 ≤ h ≤ 13 -31 ≤ k ≤ 24 -16 ≤ l ≤ 16	-16 ≤ h ≤ 16 -13 ≤ k ≤ 13 -27 ≤ l ≤ 27
Absorption correction	SADABS	None
Reflections collected	19571	22886
Independent reflections	8158[R(int) = 0.0844]	6478[R(int) = 0.1467]
Reflections observed	2976	2301
[I > 2σ(I)]		
Reflections refined	8158	6478
Parameters	389	302
Goodness-of-fit	0.927	0.863
Final R indices [I > 2σ(I)]	R1 = 0.0685, wR2 = 0.1702	R1 = 0.0608, wR2 = 0.1442
Final R indices (all data)	R1 = 0.1983, wR2 = 0.2429	R1 = 0.1936, wR2 = 0.1879
Largest diff. peak and hole [e.Å ⁻³]	0.799 -0.706	0.505 -0.562

Table 4.3. Crystallographic data for **11** and **16**.

	11	16
Empirical formula	C ₂₇ H ₂₅ BKN ₉ · CH ₃ CN	C ₂₉ H ₂₈ BN ₉ O ₂ Zn · CH ₃ OH
Formula weight	525.46 + 41.05	610.80 + 32.04
Crystal size [mm]	0.21 x 0.16 x 0.12	0.23 x 0.13 x 0.04
Crystal colour	colourless	colourless
Space group	P2(1)/c	P2(1)/c
Z	4	4
a [Å]	11.3751(18)	12.936(4)
b [Å]	16.015(3)	16.933(6)
c [Å]	16.499(3)	16.460(4)
α[°]	90	89.905(8)
β[°]	103.399(3)	120.673(18)
γ[°]	90	90.091(7)
Volume [Å ³]	2924.0(8)	3101.0(16)
d (calc.) [g/cm ³]	1.287	1.377
μ(MoKα) [mm ⁻¹]	0.219	0.839
Temperature [K]	223(2)	233(2)
Θ-range [°]	1.80 to 30.07	1.83 to 29.01
Index ranges	-15 ≤ h ≤ 8 -20 ≤ k ≤ 22 -20 ≤ l ≤ 23	-17 ≤ h ≤ 17 -22 ≤ k ≤ 22 -22 ≤ l ≤ 21
Absorption correction	SADABS	None
Reflections collected	19542	28041
Independent reflections	8052[R(int) = 0.0750]	7663[R(int) = 0.1173]
Reflections observed [I > 2σ(I)]	3088	3942
Reflections refined	8052	7663
Parameters	371	403
Goodness-of-fit	0.970	1.039
Final R indices [I > 2σ(I)]	R1 = 0.0681, wR2 = 0.1671	R1 = 0.0579, wR2 = 0.1420
Final R indices (all data)	R1 = 0.1985, wR2 = 0.2378	R1 = 0.1209, wR2 = 0.1743
Largest diff. peak and hole [e.Å ⁻³]	0.426 -0.407	0.711 -0.731

Table 4.4. Crystallographic data for **17** and **18**.

	17	18
Empirical formula	C ₂₇ H ₂₅ BN ₁₀ O ₃ Zn	C ₅₄ H ₅₁ B ₂ Cl ₂ N ₁₈ O ₁₀ Zn ₂ ·MeOH·H ₂ O
Formula weight	613.75	1335.42 + 32.04 + 18.02
Crystal size [mm]	0.10 x 0.15 x 0.20	0.26 x 0.09 x 0.09
Crystal colour	colourless	colourless
Space group	P2(1)/n	P2(1)/c
Z	4	4
a [Å]	9.918(3)	26.312(6)
b [Å]	9.280(3)	11.316(2)
c [Å]	29.539(8)	25.932(6)
α[°]	90	90
β[°]	97.220(4)	110.907(4)
γ[°]	90	90
Volume [Å ³]	2697.1(13)	7213(3)
d (calc.) [g/cm ³]	1.512	1.276
μ(MoKα) [mm ⁻¹]	0.962	0.804
Temperature [K]	243(2)	247(2)
Θ-range [°]	1.39 to 28.78	1.59 to 28.95
Index ranges	-13 ≤ h ≤ 12 -12 ≤ k ≤ 12 -38 ≤ l ≤ 39	-34 ≤ h ≤ 34 -15 ≤ k ≤ 15 -34 ≤ l ≤ 35
Absorption correction	None	SADABS
Reflections collected	22184	63184
Independent reflections	6429[R(int) = 0.0862]	17506[R(int) = 0.1492]
Reflections observed [I > 2σ(I)]	3589	5382
Reflections refined	6429	17506
Parameters	379	836
Goodness-of-fit	1.010	0.783
Final R indices [I > 2σ(I)]	R1 = 0.0525, wR2 = 0.1319	R1 = 0.0808, wR2 = 0.1975
Final R indices (all data)	R1 = 0.1116, wR2 = 0.1582	R1 = 0.1925, wR2 = 0.2350
Largest diff. peak and hole [e.Å ⁻³]	0.577 -0.809	0.497 -0.427

Table 4.5. Crystallographic data for **19** and **21**.

	19	21
Empirical formula	C ₂₈ H ₂₉ BClN ₉ O ₅ Zn	C ₅₄ H ₅₁ B ₂ N ₁₈ OZn _{1.50} · H ₂ O · 1.75 CH ₂ Cl ₂
Formula weight	683.25	1247.91
Crystal size [mm]	0.30 x 0.20 x 0.07	0.23 x 0.13 x 0.08
Crystal colour	colourless	colourless
Space group	P-1	C2/c
Z	2	8
a [Å]	10.8383(19)	20.566(3)
b [Å]	12.544(2)	16.961(3)
c [Å]	16.023(3)	33.994(5)
α [°]	90.583(3)	90
β [°]	101.794(3)	92.157(4)
γ [°]	94.111(3)	90
Volume [Å ³]	2126.3(6)	11849(3)
d (calc.) [g/cm ³]	1.067	1.399
μ(MoKα) [mm ⁻¹]	0.679	0.828
Temperature [K]	233(2)	293(2)
Θ-range [°]	1.63 to 28.80	1.20 to 28.99
Index ranges	-14 ≤ h ≤ 14 -16 ≤ k ≤ 16 -21 ≤ l ≤ 21	-27 ≤ h ≤ 27 -23 ≤ k ≤ 22 -45 ≤ l ≤ 44
Absorption correction	SADABS	None
Reflections collected	18887	53568
Independent reflections	9849[R(int) = 0.0295]	14618[R(int) = 0.0715]
Reflections observed [I > 2σ(I)]	5623	6693
Reflections refined	9849	14618
Parameters	438	745
Goodness-of-fit	0.890	0.946
Final R indices [I > 2σ(I)]	R1 = 0.0527, wR2 = 0.1432	R1 = 0.0601, wR2 = 0.1717
Final R indices (all data)	R1 = 0.0784, wR2 = 0.1561	R1 = 0.1429, wR2 = 0.2109
Largest diff. peak and hole [e.Å ⁻³]	1.024 -0.363	0.775 -0.828

Table 4.6. Crystallographic data for **22** and **27**.

	22	27
Empirical formula	C ₅₆ H ₅₃ B ₂ ClN ₁₈ O ₃ Zn ₂	C ₃₇ H ₃₄ BN ₉ O ₂ Zn · CH ₂ Cl ₂
Formula weight	1213.97	712.94 + 84.93
Crystal size [mm]	0.14 x 0.13 x 0.09	0.12 x 0.20 x 0.21
Crystal colour	colourless	colourless
Space group	C2/c	P2(1)/n
Z	8	4
a [Å]	18.409(4)	12.003(2)
b [Å]	25.757(6)	18.769(3)
c [Å]	29.688(6)	16.999(3)
α[°]	90	90
β[°]	96.427(4)	97.345(3)
γ[°]	90	90
Volume [Å ³]	13988(5)	3798.2(11)
d (calc.) [g/cm ³]	1.153	1.395
μ(MoKα) [mm ⁻¹]	0.774	0.834
Temperature [K]	236(2)	246(2)
Θ-range [°]	1.37 to 28.86	1.62 to 30.00
Index ranges	-24 ≤ h ≤ 24 -34 ≤ k ≤ 34 -39 ≤ l ≤ 39	-13 ≤ h ≤ 16 -12 ≤ k ≤ 26 -20 ≤ l ≤ 22
Absorption correction	SADABS	SADABS
Reflections collected	62060	25040
Independent reflections	16890[R(int) = 0.0768]	9946[R(int) = 0.0344]
Reflections observed [I > 2σ(I)]	6332	6038
Reflections refined	16890	9946
Parameters	740	478
Goodness-of-fit	0.905	1.032
Final R indices [I > 2σ(I)]	R1 = 0.0721, wR2 = 0.1934	R1 = 0.0601, wR2 = 0.1811
Final R indices (all data)	R1 = 0.1570, wR2 = 0.2187	R1 = 0.1019, wR2 = 0.2149
Largest diff. peak and hole [e.Å ⁻³]	1.137 -0.775	1.355 -0.879

Table 4.7. Crystallographic data for **34**.

34	
Empirical formula	C ₆₆ H ₆₃ B ₂ ClN ₁₈ O ₁₁ Zn ₂
Formula weight	1472.15
Crystal size [mm]	0.23 x 0.10 x 0.10
Crystal colour	colourless
Space group	C2/c
Z	8
a [Å]	44.40(2)
b [Å]	17.703(8)
c [Å]	19.403(9)
α[°]	90
β[°]	110.614(13)
γ[°]	90
Volume [Å ³]	14275(11)
d (calc.) [g/cm ³]	1.370
μ(MoKα) [mm ⁻¹]	0.780
Temperature [K]	193(2)
Θ-range [°]	0.98 to 29.98
Index ranges	-43 ≤ h ≤ 56 -22 ≤ k ≤ 23 -27 ≤ l ≤ 20
Absorption correction	SADABS
Reflections collected	43639
Independent reflections	16280[R(int) = 0.1260]
Reflections observed [I > 2σ(I)]	5020
Reflections refined	16280
Parameters	901
Goodness-of-fit	0.961
Final R indices [I > 2σ(I)]	R1 = 0.0958, wR2 = 0.2458
Final R indices (all data)	R1 = 0.2529, wR2 = 0.2723
Largest diff. peak and hole [e.Å ⁻³]	0.908 -0.829

Table 4.8. Atomic coordinates (10^4) and equivalent isotropic displacement parameters ($\text{\AA}^2 \cdot 10^3$) for **3**.

	x	y	z	U(eq)
K(1)	8884(1)	6428(2)	4637(1)	37(1)
O(1)	6423(4)	7346(7)	4248(4)	52(1)
O(2)	4344(4)	6868(8)	3199(5)	64(1)
O(3)	10734(4)	7927(7)	3816(4)	48(1)
O(4)	11088(4)	7915(7)	2160(4)	48(1)
N(1)	6841(4)	3794(7)	3184(4)	37(1)
N(2)	9433(4)	3994(7)	2999(4)	32(1)
N(3)	6766(4)	1961(6)	2526(4)	35(1)
N(4)	8733(4)	2318(7)	2259(4)	34(1)
B(1)	8007(6)	799(10)	2728(6)	38(1)
C(1)	5165(6)	-556(11)	964(6)	53(2)
C(2)	5553(5)	1396(11)	1818(5)	40(1)
C(3)	4833(6)	2894(10)	2035(5)	45(1)
C(4)	5683(5)	4342(9)	2893(5)	39(1)
C(5)	5383(5)	6290(11)	3440(5)	45(1)
C(6)	6219(9)	9229(13)	4861(8)	77(2)
C(7)	8000(6)	791(10)	139(5)	48(2)
C(8)	8717(5)	2433(9)	1142(5)	38(1)
C(9)	9410(5)	4202(9)	1141(5)	38(1)
C(10)	9836(5)	5115(8)	2314(5)	34(1)
C(11)	10593(5)	7110(8)	2855(5)	36(1)
C(12)	11869(6)	9862(10)	2636(7)	57(2)

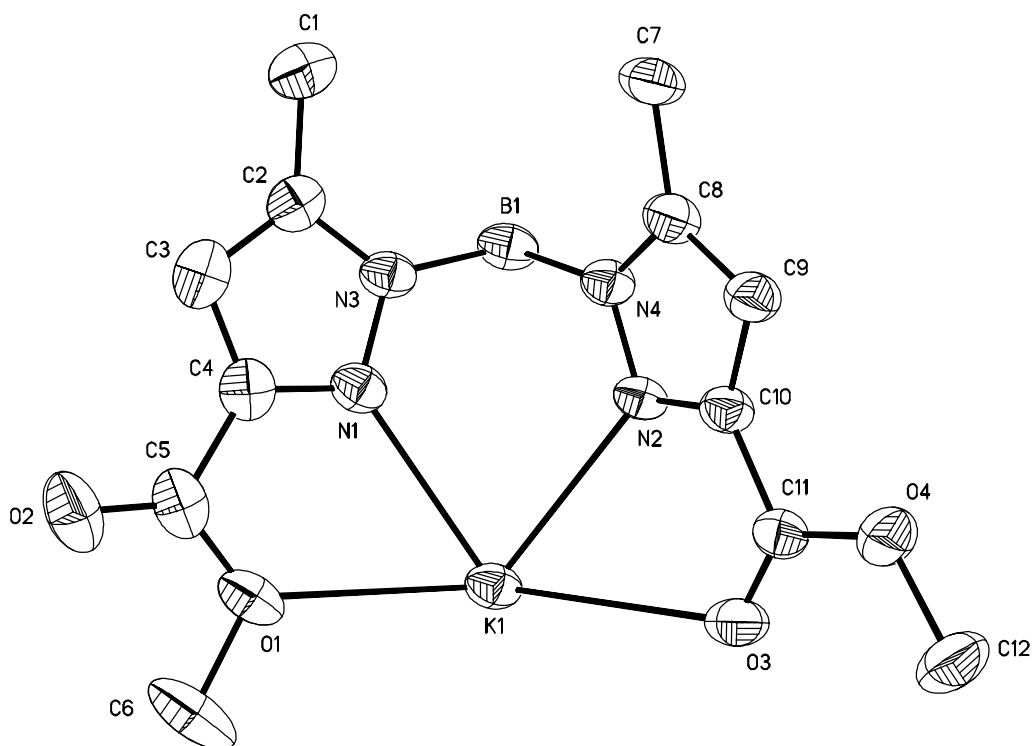


Figure 4.1. Ortep diagram with 30% thermal ellipsoids for **3**.

Table 4.9. Atomic coordinates (10^4) and equivalent isotropic displacement parameters ($\text{\AA}^2 \cdot 10^3$) for **5**.

	x	y	z	U(eq)
Zn(1)	15(1)	7815(1)	7230(1)	54(1)
O(1)	-1912(4)	9185(3)	7289(3)	64(1)
O(2)	-3596(4)	9299(4)	5841(3)	83(1)
O(3)	1040(7)	6353(4)	8508(4)	99(2)
O(4)	1284(6)	4905(4)	7919(4)	94(1)
O(5)	-2117(5)	6255(3)	5023(3)	71(1)
O(6)	-4386(4)	6290(3)	4401(3)	71(1)
O(7)	2655(5)	9519(4)	7943(3)	94(2)
O(8)	3719(5)	10668(3)	9398(3)	83(1)
N(1)	-498(4)	8594(3)	6038(3)	48(1)
N(2)	1086(4)	7066(3)	6684(3)	54(1)
N(3)	-2093(4)	6851(3)	7029(3)	53(1)
N(4)	559(4)	8459(3)	8694(3)	53(1)
N(5)	-81(4)	8457(3)	5224(3)	47(1)
N(6)	1280(4)	7205(3)	5784(3)	51(1)

N(7)	-2561(5)	7001(3)	7814(3)	60(1)
N(8)	-258(4)	8122(3)	9281(3)	53(1)
B(1)	1349(7)	8243(5)	5392(5)	59(2)
B(2)	-1567(8)	7106(6)	8944(5)	67(2)
C(1)	-979(5)	8647(4)	4378(3)	50(1)
C(2)	-2003(6)	8923(4)	4630(4)	55(1)
C(3)	-1671(5)	8887(4)	5677(3)	48(1)
C(4)	-834(7)	8543(5)	3342(4)	70(2)
C(5)	-2381(6)	9131(4)	6372(4)	56(1)
C(6)	-4386(8)	9615(9)	6438(6)	116(3)
C(7)	-3905(13)	10739(9)	6718(7)	145(4)
C(8)	1557(5)	6394(4)	5415(4)	56(1)
C(9)	1538(6)	5709(4)	6097(4)	62(1)
C(10)	1248(5)	6155(4)	6872(4)	55(1)
C(11)	1821(7)	6317(5)	4424(4)	76(2)
C(12)	1164(7)	5829(5)	7848(4)	68(2)
C(13)	1194(11)	4505(7)	8848(6)	115(3)
C(14)	-457(12)	4027(11)	8745(9)	160(5)
C(15)	-3972(6)	6894(5)	7444(4)	73(2)
C(16)	-4449(6)	6645(5)	6399(4)	71(2)
C(17)	-3258(5)	6627(4)	6166(4)	54(1)
C(18A)	-4829(13)	7243(16)	8061(10)	64(5)
C(18B)	-4735(16)	6810(20)	8182(12)	76(6)
C(19)	-3148(6)	6380(4)	5152(4)	57(1)
C(20)	-4396(7)	6077(6)	3368(4)	82(2)
C(21)	-5848(10)	5963(8)	2659(5)	126(3)
C(22)	356(6)	8764(4)	10204(4)	59(1)
C(23)	1572(6)	9518(5)	10200(4)	65(1)
C(24)	1656(5)	9302(4)	9249(4)	53(1)
C(25)	-279(8)	8606(5)	11036(4)	77(2)
C(26)	2699(6)	9812(5)	8784(4)	64(1)
C(27)	4854(8)	11206(6)	9015(7)	102(2)
C(28)	5726(11)	12153(8)	9649(9)	158(5)

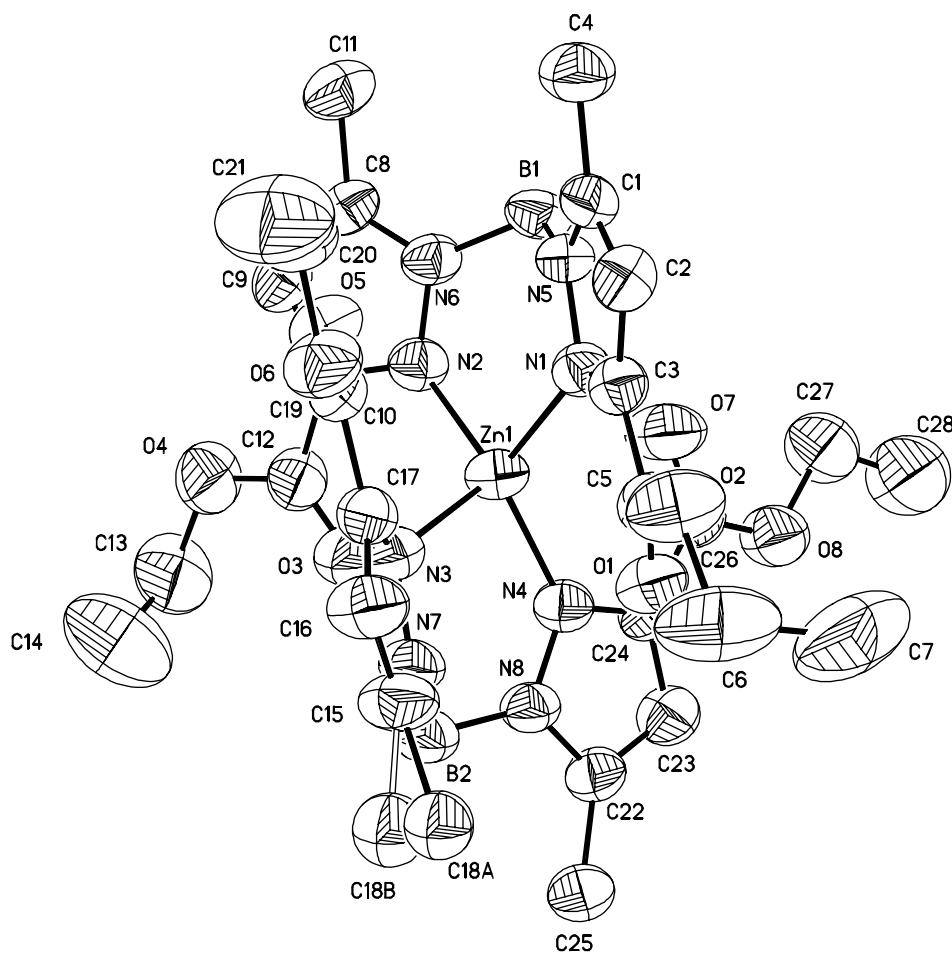


Figure 4.2. Ortep diagram with 30% thermal ellipsoids for **5**.

Table 4.10. Atomic coordinates (10^4) and equivalent isotropic displacement parameters ($\text{\AA}^2 \cdot 10^3$) for **6**.

	x	y	z	U(eq)
Zn(1)	7498(1)	3687(1)	7714(1)	44(1)
O(1)	4784(4)	2293(2)	8888(3)	62(1)
O(2)	6863(4)	2617(2)	8942(3)	51(1)
O(3)	9270(6)	4000(3)	6082(4)	92(2)
O(4)	8445(4)	4535(2)	4692(4)	69(1)
O(5)	8921(5)	4189(2)	9512(4)	70(1)
O(6)	10700(5)	3877(2)	10659(4)	67(1)
O(7)	4509(4)	3848(2)	6233(3)	59(1)
O(8)	3160(4)	3057(2)	6249(4)	61(1)
N(1)	5990(4)	3751(2)	8511(3)	40(1)

N(2)	7297(4)	4504(2)	7047(4)	47(1)
N(3)	9187(4)	3244(2)	8267(4)	46(1)
N(4)	6683(4)	3013(2)	6660(3)	41(1)
N(5)	5308(5)	4277(2)	8483(4)	45(1)
N(6)	6382(5)	4892(2)	7269(4)	47(1)
N(7)	9602(4)	2742(2)	7844(4)	47(1)
N(8)	7387(4)	2497(2)	6656(3)	42(1)
B(1)	5994(7)	4877(3)	8337(6)	51(2)
B(2)	8923(7)	2511(4)	6758(6)	58(2)
C(1)	4090(6)	4176(3)	8663(4)	49(1)
C(2)	3977(6)	3573(3)	8822(5)	55(2)
C(3)	5168(5)	3323(2)	8717(4)	41(1)
C(4)	3087(7)	4651(3)	8682(6)	76(2)
C(5)	5570(6)	2695(3)	8845(4)	46(1)
C(6)	7359(6)	2018(3)	9099(5)	57(2)
C(7)	6034(6)	5293(3)	6498(5)	52(2)
C(8)	6723(6)	5149(3)	5753(5)	55(2)
C(9)	7492(6)	4667(2)	6112(5)	46(1)
C(10)	5057(7)	5785(3)	6517(6)	77(2)
C(11)	8495(6)	4357(3)	5662(5)	52(2)
C(12)	9401(8)	4302(3)	4174(6)	79(2)
C(13)	10716(5)	2521(3)	8487(5)	53(2)
C(14)	10987(6)	2884(3)	9342(5)	53(2)
C(15)	10029(5)	3323(3)	9182(4)	44(1)
C(16)	11455(6)	1996(3)	8208(6)	75(2)
C(17)	9809(6)	3842(3)	9789(5)	54(2)
C(18)	10568(8)	4380(3)	11322(6)	80(2)
C(19)	6533(6)	2030(2)	6404(4)	42(1)
C(20)	5259(6)	2251(3)	6263(4)	46(1)
C(21)	5399(5)	2863(2)	6420(4)	40(1)
C(22)	6955(7)	1401(3)	6285(5)	63(2)
C(23)	4346(5)	3322(3)	6303(4)	45(1)
C(24)	2048(6)	3457(3)	6177(6)	77(2)

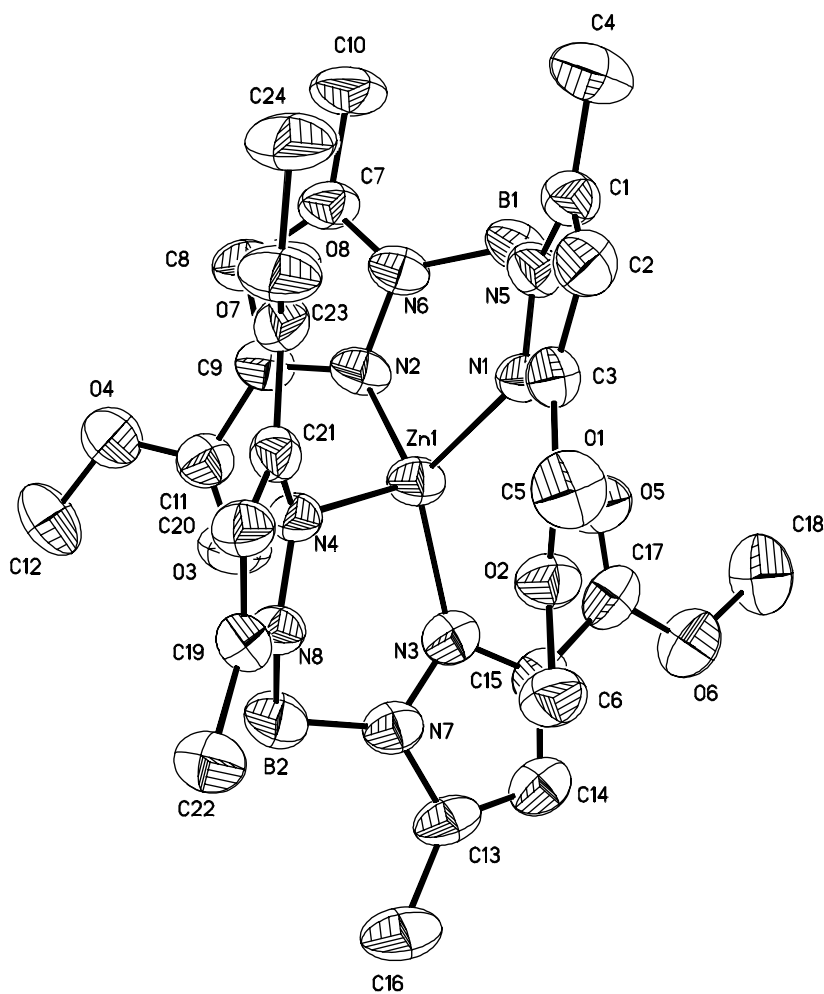


Figure 4.3. Ortep diagram with 30% thermal ellipsoids for **6**.

Table 4.11. Atomic coordinates (10^4) and equivalent isotropic displacement parameters ($\text{\AA}^2 \cdot 10^3$) for **10**.

	x	y	z	U(eq)
Zn(1)	2413(1)	947(1)	1674(1)	43(1)
Cl(1)	2362(1)	-1055(2)	1290(1)	70(1)
N(1)	3652(4)	1466(4)	2276(2)	44(1)
N(2)	1200(4)	1720(4)	2103(2)	43(1)
N(3)	3414(4)	1575(5)	2897(2)	45(1)
N(4)	1383(3)	1793(4)	2753(2)	45(1)
O(1)	2518(3)	2115(4)	938(2)	62(1)
O(2)	2536(6)	4624(6)	976(4)	125(2)
O(3)	1924(9)	5959(10)	1944(5)	193(4)
B(1)	2326(5)	978(7)	3064(3)	50(2)

C(1)	4178(6)	2463(8)	3931(3)	80(2)
C(2)	4217(5)	2206(6)	3232(3)	53(2)
C(3)	4982(5)	2516(6)	2844(3)	60(2)
C(4)	4628(4)	2055(6)	2256(3)	47(1)
C(5)	5186(4)	2068(6)	1671(3)	47(1)
C(6)	5079(5)	1060(7)	1245(3)	65(2)
C(7)	5664(6)	1068(8)	715(3)	81(2)
C(8)	6340(6)	2093(9)	619(3)	82(2)
C(9)	6451(6)	3103(9)	1035(4)	96(3)
C(10)	5873(6)	3075(7)	1563(3)	76(2)
C(11)	679(6)	2933(8)	3665(3)	81(2)
C(12)	674(5)	2626(6)	2968(3)	53(2)
C(13)	19(5)	3100(6)	2473(3)	60(2)
C(14)	362(4)	2529(6)	1936(3)	45(1)
C(15)	-79(4)	2687(6)	1285(3)	45(1)
C(16)	-149(5)	1656(6)	868(3)	64(2)
C(17)	-607(5)	1807(8)	251(3)	70(2)
C(18)	-945(5)	3024(8)	39(3)	66(2)
C(19)	-858(5)	4058(7)	444(3)	62(2)
C(20)	-430(5)	3892(6)	1066(3)	57(2)
C(21)	2512(7)	1757(9)	282(3)	106(3)
C(22)	3506(8)	5196(10)	832(6)	160(5)
C(23)	2280(11)	5531(15)	2565(6)	200(7)

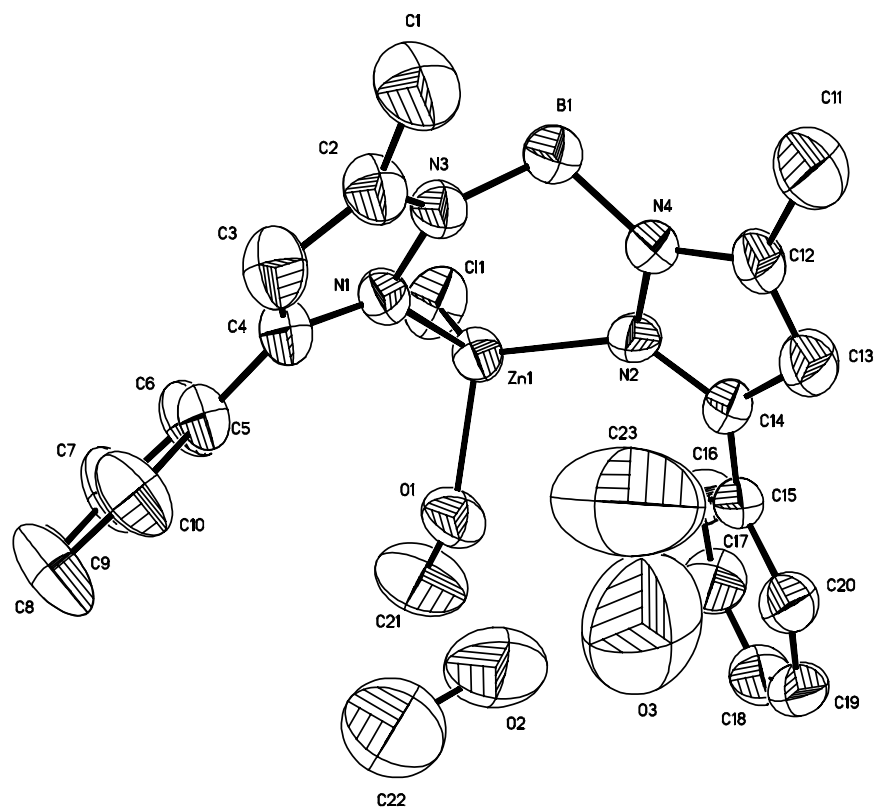


Figure 4.4. Ortep diagram with 30% thermal ellipsoids for **10**.

Table 4.12. Atomic coordinates (10^4) and equivalent isotropic displacement parameters ($\text{\AA}^2 \cdot 10^3$) for **11**.

	x	y	z	U(eq)
K(1)	6028(1)	4769(1)	7758(1)	43(1)
N(1)	8311(3)	5643(2)	7984(2)	36(1)
N(2)	7765(3)	4089(2)	9089(2)	36(1)
N(3)	7667(3)	4211(2)	6659(2)	37(1)
N(4)	9162(3)	5104(2)	7834(2)	36(1)
N(5)	8889(3)	4053(2)	8937(2)	35(1)
N(6)	8036(3)	3781(2)	7391(2)	37(1)
N(7)	6082(3)	8452(2)	7462(2)	58(1)
N(8)	5023(3)	4222(2)	11158(2)	48(1)
N(9)	5454(4)	4465(3)	3637(2)	63(1)
N(10)	11501(8)	1609(6)	10091(5)	150(3)
B(1)	9096(4)	4172(3)	8055(2)	37(1)
C(1)	10730(4)	4996(3)	6979(3)	58(1)

C(2)	9802(3)	5452(3)	7323(2)	43(1)
C(3)	9387(4)	6245(3)	7156(2)	48(1)
C(4)	8454(3)	6342(3)	7572(2)	41(1)
C(5)	7658(3)	7068(2)	7564(2)	41(1)
C(6)	7605(4)	7706(3)	6983(3)	56(1)
C(7)	6821(4)	8359(3)	6959(3)	57(1)
C(8)	6150(4)	7843(3)	8031(3)	65(1)
C(9)	6904(4)	7155(3)	8104(3)	50(1)
C(10)	11070(3)	3901(3)	9703(2)	47(1)
C(11)	9741(3)	3960(2)	9658(2)	37(1)
C(12)	9159(3)	3933(2)	10292(2)	39(1)
C(13)	7932(3)	4012(2)	9919(2)	34(1)
C(14)	6923(3)	4054(2)	10325(2)	36(1)
C(15)	5723(3)	3903(2)	9922(2)	42(1)
C(16)	4835(4)	3986(3)	10353(2)	46(1)
C(17)	6180(4)	4350(3)	11536(2)	47(1)
C(18)	7126(3)	4277(2)	11158(2)	41(1)
C(19)	7764(4)	2393(3)	8030(2)	57(1)
C(20)	7530(3)	3005(2)	7333(2)	40(1)
C(21)	6795(4)	2936(3)	6546(2)	45(1)
C(22)	6909(3)	3695(2)	6152(2)	39(1)
C(23)	6383(3)	3970(2)	5296(2)	41(1)
C(24)	6703(4)	4720(3)	4997(2)	54(1)
C(25)	6222(5)	4936(3)	4181(3)	62(1)
C(26)	5144(5)	3749(3)	3935(3)	75(2)
C(27)	5565(4)	3472(3)	4743(3)	62(1)
C(28)	9485(8)	1756(6)	10499(7)	208(6)
C(29)	10565(9)	1636(6)	10261(6)	119(3)

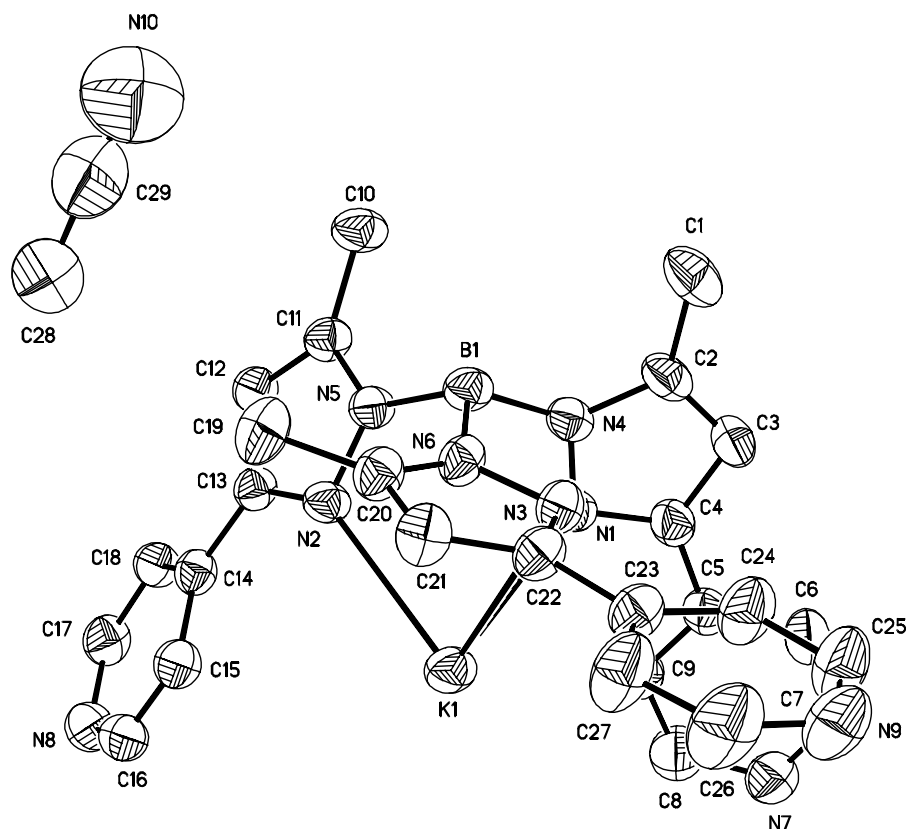


Figure 4.5. Ortep diagram with 30% thermal ellipsoids for **11**.

Table 4.13. Atomic coordinates (10^4) and equivalent isotropic displacement parameters ($\text{\AA}^2 \cdot 10^3$) for **16**.

	x	y	z	U(eq)
Zn(1)	5481(1)	2561(1)	2522(1)	36(1)
O(1)	7166(2)	2490(1)	3432(2)	51(1)
O(2)	6988(3)	3580(2)	2641(2)	64(1)
O(3)	-45(3)	427(3)	3302(3)	120(2)
N(1)	4489(2)	1546(2)	2442(2)	36(1)
N(2)	4779(2)	2503(2)	1111(2)	35(1)
N(3)	4260(2)	3303(2)	2519(2)	37(1)
N(4)	3309(2)	1638(2)	1751(2)	37(1)
N(5)	3553(2)	2510(2)	611(2)	35(1)
N(6)	3112(2)	3112(2)	1819(2)	38(1)
N(7)	7864(4)	-174(2)	4983(3)	73(1)
N(8)	8892(3)	2403(2)	1400(3)	66(1)
N(9)	7153(4)	5164(2)	5206(3)	63(1)

B(1)	2865(4)	2404(2)	1147(3)	37(1)
C(1)	1367(3)	903(2)	1012(3)	64(1)
C(2)	2678(3)	991(2)	1709(3)	44(1)
C(3)	3456(4)	474(2)	2389(3)	47(1)
C(4)	4574(3)	832(2)	2822(2)	40(1)
C(5)	5717(4)	496(2)	3558(2)	43(1)
C(6)	6810(4)	690(2)	3667(3)	48(1)
C(7)	7848(4)	346(2)	4380(3)	58(1)
C(8)	6804(5)	-370(3)	4871(4)	78(2)
C(9)	5717(4)	-67(2)	4174(3)	62(1)
C(10)	1874(4)	2577(2)	-1068(3)	59(1)
C(11)	3163(3)	2575(2)	-322(2)	39(1)
C(12)	4157(3)	2619(2)	-419(3)	41(1)
C(13)	5148(3)	2563(2)	497(2)	36(1)
C(14)	6435(3)	2522(2)	813(2)	38(1)
C(15)	6933(4)	2950(2)	395(3)	54(1)
C(16)	8128(4)	2869(3)	693(3)	68(1)
C(17)	8392(4)	1983(2)	1803(3)	57(1)
C(18)	7202(3)	2012(2)	1531(3)	44(1)
C(19)	999(3)	3560(2)	1174(3)	61(1)
C(20)	2313(3)	3608(2)	1848(3)	45(1)
C(21)	2959(4)	4124(2)	2580(3)	47(1)
C(22)	4155(3)	3927(2)	2973(3)	38(1)
C(23)	5197(4)	4333(2)	3753(2)	42(1)
C(24)	6310(4)	3988(2)	4295(3)	52(1)
C(25)	7248(4)	4422(2)	4990(3)	62(1)
C(26)	6081(4)	5490(2)	4698(3)	59(1)
C(27)	5093(4)	5113(2)	3972(3)	51(1)
C(28)	7617(4)	3105(3)	3257(3)	54(1)
C(29)	8964(4)	3192(3)	3855(4)	105(2)
C(30)	136(6)	9(5)	2577(5)	155(4)

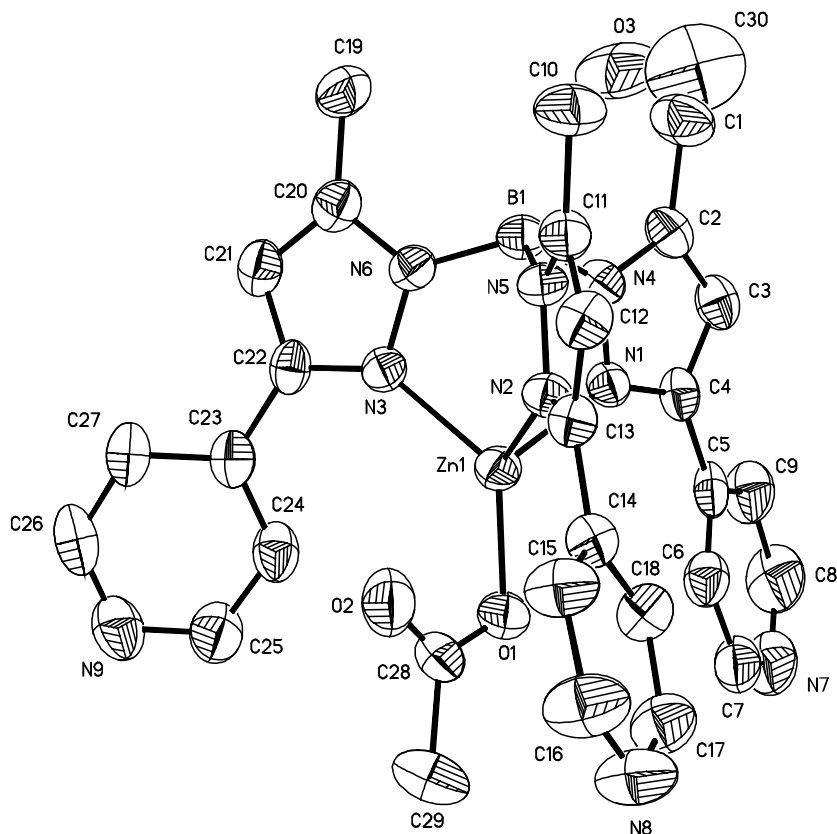


Figure 4.6. Ortep diagram with 30% thermal ellipsoids for **16**.

Table 4.14. Atomic coordinates (10^4) and equivalent isotropic displacement parameters ($\text{\AA}^2 \cdot 10^3$) for **17**.

	x	y	z	U(eq)
Zn(1)	15936(1)	2968(1)	6456(1)	30(1)
O(1)	13796(4)	2462(4)	6492(1)	60(1)
O(2)	15265(3)	904(4)	6719(1)	55(1)
O(3)	13158(4)	496(4)	6776(1)	73(1)
N(1)	15969(3)	5182(3)	6272(1)	34(1)
N(2)	15773(3)	2563(3)	5696(1)	32(1)
N(3)	18011(3)	2483(3)	6472(1)	28(1)
N(4)	17164(3)	5458(4)	6097(1)	34(1)
N(5)	16622(3)	3514(3)	5513(1)	30(1)
N(6)	18579(3)	3167(3)	6129(1)	30(1)
N(7)	12065(5)	6632(6)	7147(2)	77(2)
N(8)	11745(4)	-1028(5)	5392(2)	62(1)
N(9)	16188(3)	3827(3)	7174(1)	30(1)

N(10)	14111(3)	1362(3)	6669(1)	22(1)
B(1)	17769(5)	4277(5)	5814(2)	34(1)
C(1)	18838(5)	7455(5)	6053(2)	56(1)
C(2)	17547(5)	6839(4)	6182(1)	40(1)
C(3)	16573(5)	7476(5)	6412(1)	45(1)
C(4)	15616(4)	6412(5)	6463(1)	37(1)
C(5)	14386(5)	6502(5)	6693(1)	43(1)
C(6)	13270(5)	5618(5)	6573(2)	47(1)
C(7)	12155(5)	5724(6)	6806(2)	61(1)
C(8)	13125(7)	7481(7)	7256(2)	79(2)
C(9)	14300(6)	7463(5)	7048(2)	59(1)
C(10)	17053(5)	4534(5)	4760(1)	50(1)
C(11)	16279(4)	3613(4)	5055(1)	36(1)
C(12)	15196(4)	2729(5)	4936(1)	40(1)
C(13)	14912(4)	2073(4)	5338(1)	34(1)
C(14)	13844(4)	1003(4)	5367(1)	37(1)
C(15)	12787(5)	890(6)	5016(2)	57(1)
C(16)	11789(5)	-135(7)	5043(2)	71(2)
C(17)	12763(5)	-919(5)	5720(2)	54(1)
C(18)	13833(5)	33(5)	5719(1)	43(1)
C(19)	20691(4)	3149(6)	5751(2)	55(1)
C(20)	19825(4)	2643(5)	6097(1)	39(1)
C(21)	20103(4)	1611(5)	6425(1)	41(1)
C(22)	18955(4)	1535(4)	6655(1)	30(1)
C(23)	18830(4)	572(4)	7046(1)	28(1)
C(24)	19794(4)	-491(4)	7157(1)	36(1)
C(25)	19749(4)	-1325(4)	7539(1)	36(1)
C(26)	17849(4)	-188(4)	7708(1)	33(1)
C(27)	17819(4)	702(4)	7334(1)	34(1)

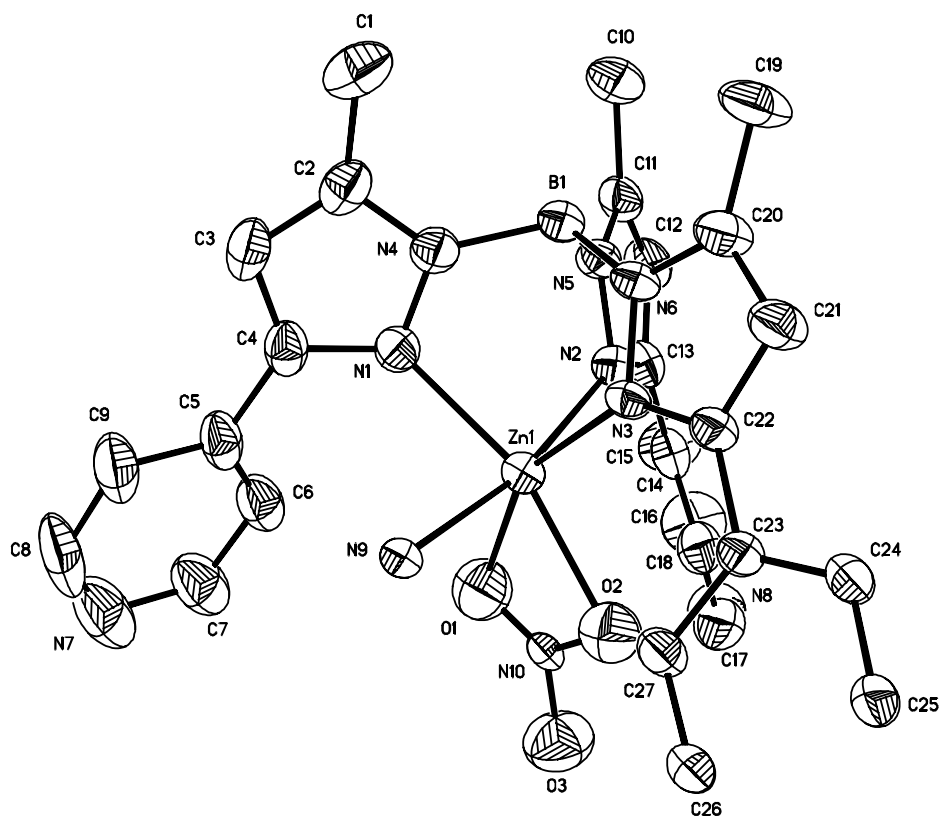


Figure 4.7. Ortep diagram with 30% thermal ellipsoids for **17**.

Table 4.15. Atomic coordinates (10^4) and equivalent isotropic displacement parameters ($\text{\AA}^2 \cdot 10^3$) for **18**.

	x	y	z	U(eq)
Zn(1)	268(1)	1997(1)	1283(1)	55(1)
Zn(2)	4766(1)	2171(1)	1064(1)	56(1)
O(1)	785(2)	1475(3)	2108(2)	60(1)
O(2)	4248(2)	1683(3)	1504(2)	62(1)
O(3)	2049(3)	7547(6)	1288(3)	136(2)
O(4)	2040(2)	5606(6)	1014(3)	136(2)
O(5)	2495(3)	6087(7)	1923(3)	153(3)
O(6)	2844(2)	6735(5)	1260(3)	105(2)
O(7)	3495(3)	3755(8)	4204(3)	160(3)
O(8)	3465(4)	5120(10)	3552(4)	213(4)
O(9)	3335(6)	3171(10)	3366(5)	253(6)
O(10)	2697(3)	4161(12)	3521(5)	255(6)
O(11)	3308(2)	563(5)	1251(2)	93(2)

O(12)	1731(2)	284(5)	2405(2)	96(2)
N(1)	-368(2)	2461(4)	1510(2)	56(1)
N(2)	-194(2)	2895(4)	425(2)	53(1)
N(3)	711(2)	3501(4)	1398(2)	57(1)
N(4)	-486(2)	3660(4)	1438(2)	51(1)
N(5)	-352(2)	3998(4)	535(2)	52(1)
N(6)	411(2)	4485(4)	1423(2)	54(1)
N(7)	-828(3)	-1592(5)	2185(2)	75(2)
N(8)	288(2)	373(4)	981(2)	54(1)
N(9)	2508(2)	1452(6)	1623(3)	79(2)
N(10)	4393(2)	3800(4)	944(2)	57(1)
N(11)	5242(2)	2919(4)	556(2)	54(1)
N(12)	5431(2)	2516(4)	1739(2)	53(1)
N(13)	4765(2)	4686(4)	1176(2)	59(1)
N(14)	5437(2)	4041(4)	753(2)	56(1)
N(15)	5630(2)	3637(4)	1756(2)	58(1)
N(16)	2402(3)	2395(7)	160(3)	95(2)
N(17)	4714(2)	547(4)	734(2)	57(1)
N(18)	5694(3)	-1576(5)	2749(2)	72(2)
Cl(1)	2355(1)	6516(2)	1362(1)	96(1)
Cl(2)	3231(1)	4029(3)	3681(1)	126(1)
C(1)	-1130(3)	5139(6)	1572(3)	79(2)
C(2)	-912(3)	3912(5)	1592(2)	62(2)
C(3)	-1075(3)	2882(5)	1756(3)	65(2)
C(4)	-733(2)	1989(5)	1710(2)	56(2)
C(5)	-753(3)	739(5)	1844(2)	56(2)
C(6)	-1253(3)	251(6)	1813(3)	70(2)
C(7)	-1263(3)	-882(6)	1985(3)	71(2)
C(8)	-351(3)	-1140(5)	2216(3)	66(2)
C(9)	-301(3)	13(5)	2054(3)	62(2)
C(10)	-909(3)	5721(5)	22(3)	65(2)
C(11)	-667(2)	4505(5)	68(2)	55(2)
C(12)	-725(2)	3724(5)	-360(2)	56(2)
C(13)	-421(2)	2747(5)	-119(2)	49(1)
C(14)	-345(2)	1681(5)	-405(2)	50(2)
C(15)	-818(2)	1198(5)	-800(2)	55(2)
C(16)	768(2)	-185(5)	1077(2)	57(2)

C(17)	-163(2)	-135(5)	614(2)	54(2)
C(18)	-144(2)	-1144(5)	324(2)	57(2)
C(19)	537(3)	6572(5)	1749(3)	74(2)
C(20)	748(3)	5386(5)	1666(2)	59(2)
C(21)	1274(3)	4998(5)	1805(2)	62(2)
C(22)	1244(2)	3813(5)	1624(2)	57(2)
C(23)	1679(2)	3001(5)	1632(3)	58(2)
C(24)	1579(3)	2163(6)	1213(3)	66(2)
C(25)	2016(3)	1421(6)	1230(3)	71(2)
C(26)	2580(3)	2264(7)	2025(3)	79(2)
C(27)	2179(3)	3058(6)	2050(3)	67(2)
C(28)	4787(3)	6785(5)	1517(3)	80(2)
C(29)	4498(3)	5636(6)	1272(3)	68(2)
C(30)	3959(3)	5382(6)	1099(3)	67(2)
C(31)	3902(3)	4249(5)	888(3)	64(2)
C(32)	3403(3)	3596(6)	637(3)	63(2)
C(33)	2945(3)	3871(7)	758(3)	82(2)
C(34)	2465(3)	3276(8)	513(4)	92(2)
C(35)	2838(3)	2101(7)	39(3)	82(2)
C(36)	3332(3)	2684(6)	263(3)	69(2)
C(37)	5990(3)	5669(5)	585(3)	79(2)
C(38)	5740(3)	4501(5)	484(3)	60(2)
C(39)	5759(3)	3647(5)	106(3)	65(2)
C(40)	5446(2)	2708(5)	153(2)	53(2)
C(41)	4633(2)	-1590(5)	156(2)	52(2)
C(42)	5131(3)	-1100(5)	471(2)	60(2)
C(43)	5161(2)	-69(5)	746(2)	55(2)
C(44)	4226(2)	52(5)	450(3)	62(2)
C(45)	4177(3)	-990(5)	161(3)	63(2)
C(46)	6422(3)	4886(7)	2304(3)	112(3)
C(47)	6102(3)	3767(6)	2182(3)	68(2)
C(48)	6214(3)	2718(6)	2458(3)	75(2)
C(49)	5792(2)	1938(5)	2171(2)	60(2)
C(50)	5748(2)	704(5)	2323(2)	56(2)
C(51)	5250(3)	174(5)	2280(2)	60(2)
C(52)	5246(3)	-943(6)	2485(3)	67(2)
C(53)	6166(3)	-1077(6)	2780(3)	77(2)

C(54)	6208(3)	42(6)	2576(3)	67(2)
C(55)	3199(4)	-567(9)	1111(5)	135(4)
B(1)	-206(3)	4468(6)	1128(3)	54(2)
B(2)	5362(3)	4517(6)	1276(3)	57(2)

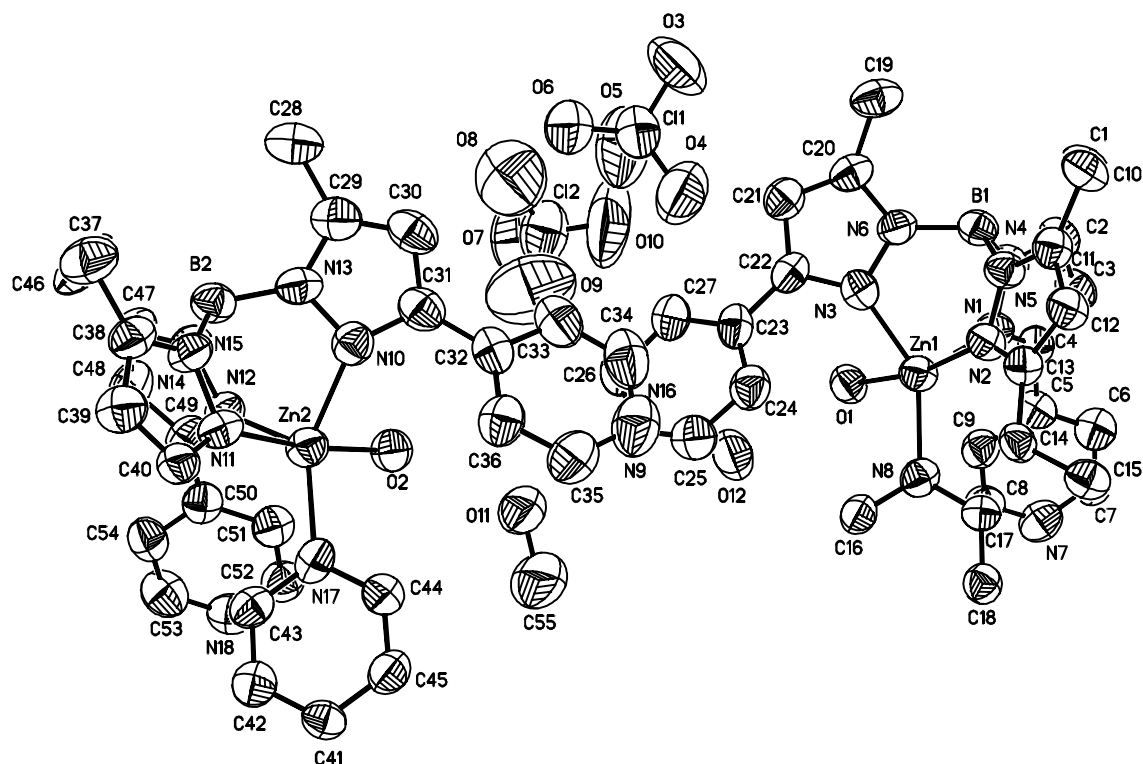


Figure 4.8. Ortep diagram with 30% thermal ellipsoids for **18**.

Table 4.16. Atomic coordinates (10^4) and equivalent isotropic displacement parameters ($\text{\AA}^2 \cdot 10^3$) for **19**.

	x	y	z	U(eq)
Zn(1)	4239(1)	-3141(1)	3170(1)	42(1)
O(1)	5511(2)	-1690(2)	3292(2)	52(1)
O(2)	6489(11)	2707(8)	3238(6)	282(5)
O(3)	5061(17)	1833(15)	2851(10)	277(10)
O(4)	6122(11)	1887(11)	1865(6)	335(6)
O(5)	7200(20)	1397(9)	2877(10)	300(12)
O(6)	7739(17)	2947(8)	2396(10)	266(10)
O(7)	5362(11)	3398(6)	2218(6)	152(4)
N(1)	3018(2)	-4646(2)	2922(1)	39(1)

N(2)	2708(2)	-2277(2)	2756(2)	44(1)
N(3)	4648(2)	-3504(2)	2013(1)	46(1)
N(4)	2110(2)	-4551(2)	2197(1)	42(1)
N(5)	2062(2)	-2584(2)	1949(2)	47(1)
N(6)	3594(2)	-3630(2)	1367(1)	45(1)
N(7)	5209(2)	-3444(2)	4360(1)	37(1)
N(8)	3686(3)	525(2)	5217(2)	57(1)
N(9)	9379(3)	-3606(4)	3161(2)	86(1)
B(1)	2265(3)	-3667(3)	1559(2)	48(1)
Cl(1A)	7095(7)	2403(4)	2695(4)	149(2)
Cl(1B)	5975(6)	2494(3)	2482(2)	123(1)
C(1)	21(3)	-5413(4)	1451(2)	77(1)
C(2)	1154(3)	-5315(3)	2163(2)	52(1)
C(3)	1449(3)	-5916(3)	2879(2)	53(1)
C(4)	2613(3)	-5484(2)	3324(2)	41(1)
C(5)	3372(3)	-5869(2)	4115(2)	38(1)
C(6)	2813(3)	-6165(2)	4791(2)	43(1)
C(7)	6465(3)	-3496(2)	4472(2)	42(1)
C(8)	4666(3)	-3691(2)	5021(2)	38(1)
C(9)	4666(2)	-5988(2)	4215(2)	37(1)
C(10)	520(5)	-1904(4)	743(3)	114(2)
C(11)	1352(4)	-1791(3)	1608(2)	68(1)
C(12)	1553(4)	-965(3)	2200(2)	69(1)
C(13)	2389(3)	-1297(3)	2903(2)	49(1)
C(14)	2873(3)	-693(2)	3712(2)	47(1)
C(15)	3152(4)	412(3)	3699(2)	63(1)
C(16)	3550(4)	961(3)	4460(2)	66(1)
C(17)	3414(3)	-534(3)	5223(2)	56(1)
C(18)	3013(3)	-1154(3)	4497(2)	49(1)
C(19)	3050(4)	-3885(4)	-223(2)	88(1)
C(20)	3969(3)	-3725(3)	615(2)	63(1)
C(21)	5264(3)	-3673(4)	776(2)	75(1)
C(22)	5645(3)	-3547(3)	1656(2)	51(1)
C(23)	6964(3)	-3544(3)	2174(2)	51(1)
C(24)	7811(4)	-2696(4)	2238(3)	96(2)
C(25)	9008(4)	-2773(5)	2739(4)	113(2)
C(26)	8534(4)	-4436(4)	3079(3)	84(1)

C(27)	7353(3)	-4426(3)	2605(3)	72(1)
C(28)	5476(4)	-916(3)	2628(3)	82(1)

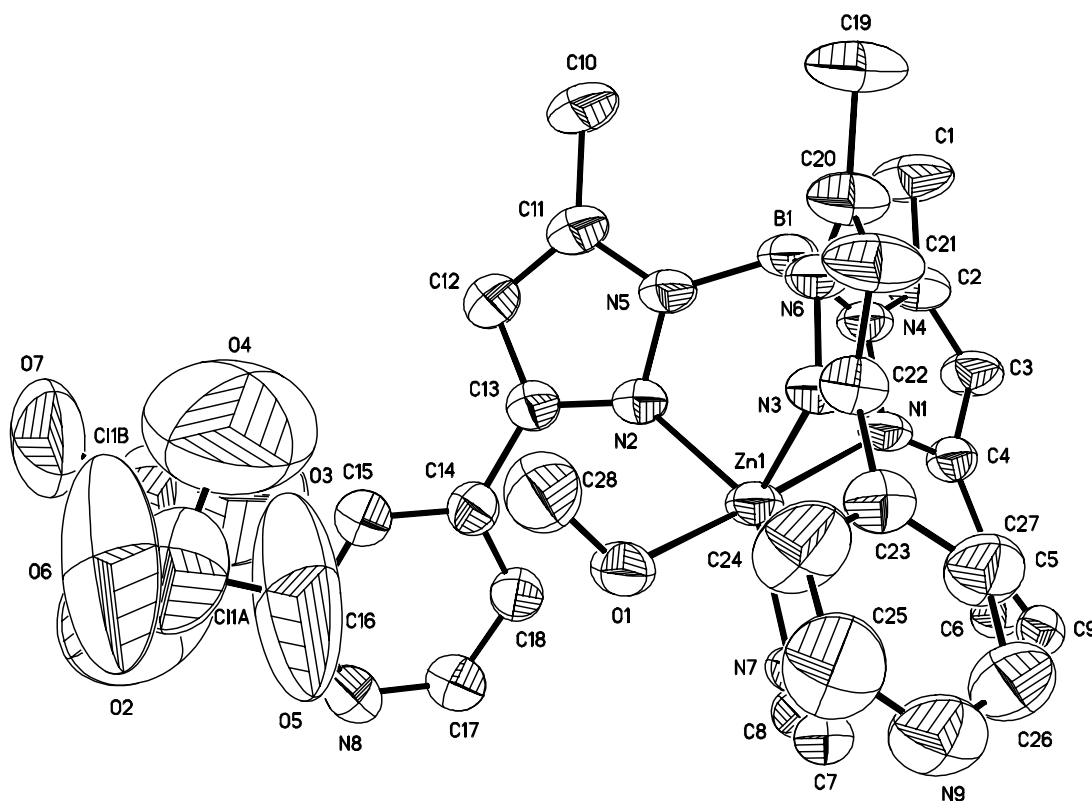


Figure 4.9. Ortep diagram with 30% thermal ellipsoids for **19**.

Table 4.17. Atomic coordinates (10^4) and equivalent isotropic displacement parameters ($\text{\AA}^2 \cdot 10^3$) for **21**.

	x	y	z	U(eq)
Zn(1)	-5000	12736(1)	2500	37(1)
Zn(2)	-4415(1)	12623(1)	175(1)	43(1)
O(1)	-3626(1)	12466(2)	-73(1)	53(1)
O(2)	-2510(2)	13420(2)	-152(1)	85(1)
N(2)	-5295(2)	13683(2)	2082(1)	37(1)
N(3)	-5215(2)	11884(2)	2030(1)	38(1)
N(4)	-6481(2)	12647(2)	2360(1)	39(1)
N(5)	-5887(2)	13526(2)	1896(1)	42(1)
N(6)	-5801(2)	12030(2)	1838(1)	41(1)
N(8)	-3448(3)	15779(3)	2309(2)	105(2)

N(9)	-3149(2)	10053(3)	2092(2)	87(2)
N(10)	-3944(2)	12644(2)	2318(1)	37(1)
N(16)	-4143(2)	12547(2)	781(1)	43(1)
N(19)	-5004(2)	12988(2)	-560(1)	49(1)
N(20)	-5123(2)	11775(2)	178(1)	42(1)
N(21)	-4966(2)	13610(2)	242(1)	42(1)
N(22)	-5649(2)	12864(2)	-499(1)	44(1)
N(23)	-5753(2)	12041(2)	117(1)	43(1)
N(24)	-5622(2)	13533(2)	168(1)	41(1)
N(25)	-3134(2)	13547(3)	-1464(2)	81(2)
N(26)	-3555(2)	9529(3)	645(1)	75(1)
N(27)	-3004(2)	15078(3)	872(2)	86(2)
B(1)	-6238(2)	12735(3)	1942(1)	41(1)
B(2)	-5908(2)	12846(3)	-81(1)	44(1)
Cl(1)	-5000	12304(8)	-2500	498(9)
Cl(2)	-5347(15)	11154(14)	-2213(7)	1188(17)
Cl(3)	-1808(11)	14220(11)	1692(4)	900(16)
Cl(4)	-1622(7)	13873(9)	1065(3)	748(13)
C(1)	-7682(2)	12579(4)	2191(2)	82(2)
C(2)	-7100(2)	12568(3)	2470(1)	54(1)
C(10)	-6737(3)	14184(4)	1461(2)	99(2)
C(11)	-6089(2)	14155(3)	1681(1)	56(1)
C(12)	-5629(2)	14723(3)	1722(1)	59(1)
C(13)	-5137(2)	14425(2)	1977(1)	44(1)
C(14)	-4549(2)	14863(3)	2098(1)	48(1)
C(15)	-3959(2)	14532(3)	2212(2)	59(1)
C(16)	-3437(3)	15013(3)	2314(2)	82(2)
C(17)	-4011(3)	16101(4)	2198(2)	113(3)
C(18)	-4563(3)	15672(3)	2095(2)	88(2)
C(19)	-6533(3)	11477(4)	1298(2)	103(2)
C(20)	-5917(2)	11494(3)	1553(1)	62(1)
C(21)	-5398(2)	10995(3)	1554(2)	67(2)
C(22)	-4969(2)	11249(2)	1853(1)	43(1)
C(23)	-4337(2)	10867(2)	1951(1)	48(1)
C(24)	-4055(2)	10793(3)	2322(1)	59(1)
C(25)	-3470(3)	10403(3)	2375(2)	74(2)
C(26)	-3427(3)	10125(4)	1737(2)	88(2)

C(27)	-4003(2)	10522(3)	1651(2)	68(1)
C(30)	-2913(2)	12497(3)	2128(1)	60(1)
C(31)	-3566(2)	12552(2)	2003(1)	42(1)
C(32)	-3792(2)	12544(2)	1590(1)	41(1)
C(33)	-3374(2)	12271(3)	1306(1)	50(1)
C(34)	-3554(2)	12304(3)	914(1)	49(1)
C(35)	-4550(2)	12798(2)	1056(1)	43(1)
C(36)	-4392(2)	12814(3)	1451(1)	46(1)
C(55)	-6700(2)	12633(4)	-888(2)	76(2)
C(56)	-5986(2)	12779(3)	-852(1)	50(1)
C(57)	-5542(2)	12856(3)	-1139(1)	56(1)
C(58)	-4942(2)	12987(3)	-948(1)	47(1)
C(59)	-4318(2)	13164(3)	-1122(1)	48(1)
C(60)	-4220(3)	13040(3)	-1520(1)	64(1)
C(61)	-3633(3)	13244(4)	-1672(2)	78(2)
C(62)	-3230(2)	13658(3)	-1081(2)	64(1)
C(63)	-3799(2)	13483(3)	-907(1)	55(1)
C(64)	-6890(2)	11559(3)	198(2)	71(2)
C(65)	-6169(2)	11478(3)	225(1)	50(1)
C(66)	-5813(2)	10841(3)	365(1)	54(1)
C(67)	-5164(2)	11045(2)	329(1)	45(1)
C(68)	-4598(2)	10541(2)	432(1)	47(1)
C(69)	-4693(3)	9842(3)	635(2)	62(1)
C(70)	-4164(3)	9366(3)	733(2)	77(2)
C(71)	-3474(3)	10189(3)	451(2)	71(2)
C(72)	-3969(2)	10707(3)	334(1)	55(1)
C(73)	-6658(2)	14225(3)	312(2)	75(2)
C(74)	-5930(2)	14137(3)	337(1)	54(1)
C(75)	-5477(2)	14616(3)	515(2)	58(1)
C(76)	-4873(2)	14272(2)	453(1)	45(1)
C(77)	-4237(2)	14542(3)	592(1)	50(1)
C(78)	-4157(3)	15003(3)	930(2)	72(2)
C(79)	-3547(3)	15239(4)	1054(2)	92(2)
C(80)	-3077(3)	14646(3)	552(2)	78(2)
C(81)	-3669(2)	14361(3)	402(2)	63(1)
C(82)	-5000	11557(9)	-2500	360(20)
C(83)	-1162(14)	14046(7)	1382(6)	374(16)

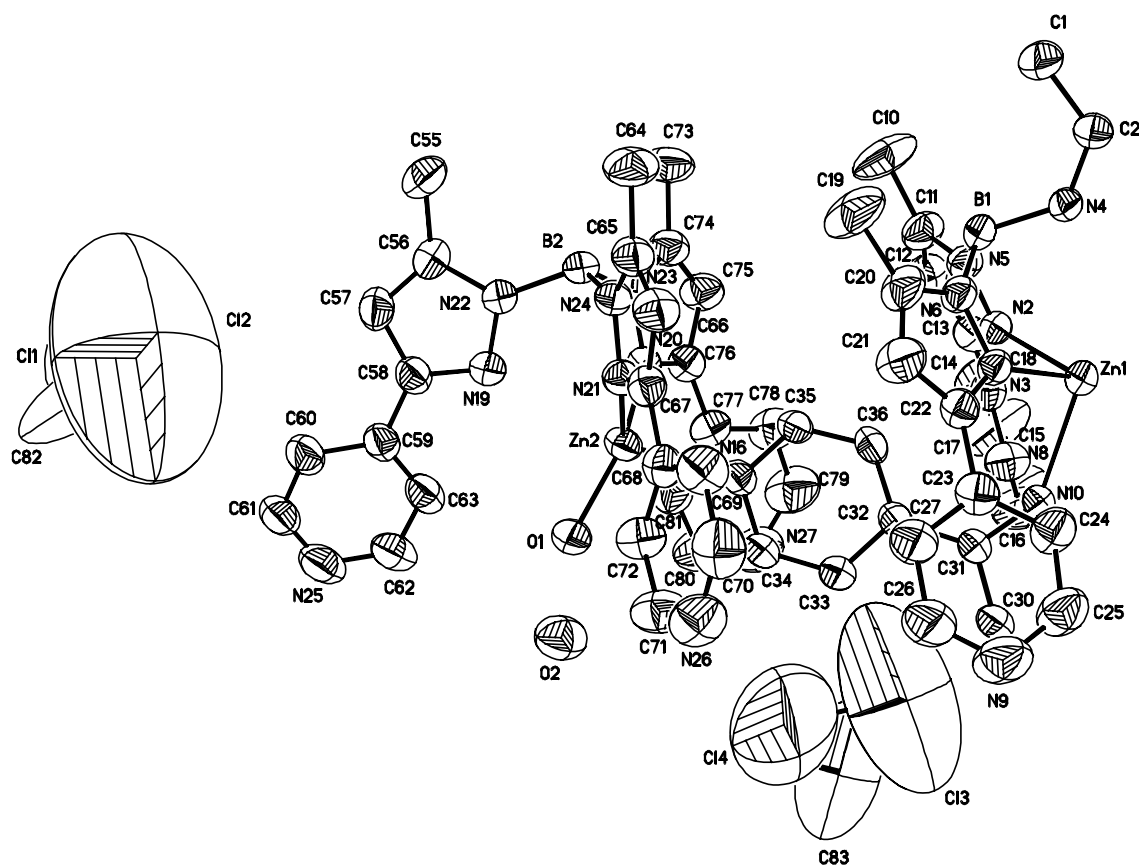


Figure 4.10. Ortep diagram with 30% thermal ellipsoids for **21**.

Table 4.18. Atomic coordinates (10^4) and equivalent isotropic displacement parameters ($\text{\AA}^2 \cdot 10^3$) for **22**.

	x	y	z	U(eq)
Zn(1)	5679(1)	2045(1)	1203(1)	52(1)
Zn(2)	2427(1)	-87(1)	567(1)	64(1)
O(1)	4640(2)	2024(1)	1022(1)	65(1)
O(2)	3480(3)	2091(2)	1149(2)	164(3)
O(3)	4363(2)	1845(2)	1710(2)	93(1)
Cl(1)	2071(2)	-541(1)	1166(1)	239(2)
N(1)	6565(2)	1780(1)	896(1)	52(1)
N(2)	6247(2)	2326(2)	1780(1)	55(1)
N(3)	5770(2)	1223(1)	1508(1)	52(1)
N(4)	7130(2)	1585(2)	1187(1)	55(1)
N(5)	6914(2)	2103(2)	1880(1)	57(1)
N(6)	6426(2)	1194(1)	1780(1)	49(1)

N(7)	5587(4)	2319(2)	-741(2)	102(2)
N(8)	4520(5)	3886(3)	1810(2)	120(2)
N(9)	3314(2)	326(2)	965(1)	55(1)
N(10)	3011(2)	-256(2)	36(2)	59(1)
N(11)	1901(2)	565(2)	318(1)	52(1)
N(12)	1486(2)	-583(1)	21(1)	48(1)
N(13)	2687(2)	-106(1)	-377(1)	51(1)
N(14)	1902(2)	628(1)	-141(1)	51(1)
N(15)	1340(2)	-238(1)	-321(1)	45(1)
N(16)	5305(5)	-991(3)	971(3)	142(3)
N(17)	1583(4)	1324(3)	1874(2)	131(2)
N(18)	5716(2)	2793(2)	855(1)	51(1)
B(1)	7049(3)	1559(2)	1696(2)	50(1)
B(2)	1921(3)	143(2)	-455(2)	48(1)
C(1)	8397(3)	1233(2)	1182(2)	86(2)
C(2)	7707(3)	1452(2)	962(2)	61(1)
C(3)	7505(3)	1569(2)	506(2)	67(2)
C(4)	6800(3)	1771(2)	472(2)	53(1)
C(5)	6370(3)	1955(2)	65(2)	61(1)
C(6)	5610(3)	1971(2)	5(2)	76(2)
C(7)	5264(4)	2143(3)	-391(2)	101(2)
C(8)	6310(5)	2305(3)	-679(2)	97(2)
C(9)	6713(3)	2128(2)	-299(2)	74(2)
C(10)	8151(3)	2299(2)	2285(2)	89(2)
C(11)	7372(3)	2428(2)	2133(2)	65(1)
C(12)	6993(3)	2867(2)	2194(2)	78(2)
C(13)	6300(3)	2801(2)	1968(2)	63(1)
C(14)	5673(3)	3163(2)	1915(2)	67(1)
C(15)	5801(4)	3701(2)	1872(2)	90(2)
C(16)	5212(6)	4026(3)	1826(3)	122(3)
C(17)	4400(4)	3370(4)	1859(2)	103(2)
C(18)	4968(4)	3003(3)	1903(2)	82(2)
C(19)	7047(3)	650(2)	2404(2)	73(2)
C(20)	6413(2)	792(2)	2077(2)	52(1)
C(21)	5738(2)	561(2)	2001(2)	53(1)
C(22)	5353(2)	841(2)	1645(2)	46(1)
C(23)	4639(2)	701(2)	1412(2)	49(1)

C(24)	4400(2)	831(2)	963(2)	52(1)
C(25)	3757(2)	644(2)	756(2)	54(1)
C(26)	3527(3)	220(2)	1396(2)	63(1)
C(27)	4170(3)	386(2)	1626(2)	62(1)
C(28)	4129(3)	2002(2)	1279(3)	87(2)
C(29)	3807(5)	1778(3)	2001(3)	161(4)
C(30)	2959(3)	-73(3)	-1189(2)	88(2)
C(31)	3146(3)	-203(2)	-701(2)	66(1)
C(32)	3766(3)	-415(2)	-493(2)	75(2)
C(33)	3681(3)	-446(2)	-43(2)	66(2)
C(34)	4205(4)	-633(2)	325(3)	87(2)
C(35)	4956(3)	-633(2)	260(3)	114(3)
C(36)	5471(5)	-816(3)	550(4)	144(4)
C(37)	4592(6)	-1011(4)	1053(4)	158(4)
C(38)	4030(4)	-832(3)	723(3)	105(2)
C(39)	1769(3)	1324(2)	-741(2)	77(2)
C(40)	1799(3)	1129(2)	-254(2)	55(1)
C(41)	1738(3)	1397(2)	135(2)	65(1)
C(42)	1803(2)	1042(2)	487(2)	56(1)
C(43)	1730(3)	1129(2)	967(2)	63(1)
C(44)	1884(4)	1599(3)	1164(2)	111(2)
C(45)	1809(6)	1672(4)	1602(3)	143(4)
C(46)	1452(4)	849(3)	1690(2)	106(2)
C(47)	1522(3)	749(3)	1245(2)	83(2)
C(48)	314(3)	56(2)	-888(2)	91(2)
C(49)	626(2)	-277(2)	-511(2)	56(1)
C(50)	319(3)	-661(2)	-282(2)	62(1)
C(51)	864(2)	-843(2)	47(2)	53(1)
C(52)	5822(2)	3708(2)	348(2)	50(1)
C(53)	5147(3)	3474(2)	396(2)	67(1)
C(54)	5122(3)	3029(2)	646(2)	67(1)
C(55)	6358(3)	3023(2)	819(2)	52(1)
C(56)	6424(2)	3473(2)	573(2)	50(1)

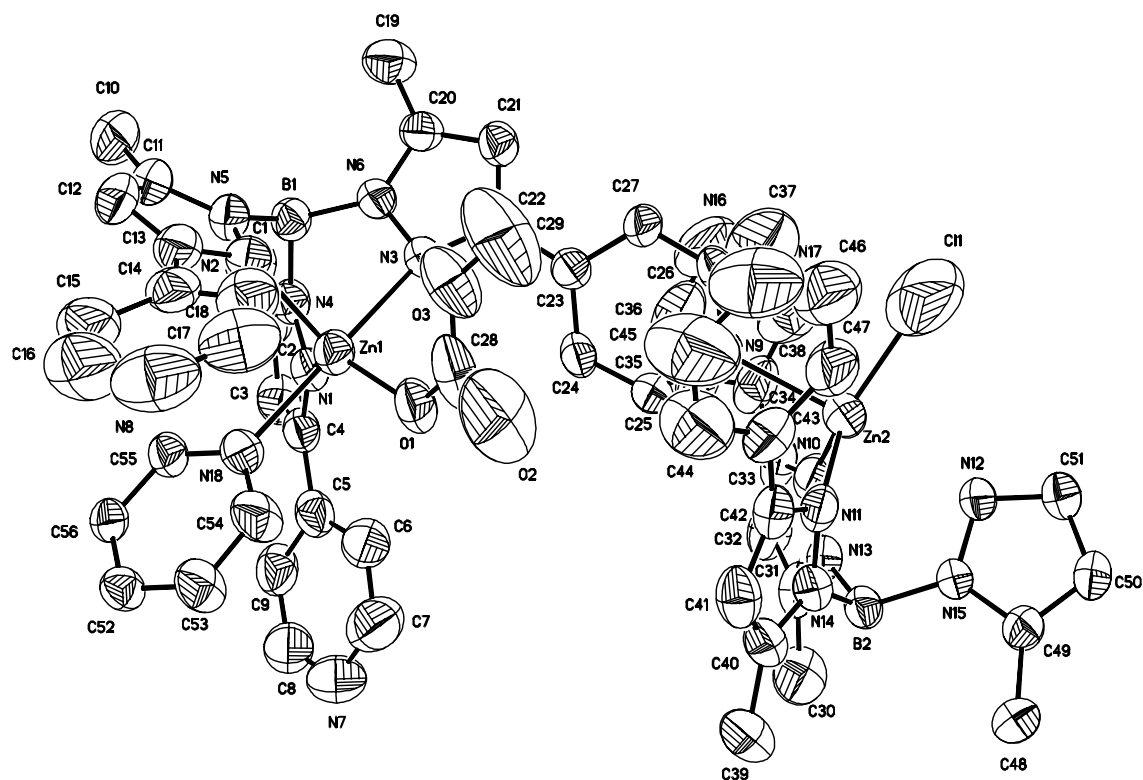


Figure 4.11. Ortep diagram with 30% thermal ellipsoids for **22**.

Table 4.19. Atomic coordinates (10^4) and equivalent isotropic displacement parameters ($\text{\AA}^2 \cdot 10^3$) for **27**.

	x	y	z	U(eq)
Zn(1)	2988(1)	7910(1)	1118(1)	32(1)
O(1)	3241(2)	8946(1)	958(2)	41(1)
O(2)	1369(2)	8111(1)	1218(2)	45(1)
N(1)	2969(2)	7353(1)	71(2)	33(1)
N(2)	2813(2)	6960(1)	1792(2)	35(1)
N(3)	4739(2)	7723(1)	1437(2)	33(1)
N(4)	3498(2)	6706(1)	134(2)	34(1)
N(5)	3375(2)	6383(1)	1540(2)	34(1)
N(6)	5071(2)	7062(1)	1218(2)	35(1)
N(7)	393(3)	9168(2)	-1516(2)	66(1)
N(8)	133(5)	8012(2)	3608(3)	84(2)
N(9)	5768(4)	10143(2)	2794(2)	62(1)
B(1)	4194(3)	6480(2)	920(2)	35(1)
C(1)	3607(4)	5577(2)	-648(3)	61(1)

C(2)	3162(3)	6308(2)	-517(2)	40(1)
C(3)	2397(4)	6704(2)	-1011(2)	45(1)
C(4)	2307(3)	7350(2)	-626(2)	36(1)
C(5)	1648(3)	7979(2)	-924(2)	35(1)
C(6)	610(4)	7902(2)	-1371(2)	51(1)
C(7)	28(4)	8503(3)	-1646(3)	67(1)
C(8)	1394(4)	9237(2)	-1093(3)	54(1)
C(9)	2048(3)	8668(2)	-787(2)	43(1)
C(10)	3498(4)	5058(2)	1742(3)	60(1)
C(11)	3026(3)	5776(2)	1878(2)	40(1)
C(12)	2235(3)	5965(2)	2351(2)	44(1)
C(13)	2124(3)	6707(2)	2286(2)	36(1)
C(14)	1429(3)	7171(2)	2720(2)	42(1)
C(15)	320(4)	7001(2)	2795(3)	56(1)
C(16)	-280(5)	7436(3)	3238(3)	78(2)
C(17)	1201(5)	8168(2)	3551(3)	73(2)
C(18)	1884(4)	7776(2)	3110(3)	54(1)
C(19)	6842(4)	6353(2)	1191(4)	72(2)
C(20)	6202(3)	7014(2)	1352(3)	43(1)
C(21)	6609(3)	7653(2)	1649(2)	44(1)
C(22)	5674(3)	8083(2)	1703(2)	33(1)
C(23)	5667(3)	8805(2)	2046(2)	37(1)
C(24)	6491(3)	9295(2)	1928(2)	50(1)
C(25)	6494(4)	9949(2)	2311(3)	65(1)
C(26)	4974(4)	9665(2)	2895(2)	53(1)
C(27)	4890(3)	9000(2)	2539(2)	42(1)
C(28)	-256(4)	8723(2)	1472(3)	63(1)
C(29)	925(3)	8723(2)	1275(2)	43(1)
C(30)	1446(3)	9374(2)	1165(2)	45(1)
C(31)	2519(3)	9454(2)	963(2)	37(1)
C(32)	2928(3)	10169(2)	724(2)	40(1)
C(33)	4052(4)	10269(2)	689(3)	53(1)
C(34)	4450(5)	10923(2)	448(3)	70(1)
C(35)	3723(5)	11481(2)	263(3)	64(1)
C(36)	2606(5)	11385(2)	304(3)	66(1)
C(37)	2192(4)	10739(2)	523(3)	55(1)
C(38)	283(8)	6396(5)	610(5)	133(3)

Cl(1)	520(17)	5687(9)	161(7)	789(15)
Cl(2)	-971(7)	6434(6)	-310(6)	480(7)

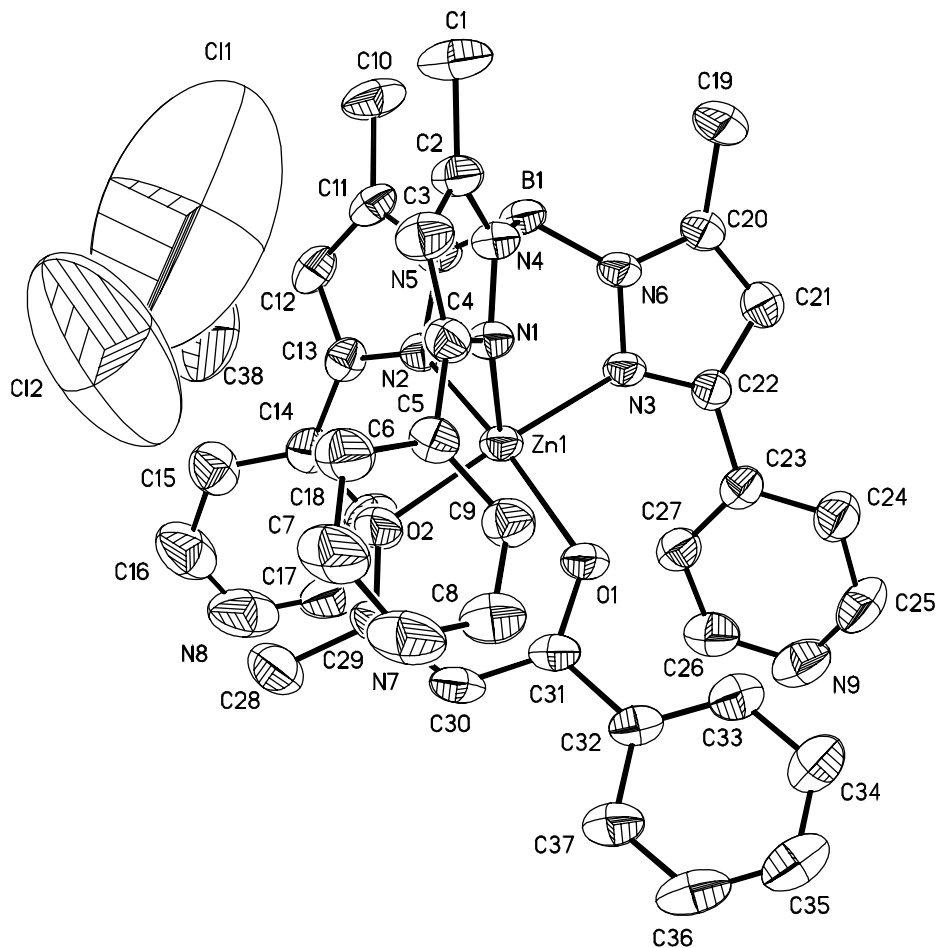


Figure 4.12. Ortep diagram with 30% thermal ellipsoids for **27**.

Table 4.20. Atomic coordinates (10^4) and equivalent isotropic displacement parameters ($\text{\AA}^2 \cdot 10^3$) for **34**.

	x	y	z	U(eq)
Zn(1)	1524(1)	2467(1)	8808(1)	45(1)
Zn(2)	1021(1)	2866(1)	7150(1)	44(1)
O(1)	1799(2)	4950(3)	10187(3)	56(2)
O(2)	2497(2)	2418(4)	8234(3)	76(2)
O(3)	809(1)	2176(3)	7942(3)	46(1)
O(4)	1704(1)	3902(3)	7454(3)	55(2)
O(5)	1396(2)	1435(3)	7670(3)	49(2)

O(6)	392(2)	4783(3)	7844(3)	59(2)
O(7)	1351(1)	3166(3)	8036(3)	36(1)
O(8)	741(2)	9139(4)	6804(5)	120(3)
O(9)	957(2)	7949(5)	6782(5)	134(4)
O(10)	452(2)	8188(6)	5984(5)	151(4)
O(11)	871(3)	8833(7)	5812(6)	178(5)
N(1)	1680(2)	3012(4)	9841(4)	45(2)
N(2)	1943(2)	1945(4)	9099(4)	52(2)
N(3)	1294(2)	1647(4)	9128(4)	47(2)
N(4)	1740(2)	2464(4)	10380(3)	44(2)
N(5)	2035(2)	1635(4)	9804(4)	47(2)
N(6)	1478(2)	1297(4)	9768(4)	46(2)
N(7)	1527(2)	4443(4)	9076(4)	47(2)
N(8)	1979(2)	2139(4)	7627(4)	57(2)
N(9)	559(2)	1043(4)	7754(4)	50(2)
N(10)	1142(2)	3423(4)	6314(3)	42(2)
N(11)	908(2)	1971(4)	6513(4)	47(2)
N(12)	589(2)	3417(4)	6757(4)	47(2)
N(13)	921(2)	3264(4)	5633(4)	48(2)
N(14)	674(2)	2064(4)	5860(4)	46(2)
N(15)	442(2)	3330(4)	6015(4)	45(2)
N(16)	1859(2)	4520(4)	6637(4)	50(2)
N(17)	1249(2)	208(4)	7345(4)	57(2)
N(18)	644(2)	3677(4)	8260(4)	54(2)
B(1)	1800(3)	1646(6)	10227(6)	55(3)
B(2)	604(2)	2880(5)	5575(5)	42(2)
Cl(1)	752(1)	8506(2)	6349(2)	85(1)
C(1)	1824(2)	2374(5)	11708(4)	56(3)
C(2)	1778(2)	2812(5)	11031(4)	45(2)
C(3)	1758(2)	3552(5)	10919(4)	52(2)
C(4)	1691(2)	3668(5)	10162(4)	40(2)
C(5)	1675(2)	4404(5)	9810(5)	42(2)
C(6)	1459(3)	5117(5)	8649(5)	54(3)
C(7)	1633(3)	5771(6)	8847(5)	73(3)
C(8)	1548(4)	6415(6)	8397(8)	106(5)
C(9)	1293(4)	6374(8)	7734(7)	109(5)
C(10)	1138(3)	5703(7)	7542(7)	99(4)

C(11)	1205(3)	5073(6)	7979(6)	77(3)
C(12)	2499(2)	1048(5)	10748(5)	69(3)
C(13)	2340(2)	1403(5)	10026(5)	52(2)
C(14)	2460(2)	1592(5)	9478(5)	59(3)
C(15)	2215(2)	1903(4)	8935(5)	44(2)
C(16)	2244(3)	2183(5)	8222(5)	56(2)
C(17)	1957(2)	2274(5)	6892(5)	49(2)
C(18)	1701(2)	1967(5)	6330(5)	58(3)
C(19)	1675(3)	2063(6)	5621(5)	76(3)
C(20)	1899(3)	2489(7)	5436(7)	87(4)
C(21)	2143(3)	2806(7)	5993(6)	84(3)
C(22)	2181(2)	2715(5)	6730(5)	60(3)
C(23)	1455(2)	170(5)	10519(6)	74(3)
C(24)	1313(2)	688(6)	9841(5)	60(3)
C(25)	1025(2)	614(4)	9268(5)	54(3)
C(26)	1022(2)	1248(5)	8837(5)	52(2)
C(27)	786(2)	1523(5)	8126(5)	44(2)
C(28)	299(2)	1196(5)	7112(5)	44(2)
C(29)	180(2)	1891(6)	6911(6)	59(3)
C(30)	-88(3)	1984(7)	6272(6)	77(3)
C(31)	-228(3)	1419(9)	5839(6)	87(4)
C(32)	-102(3)	713(8)	6031(7)	92(4)
C(33)	152(3)	595(6)	6666(7)	75(3)
C(34)	849(2)	3377(6)	4297(4)	65(3)
C(35)	1029(2)	3502(5)	5086(4)	44(2)
C(36)	1315(2)	3817(4)	5437(4)	44(2)
C(37)	1378(2)	3789(4)	6188(4)	37(2)
C(38)	1657(2)	4058(5)	6811(5)	45(2)
C(39)	2133(2)	4866(5)	7143(5)	55(2)
C(40)	2107(3)	5271(6)	7720(5)	69(3)
C(41)	2378(4)	5636(7)	8207(6)	101(4)
C(42)	2665(4)	5586(7)	8068(8)	106(5)
C(43)	2683(3)	5231(8)	7485(10)	108(5)
C(44)	2413(3)	4844(7)	6998(7)	92(4)
C(45)	339(3)	1320(6)	4762(6)	95(4)
C(46)	580(2)	1384(5)	5490(5)	55(3)
C(47)	755(3)	829(6)	5944(6)	69(3)

C(48)	957(2)	1214(6)	6572(6)	61(3)
C(49)	1228(3)	967(6)	7266(6)	52(3)
C(50)	1498(3)	-168(5)	7908(6)	55(3)
C(51)	1677(3)	138(6)	8565(6)	70(3)
C(52)	1918(3)	-285(7)	9073(6)	77(3)
C(53)	1986(3)	-997(7)	8984(7)	96(4)
C(54)	1821(3)	-1347(7)	8300(8)	101(4)
C(55)	1579(3)	-896(6)	7756(7)	91(4)
C(56)	-39(2)	3825(6)	5001(5)	72(3)
C(57)	176(2)	3767(6)	5766(5)	61(3)
C(58)	155(2)	4163(5)	6377(5)	53(3)
C(59)	406(2)	3914(5)	6952(5)	44(2)
C(60)	480(2)	4186(5)	7745(5)	42(2)
C(61)	741(2)	3775(6)	9045(5)	51(2)
C(62)	831(2)	3129(6)	9458(5)	59(3)
C(63)	934(2)	3217(7)	10213(6)	75(3)
C(64)	940(3)	3890(10)	10545(6)	96(5)
C(65)	863(3)	4497(8)	10151(7)	94(4)
C(66)	753(2)	4490(6)	9352(5)	70(3)

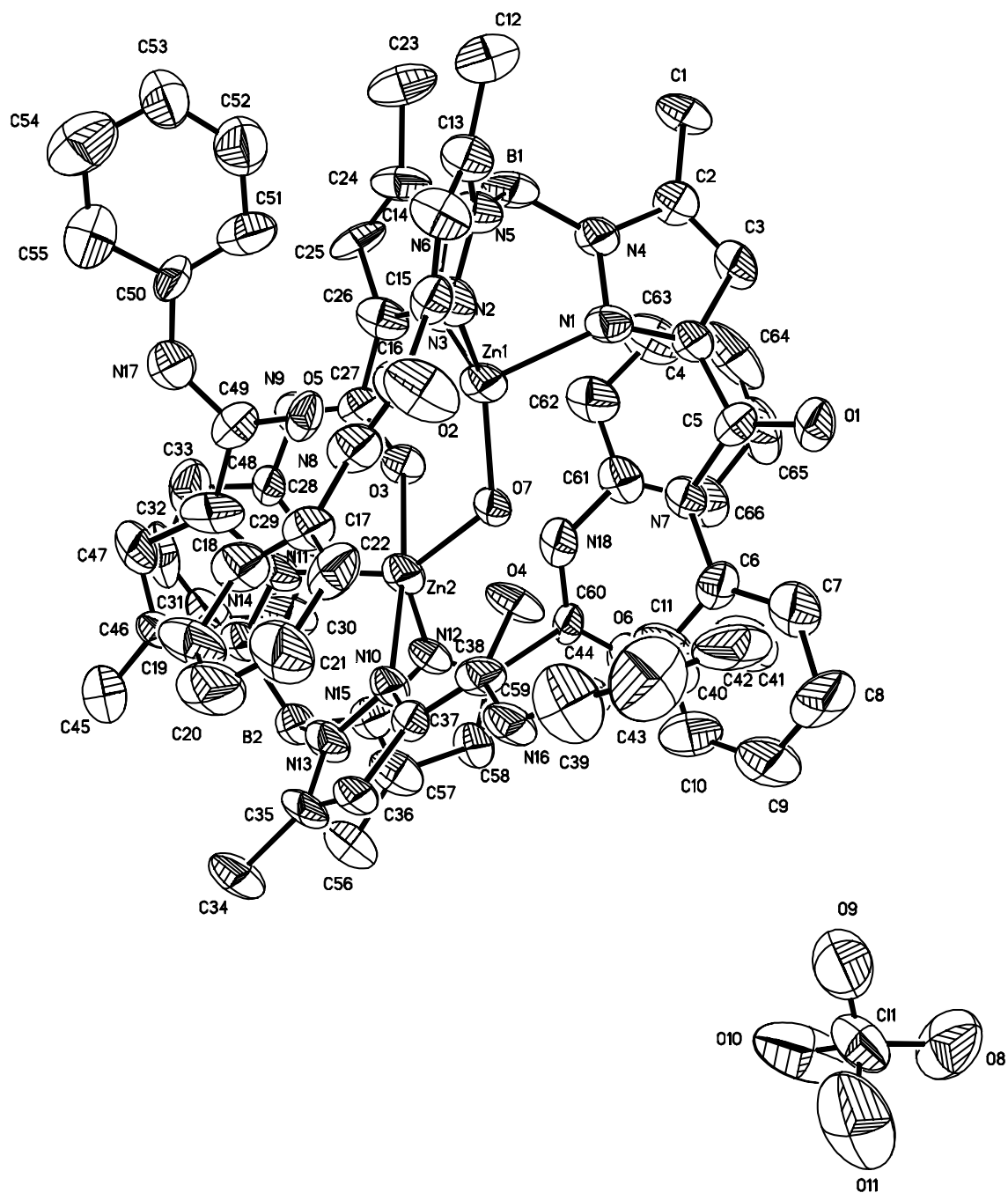


Figure 4.13. Ortep diagram with 30% thermal ellipsoids for **34**.

5. Summary

The ultimate aim of this work was to understand the importance of secondary interactions of hydrophilic nature in the catalytic activity of zinc metalloenzymes. The zinc complexes of novel tris(pyrazolyl)borate ligands bearing polar substituents on the 3-position of the pyrazoles were expected to contribute to this. On the one hand, structural models of a protecting cavity around zinc incorporating hydrogen bonding groups had to be constructed. On the other hand, not only the stoichiometric but more the catalytic modeling of an enzymatic process had to be achieved in aqueous solution. With these purposes, the synthesis and zinc coordination chemistry of three classes of polar poly(pyrazolyl)borate ligands were studied. These comprise the carboxyester substituted $\text{Bp}^{\text{C(O)OR,Me}}$ ($\text{R} = \text{Me, Et}$), the pyridyl substituted $\text{Tp}^{4\text{'Py,Me}}$ and $\text{Tp}^{4\text{'(6'Me)Py,Me}}$, and the carboxamide substituted $\text{Tp}^{\text{C(O)NHPh,Me}}$ ligands.

The carboxyester substituted pyrazoles $\text{Hpz}^{\text{Me,C(O)OR}}$ ($\text{R} = \text{Me, Et}$) were revealed to be good precursors of the water soluble bis(pyrazolyl)borates $\text{KBp}^{\text{C(O)OEt,Me}}$ **2** and $\text{KBp}^{\text{C(O)OMe,Me}}$ **3**, but not of the corresponding tris(pyrazolyl)borates $\text{KTp}^{\text{C(O)OR,Me}}$ ($\text{R} = \text{Me, Et}$). The X-ray structure determination of **3** revealed that such species build polymers in the solid state. The thallium salt $\text{TlBp}^{\text{C(O)OMe,Me}}$ **4** was easily accessible by metathesis of **3** with thallium nitrate. By reaction with zinc perchlorate, **2** and **3** gave the bis(ligand) complexes $(\text{Bp}^{\text{C(O)OEt,Me}})_2\text{Zn}$ **5** and $(\text{Bp}^{\text{C(O)OMe,Me}})_2\text{Zn}$ **6**, respectively, which were structurally characterized. The methyl ester substituted complex **6** was also obtained by the reaction of the ethyl ester substituted ligand **2** with zinc chloride in methanol, thereby providing a process of self-transesterification often found to be catalysed by carboxyester substituted poly(pyrazolyl)borates.

The bis(pyrazolyl)borate $\text{KBp}^{\text{Ph,Me}}$ **7** could be easily prepared under melting conditions, and purified by metathesis with thallium nitrate as $\text{TlBp}^{\text{Ph,Me}}$ **8**. By reaction of **7** with zinc salts of poorly coordinating counter ions, i.e. perchlorate or sulphate, the bis(ligand) complex $(\text{Bp}^{\text{Ph,Me}})_2\text{Zn}$ **9** always resulted, while with zinc chloride, the

complex $(\text{Bp}^{\text{Ph,Me}})\text{Zn}(\text{Cl})(\text{MeOH})$ **10** was obtained. The X-ray structure determination of **10** revealed that a methanol molecule is coordinated to zinc.

In analogy to the already known pyridyl substituted ligands $\text{Tp}^{3'\text{Py,Me}}$ and $\text{Tp}^{3'(6'\text{Me})\text{Py,Me}}$, the new 4'-pyridyl substituted tris(pyrazolyl)borates $\text{KTp}^{4'\text{Py,Me}}$ **11** and $\text{KTp}^{4'(6'\text{Me})\text{Py,Me}}$ **12** were synthesized. The 4'-position of the pyridyl nitrogens was found to favour the hydrophilic interactions of the ligand system with the solvent and to enhance its solubility in protic solvents and water. Indeed, **11** represents the first example of a water soluble tris(pyrazolyl)borate able to build a hydrophobic cavity around zinc. The X-ray structure determination of **11** showed that it has a polymeric structure in which all pyridyl nitrogen atoms are coordinated to neighbouring potassium ions.

By reaction of **11** with zinc halides, the complexes $\text{Tp}^{4'\text{Py,Me}}\text{Zn-Cl}$ **13**, $\text{Tp}^{4'\text{Py,Me}}\text{Zn-Br}$ **14** and $\text{Tp}^{4'\text{Py,Me}}\text{Zn-I}$ **15** were isolated and spectroscopically characterized. The versatile coordination behaviour of $\text{Tp}^{4'\text{Py,Me}}$ towards zinc was revealed in the crystal structures of the acetate and nitrate complexes $\text{Tp}^{4'\text{Py,Me}}\text{Zn-OC}(\text{O})\text{CH}_3$ **16** and $\text{Tp}^{4'\text{Py,Me}}\text{Zn-ONO}_2$ **17**. Complex **16** has a monomeric structure which shows the expected monodentate coordination of acetate to zinc and the hydrophilic character of the ligand $\text{Tp}^{4'\text{Py,Me}}$ by the fact that a pyridyl nitrogen is hydrogen bound to a co-crystallized methanol molecule. In contrast, complex **17** forms one-dimensional chains, in which the adjacent $\text{Tp}^{4'\text{Py,Me}}\text{Zn-ONO}_2$ units are linked to each other through a pyridyl ring. The ability of $\text{Tp}^{4'\text{Py,Me}}$ to stabilize zinc coordination to small neutral co-ligands was demonstrated in the crystal structures of the novel aqua and methanol complexes $[\text{Tp}^{4'\text{Py,Me}}\text{Zn-OH}_2]\text{ClO}_4$ **18** and $[\text{Tp}^{4'\text{Py,Me}}\text{Zn-HOMe}]\text{ClO}_4$ **19**, which form dimeric species in the solid state due to pyridine coordination to zinc. Furthermore, the intermolecular H-bonding network found in the crystal structure of **18**, which involves the zinc bound water molecule, the pyridine nitrogens of the $\text{Tp}^{4'\text{Py,Me}}$ system and different solvent molecules, possesses remarkable structural similarities with the resting state of carbonic anhydrase.

For the functional modeling of zinc metalloenzymes the hydroxo complex $\text{Tp}^{4'\text{Py,Me}}\text{Zn-OH}$ **20** was isolated and spectroscopically characterized. Upon attempts to crystallize **20**, it dismutated into the bis(ligand) complex $(\text{Tp}^{4'\text{Py,Me}})_2\text{Zn}$ and $\text{Zn}(\text{OH})_2$, and the mixed compound $[(\text{Tp}^{4'\text{Py,Me}})_2\text{Zn}][\text{Tp}^{4'\text{Py,Me}}\text{Zn-OH}]_2$ **21** was obtained and

structurally characterized. The carbonic anhydrase catalysed hydration of CO₂ was modelled by the insertion reactions of **20** with CO₂ and CS₂ in alcoholic solutions. Thereby, the mixed methylcarbonate-chloride complex [Tp^{4Py,Me}Zn-OC(O)OMe][Tp^{4Py,Me}Zn-Cl] **22**, and the alkylxanthogenate complexes Tp^{4Py,Me}Zn-SC(S)OMe **23** and Tp^{4Py,Me}Zn-SC(S)OEt **24** were obtained. The X-ray structure determination of **22** revealed that it forms one-dimensional polymers in which the methylcarbonate complex Tp^{4Py,Me}Zn-OC(O)OMe and the chloride complex Tp^{4Py,Me}Zn-Cl are linked to each other through their pyridyl nitrogen donors.

The β-ketoenolate complexes Tp^{4Py,Me}Zn(acac) **26** and Tp^{4Py,Me}Zn(benzoylac) **27** were prepared by the reaction of **20** with acetylacetone and benzoylacetone, respectively. The structural characterization of **27** provided a new example of “*transition state analogue*” of zinc containing metalloproteases. The hydrolytic cleavage of phosphotriesters and carboxyesters was modelled by the reactions of **20** with tris(*p*-nitrophenyl)phosphate and *p*-nitrophenylacetate, respectively. Thereby, the new *p*-nitrophenolate complex Tp^{4Py,Me}Zn-ONit **25**, the new bis(*p*-nitrophenyl) phosphate complex Tp^{4Py,Me}Zn-OP(O)(ONit)₂ **28** and the acetate complex **16** were obtained. The hydroxo complex **20** did not promote the hydrolytic cleavage of carboxyamides. Instead, by reaction with trifluoroacetamide the amidate complex Tp^{4Py,Me}Zn-NHC(O)CF₃ **29** was obtained.

The isolation of the polar aqua complex **18** provided a unique opportunity for the functional modeling of zinc metalloenzymes under more natural conditions than those demanded by the hydrophobic *t*-butyl, phenyl and cumenyl substituted Tp^{R,Me}Zn-OH complexes. Indeed, complex **18** was found to be an appropriate catalyst for the hydrolytic cleavage of the activated phosphotriesters tris(*o*-dichlorophenyl)phosphate and tris(*p*-nitrophenyl)phosphate, and of carboxyesters like trifluoro(*p*-nitrophenyl) acetate and *p*-nitrophenylacetate, in aqueous solution. In accordance with the catalytic nature of these hydrolyses, the hydrolysis products were spectroscopically demonstrated not to be bound to the Tp^{4Py,Me}Zn unit.

Finally, the synthesis of the ligand Tp^{C(O)NHPh,Me} incorporating for the first time NH hydrogen donor groups in a pyrazolylborate system, was achieved. Its potassium salt KTp^{C(O)NHPh,Me} **30** is soluble in alcohols and in alcohol/water mixtures. The coordination

behaviour of $\text{Tp}^{\text{C(O)NHPH,Me}}$ towards zinc was studied by reactions of **30** with zinc chloride, nitrate and acetate. The corresponding complexes $\text{Tp}^{\text{C(O)NHPH,Me}}\text{Zn-Cl}$ **31**, $\text{Tp}^{\text{C(O)NHPH,Me}}\text{Zn-ONO}_2$ **32** and $\text{Tp}^{\text{C(O)NHPH,Me}}\text{Zn-OC(O)CH}_3$ **33** were isolated and spectroscopically characterized. By reaction of **30** with zinc perchlorate the hydroxide bridged binuclear complex $[(\text{Tp}^{\text{C(O)NHPH,Me}}\text{Zn})_2(\mu_2\text{-OH})]\text{ClO}_4$ **34** was obtained. The crystal structure of **34** revealed the existence of a series of secondary interactions of hydrophobic and hydrophilic nature, which are influencing the chemistry of $\text{Tp}^{\text{C(O)NHPH,Me}}$ based zinc complexes as they do in the active sites of zinc metalloenzymes.

In summary, 3 new bis(pyrazolyl)borate and 3 novel polar tris(pyrazolyl)borate ligands were synthesized. 7 potassium, 2 thallium and 25 zinc complexes were isolated. 12 compounds were structurally characterized, providing a better structural modeling of the secondary interactions present in the active sites of zinc metalloenzymes. The carbonic anhydrase catalysed hydration of CO_2 and the biologically relevant hydrolytic cleavages of phosphotriesters and carboxyesters were modelled with the new hydroxo complex $\text{Tp}^{4\text{-Py,Me}}\text{Zn-OH}$ **20**. The novel aqua complex $[\text{Tp}^{4\text{-Py,Me}}\text{Zn-OH}_2]\text{ClO}_4$ **18** was demonstrated to behave as a catalyst towards the hydrolytic cleavage of tris(*p*-nitrophenyl)phosphate in aqueous solution.

6. References

-
- ¹ Franks, F. (ed.) *The chemistry and physics of water. A comprehensive treatise*. Vols. 1-7, Plenum Press, New York London, **1972-1982**.
 - ² Jeffrey, G. A. Saenger, W. *Hydrogen bonding in biological structures*. Springer-Verlag, Berlin Heidelberg, **1994**.
 - ³ Hughes, M. N. *The inorganic chemistry of biological processes*. 2. ed. Chichester, Wiley, **1981**.
 - ⁴ Vallee, B. L., Auld, D. S. *Acc. Chem. Res.* **1993**, *26*, 543-551.
 - ⁵ Lipscomb, W. N., Sträter, N. *Chem. Rev.* **1996**, *96*, 2375-2433.
 - ⁶ Reichwein, A. M., Verboom, W., Reinhoudt, D. N. *Recl. Trav. Chim. Pays-Bas* **1994**, *113*, 343-349.
 - ⁷ Chin, J. *Acc. Chem. Res.* **1991**, *24*, 145-152.
 - ⁸ Coleman, J. E. In *Zinc Enzymes*; Bertini, I., Luchinat, C., Maret, W., Zeppezauer, M., Eds., Birkhäuser, Boston, **1986**, Vol. 1, 49-58.
 - ⁹ Hakansson, K., Carlsson, M., Svensson, L. A., Liljas, A., *J. Mol. Biol.* **1992**, *227*, 1192-1204.
 - ¹⁰ Bertini, I., Luchinat, C. In *Bioinorganic Chemistry*; Bertini, I., Gray, H. B., Lippard, S. J., Valentine, J., Eds., Univ. Science Books, Mill Valley, Calif., **1994**.
 - ¹¹ Ibers, J. A., Holm, R. H. *Science* **1980**, *209*, 223-235.
 - ¹² Karlin, K. D. *Science* **1993**, *261*, 701-708.
 - ¹³ Meldrum, N.M., Roughton, F. H. *Nature (London)* **1993**, *80*, 113-142.
 - ¹⁴ Keilin, D., Mann, T. *Biochem. J.* **1940**, *34*, 1163-1176.
 - ¹⁵ Nagase, H., Woessner, J. F., Jr. *J. Biol. Chem.* **1999**, *274*, 21491-21494.
 - ¹⁶ McDonnell, S., Morgan, M., Lynch, C. *Biochem. Soc. Trans.* **1999**, *27*, 734-740.
 - ¹⁷ Nagase, H. *Biol. Chem.* **1997**, *378*, 151-160.
 - ¹⁸ Pelmeshnikov, V., Siegbahn, P. E. M. *Inorg. Chem.* **2002**, *41*, 5659-5666.
 - ¹⁹ Parkin, G. *Chem. Rev.* **2004**, *104*, 699-767.
 - ²⁰ Jairam, R., Potvin, P. G., Balsky, S. *J. Chem. Soc., Perkin Trans.* **1999**, 363-367.

-
- ²¹ Fujii, Y., Itoh, T., Onodera, K., Tada, T. *Chem. Lett.* **1995**, *24*, 305-306.
- ²² Cronin, L., Foxon, S. P., Lusby, P. J., Walton, P. H. *J. Biol. Inorg. Chem.* **2001**, *6*, 367-377.
- ²³ Tecilla, P., Tonellato, U., Veronese, A., Felluga, F., Scrimin, P. *J. Org. Chem.* **1997**, *62*, 7621-7628.
- ²⁴ Gregorzik, R., Hartmann, U., Vahrenkamp, H. *Chem. Ber.* **1994**, *127*, 2117-2122.
- ²⁵ Hartmann, U., Gregorzik, R., Vahrenkamp, H. *Chem. Ber.* **1994**, *127*, 2123-2127.
- ²⁶ Breslow, R., Hunt, J. T., Smiley, R., Tarnowski, T. *J. Am. Chem. Soc.* **1983**, *105*, 5337-5342.
- ²⁷ Hannon, M. J., Mayers, P. C., Taylor, P. C. *Angew. Chem., Int. Ed.* **2001**, *40*, 1081-1084.
- ²⁸ Kimblin, C., Allen, W. E., Parkin, G. *J. Chem. Soc., Chem. Commun.* **1995**, 1813-1815.
- ²⁹ Sénèque, O., Rager, M. N., Giorgi, M., Reinaud, O. *J. Am. Chem. Soc.* **2000**, *122*, 6183-6189.
- ³⁰ Sénèque, O., Rager, M. N., Giorgi, M., Reinaud, O. *J. Am. Chem. Soc.* **2001**, *123*, 8442-8443.
- ³¹ Voo, J. K., Incarvito, C. D., Yap, G. P. A., Rheingold, A. L., Riordan, C. G. *Polyhedron* **2004**, *23*, 405-412.
- ³² Zvargulis, E. S., Buys, I. E., Hambley, T. W. *Polyhedron* **1995**, *14*, 2267-2273.
- ³³ Titze, C., Hermann, J., Vahrenkamp, H. *Chem. Ber.* **1995**, *128*, 1095-1103.
- ³⁴ Chaudhuri, P., Stockheim, C., Wieghardt, K., Deck, W., Gregorzik, R., Vahrenkamp, H., Nuber, B., Weiss, J. *Inorg. Chem.* **1992**, *31*, 1451-1457.
- ³⁵ Kimura, E., Shiota, T., Koike, T., Shiro, M., Kodama, M. *J. Am. Chem. Soc.* **1990**, *112*, 5805-5811.
- ³⁶ Kimura, E. *Acc. Chem. Res.* **2001**, *34*, 171-179.
- ³⁷ Brandsch, T., Schell, F. A., Weis, K., Ruf, M., Müller, B., Vahrenkamp, H. *Chem. Ber./Recl.* **1997**, *130*, 283-289.
- ³⁸ Nakata, K., Uddin, M. K., Ogawa, K., Ichikawa, K. *Chem. Lett.* **1997**, *26*, 991-992.
- ³⁹ Echizen, T., Ibrahim, M. M., Nakata, K., Izumi, M., Ichikawa, K., Shiro, M. *J. Inorg. Biochem.* **2004**, *98*, 8, 1347-1360.
- ⁴⁰ Trofimenko, S. *Chem. Rev.* **1972**, *72*, 497-509.

-
- ⁴¹ Trofimenko, S. *Prog. Inorg. Chem.* **1986**, *34*, 115-210.
- ⁴² Trofimenko, S. *Scorpionates. The coordination chemistry of polypyrazolborate ligands*. Imperial College Press., London, **1999**.
- ⁴³ Alsfasser, R., Trofimenko, S., Looney, A., Parkin, G., Vahrenkamp, H. *Inorg. Chem.* **1991**, *30*, 4098-4100.
- ⁴⁴ Alsfasser, R., Ruf, M., Trofimenko, S., Vahrenkamp, H. *Chem. Ber.* **1993**, *126*, 703-710.
- ⁴⁵ Looney, A., Han, R., McNeill, K., Parkin, G. *J. Am. Chem. Soc.* **1993**, *115*, 4690-4697.
- ⁴⁶ Kitajima, N., Hikichi, S., Tanaka, M., Morooka, Y. *J. Am. Chem. Soc.* **1993**, *115*, 5496-5508.
- ⁴⁷ Ruf, M., Vahrenkamp, H. *Inorg. Chem.* **1996**, *35*, 6571-6578.
- ⁴⁸ Looney, A., Parkin, G., Alsfasser, R., Ruf, M., Vahrenkamp, H. *Angew. Chem.* **1992**, *104*, 57-58.
- ⁴⁹ Vahrenkamp, H. *Acc. Chem. Res.* **1999**, *32*, 589-596.
- ⁵⁰ Brombacher, H., Vahrenkamp, H., *Inorg. Chem.* **2004**, *43*, 6042-6049.
- ⁵¹ Brombacher, H., Vahrenkamp, H., *Inorg. Chem.* **2004**, *43*, 6050-6053.
- ⁵² Brombacher, H., Vahrenkamp, H., *Inorg. Chem.* **2004**, *43*, 6054-6060.
- ⁵³ Rombach, M., Brombacher, H., Vahrenkamp, H. *Eur. J. Inorg. Chem.* **2002**, 153-159.
- ⁵⁴ Kläui, W., Berghahn, M., Rheinwald, G., Lang, H. *Angew. Chem.* **2000**, *112*, 2590-2592.
- ⁵⁵ Kläui, W., Berghahn, M., Frank, W., Reiß, G. J., Schönherr, T., Rheinwald, G., Lang, H. *Eur. J. Inorg. Chem.* **2003**, 2059-2070.
- ⁵⁶ Kunz, P. C., Reiß, G. J., Frank, W., Kläui, W. *Eur. J. Inorg. Chem.* **2003**, 3945-3951.
- ⁵⁷ Hammes, B. S., Carrano, M. W., Carrano, C. J., *J. Chem. Soc., Dalton Trans.* **2001**, 1448-1451.
- ⁵⁸ Hammes, B. S., Luo, X. M., Carrano, M. W., Carrano, C. J. *Inorg. Chim. Acta* **2002**, *341*, 33-38.
- ⁵⁹ Weis, K., Vahrenkamp, H. *Inorg. Chem.* **1997**, *36*, 5589-5591.
- ⁶⁰ Weis, K., Vahrenkamp, H. *Inorg. Chem.* **1997**, *36*, 5592-5596.
- ⁶¹ Rheingold, A.L., Incarvito, C. D., Trofimenko, S. *J. Chem. Soc., Dalton Trans.* **2000**, 1233-1234.

-
- ⁶² Hammes, B. S., Young, V. G., Jr., Borovik, A. S. *Angew. Chem., Int. Ed.* **1999**, *38*, 666-669.
- ⁶³ MacBeth, C. E., Hammes, B. S., Young, V. G., Jr., Borovik, A. S. *Inorg. Chem.* **2001**, *40*, 4733-4741.
- ⁶⁴ Trofimenko, S. *J. Am. Chem. Soc.* **1966**, *88*, 1842-1844.
- ⁶⁵ Trofimenko, S. *Chem. Rev.* **1993**, *93*, 943-980.
- ⁶⁶ Curtis, M. D., Shiu, K.-B., Butler, W. M. *J. Am. Chem. Soc.* **1986**, *108*, 1550-61.
- ⁶⁷ Trofimenko, S., Calabrese, J. C., Thompson, J. S. *Inorg. Chem.* **1987**, 1508-14.
- ⁶⁸ Weis, K., Rombach, M., Vahrenkamp, H. *Inorg. Chem.* **1998**, *37*, 2470-2475.
- ⁶⁹ Rombach, M., Gelinsky, M., Vahrenkamp, H. *Inorg. Chim. Acta* **2002**, *334*, 25-33.
- ⁷⁰ Badura, D., Vahrenkamp, H. *Inorg. Chem.* **2002**, *41*, 6013-6019.
- ⁷¹ Badura, D., Vahrenkamp, H. *Inorg. Chem.* **2002**, *41*, 6020-6027.
- ⁷² Armstrong, N. *Biochemistry* **2000**, *39*, 13625-13632.
- ⁷³ Hammes, B. S., Luo, X. M., Chohan, B. S., Carrano, M. W., Carrano, C. J. *J. Chem. Soc., Dalton Trans.* **2002**, 3374-3380.
- ⁷⁴ Buchen, Th., Gütllich, P. *Inorg. Chim. Acta* **1995**, *231*, 221-223.
- ⁷⁵ Dowling, C., Parkin, G. *Polyhedron* **1996**, *15*, 2463-2465.
- ⁷⁶ Ghosh, P., Parkin, G. *J. Chem. Soc., Dalton Trans.* **1998**, 2281-2283.
- ⁷⁷ Ghosh, P., Parkin, G. *Chem. Commun.* **1998**, 413-414.
- ⁷⁸ Ji, M. *Dissertation*, Freiburg, **2004**.
- ⁷⁹ Trofimenko, S., Calabrese, J. C., Thompson, J. S., *Inorg. Chem.* **1987**, *26*, 1507-1514.
- ⁸⁰ Calabrese, J. C., Domaille, P. J., Thompson, J. S., Trofimenko, S., *Inorg. Chem.* **1990**, *29*, 4429-4437.
- ⁸¹ Dowling, C., Ghosh, P., Parkin, G. *Polyhedron* **1995**, *16*, 3469-3473.
- ⁸² Ghosh, C. K.; Hoyano, J. K.; Krentz, R.; Graham, W. A. G. *J. Am. Chem. Soc.* **1989**, *111*, 5480-5481.
- ⁸³ Dias, H. V. R.; Kim, H. J. *Organometallics* **1996**, *15*, 5374-5379.
- ⁸⁴ Jones, P. L.; Amoroso, A. J.; Jeffery, J. C.; McCleverty, J. A.; Psillakis, E.; Rees, L. H.; Ward, M. D. *Inorg. Chem.* **1997**, *36*, 10-18.
- ⁸⁵ Amoroso, A. J.; Jeffery, J. C.; Jones, P. L.; McCleverty, J. A.; Thornton, P.; Ward, M. D. *Angew. Chem., Int. Ed. Engl.* **1995**, *34*, 1443-1446.
- ⁸⁶ Weis, K., Rombach, M., Vahrenkamp, H. *Inorg. Chem.* **1998**, *37*, 2470-2475.

-
- ⁸⁷ Ruf, M., Weis, K., Vahrenkamp, H. *J. Am. Chem. Soc.* **1996**, *118*, 9288-9294.
- ⁸⁸ Davies, G. M., Jeffrey, J. C., Ward, M. D., *New J. Chem.* **2003**, *27*, 1550-1553.
- ⁸⁹ Swamer, F. W., Hauser, C. R. *J. Am. Chem. Soc.* **1950**, *72*, 1352-1356.
- ⁹⁰ Efimovsky, O., Rumpf, P. *Bull. Soc. Chim. Fr.* **1954**, 648-649.
- ⁹¹ Gough, G. A. C., King, H. *J. Chem. Soc.* **1933**, 350-351.
- ⁹² Weis, K. *Dissertation*, Freiburg, **1997**.
- ⁹³ Akita, M., Ohta, K., Takahashi, Y., Hikichi, S., Moro-oka, Y. *Organometallics* **1997**, *16*, 4121-4128.
- ⁹⁴ Sugawara, K., Hikichi, S., Akita, M. *J. Chem. Soc., Dalton Trans.* **2003**, 4346-4355.
- ⁹⁵ Rombach, M., Gelinsky, M., Vahrenkamp, H. *Inorg. Chim. Acta* **2002**, *334*, 25-33.
- ⁹⁶ Kremer-Aach, A., Kläui, W., Bell, R., Strerath, A., Wunderlich, H., Mootz, D., *Inorg. Chem.* **1997**, *36*, 1552.
- ⁹⁷ Botre, F., Gros, G., Storey, B. T., Eds. *Carbonic Anhydrase*, VCH, New York, **1991**.
- ⁹⁸ Looney, A., Han, R., McNeill, K., Parkin, G. *J. Am. Chem. Soc.* **1993**, *115*, 4690-4697.
- ⁹⁹ Han, R., Parkin, G. *J. Am. Chem. Soc.* **1991**, *113*, 9707-9708.
- ¹⁰⁰ Kimblin, C., Murphy, V. J., Hascall, T., Bridgewater, B. M., Bonanno, J. B., Parkin, G. *Inorg. Chem.* **2000**, *39*, 967-974.
- ¹⁰¹ Cronin, L., Foxon, S. P., Lusby, P. J., Walton, P. H. *J. Biol. Inorg. Chem.* **2001**, *6*, 367-377.
- ¹⁰² Eklund, H., Nordström, B., Zeppezauer, E., Söderlund, G., Ohlsson, I., Boiwe, T., Söderberg, B. O., Tapia, O., Brändén, C. I., Akesson, A. *J. Mol. Biol.* **1976**, *102*, 27-
- ¹⁰³ Bergquist, C., Parkin, G. *J. Am. Chem. Soc.* **1999**, *121*, 6322-6323.
- ¹⁰⁴ Seebacher, J., Shu, M., Vahrenkamp, H. *Chem. Commun.* **2001**, 1026-1027.
- ¹⁰⁵ Bergquist, C., Fillebeen, T., Morlok, M. M., Parkin, G. *J. Am. Chem. Soc.* **2003**, *125*, 189-6199.
- ¹⁰⁶ Kimblin, C., Bridgewater, B. M., Churchill, D. G., Parkin, G. *Chem. Commun.* **1999**, 301-2302.
- ¹⁰⁷ Ibrahim, M. M., Shimomura, N., Ichikawa, K., Shiro, M. *Inorg. Chim. Acta* **2001**, *313*, 125-136.
- ¹⁰⁸ Denisov, V. P., Jonsson, B.-H., Halle, B. *J. Am. Chem. Soc.* **1999**, *121*, 2327-2328.
- ¹⁰⁹ Ruf, M.; Schell, F. A.; Walz, R.; Vahrenkamp, H. *Chem. Ber.* **1997**, *130*, 101-104.

-
- ¹¹⁰ Alsfasser, R.; Powell, A. K.; Trofimenko, S.; Vahrenkamp, H. *Chem. Ber.* **1993**, *126*, 685-694.
- ¹¹¹ Bräuer, M., Anders, E., Sinnecker, S., Koch, W., Rombach, M., Brombacher, H., Vahrenkamp, H. *Chem. Commun.* **2000**, 647-648.
- ¹¹² Bergquist, C., Parkin, G. *Inorg. Chem.* **1999**, *38*, 422-423.
- ¹¹³ Peter, A. *Zulassungsarbeit*, Freiburg, **2003**.
- ¹¹⁴ Walz, R., Weis, K., Ruf, M., Vahrenkamp, H. *Chem. Ber.* **1997**, *130*, 975-980.
- ¹¹⁵ Weis, K., Rombach, M., Ruf, M., Vahrenkamp, H. *Eur. J. Inorg. Chem.* **1998**, 263-270.
- ¹¹⁶ Rombach, M., Maurer, C., Weis, K., Keller, E., Vahrenkamp, H. *Chem. Eur. J.* **1999**, *5*, 1013-1027.
- ¹¹⁷ Wolfenden, R., *Acc. Chem. Res.* **1972**, *5*, 10-18.
- ¹¹⁸ Ruf, M., Weis, K., Brasack, I., Vahrenkamp, H. *Inorg. Chim. Acta* **1996**, *250*, 271-281.
- ¹¹⁹ Rombach, M., Vahrenkamp, H. *Inorg. Chem.* **2001**, *40*, 6144-6150.
- ¹²⁰ Fitzgerald, P. M. D., Wu, J. K., Toney, J. H. *Biochemistry* **1998**, *37*, 6791-6800.
- ¹²¹ Payne, D. J., Bateson, J. H., Gasson, B. C., Proctor, D., Khushi, T., Farmer, T. H., Tolson, D. A., Bell, D., Skett, P. W., Marshall, A. C., Reid, R., Ghosez, L., Combred, Y., Marchand-Brynaert, J. *Antimicrob. Agents Chemoter.* **1997**, *41*, 135-140.
- ¹²² Coussens, L. M., Fingleton, B., Matrisian, L. M. *Science* **2002**, *295*, 2387-2392.
- ¹²³ Hikichi, S., Tanaka, M., Moro-oka, Y., Kitajima, N. *J. Chem. Soc., Chem. Commun.*, **1992**, 814-815.
- ¹²⁴ Kaim, W., Schwerderski, B. *Bioanorganische Chemie*, 2. ed., Teubner, Stuttgart, **1995**.
- ¹²⁵ Rice, L. B., Bonomo, R. A. *Drug Resist. Updates* **2000**, *3*, 178-189.
- ¹²⁶ Groß, F. *Dissertation*, Freiburg, **2004**.
- ¹²⁷ Boerzel, H., Koeckert, M., Bu, W. M., Spingler, B., Lippard, S. J. *Inorg. Chem.* **2003**, *42*, 1604-1615.
- ¹²⁸ Cricco, J. A., Orellano, E. G., Rasia, R. M., Ceccarelli, E. A., Vila, A. J. *Coord. Chem. Rev.* **1999**, *192*, 519-535.
- ¹²⁹ Maldonado Calvo, J. A. *Dissertation*, Freiburg, **2005**.

-
- ¹³⁰ Koike, T., Kimura, E. *J. Am. Chem. Soc.* **1991**, *113*, 8935-8941.
- ¹³¹ Eklund, H., Brändén, C.-I. In *Zinc Enzymes*, Spiro, T. G., Ed., Wiley, New York, **1983**.
- ¹³² Bergquist, C., Storrie, H., Koutcher, L., Bridgewater, B. M., Friesner, R. A., Parkin, G. *J. Am. Chem. Soc.* **2000**, *122*, 12651-12658.
- ¹³³ Walz, R., Vahrenkamp, H. *Inorg. Chim. Acta* **2001**, *314*, 58-62 and references therein.
- ¹³⁴ Ramaswamy, S., Park, D.-H., Plapp, B. V. *Biochemistry* **1999**, *38*, 13951-13959.
- ¹³⁵ Garner, D. K., Allred, R. A., Tubbs, K. J., Arif, A. M., Berreau, L. M. *Inorg. Chem.*, **2002**, *41*, 3533-3541.
- ¹³⁶ Makowska-Grzyska, M. M., Jeppson, P. C., Allred, R. A., Arif, A. M., Berreau, L. M. *Inorg. Chem.*, **2002**, *41*, 4872-4887.
- ¹³⁷ MacBeth, C. E., Gupta, R., Mitchell-Koch, K. R., Young, V. G., Lushington, G. H., Thompson, W. H., Hendrich, M. P., Borovik, A. S. *J. Am. Chem. Soc.* **2004**, *126*, 2556-2567.
- ¹³⁸ Hesse, M., Meier, H., Zeeh, B. *Spektroskopische Methoden in der organischen Chemie*, Thieme-Verlag, Stuttgart-New York, **1995**.
- ¹³⁹ Lopez, C., Claramunt, R. M., Sanz, D., Foces, C. F., Cano, F. H., Faure, R., Cayon, E., Elguero, J. *Inorg. Chim. Acta* **1990**, *176*, 195-204.
- ¹⁴⁰ Lobbia, G. G., Cecchi, P., Spagna, R., Colapietro, M., Pifferi, A., Pettinari, C. *J. Organomet. Chem.* **1995**, *485*, 45-53.
- ¹⁴¹ Dowling, C. M., Leslie, D., Chisholm, M. H., Parkin, G. *Main Group Chem.* **1995**, *1*, 29.
- ¹⁴² Dias, H. V. R., Lu, H.-L., Ratcliff, R. E., Bott, S. G. *Inorg. Chem.* **1995**, *34*, 1975-1976.
- ¹⁴³ Dias, H. V. R.; Gorden, J. D. *Inorg. Chem.* **1996**, *35*, 318-324.
- ¹⁴⁴ Pelli, M., Benetollo, F., Lobbia, G. G., Alidori, S., Santini, C. *Inorg. Chem.* **2005**, *44*, 846-848.
- ¹⁴⁵ Looney, A., Han, R., Gorrell, I. B., Cornebise, M., Yoon, K., Parkin, G., Rheingold, A. L. *Organometallics* **1995**, *14*, 274-288.
- ¹⁴⁶ Tesmer, M., Shu, M., Vahrenkamp, H. *Inorg. Chem.* **2001**, *40*, 4022-4029.
- ¹⁴⁷ Beck, A., Weibert, B., Burzlaff, N. *Eur. J. Inorg. Chem.* **2001**, 521-527.

- ¹⁴⁸ Fenton, D. E. In *Comprehensive Coordination Chemistry*; Wilkinson, G., Gillard, R. D., McCleverty, J. A., Eds.; Pergamon Press: Oxford, U.K., **1987**; Vol. 3, pp 1-80.
- ¹⁴⁹ Lindoy, L. F. *The Chemistry of macrocyclic ligand complexes*; Cambridge University Press: Cambridge, U.K., **1989**.
- ¹⁵⁰ Zemann, J. Z. *Anorg. Allg. Chem.* **1963**, 324, 241.
- ¹⁵¹ Janiak, C. *J. Chem. Soc., Dalton Trans.* **2000**, 3885-3896.
- ¹⁵² Holmes, R. R. *Prog. Inorg. Chem.* **1984**, 32, 119-235.
- ¹⁵³ Addison, A. W., Nageswara Rao, T., Reedijk, J., Van Rijn, J., Verschoor, G. C. *J. Chem. Soc., Dalton Trans.* **1984**, 1349-1356.
- ¹⁵⁴ Xue, Y., Vidgren, J., Svensson L.A., Liljas, A., Honsson B. H., Lindskog, S. *Proteins Struct. Funct. Genet.* **1993**, 15, 80-87.
- ¹⁵⁵ Hartmann, F., Kläui, W., Kremer-Aach, A., Mootz, D., Strerath, A., Wunderlich, H. *Z. Anorg. Allg. Chem.* **1993**, 619, 2071.
- ¹⁵⁶ Kleywegt, G. J., Wiesmeijer, W. G. R., Van Driel, G. J., Driessen, W. L., Reedijk, J., Noordik, J. H. *J. Chem. Soc., Dalton Trans.* **1985**, 2177-2184.
- ¹⁵⁷ Spek, A. L., *J. Appl. Cryst.* **2003**, 36, 7-13.
- ¹⁵⁸ Tesmer, M., Shu, M., Vahrenkamp, H. *Inorg. Chem.* **2001**, 40, 4022-4029.
- ¹⁵⁹ Ibrahim, M. M., Ichikawa, K., Shiro, M. *Inorg. Chem. Comm.* **2003**, 6, 1030-1034.
- ¹⁶⁰ Hartmann, F., Kläui, W., Kremer-Aach, A., Mootz, D., Strerath, A., Wunderlich, H. *Z. Anorg. Allg. Chem.* **1993**, 619, 2071.
- ¹⁶¹ Weis, K., Vahrenkamp, H. *Eur. J. Inorg. Chem.* **1998**, 271-274.
- ¹⁶² Marvel, C. S., Dreger, E. E. *Org. Synth. Coll.* Vol.1, 238-240, **1941**.
- ¹⁶³ Royals, E. E. *J. Am. Chem. Soc.* **1945**, 67, 1508-1509.
- ¹⁶⁴ Henke, B., Aquino, A.J., Bikermo, L.S., Croom, D.K., Dougherty, R.W. *J. Med. Chem.*, **1997**, 40, 2706-2725.
- ¹⁶⁵ Elguero, J., Jaquier, R. *Bull. Soc. Chim. Fr.* **1966**, 2832-2845.
- ¹⁶⁶ E.W. Abel, G. Wilkinson, *J. Chem. Soc.*, **1959**, 1501.
- ¹⁶⁷ Seki, K., Isegawa, J., Fukuda, M., Ohki, M. *Chem. Pharm. Bull.* **1984**, 32, 4, 1568-1577.
- ¹⁶⁸ Musante, C. *Gazz. Chim. Ital.* **1945**, 75, 121-123.
- ¹⁶⁹ SAINT+, V6.02, Bruker AXS, Madison, WI, **1999**.
- ¹⁷⁰ G.M.Sheldrick, SADABS, Area-Detector Absorption Correction, Göttingen, **1996**.

-
- ¹⁷¹ G.M.Sheldrick, Program SHELXS, Program for Crystal Structure Determination, Göttingen, **1997**.
- ¹⁷² G.M.Sheldrick, Program SHELXL, Program for Crystal Structure Determination, Göttingen, **1997**.
- ¹⁷³ A.L.Spek PLATON, *A Multipurpose Crystallographic Tool*, Utrecht University, Utrecht, The Netherlands, **2005**.
- ¹⁷⁴ XP program, Interactive Molecular Graphics, **1992**, Ver. 4.3, Siemens Analytical X-ray Inst. Inc.